Title

The Committor in Quantum Systems for Transition States, Reaction Mechanisms, and Coherent Control

Author

Anderson, Michelle

Publication Date

2024

Peer reviewed|Thesis/dissertation

The Committor in Quantum Systems for Transition States, Reaction Mechanisms, and Coherent Control

by

Michelle Anderson

A dissertation submitted in partial satisfaction of the

requirements for the degree of

Doctor of Philosophy

in

Chemistry

in the

Graduate Division

of the

University of California, Berkeley

Committee in charge:

Professor David T. Limmer, Chair
Professor Eran Rabani
Professor Jeffrey B. Neaton

Spring 2024

The Committor in Quantum Systems for Transition States, Reaction Mechanisms, and Coherent Control

Abstract

The Committor in Quantum Systems for Transition States, Reaction Mechanisms, and Coherent Control

by

Michelle Anderson

Doctor of Philosophy in Chemistry

University of California, Berkeley

Professor David T. Limmer, Chair

Understanding reaction dynamics in chemical systems is the first step towards manipulating those reactions to improve efficiency or avoid undesired products. Computational modeling plays a central role in the understanding of reaction dynamics, with that role ever increasing as computational power grows. Such modeling remains challenging, however. Studying reaction mechanisms in classical systems often proves extremely complicated due to the rare nature of reactive events and the many degrees of freedom that are involved. Classical reactions in solution are complicated further by the interactions of the system with the solvent degrees of freedom. The study of reaction mechanisms becomes more complicated still in quantum systems, where confounding behaviors such as interference and tunneling may occur.

Many powerful methods for understanding classical reaction mechanisms, adept at circumventing the problems posed by many degrees of freedom and rare events, have been developed, including transition path theory. Transition path theory is a method built on the committor, the probability for a reaction to occur, which defines a perfect reaction coordinate and the transition state. In this thesis we employ the Redfield quantum master equations to extend transition path theory to address the problems in common between classical and quantum reaction mechanism studies as well as those unique to quantum reactions. We extend this quantum transition path theory to address systems in and out of equilibrium, then derive a general quantum committor which is applicable to the study of systems in which the assumptions underlying quantum transition path theory do not apply, allowing us to quantify the impact of coherent effects on quantum reactions and propose means for coherent quantum control.

To friends and family near and far. May we cross paths again.

Contents

Acknowledgments

Although theoreticians may sometimes claim that we like to work in frictionless vacuums, this is a lie. I do not work in a vacuum and it is definitely not frictionless. Many people and organizations have helped me through my research, during smooth periods when "frictionless" seemed a decently apt term for research progress but especially during periods when "Brownian motion" or "quagmire" seemed a more appropriate description.

It is typical to thank one's advisor first and I will follow suit in this case. David Limmer is a wonderful and inspiring person to work for, his interests and knowledge seemingly encompassing every nook and cranny of physical chemistry. He has been a supportive advisor throughout all manners of tumultuous events ranging from a pandemic to industrial action to projects that just would not work no matter how much I glowered at them. I would like to thank him for guiding me along a path through the first years of graduate school and for then allowing me to choose my own path as I gained more experience.

One's research advisor may be the single most important piece of infrastructure that supports success in graduate school, but is hardly the only piece. I think the other pieces, taken together, are at least as important and I would like to thank some of them in particular.

First because they are the easiest to think of due to their similarly advisorly roles, several professors helped me both with difficult problems in course work at Berkeley and with applications for grants and positions afterwards. Thank you, Dr. Whaley, Dr. Martin Head-Gordon, Dr. Geissler and Dr. Neuscamann. I would also like to thank Dr. Laura Gagliardi and Dr. Doreen Leopold from my undergraduate institution. We still keep in contact and they have been kind and provided help with graduate school navigation and grant applications even though I have not been their student proper for a long time.

My first year of research was rudely interrupted by the pandemic. This interruption was not nearly so rude or tragic as that experienced by many others but it was rude none the less. My personal computer had given up the ghost only two days before lockdown began and my housemates, all law students, had either departed for their homes in other states already or were about to. So it came to pass that Leslie the Limmer group administrator (and actual superhero) gave me a ride home in her car with my oversized desktop work computer clutched in my lap so that I would have internet access and be able to attend virtual classes, get some work done, and order myself a new personal computer. I don't know what I would have done without her but it would not have been pleasant. Leslie also gave me a ride home on the day it was pouring, nearly freezing, and blowing branches around at forty miles an hour, but car rides are far from the only favor she has done for me over the years. I have no idea how I would have navigated conference attendance, travel arrangements and grant disbursements without her. Thank you, Leslie, for all your help.

Many students and postdocs have come and gone from the group in my time here, all of whom have been helpful and kind to me. I must extend special thanks to Addison, the one who took the time to teach me how to implement many of the algorithms I use, Amr, a truly admirable man who knows an incredible amount of stuff about all the things I need to do and is happy to explain, Tom, who also knows a lot about stuff I need to do and

always has good ideas about other things I could be doing instead, Avishek, a wonderful TA who disagreed with me in interesting ways during every single philosophical discussion we ever shared over lunch, Yoon, a good friend who was always happy to chat about problems and their solutions whether those problems were personal or professional, Old Sam, with whom I once wasted a happy half hour learning that African porcupines do exist and thus porcupines are not American hedgehogs, and Songela, who is a close friend and always available for brainstorming, commiserating, and hiking. I owe thanks to the rest of the group, past and present, for the pleasant and supportive work environment they provide. Thank you to Chloe, Trevor, Phillip, Anthony, Aditya, Rohit, Leonardo, New Sam, Eric, Jorge, Ashesh, Kritanjan, Joseph, Constantine, Artur, Ben and Mirza. The entire Berkeley community, stretching far beyond my research group, from college of chemistry up, has formed a pleasant environment in which to work. There are countless invisible people, like Heidi, Joel and the magical NMR technician who can fix any problem be it technical or personal, without whom there would be no Berkeley or College of Chemistry. I would like to extend thanks to these people as well.

I would not have survived undergraduate studies let alone graduate studies without unceasing support from my parents and my sister, who always seem to arrange for chocolate bars to arrive in the mail on the days when I really need them. As they all live far away, it is local friends who have been subject to, and helpful in defusing, my occasional histrionics over the years. I would like to extend my thanks, and my apologies for said histrionics, to both Daniel's, Juan, Liz, Grace, Phalen, Kayleigh, Kshitiz, and several neighbors whose names were told to me once, whose names I have forgotten, and whose names I am too embarrassed to admit to them that I cannot remember. This list is hardly exhaustive. I would also like to extend thanks to Merrick, Benjamin, Jupiter and Aysa, my undergraduate D&D group, a support network without whom I might have decided to spend all of my second sophomore semester hiding under my bed instead of attending class, certainly ending any chance at graduate studies.

Finally, I acknowledge Selkie, Xana and Tasset, my three pet rats throughout graduate school, and my frog Glyph and wall lizard Charlie. No matter what sort of quagmire I found myself in at work, I have always been lucky enough to know that, when I made it home at last, somebody would be unequivocally happy to see me. Life is easier and better with a pet rat (or two) waiting at home. In a similar vein, the hundreds of people who provided feedback on the internet creative writing projects with which I kept myself busy during the pandemic isolation deserve my acknowledgment and thanks. I'm not sure how I would have made it through lockdown without some form of escape.

It has been a long journey, challenging and rewarding both, and here is its conclusion. I dare not look back as something might be gaining on me. I look forward to new problems, new solutions, and new quagmires wherever my path takes me next and can only hope for guides and support as wonderful as those I have named here.

Chapter 1

Introduction

> 'What're quantum mechanics?' 'I don't know. People who repair quantums, I suppose.'
>
> Terry Pratchett, *Eric*

1.1 Reaction Rates and Life as We Know It

The existence of the universe as we know it depends on the right set of chemical reactions occurring quickly and the right set of chemical reactions occurring slowly or not at all. In the set of necessary reactions whose speed is essential we can put photosynthesis, perhaps the most important chemical reaction on Earth,[156, 110] which granted the planet its oxygen atmosphere at the hands of tiny bacteria eons ago.[74, 30, 172] Less immediately relevant to the existence of the planet as we know it but plenty important to the existence of society as we know it are reactions such as the Haber-Bosch process which allows artificial synthesis of the ammonia-based fertilizers that have fed billions of people over the last century.[262, 84] In the set of reactions which are deleterious and would be utterly disastrous should they occur with greater speed we can count everyday processes such as the corrosion of metals,[27, 191] an age old enemy of manufacturers everywhere, photodamage to DNA,[165, 241] and spontaneous combustion of coal,[196, 22] a menace that has led to countless destructive fires.

What can we do to discourage destructive reactions? Metallurgists are constantly researching new alloys to resist corrosion while maintaining the strength, flexibility or magnetic properties necessary for specialized applications.[12, 27, 191] Given the enormous costs of extinguishing fires in mines, serious research into conditions to prevent the self heating of coal continue in earnest.[51, 196, 22]

What can we do to improve the speed and efficiency of constructive reactions? Photosynthesis occurs quickly enough, but with looming food insecurity it pays to wonder what would make the process more efficient, or how we can artificially imitate and improve the

process of photon capture to address the crisis of energy insecurity which looms nearly as large as food insecurity.[238, 301, 124, 258, 163]

What can we do to achieve the speed and efficiency of chemical reactions we rely on while avoiding the destructive side effects of current processes? The Haber-Bosch process is an enormous source of CO_2 pollution.[84, 135, 105] The production of specialized molecules for pharmaceutical or engineering purposes can similarly produce an immense amount of waste.[128, 111, 227, 139] Improved synthetic methods are direly needed.

These three questions tie together into a deeper one: why are some chemical reactions fast and others slow? This is a fundamental question not just for understanding the somewhat precarious balance of rates that allows for the existence of life and civilization as we know it but for understanding what civilization may become in the near future. In order to address this question, it is necessary to understand how a reaction occurs, to understand its mechanism.

1.2 Reaction Mechanisms and Computational Modeling

To understand and improve on a chemical reaction, it is necessary to understand the reaction mechanism in detail, not just what bonds form or break but how they break, what vibrations are involved, what the intermediate states are, and whether quantum mechanical effects like interference or tunneling play an important role. Simulations of molecular systems carried out on computers are a key tool in understanding reaction mechanisms, with the steady increase of computing power over the decades arming researchers with more versatile techniques for seeking out the hidden details of how reactions occur and how reactions can be manipulated.[32, 48, 228, 4, 28, 53] Countless methods for computationally modeling a chemical system exist ranging from molecular mechanics, which simply solves Newton's equations for a classical model of interacting atoms,[220, 276, 245] to Multi-Configurational Time Dependent Hartree approaches,[29] which solve the time-dependent Schrödinger equation for systems in which quantum effects must be addressed with exact numerical precision. Both describe how a chemical system evolves in time and can describe how reactants transform into products.

Particularly coveted information obtained from simulation is the nature of the transition state, the state of the molecule as it changes from reactant to product. Armed with knowledge of the transition state, a great deal of mechanistic insight can be obtained, but locating a transition state can be very difficult, even in a system behaving entirely classically.[298, 257, 303] When quantum mechanical effects are involved in the reaction, and they are involved in many important reactions, numerous additional complications arise, not least among them the challenge of even defining a transition state.[216, 236, 206]

1.3 Condensed Phase Reaction Mechanisms and the Committor

Each configuration of a chemical system has an energy. Under the simplifying Born-Oppenheimer assumptions,[187, 38] the function providing the energy of the system given its current configuration defines the potential energy surface. In a classical system, a reaction can be viewed as a pathway taken along a potential energy surface from reactants to products.[206, 187] The transition state would be a saddle point on this surface. However, potential energy surfaces are very high in dimension making these pathways very complicated.[297, 127, 235] The problem of finding reactive pathways across the surface is exacerbated by how unusual reactive events are. A simulated system left to its own devices is unlikely to undergo a reaction in a reasonable amount of time.[187, 69, 211]

Even more complications arise if the system is in solution rather than in gas phase. All of the solvent degrees of freedom may participate in the reaction, as they do in electron transfer between iron atoms[187] or during dissociation of $NaCl$ ions.[162, 103] This drastically increases the complexity of the model and complicates the search for reaction mechanisms, making the transition state very difficult to locate.

A variety of analysis methods have risen to the challenge of describing reactions in classical condensed systems. Transition path sampling, by means of a Monte Carlo sampling method, obtains the system's pathways from reactants to products directly, without knowing anything about the transition state and without having to wait for long time periods to observe reactions.[69, 68] Transition path theory, originally developed for the monumental task of modelling the mechanisms of proteins folding in solution, combines numerous, independent short calculations into an overall model of reactive behavior in the system.[277, 188] Both methods can efficiently obtain rates as well as mechanisms and transition states.

Both transition path sampling and transition path theory involve a key probability called the committor, which is simply the chance that, given the current state of the system, a reaction will occur. When a reaction is as likely to occur as not, meaning when the committor is equal to 0.5, the system has reached a transition state.[287, 210, 211, 69, 277] In this way, the committor describes a perfect coordinate through which to understand the progress of a reaction. Transition path sampling and theory have proved extremely useful for analyzing reactions in classical systems under many different circumstances. [278, 168, 218, 67, 73, 193]

1.4 Quantum Condensed Phase Reactions

Quantum condensed phase reactions include any reaction in solution in which quantum mechanical effects, including quantum interference or tunneling, are important to the outcome. Understanding reactions in quantum systems poses all the problems of classical systems plus a host of new ones.[206, 282, 118]

Photosynthetic systems, which capture the energy of photons, involve quantum reactions as do many other systems of increasing importance to applications in engineering and catalysis.[238, 156] Included among these are light-matter hybrid systems known as polaritons which show promise for selectively manipulating the products of chemical reactions, opening intriguing possibilities for catalysis.[267, 268, 140] Also included are photoswitches, molecules which change their conformation upon excitation by a photon, a property that has potential for numerous applications ranging from memory storage to telecommunications to holographic materials.[252, 186, 11, 255, 102]

Addressing dynamics in photoswitches and photosynthetic materials are more difficult than addressing dynamics in polaritonic systems because the former two nearly always contain conical intersections, yet another serious complication to understanding reaction dynamics.[165, 118] All quantum mechanical systems have several different potential energy surfaces, one for each electronic excitation the system may experience. In many cases, it is possible to model the system's evolution by considering only a single electronic potential energy surface. This is known as adiabatic dynamics. In a system behaving adiabatically the degrees of freedom of the nuclei in the system are separated from the electronic degrees of freedom by the Born-Oppenheimer approximation,[38] a simplification which argues that the nuclei move so slowly that they can be regarded as fixed in position relative to electrons.[187] At conical intersections, however, two different electronic state potential energy surfaces touch leading to a breakdown of the Born-Oppenheimer approximation and nonadiabatic dynamics. This necessitates a full quantum dynamical treatment for both the electronic states of the system and the nuclear degrees of freedom, greatly complicating the simulation.[291, 142, 244, 33, 273, 122]

Despite the added complexity, the dynamics around conical intersections cannot be ignored any more than the impact of the solvent can be ignored. Conical intersections allow the system to relax extremely quickly from an electronic excited state without emitting a photon, a phenomenon with critical implications for the system's dynamics.[184, 164, 60]

Regardless of whether adiabatic or nonadiabatic dynamics are appropriate for the system in question, the problem of understanding a quantum reaction mechanism involves defining a quantum transition state. It is not immediately clear how to define a transition state in a system where tunneling may occur or quantum interference effects may impact dynamics in unexpected ways. Quantum variations on the classical transitions state theory for calculating rates must make corrections to attempt to account for such phenomena.[282, 283, 173] The powerful transition path sampling and transition path theory methods for analyzing the mechanisms of classical systems and identifying their transition states depend on the ability to define a committor probability for the system. It is no more obvious, unfortunately, how a quantum committor ought to be defined than how a quantum transition state ought to be defined.

1.5 Quantum Control

Overcoming these challenges to achieve deeper understanding of quantum reaction mechanisms could yield great benefits. A principal goal of analyzing quantum reaction mechanisms is to use the understanding gained to improve on an existing reaction or develop a new one entirely. If we understand how a photoswitch changes form, perhaps we can manipulate that system in order to optimize the efficiency of the transformation.[1, 146, 243, 143] If we understand how energy is transferred through a light harvesting system, perhaps we can improve that efficiency.[258, 124, 301] Quantum control around conical intersections is especially interesting due to the role of these structures in nonradiative relaxation and photoisomerizations. By controlling how a wavepacket passes through a conical intersection, the outcome of isomerization in a photoswitch might be controlled completely.[13, 150]

Understanding a reaction in a quantum system, even a comparatively simple adiabatic reaction, is already difficult. Using that understanding to manipulate a quantum reaction to obtain the desired product, or product ratio from competing mechanisms, adds yet another layer of complexity.[285] Nonetheless, numerous researchers have explored means of controlling the reactions of quantum systems and some have succeeded.[1, 146, 243, 143, 13, 150, 26] Manipulating the state of a quantum system with a laser to guide it along a particular reaction pathway is a popular means of quantum control, with several different approaches dictating how the laser's setup is adjusted.[26, 146, 285, 192]

1.6 The Committor in Quantum Systems

To gain understanding of quantum reaction mechanisms, making way for new ways to manipulate reactions, we have extended the extremely successful classical transition path theory[9, 10] into the quantum realm, building on previous work to extend transition path sampling to quantum systems.[233, 234] We have modeled dynamics with the Redfield quantum master equations, which are a means for describing the dynamics of a quantum system weakly interacting with a Markovian bath.[222, 187, 41] Several variations on these equations, with different applicabilities and accuracies, are available and we will make use of two different levels of approximation to address systems in which different varieties of quantum effects are relevant.

Obtaining the committor in quantum systems will allow us to define a quantum transition state and determine reaction mechanisms in both adiabatic and nonadiabatic cases for reactions taking place in thermal equilibrium. Extensions to this theory will allow us to address relaxations following photoexcitation, relevant for conical intersection dynamics. Extending this method further, we will determine means to coherently control dynamics around conical intersections and quantitatively measure the impact of quantum coherent effects on the relaxation dynamics in a small piece of a photosynthetic light harvesting complex, the Fenna-Matthews-Olson complex.[91]

1.7 Outline

We will first review the Redfield equations, our chosen means of quantum dynamical modelling. We will then consider classical reaction mechanisms so that we may discuss some of the aforementioned universal challenges in reaction modelling in depth and encounter the committor in its native habitat. We will extend the committor definition through the development of quantum transition path theory, whose limitations and capabilities we will explore. We will then use a Redfield master equation with different approximations[272, 46] to define a more general quantum committor which will give us a means of quantifying the impact of quantum coherent effects on reactions.

Our methods will first be applied to conical intersections, nonadiabatic dynamics. The mechanism of thermal barrier crossing around conical intersections as well as the mechanisms of relaxation after photoexcitation will be addressed. We will then treat a quantum coherent control problem around a conical intersection with the more general formulation of the committor.

Our second application will treat polariton systems, adiabatic dynamics. We will identify one potential mechanism of the selective reaction rate suppression observed in polariton experiments.[268, 267, 140] We will also explore the implications of the more general quantum committor definition, illustrating what really constitutes a quantum transition state in the more general case.

Finally, we will turn our attention to the Fenna-Matthews-Olson complex, a small piece of photosynthetic machinery. We will use the general quantum committor definition to search for coherent effects on dynamics in this system by means of a time-dependent version of the general quantum committor.

These variations of analysis methods, all drawing on the quantum committor's power to define a transition state, together provide a reasonably versatile toolbox for gaining a deeper understanding of quantum reactions. Whether we wish to identify properties of an ideal photoswitch or study something as fundamental as how to modify photosynthetic efficiency, an appropriate technique is available.

Chapter 2

Modelling Quantum Systems in Condensed Phase

> I think I can safely say that nobody really understands quantum mechanics
>
> Richard Feynman

Computational quantum dynamics concerns itself with modelling how the properties of a quantum system evolve over time. A variety of prerequisite information about a system of interest must be acquired before any attempt to compute time-dependent behavior, or interpret that time-dependent behavior, can be made. The most important prerequisite for many quantum dynamics methods is an accurate, comprehensive description of the system at rest, particularly the potential energy surfaces of the system. We will largely not concern ourselves with this crucial step as it is beyond our scope. A huge body of work on this subject awaits those interested.[230, 231, 204, 14] Generally, we will assume that a Hamiltonian operator, which provides us the system's energy, as well as all additional operators of interest, have been acquired in an analytical form which we can make immediate use of and address the complications which arise when we attempt to model the time evolution of the system.

We will initially discuss some quantum mechanical background and closed quantum systems before turning to open systems, which may be addressed by numerous different quantum dynamical approaches, all with advantages and disadvantages that must be weighed carefully. As Markovian master equation approaches will be our focus, we will discuss these in great detail.

2.1 Closed Systems and the Curse of Dimensionality

A closed system is completely isolated. Within the closed system energy is conserved. Nothing, be that heat or particles, flows between the system and its surroundings. In reality no system is perfectly closed, but closed system conditions can be experimentally approximated and due to the simplicity of their treatment, we will address them first.

Quantum Mechanical Background

Prior to the discussion of quantum dynamics in closed systems, it is necessary to introduce some basic concepts and notation, including the wavefunction itself, basis representations, the density matrix and bra-ket notation.

Wavefunctions, Operators and the Schrödinger Equation

A classical system is usually described by a complete set of phase space coordinates, position and momentum, for all the particles in the system. This state vector, often written as $\{\boldsymbol{x}, \boldsymbol{p}\}$, where the boldface indicates that these are vectors of positions and momenta in R^3, in combination with a potential energy function is sufficient to describe the current state of the system and derive all future states.

This picture does not translate well into a quantum world. Heisenberg's uncertainty principle states that it is impossible to know both where a particle is and where a particle is going at the same time.[89, 119] A state vector of positions and momenta is insufficient to describe a quantum system, which is described, instead, by a wavefunction, $\Psi(\boldsymbol{x}, t)$ where $\boldsymbol{x}$ refers to spacial coordinates and t to time in the case that the wavefunction is time-dependent.

The wavefunction is a complex function which, when multiplied with its complex conjugate, describes the probability distribution for where a particle may be found. Like all probability distributions, it must be normalized over space, meaning that the integral

$$\int_{\boldsymbol{x}} \Psi^*(\boldsymbol{x}, t)\Psi(\boldsymbol{x}, t)\, d\boldsymbol{x} \tag{2.1}$$

must be equal to one, where the $\int_{\boldsymbol{x}} d\boldsymbol{x}$ is shorthand for integrating over all space on which the wavefunction is defined. For simplicity, assume that this system has a single $\boldsymbol{x}$ position degree of freedom. The finite probability to observe a particle at some $\boldsymbol{x}$ in the region bounded by $\boldsymbol{x_1}$ and $\boldsymbol{x_2}$ is found in the usual way for a probability distribution. Specifically,

$$\int_{\boldsymbol{x}=\boldsymbol{x_1}}^{\boldsymbol{x}=\boldsymbol{x_2}} \Psi^*(\boldsymbol{x}, t)\Psi(\boldsymbol{x}, t)\, d\boldsymbol{x}, \tag{2.2}$$

gives the finite probability to find the system in the region bounded by $\boldsymbol{x_1}$ and $\boldsymbol{x_2}$.

An average value of any observable for the system can be calculated by inserting the operator for the observable ($\boldsymbol{x}$ in the case of position, $-i\hbar\partial/\partial\boldsymbol{x}$ for momentum) into the integral between $\Psi^*(\boldsymbol{x}, t)$ and $\Psi(\boldsymbol{x}, t)$. For example, to find average momentum we calculate

$$\int_{\boldsymbol{x}} \Psi^*(\boldsymbol{x}, t)\frac{-i\hbar\, \partial\Psi(\boldsymbol{x}, t)}{\partial\boldsymbol{x}}\, d\boldsymbol{x}, \tag{2.3}$$

in a manner analogous to calculating an average over any conventional, continuous probability distribution.

Having reviewed notation for the wavefunction, we can discuss evolution of a closed quantum mechanical system. The time-independent Schrödinger equation defines eigenfunctions, $\phi_i(\boldsymbol{x})$ of the Hamiltonian operator, H, as,

$$H\phi_i(\boldsymbol{x}) = \epsilon_i\phi_i(\boldsymbol{x}), \tag{2.4}$$

where ϵ_i are the energies of the eigenfunctions. The evolution of a closed system is deterministic,[187, 89, 166] completely defined by the time-dependent incarnation of the Schrödinger equation,

$$\Psi(\boldsymbol{x}, t) = e^{-iHt/\hbar}\Psi(\boldsymbol{x}, t), \tag{2.5}$$

where H is the Hamiltonian operator for the energy, and $\hbar$ is Planck's constant.

No time-dependence is included for the eigenfunctions because, provided that the Hamiltonian itself is not time-dependent, its eigenfunctions are constant in time. The time-dependent Schrödinger equation is the only equation necessary to describe evolution of a closed quantum system. In this sense, all of quantum mechanics has been solved for a century.[187] If we knew the exact eigenfunctions and eigenvalues of a system's Hamiltonian, we could immediately calculate its state at all times. Generally speaking, however, analytical solutions for all but the very simplest problems in quantum mechanics do not exist.[166, 187] The time-independent Schrödinger equation can be solved and the energy eigenstates found exactly for a quantum harmonic oscillator, a free particle, or even a hydrogen atom but as soon as we try to address a helium atom, electron-electron repulsion terms thwart all efforts at analytical solutions and approximations for the solutions must be found, generally by calculations carried out on computers.[166, 89, 187]

Basis Representation

In theory, a wavefunction can be any continuous function satisfying certain requirements about the continuity of its first derivative and probability normalization.[89, 166, 187] Wavefunctions are generally described as a linear combination of easily manipulated basis functions, meaning $\Psi(\boldsymbol{x}, t) = \sum_i c_i(t)\phi_i(\boldsymbol{x})$ where $\phi_i(\boldsymbol{x})$ are a set of convenient basis functions which are time-independent and c_i are a set of time-dependent coefficients. The time-dependence can be freely distributed between functions and coefficients, but time-independent functions and time-dependent coefficients is often most convenient. Given a set of (usually infinitely numerous, linearly independent) basis functions which span the region over which the wavefunction is defined, it is possible to exactly express any wavefunction $\Psi(\boldsymbol{x}, t)$ as a linear combination of these functions. The basis will usually be chosen to be orthonormal, meaning

$$\int_{\boldsymbol{x}} \phi_i^*(\boldsymbol{x})\phi_j(\boldsymbol{x}) = \delta_{i,j}, \tag{2.6}$$

where $\delta_{i,j} = 1$ if $i = j$ and is 0 otherwise. Complications will arise if the basis is not orthonormal. For an orthonormal basis, the normalization of the wavefunction is simply $\sqrt{\sum_i c_i^* c_i}$, but when the basis is not orthonormal it is necessary to know the overlap integral

between every single pair of functions in the basis in order to calculate the normalization.[89] From here forward, unless specified otherwise, the basis will be orthonormal. A particularly convenient basis in some problems is the eigenbasis of the Hamiltonian, $\phi_i(\boldsymbol{x})$. This is a convenient choice in exactly solvable systems such as the particle in a box problem or the quantum harmonic oscillator. In most cases, however, explicit functions for the energy eigenbasis are difficult or impossible to find and alternative bases will be used. In calculations of molecular energies, for example, the wavefunction basis may consist of three dimensional Gaussian functions, Slater orbitals, or the energy eigenbasis for the hydrogen atom.[261] Simpler problems may employ the particle in a box, quantum harmonic oscillator wavefunctions, plane waves or bases specially designed to simplify the description of the Hamiltonian such as a discrete variable representation basis using $sinc(x) = sin(x)/(x)$ functions with their centers evenly distributed across a relevant region.[57]

To begin a quantum dynamics calculations in its simplest form, a basis for the system is selected and then the wavefunction and necessary operators are calculated in that basis. The wavefunction is stored as a vector of c_i values whereas each operator is a matrix such that element i, j of the matrix description of operator A is given by

$$A_{i,j} = \int_{\boldsymbol{x}} \phi_i(\boldsymbol{x}) A \phi_j(\boldsymbol{x}) \, d\boldsymbol{x}. \tag{2.7}$$

As previously stated, generally an infinitely large basis is needed to describe any wavefunction exactly as a linear combination of basis functions. Of course, a computer is of finite size and a finite number of functions from the basis of infinite size must be selected to describe the wavefunction. Often, a large primitive basis will be selected, the wavefunction and operators prepared in the primitive basis, and then the Hamiltonian diagonalized and a basis transformation carried out to work in this energy eigenbasis (as approximated by a linear combination of primitive basis functions.) It may be possible to use a smaller number of eigenbasis functions than primitive basis functions as the highest energy eigenstates are rarely relevant to dynamics. This kind of trimming of basis size is known as basis truncation. When truncating the basis, it is foremost necessary that $\int_{\boldsymbol{x}} \Psi^*(\boldsymbol{x}, 0)(\sum_i c_i(0)\phi_i(\boldsymbol{x})) \, d\boldsymbol{x} \approx 1$, meaning that the initial wavefunction is described with sufficient accuracy by the truncated basis, with no large portion of the wavefunction density being lost by the truncation. As quantum dynamics deals with a wavefunction evolving through time, a basis which describes $\Psi(\boldsymbol{x}, 0)$ sufficiently may not sufficiently describe the evolution of $\Psi(\boldsymbol{x}, t)$ for every relevant time t and several calculations with increasingly larger basis sizes will be necessary to confirm that the basis truncation is appropriate. If the results of two calculations of different sizes agree, the basis is likely of sufficient size.

Regardless of how the basis is selected and truncated, computers typically store all information about the problem in the form of vectors and matrices rather than as abstract analytical functions and associated integrals. In order to discuss computational quantum dynamics, it is convenient to adopt notation for quantum mechanical operations tailored to the computer's representation of the problem.

Bra-Ket Notation and Matrix Representation of Operators

Computational chemistry is best discussed using bra-ket notation as it corresponds intuitively with the representation of operators and wavefunctions in the computer. The ket, $|\Psi(\boldsymbol{x},t)\rangle$, represents a wavefunction. It is stored in computer memory as an n by 1 column vector, where n is the dimension of the chosen basis and entry $(i,1)$ of the vector is $c_i(t)$. The bra, $\langle\Psi(\boldsymbol{x},t)|$ represents the conjugate transpose of the ket, given by a 1 by n row vector with entry $(1,i)$ equal to $c_i^*(t)$. Moving forward, the implied degrees of freedom such as $(\boldsymbol{x},t)$ may be omitted for brevity.[89]

A bra and ket together, $\langle\Psi|\Psi\rangle$ is shorthand for the matrix multiplication of the bra row vector by the ket column vector, equivalent for an orthonormal basis to

$$\int_x \Psi(\boldsymbol{x},t)^*\Psi(\boldsymbol{x},t)\; d\boldsymbol{x} = 1 \tag{2.8}$$

and insertion of an operator between bra and ket, $\langle\Psi|A|\Psi\rangle$, indicates calculation of the integral,

$$\int_x \Psi(\boldsymbol{x},t)^* A\Psi(\boldsymbol{x},t)\; d\boldsymbol{x}, \tag{2.9}$$

given by the matrix multiplication of the 1 by n bra by the n by n matrix representation of operator A by the n by 1 ket. This representation simplifies mathematical discussions in quantum mechanics especially when discussing the density matrix.

The Density Matrix

Multiplication of a column vector by a row vector, $\langle\Psi|\Psi\rangle$, returns a 1 by 1 matrix, a single number, 1 if the wavefunction is normalized. If the order of bra and ket is flipped, $|\Psi\rangle\langle\Psi|$ represents multiplication of a column vector by a row vector, resulting in an n by n operator. This operator is called the density matrix, ρ. A density matrix which can be written as $|\Psi\rangle\langle\Psi|$ for some $|\Psi\rangle$ is called a pure state density matrix. The diagonal entries, $c_i^*c_i$, of the density matrix indicate the probability to be found in any given $|\phi_i\rangle$ of the basis set whereas the off diagonal entries, $c_i^*c_j$, for diagonal entry i,j, are called coherences and represent the quantum coherence between basis states i and j. A pure state density matrix and wavefunction convey the same information.[89, 187]

For a density matrix to describe a physically realizable quantum state, populations must be nonnegative and sum to 1 and the absolute value of coherence i,j must not be larger than $\sqrt{\rho_{i,i}}\sqrt{\rho_{j,j}}$. A valid density matrix must also be Hermitian, meaning the conjugate transpose of the density matrix, ρ^*, is equal to ρ, and like any Hermitian matrix, a basis can always be determined in which it is diagonal.[187, 41, 89] It is always the case that the populations in the density matrix indicate the probability to be in each given basis state. However, there are density matrices which cannot be written as $|\Psi\rangle\langle\Psi|$ for any wavefunction. If more than one diagonal entry of the density matrix is nonzero and all other entries are zero, no wavefunction exists such that $\rho = |\Psi\rangle\langle\Psi|$. Rather, a sum of several terms would be

necessary to describe the density matrix, $\rho = \sum_i p_i |\phi_i\rangle\langle\phi_i|$ where p_i is the probability to find the system in basis state $|\phi_i\rangle$. Density matrices which cannot be written as $\rho = |\Psi\rangle\langle\Psi|$ are called mixed state density matrices or statistical mixtures. They convey more information than any single wavefunction and are interpreted differently.

Intuitively, a mixed state represents a different kind of uncertainty than that described by a single wavefunction. A single wavefunction describes the uncertainty inherent in any quantum mechanical description, our inability to know the momentum and position at the same time which necessitates a probabilistic description of the system's state. A mixed state indicates that not only is the position and momentum of the system described probabilistically, there is also uncertainty in which probabilistic function describes the state of the system. For example, a system in thermal equilibrium will be Boltzmann distributed among energy eigenstates with no coherences between them, a statistical mixture.[187]

Mixed and pure states are very different constructs. For example, take an arbitrary two state system and consider the pure state wavefunction $|\Psi\rangle = \sqrt{0.5}|\phi_1\rangle + \sqrt{0.5}|\phi_2\rangle$ where $|\phi_1\rangle$ and $|\phi_2\rangle$ are orthonormal and isoenergetic. The density matrix corresponding to this pure state is,

$$\begin{bmatrix} 0.5 & 0.5 \\ 0.5 & 0.5 \end{bmatrix} \tag{2.10}$$

whereas a statistical mixture representing this system in thermodynamic equilibrium is,

$$\begin{bmatrix} 0.5 & 0 \\ 0 & 0.5 \end{bmatrix}, \tag{2.11}$$

and although the probability to be in either basis state is equivalent for the pure and mixed state, the density matrices do not describe comparable quantum states. To see this clearly, consider the average of an operator A for these systems. The average value of an operator can be found from the trace, $\langle A\rangle = Tr[\rho A]$. This average will not generally be equivalent for the pure state and statistical mixture shown above.[187] Unless A is an operator dependent solely on populations in the basis states, the pure and mixed state will not have the same $\langle A\rangle$. To see that the trace provides the average, consider the basis in which the density matrix is diagonal, $|\zeta_i\rangle$, and the cyclic property of the trace

$$Tr[A\rho] = Tr\left[A\sum_j p_j|\zeta_j\rangle\langle\zeta_j|\right] = Tr\left[\sum_j p_j\langle\zeta_j|A|\zeta_j\rangle\right] = \sum_j p_j\langle A_j\rangle \tag{2.12}$$

where p_j is the population in state j and $\langle A_j\rangle$ is the average value of A for basis function $|\zeta_j\rangle$. This operation yields the average for the operator by weighting the operator average of each basis function by its population.

For a closed system in a pure state it is only necessary to evolve the wavefunction in time with the Schrödinger equation to describe the evolution of the quantum system as there is no process which can change a pure state to a mixed state in a closed system. For a mixed state, however, evolving a single wavefunction is not sufficient, and the time evolution of the

full density matrix must usually be dealt with directly. The time evolution of the density matrix, $\rho = |\Psi(t)\rangle\langle\Psi(t)|$, is described by

$$\frac{d\rho(t)}{dt} = -i/\hbar[H, \rho(t)] = \mathcal{L}\rho, \tag{2.13}$$

which is known as the Liouville-von Neumann equation where $\mathcal{L}$ is a superoperator encompassing all dynamics in the commutator.[187, 41] Again, note that a pure state density matrix will not spontaneously become a mixed state density matrix or vice versa under the Liouville-von Neumann equation.

The Schrödinger, Heisenberg and Interaction Representations

The Liouville-von Neumann equation may be written in several different "pictures" depending how the time-dependence of the system is represented. In some cases one representation may simplify the mathematical treatment and thus be preferred. The most commonly used representation of a quantum system designates the wavefunction to be time-dependent and the operators to be time-independent unless they are inherently time-dependent, such as the density matrix operator or the Hamiltonian in a system with an oscillating electric field. Placing time-dependence on the wavefunction is known as the Schrödinger representation, or picture. This will be our default representation and usually merit no special notation, but for clarity, in this section only, a subscript of s will indicate a Schrödinger representation object. In contrast, in the Heisenberg representation, indicated with subscript H, the wavefunctions are time-independent and all the time-dependence is carried by the operators.[187] The Heisenberg wavefunction at time t is defined as,

$$|\Psi_H(t)\rangle = e^{iHt/\hbar}|\Psi_s(t)\rangle = e^{iHt/\hbar}e^{-iHt/\hbar}|\Psi_s(0)\rangle = |\Psi_s(0)\rangle, \tag{2.14}$$

meaning that the Heisenberg wavefunction at all times is the Schrödinger wavefunction at time zero. The time-dependence is transferred to the operators such that

$$A_H(t) = e^{iHt/\hbar}A_s(0)e^{-iHt/\hbar}. \tag{2.15}$$

The Heisenberg representation and the Schrödinger representation are equivalent, conveying the exact same information. This is easy to see when considering the time-dependent average of operator A_s. Start from the Schrödinger picture for the average of A,

$$\langle A_s\rangle = \langle\Psi_s(t)|A_s|\Psi_s(t)\rangle = \langle\Psi_s(0)|e^{iHt/\hbar}A_s e^{-iHt/\hbar}|\Psi_s(0)\rangle = \langle\Psi_H|A_H(t)|\Psi_H\rangle = \langle A_H\rangle, \tag{2.16}$$

and find the corresponding average in the Heisenberg representation.

There is a third representation, the interaction representation, indicated with the subscript i because H_I is more commonly used for a different purpose. The interaction picture splits H_s into $H_s = H_0 + H_i$. The time-dependence is then distributed between the operators and the wavefunction, with $|\Psi_i(t)\rangle = e^{iH_0t}|\Psi_s(0)\rangle$ and the operator $A_i(t) =$

$e^{iH_0t/\hbar}A_se^{-iH_0t/\hbar}$.[187] Note that there are potentially an infinite number of different interaction representations depending on how the Hamiltonian is split. The time evolution of the interaction wavefunction,

$$\frac{d|\Psi_i(t)\rangle}{dt} = -\frac{i}{\hbar}H_i|\Psi_i(t)\rangle \tag{2.17}$$

is described purely by the effect of H_i. The evolution of the density matrix is

$$\frac{d\rho}{dt} = -\frac{i}{\hbar}[H_i, \rho_i], \tag{2.18}$$

which, again, involves only H_i. Depending on the problem and the distribution of Hamiltonian terms between H_0 and H_i, the interaction representation may significantly simplify algebra or allow for more intuitive understanding of the timescales of different processes influencing the system.

Dimensionality

Although changing representation may simplify our math at times, it will not save us from the curse of dimensionality, one of the most serious problems for computational quantum dynamics.

The time evolution of the density matrix and wavefunction, regardless of basis or representation, is deterministic in a closed system, and it seems, initially, that all we need to do to solve any problem of our choosing is determine a Hamiltonian (easier said than done, but that is another story) an initial wavefunction, and any other operators of interest, choose a basis and basis truncation, transform our operators into that basis, and then propagate the time-dependent Schrödinger equation to evolve the wavefunction forward in time.

Unfortunately, there is a catch that prevents us from solving all open questions in quantum dynamics: the exponential increase in complexity with each additional degree of freedom. Consider a system that consists of a single spin in a magnetic field. This system may be completely described by a wavefunction, $|\Psi\rangle = c_\uparrow|\uparrow\rangle + c_\downarrow|\downarrow\rangle$, which gives the probabilities to find the system in a spin up $|\uparrow\rangle$ or spin down $|\downarrow\rangle$ state. This system is trivial to address because there are only two states in the wavefunction. When we add a second spin, however, there are now four potential states, $|\uparrow\uparrow\rangle$, $|\uparrow\downarrow\rangle$, $|\downarrow\uparrow\rangle$ and $|\downarrow\downarrow\rangle$, and if we add an additional spin the number of basis states rises to eight. To model 40 spins, over a terabyte of storage space would be necessary just to store a wavefunction, let alone a density matrix and the Hamiltonian necessary to evolve the system in time. The computational cost to solve the Schrödinger equation, usually accomplished by diagonalizing the Hamiltonian, scales with the cube of the number of basis states and quickly becomes immense.

Closed systems of interest involve many degrees of freedom and the storage and computation requirements to model them increase exponentially with each additional degree of freedom. This approach to quantum dynamics quickly becomes untenable. Good basis selection, aggressive basis truncation approaches and certain specialized methods, such as the Lanczos solver,[292, 213] can extend the applicability of closed system modeling, but

the curse of dimensionality will quickly catch up with even these methods. Models for most systems of interest are out of reach.

This leaves us in an unfortunate position. We have a solution to all of our problems. We simply cannot apply it, however, except in very small systems. The alternative, and only path forward, is the open quantum system approach.

2.2 Open Systems

An open quantum system is the opposite of a closed system in the sense that it is not isolated. It exchanges energy with a bath. To model an open system, we split the universe into two portions: the system, in which we are interested, and the bath, the rest of the universe which we are interested in only in so far as it influences the system. The goal is to avoid explicitly modelling the degrees of freedom in the bath, thereby cutting down on computational cost. Note that the basis size still scales exponentially with the explicit degrees of freedom in the system; the advantage gained is that there are now far fewer of them.

A common case for the application of an open system approach is a simple molecular reaction occurring in solution. The solvent degrees of freedom far outnumber the degrees of freedom of interest in the molecule undergoing reaction and although solvent degrees of freedom might influence the reaction, modeling them explicitly is not feasible nor desirable as we have no particular interest in them. The solvent degrees of freedom can be included in the bath, preserving their influence but avoiding the cost of their addition to the simulation.

The first step in modeling an open quantum system is partitioning the universe into the Hamiltonian H_S (not to be confused with the H_s indicating the Schrödinger representation Hamiltonian) of the system and the Hamiltonian H_B of the bath. The total Hamiltonian of the system and bath is then

$$H = H_S + H_B + H_I, \tag{2.19}$$

where H_I represents the interaction between system and the bath (not to be confused with the interaction picture Hamiltonian).

2.3 Master Equations

One approach to modeling open quantum systems is through constructs known as master equations. A quantum master equation simply means an equation that fully describes the evolution of the system density matrix. The general form of a master equation is[41]

$$\frac{d\sigma(t)}{dt} = \mathcal{K}(t)\sigma(t), \tag{2.20}$$

where $\mathcal{K}$ is a superoperator, meaning an operator operating on another operator, in this case on $\sigma(t)$, the reduced density matrix of the system. The reduced density matrix of the

system includes only the degrees of freedom explicitly modeled by the system. It is given by $\sigma(t) = Tr_B[\rho(t)] = \sigma(t) \otimes Tr_B[\rho_B(t)]$, where $\rho(t)$ is the density matrix for the full universe consisting of system and bath, $\rho_B(t)$ is the density matrix of the bath alone, and Tr_B indicates the operation of performing the trace over the bath degrees of freedom.

If $\mathcal{K}$ is time-independent, then the Master equation is Markovian, meaning the history of the evolution of the system has no influence on its future evolution. Only the current state of the system matters.[187, 64, 41] Markovian master equations are comparatively simple and easy to analyze. Closed system dynamics are, of course, Markovian and any non-Markovianity in an open quantum system is an effect of integrating out the bath degrees of freedom and losing explicit access to information in the bath.

There is no guarantee that an arbitrary $\mathcal{K}(t)$ will produce a physically reasonable density matrix at all times t. To guarantee that a quantum master equation has the semigroup property, which guarantees that it will result in a physically reasonable density matrix at all times,[41] $\mathcal{K}$ must have a very specific form. In order to guarantee that $\sigma(t)$ is a physically reasonable density matrix, it must be possible to write $\mathcal{K}\sigma(t)$ in the Gorini-Kossakowski-Sudarshan-Lindblad (GKSL) form[109, 148, 41, 61]

$$\mathcal{K}\sigma(t) = -i[H, \sigma(t)] + \sum_k \gamma_k \left(S_k \sigma(t) S_k^* - \frac{1}{2} \{S_k^* S_k, \sigma\} \right), \tag{2.21}$$

where $\{\}$ indicates an anticommutator, S_k are operators often referred to as jump operators, and γ_k is a rate, often called the jump rate.[62] The GKSL equation, or Lindblad master equation as it may be called, is often used phenomenologically, with rates and operators selected to match experimental data or physical consideration of the system but not taken from a rigorous microscopic derivation.[195, 221, 31, 104] A GKSL form master equation is often desirable due to the semigroup property guaranteeing the non-negativity of populations and trace preservation of the matrix, but many quantum master equations which perform very well when compared to expensive, numerically exact benchmarking methods cannot be written in GKSL form.

The Nakajima-Zwanzig Equation: An Exact Solution

The accuracy and regions of applicability of master equations vary widely depending on what kinds of approximations are made in their derivations. Many are only accurate in very specific situations, but one, the Nakajima-Zwanzig equation, is completely accurate in all situations.

The Nakajima-Zwanzig master equation is formally exact.[187, 182, 304] Unfortunately, its solution is just as odious to obtain as that of the corresponding closed system dynamics and it cannot, generally, be used. It does serve as a useful starting point for some derivations of other quantum master equations and serves to illustrate the nature of the complications that thwart efforts to simply describe quantum systems. The derivation begins from the Liouville-von Neumann equation, assuming $\hbar = 1$, and defines two projectors, P and Q such

that $P\rho = \sigma$, $Q\rho = \rho_B$ and $(P + Q)\rho = \rho$, meaning the first projector selects out system degrees of freedom while eschewing the bath and the latter does the precise opposite. The time evolution of the system is then

$$\frac{dP\rho(t)}{dt} = -iP\mathcal{L}\rho(t) \tag{2.22}$$

and the bath evolution is

$$\frac{dQ\rho(t)}{dt} = -iQ\mathcal{L}\rho(t), \tag{2.23}$$

where $\mathcal{L}$ is the superoperator defined in Eq. 2.13.

Substituting in $P\rho + Q\rho = \rho$, we arrive at a coupled set of linear equations,

$$\frac{dP\rho(t)}{dt} = -iP\mathcal{L}P\rho(t) - iP\mathcal{L}Q\rho(t) \tag{2.24}$$

and

$$\frac{dQ\rho(t)}{dt} = -iQ\mathcal{L}P\rho(t) - iQ\mathcal{L}Q\rho(t), \tag{2.25}$$

which can be integrated, presuming that our initial time is 0, to find an expression for the bath evolution,

$$Q\rho(t) = e^{-iQ\mathcal{L}(t)}Q\rho(0) - i\int_0^t e^{-iQ\mathcal{L}(t-\tau)}Q\mathcal{L}P\rho(\tau)\, d\tau, \tag{2.26}$$

which we can insert into the derivative for $P\rho(t)$ to obtain the Nakajima-Zwanzig equation,[187, 182, 304]

$$\frac{dP\rho(t)}{dt} = -iP\mathcal{L}P\rho(t) - iP\mathcal{L}e^{-iQ\mathcal{L}(t)}Q\rho(0) - iP\int_0^t e^{-iQ\mathcal{L}(t-\tau)}Q\mathcal{L}P\rho(\tau)\, d\tau, \tag{2.27}$$

a formally exact quantum master equation.[187, 182, 304]

The three terms reflect different physical processes. The first term reflects the effect that the current state of the system will have on the system states without any interaction with the bath components. In other words, if there were no bath, this term would completely describe the evolution of the system. The second term reflects the impact that the initial state of the bath, propagated forward to the current time, will have on the evolution of the system now, the impact of the initial correlations between the system and the bath. The third term is the most complicated. It reflects the feedback on the system caused by all prior system states up until time t impacting the bath. The past states' impact on it is propagated through the bath until the current time where the bath impacts the system. This term describes the bath's memory of prior system states. Similarly to an echo in a canyon which reflects back to the ear of the one who has shouted, the origin of this term is actually in the system despite the fact that it is the bath that delivers the feedback.[187]

Although this equation is exact, due to the presence of the full density matrix and propagators for both the system and bath, it is no easier to solve than the complete, closed

system dynamics. Even if we demand that the system and bath are uncorrelated at time 0, eliminating the second term, the third term cannot be eliminated and there is no convenient way to solve it.

The Generalized Quantum Master Equation with Approximated Kernels

Since the third term in the Nakajima-Zwanzig equation cannot be conveniently solved, numerous different approaches have been employed to determine approximations for it. The Nakajima-Zwanzig equation, after applying the projection operators and eliminating the second term by assuming no initial system-bath correlation, can be retooled as the generalized quantum master equation,

$$\frac{d\sigma(t)}{dt} = -i\mathcal{L}_s\sigma(t) - i\int_0^t \mathcal{W}(\tau)\sigma(\tau)\, d\tau, \tag{2.28}$$

where $\mathcal{L}_s = P\mathcal{L}P$ and $\mathcal{W}(\tau)$ is a time-dependent memory kernel, an operator to approximate the exact memory described in the Nakajima-Zwanzig equation. Methods for determining $\mathcal{W}(\tau)$, and even designating its form, number in the dozens[179] ranging from performing quantum-classical path integrals[49] to running mean field Ehrenfest dynamics.[7, 180] The generalized quantum master equation approach excels in cases where a clear partitioning between system and bath degrees of freedom can be found for which $\mathcal{W}(\tau)$ decays quickly, making it easy to calculate and easy to store, and when there are a small number of electronic states to model. Scaling of memory storage requirements with electronic states is very unfavorable for most of these approaches.[248, 179] The limitations for any particular method for determining $\mathcal{W}(\tau)$ must be considered carefully, but they are a thesis unto themselves.

The Redfield Equation and Relatives

An alternative treatment in quantum master equations involves a perturbative approach, in which the system and the bath are assumed to weakly interact with each other, allowing for many approximations to simplify the equations of motion of the density matrix. The stronger the approximations made, the more limited the applicability of the resulting master equation. The Redfield equation and its relatives are among the most commonly used quantum master equations. All depend on both a perturbative approximation and assumption of fast relaxation of the bath, but the nature of the additional approximations made varies and changes the applicability of the equation.

The Time Convolutionless Master Equation

There are several ways to derive the Redfield equation and its relatives, including a method based on the thermal projectors introduced in the Nakajima-Zwanzig equation. An-

other, more straightforward, method is covered in Breuer and Petruccione.[41] This method begins from the usual splitting of the Hamiltonian into system, bath, and interaction terms,

$$H = H_S + H_B + \lambda H_I, \tag{2.29}$$

where λ is a perturbation parameter which may be absorbed into H_I but is useful to consider explicitly in order to analyze the accuracy of the approximations. The total density matrix, $\rho = \sigma \otimes \rho_B$, evolves according to

$$\dot{\rho}(t) = -i\,[H, \rho(t)] \tag{2.30}$$

in the Schrödinger representation, as usual using atomic units in which $\hbar = 1$. In this section we will designate the time derivative of an operator A, dA/dt with $\dot{A}$ and use a tilde, $\tilde{A}$ to designate that an operator is given in the interaction picture, rather than using a subscript, to avoid a surplus of subscripts. Designating $H_0 = H_S + H_B$,

$$\dot{\tilde{\rho}}(t) = -i\lambda[\tilde{H}_I(t), \tilde{\rho}(t)] \tag{2.31}$$

is the interaction picture evolution of the density matrix. At time t, the exact full density matrix is given by

$$\tilde{\rho}(t) = \tilde{\rho}(0) - i\lambda \int_0^t [\tilde{H}_I(s), \tilde{\rho}(s)]\, ds, \tag{2.32}$$

where the first term, $\tilde{\rho}(0)$, is the initial condition of the system and bath. This solution can then be inserted into the derivative, which allows a perturbative expansion by repeatedly substituting an integral for $\tilde{\rho}(s)$, obtaining commutator terms of progressively higher orders in $\tilde{H}_I(s)$. An infinite number of substitutions and hence infinite number of terms would result in a formally exact equation which, again, could not be solved any more easily than the closed system dynamics. However, by ceasing to continue the expansion and keeping only the lowest order term in $\tilde{H}_I$, we obtain a perturbative expansion of second order,

$$\dot{\tilde{\rho}}(t) = -i\lambda[\tilde{H}_I(t), \tilde{\rho}(0)] - \lambda^2 \int_0^t [\tilde{H}_I(t), [\tilde{H}_I(s), \tilde{\rho}(s)]]\, ds + O(\lambda^3), \tag{2.33}$$

which is accurate when λ and hence $O(\lambda^3)$ is small, meaning that the coupling between the system and the bath is weak. This is the usual requirement for accuracy in a perturbative expansion. This equation, however, still describes the evolution of the full system and bath. We proceed by tracing out the bath degrees of freedom to find

$$\dot{\tilde{\sigma}}(t) = Tr_B \left[-i\lambda[\tilde{H}_I(t), \tilde{\rho}(0)] - \lambda^2 \int_0^t [\tilde{H}_I(t), [\tilde{H}_I(s), \tilde{\rho}(s)]]\, ds + O(\lambda^3) \right], \tag{2.34}$$

but this operation has not yet eliminated the contribution of $\tilde{\rho}$ and additional simplifications must be made. The first term will be zero if the system and the bath are initially uncorrelated, resulting in commutation of $\tilde{H}_I(t)$ and $\tilde{\rho}(0)$. We will assume this is the case. The new

equation,

$$\dot{\tilde{\sigma}}(t) = Tr_B \left[-\lambda^2 \int_0^t [\tilde{H}_I(t), [\tilde{H}_I(s), \tilde{\rho}_T(s)]] \, ds + O(\lambda^3) \right], \tag{2.35}$$

can be further simplified by two assumptions. First, assume that the relaxation time of the bath is very fast in comparison to system relaxation timescales, meaning that any fluctuations in the bath induced by the system will decay too quickly to be resolved on the timescales which interest us. This allows us to approximate that the bath is always in its equilibrium, thermal state, $\sigma_B = \sigma_{eq} = e^{-\beta H_B}|i\rangle\langle i|/\left(\sum_i e^{-\beta H_B}|i\rangle\langle i|\right)$ with $|i\rangle$ being eigenstates of the bath Hamiltonian. This simplification eliminates the full system density matrix to give,

$$\dot{\tilde{\sigma}}(t) = Tr_B \left[-\lambda^2 \int_0^t [\tilde{H}_I(t), [\tilde{H}_I(s), \tilde{\sigma}(s) \otimes \tilde{\sigma}_B]] \, ds \right] + O(\lambda^3), \tag{2.36}$$

where the system density matrix tensor producted with the equilibrium bath matrix has substituted for the full system density matrix. This equation is known as the time convolutionless master equation, TCL2,[249, 50, 93] or colloquially as time-dependent Redfield theory. The assumptions required to derive it are that the bath and the system interact weakly and the bath relaxes to equilibrium much faster than the system evolves. TCL2 still lacks several desirable properties, including true Markovianity, as the integral serves as a memory term.

The Redfield Equation

Markovianity can be achieved by assuming that the integrand will decay to zero quickly in comparison to the timescale over which the system evolves appreciably. This is another assumption of fast bath relaxation, or, more precisely, small bath correlation times. This allows us to replaces $\tilde{\sigma}(s)$ with $\tilde{\sigma}(t)$ in the integrand, set $s = t - s$, and raise the integration limit to infinity, resulting in[41]

$$\dot{\tilde{\sigma}}(t) = -\lambda^2 \int_0^\infty Tr_B[\tilde{H}_I(t), [\tilde{H}_I(t-s), \tilde{\sigma}(t) \otimes \sigma_B]] \, ds, \tag{2.37}$$

which is now the fully Markovian Redfield equation. This equation lacks one additional desirable property, however. It cannot be written in GKSL form, meaning that it is possible for unphysical negative populations to appear in the system density matrix during propagation. This unphysical behavior reflects cases in which the underlying assumptions of the model are not merited. Negative populations over short times result from cases in which relaxation of excitations in the bath caused by interaction with the system is slow enough that the bath state should significantly influence the system over timescales resolved by the Redfield equation.

The Secular Redfield Equation

An additional approximation can be applied to the Redfield equation so that it enforces physical behavior of the density matrix. This is known as the secular approximation. In

some cases the term rotating wave approximation (RWA) and secular approximation may be used interchangeably, although the RWA actually refers to a different procedure for excluding rapidly oscillating terms from a master equation. The RWA may be implemented by excluding terms from the system-bath coupling operator rather than modifying the master equation itself, is known to cause fundamental problems in certain systems and should be used carefully.[154, 41, 96, 95]

The secular approximation is very widely used as a guarantor of physical density matrix behavior, although in cases where the Redfield equation produces unphysical results, there is no reason to trust the results of the secular Redfield equation, either, because it depends on the same assumptions which are not holding for the general Redfield equation. Secular Redfield results may be deceptively reasonable but completely incorrect, and disagreement between secular and nonsecular Redfield results could indicate either a breakdown in the validity of the secular approximation or breakdown in the validity of the overall Redfield approximations.[177, 82]

The secular approximation begins by defining H_I such that $H_I = \sum_\alpha S_\alpha \otimes \sum_\beta B_\beta$ where S_α is an operator only on the system and B_β is an operator only on the bath. Each S_α is then decomposed by projectors, $P(\omega)$, where $P(\omega)S_\alpha = S_\alpha(\omega) = \sum_{\omega_{i,j}=\omega} |i\rangle\langle i|S_\alpha|j\rangle\langle j|$, where $|j\rangle$ is the jth entry of the energy eigenbasis and $\omega_{i,j} = \epsilon_j - \epsilon_i$, with ϵ_i being the ith energy eigenvalue of H_S. This results in a very simple commutation relationship between $S_\alpha(\omega)$ and H_S,

$$[H_S, S_\alpha(\omega)] = \sum_{\omega_{i,j}=\omega} H_S|i\rangle\langle i|S_\alpha|j\rangle\langle j| - \sum_{\omega_{i,j}=\omega} |i\rangle\langle i|S_\alpha|j\rangle\langle j|H_S = (\epsilon_i - \epsilon_j)S_\alpha(\omega) = -\omega S_\alpha(\omega), \tag{2.38}$$

which leads to a similarly simple description of the full interaction Hamiltonian,

$$\tilde{H}_I(t) = \sum_{\alpha\omega} e^{iH_S t} S_\alpha(\omega) e^{-iH_S t} \otimes \tilde{B}_\alpha(t) = \sum_{\alpha\omega} e^{-i\omega t} S_{\alpha\omega} \otimes \tilde{B}_\alpha(t). \tag{2.39}$$

With this infrastructure in place, we can expand out the nested commutator in the Redfield equation,[41]

$$\begin{aligned}\int_0^\infty \left[\tilde{H}_I(t), \left[\tilde{H}_I(t-s), \tilde{\sigma}(t) \otimes \sigma_B\right]\right] ds = \sum_{\alpha\omega'}\sum_{\beta\omega} e^{i(\omega'-\omega)t} \\ \left(\left(\Gamma_{\alpha\beta}(\omega) + \Gamma^*_{\beta\alpha}(\omega')\right) \left(S_\beta(\omega)\tilde{\sigma}(t)S^*_\alpha(\omega') - \frac{1}{2}\{S^*_\alpha(\omega')S_\beta(\omega), \tilde{\sigma}(t)\} \right) - \right. \\ \left. \frac{1}{2}\left(\Gamma_{\alpha\beta}(\omega) - \Gamma^*_{\beta\alpha}(\omega')\right) [S^*_\alpha(\omega')S_\beta(\omega), \tilde{\sigma}(t)] \right)\end{aligned} \tag{2.40}$$

where the one-sided Fourier transform of the bath correlation function, which includes the conjugate transpose of the interaction bath operators, $\tilde{B}^*_\alpha$, is

$$\Gamma_{\alpha\beta}(\omega) = \int_0^\infty e^{-i\omega s} Tr_B[\tilde{B}^*_\alpha(s)\tilde{B}_\beta(0)\sigma_B] ds \tag{2.41}$$

and it is useful to define both

$$\gamma_{\alpha\beta}(\omega,\omega') = \int_0^\infty e^{-i\omega s} Tr_B[\tilde{B}^*_\alpha(s)\tilde{B}_\beta(0)\sigma_B]ds + \int_0^\infty e^{i\omega' s} Tr_B[\tilde{B}^*_\alpha(0)\tilde{B}_\beta(s)\sigma_B]ds, \tag{2.42}$$

and

$$\begin{aligned}\Pi_{\alpha,\beta}(\omega,\omega') =& \frac{1}{2i}\left(\int_0^\infty e^{-i\omega s} Tr_B[\tilde{B}^*_\alpha(s)\tilde{B}_\beta(0)\sigma_B]ds - \right.\\ & \left.\int_0^\infty e^{i\omega' s} Tr_B[\tilde{B}^*_\alpha(0)\tilde{B}_\beta(s)\sigma_B]ds\right)\end{aligned} \tag{2.43}$$

from these Fourier transforms in order to simplify the equation. The Lamb Shift Hamiltonian is given in the interaction picture by

$$\tilde{H}_{LS}(t) = \sum_{\alpha\omega'}\sum_{\beta\omega} \Pi_{\alpha,\beta}(\omega,\omega') e^{i(\omega'-\omega)t} S^*_\alpha(\omega') S_\beta(\omega). \tag{2.44}$$

The overall master equation after simplification is

$$\begin{aligned}\dot{\tilde{\sigma}} =& -i\left[\tilde{H}_{LS}, \tilde{\sigma}(t)\right] + \sum_{\alpha,\omega'}\sum_{\beta,\omega} \gamma_{\alpha,\beta}(\omega',\omega) e^{i(\omega'-\omega)t}\left(S_\beta(\omega)\tilde{\sigma}(t)S^*_\alpha(\omega') - \right.\\ & \left.\frac{1}{2}\{S^*_\alpha(\omega)S_\beta(\omega),\ \tilde{\sigma}(t)\}\right),\end{aligned} \tag{2.45}$$

which still cannot be put into GKSL form but is very close. The complex exponential thwarts any attempts to manipulate the equation further in that direction. In order to achieve GKSL form, we must make an additional approximation, the secular approximation. When ω' and ω are significantly different from each other, the complex exponential should result in rapid oscillation of the terms and, as we integrate over time, the contributions of terms where $\omega' \neq \omega$ should average to zero. The secular approximation demands that all $\omega = \omega'$, resulting in,[41]

$$\dot{\tilde{\sigma}} = -i\left[\tilde{H}_{LS}, \tilde{\sigma}(t)\right] + \sum_{\alpha\omega}\sum_{\beta} \gamma_{\alpha,\beta}(\omega,\omega)\left(S_\beta(\omega)\tilde{\sigma}(t)S^*_\alpha(\omega) - \frac{1}{2}\{S^*_\alpha(\omega)S_\beta(\omega),\ \tilde{\sigma}(t)\}\right), \tag{2.46}$$

which can be put into GKSL form by diagonalizing the matrix $\gamma_{\alpha,\beta}$ to flatten the summation and applying the resulting basis transformation to all operators to find

$$\dot{\tilde{\sigma}} = -i\left[\tilde{H}_{LS}, \tilde{\sigma}(t)\right] + \sum_{k\omega} \gamma_k(\omega,\omega)\left(S_k(\omega)\tilde{\sigma}(t)S^*_k(\omega) - \frac{1}{2}\{S^*_k(\omega)S_k(\omega),\ \tilde{\sigma}(t)\}\right), \tag{2.47}$$

which at last gives us the secular Redfield master equation. The secular Redfield equation, as it achieves GKSL form, is guaranteed to preserve the trace and positivity of the density matrix. Although this change of form is a useful exercise, the secular Redfield equation is

virtually never used in this form because there is a much simpler means of writing it in which populations of the density matrix evolve according to an apparently classical master equation and the coherences undergo exponential decay.[20] We will return to this point later.

The further assumption that the secular approximation has made, averaging out the quickly oscillating terms, has isolated the populations of the density matrix from the coherences. The coherences in the density matrix will decay exponentially, with their evolution having no effect on the evolution of the populations which, in turn, will have no impact on the evolution of the coherences.[41] In other words, quantum coherent effects between energy eigenstates have been removed from the master equation, which can be reformulated as a classical, Markovian master equation over the energy eigenstates, another point we will return to. The rates within this master equation are quantum informed rates, however.

This assumption of separation of timescales between the populations and coherences is only valid when the Bohr frequencies, $\omega = \epsilon_i - \epsilon_j$, are large in comparison to the system timescales, meaning the rates of population transfer between eigenstates in the system. In the case of a near degeneracy in the energy eigenspectrum, this approximation will not be met.

The Partial Secular Redfield Equation

Partial secular approximations are alternatives to the full secular approximation which can guarantee the positivity of the density matrix and preservation of the trace by achieving a GKSL form but without completely eschewing the influence of coherences on populations. There are several variations of the partial secular Redfield equation.[46, 272] The most straightforward partial secular equation assumes that there are no pathological features of the system Hamiltonian that would result in two Bohr frequencies ω and ω' being nearly degenerate without near degeneracies appearing in the eigenspectrum. In other words, if $\omega = \epsilon_i - \epsilon_j \approx \omega' = \epsilon_k - \epsilon_l$, this is because $\epsilon_i \approx \epsilon_k$ and $\epsilon_j \approx \epsilon_l$.

To carry out the partial secular approximation, each group of nearly degenerate eigenstates is designated as a nonsecular block. Within these nearly degenerate blocks where population transfer rates are large in comparison to energy gaps, quantum coherent effects are expected to be important and the evolution of populations and coherences in the density matrix should not be decoupled.

The average energy of each nonsecular block is designated $\bar{\epsilon}$ and a new set of Bohr frequencies, $\bar{\omega}_{i,j} = \bar{\epsilon}_i - \bar{\epsilon}_j$ are defined. This situation is shown in Fig. 2.1 with four nonsecular blocks pictured, one with a single member and the others with either two or three members. Using an equivalent projection operator approach as we used for the fully secular approximation, we define $S_\alpha(\bar{\omega})$,

$$P(\bar{\omega})S_\alpha = S_\alpha(\bar{\omega}) = \sum_{i,j} |i\rangle\langle i|S_\alpha|j\rangle\langle j|, \tag{2.48}$$

where i indexes over all eigenstates in the nonsecular block with $\bar{\epsilon} = \bar{\epsilon}_i$ and j indexes over all eigenstates in the nonsecular block with $\bar{\epsilon} = \bar{\epsilon}_j$. Following steps equivalent to the full

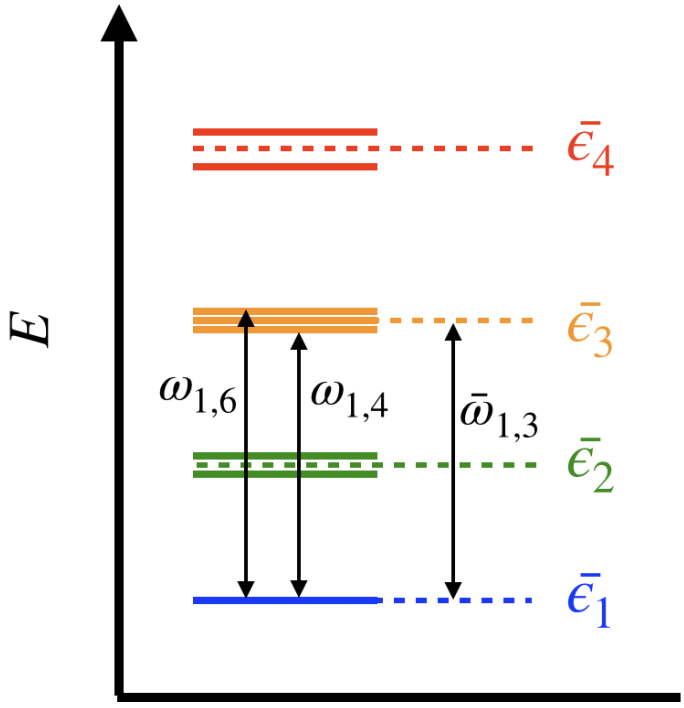

Figure 2.1: A cartoon energy eigenspectrum illustrating the meaning of ω between individual eigenstates, $\bar{\omega}$ between nonsecular block average energies, and $\bar{\epsilon}$, nonsecular block average energies.

secular derivation leads us to,[272]

$$\dot{\tilde{\sigma}}(t) = -i\left[\tilde{H}_{LS}, \tilde{\sigma}(t)\right] + \sum_{\alpha\bar{\omega}'}\sum_{\beta\bar{\omega}} \gamma_{\alpha,\beta}(\bar{\omega},\bar{\omega}')e^{i(\bar{\omega}'-\bar{\omega})t}\left(S_\beta(\bar{\omega})\tilde{\sigma}(t)S^*_\alpha(\bar{\omega}') - \frac{1}{2}\{S^*_\alpha(\bar{\omega})S_\beta(\bar{\omega}),\ \tilde{\sigma}(t)\}\right), \tag{2.49}$$

with the Lamb shift Hamiltonian

$$\tilde{H}_{LS}(t) = \sum_{\alpha\bar{\omega}'}\sum_{\beta\bar{\omega}} \Pi_{\alpha,\beta}(\bar{\omega},\bar{\omega}')e^{i(\bar{\omega}'-\bar{\omega})t}S^*_\alpha(\bar{\omega}')S_\beta(\bar{\omega}). \tag{2.50}$$

Now, the partial secular approximation is applied by eliminating all terms in which $\bar{\omega} \neq \bar{\omega}'$, with the same justification as for the full secular approximation. These rapidly oscillating terms should average out to zero. There are different ways to treat the Lamb Shift

Hamiltonian[272] during this approximation. We will use,

$$\tilde{H}_{LS}(t) = \sum_{\alpha\beta\bar{\omega}} \Pi_{\alpha,\beta}(\bar{\omega},\bar{\omega}) S^*_\alpha(\bar{\omega}) S_\beta(\bar{\omega}), \tag{2.51}$$

which is the simplest solution.

The partial secular Redfield equation is, in the Schrödinger representation,

$$\dot{\sigma}(t) = -i\left[H_s + H_{LS}, \rho(t)\right] + \sum_{\bar{\omega}} \sum_k \gamma_k(\bar{\omega}) \left(S_k(\bar{\omega}) \sigma(t) S_k^*(\bar{\omega}) - \frac{1}{2}\{S_k^*(\bar{\omega}) S_k(\bar{\omega}), \sigma(t)\} \right) \tag{2.52}$$

after any necessary diagonalization of $\gamma_{\alpha,\beta}$ and corresponding basis change to other operators. This is a GKSL form, guaranteeing physically reasonable behavior of the density matrix. However, it has not completely eschewed potentially important coherences from the system evolution. Within nonsecular blocks, quantum coherent effects are preserved, with the relevant terms being hidden in the $S_k(\bar{\omega})$ operators and the Lamb Shift Hamiltonian, which is not diagonal in the energy eigenbasis as it is for the fully secular master equation.

In Fig. 2.2, a cartoon shows the structure of the jump operators for the fully and partially secular approaches, working in the energy eigenbasis for a fictional system with two nonsecular blocks, one with a single state and one with two states. The entries of the operators are irrelevant and have been replaced with 1 for the sake of simplicity. It is always possible to factor out constants from the operators and place them in the rates, γ, so this is a reasonable way to think about the structure of the operators. The fully secular approximation treats each state as being in its own nonsecular block, a block of one, and each jump operator is a matrix with only a single entry, describing independent jumps between each eigenstate. The fully secular master equation needs two operators, $S(\omega_{3,1})$ and $S(\omega_{2,1})$ to describe jumps from eigenstates 2 and 3 into eigenstate 1 and also requires operators to describe jumps between states 2 and 3, $S(\omega_{2,3})$. All, again, have only a single entry. In contrast, the partial secular approximation requires only a single operator to describe the jumps between the nonsecular block of two and the nonsecular block of one, with this operator having two entries, indicating that population departures from eigenstates 2 and 3 to eigenstate 1 are no longer independent. The dephasing operators, the operators where $\omega = 0$, are very different in structure as well. For the fully secular approximation the operator is diagonal. In the partial secular approximation, the nonsecular block structure is reflected in the operator because eigenstates 2 and 3, which are treated as having different energies in the fully secular approximation, are treated as having the same energy, $\bar{\epsilon}_2$, the energy of their shared nonsecular block. The structure of the Lamb Shift Hamiltonians, H_{LS}, is the same, with that for the fully secular approximation being diagonal and that for the partial secular approximation having the structure of the nonsecular blocks.

The partial secular Redfield equation may be the best of both worlds. It can preserve important quantum coherences while also preserving the physicality of the density matrix. However, it relies on the same weak coupling and fast bath assumptions as all variations on the Redfield equation, and in regions where these approximations breakdown, the results will

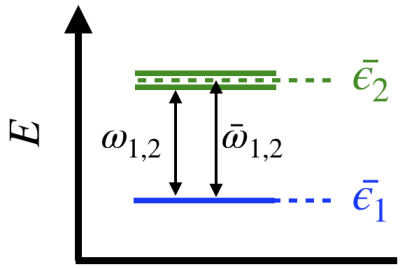

$S(\bar{\omega}_{1,2}) =$

	$\|1\rangle$	$\|2\rangle$	$\|3\rangle$
$\langle 1\|$	0	1	1
$\langle 2\|$	0	0	0
$\langle 3\|$	0	0	0

$S(\omega_{3,2}) =$

	$\|1\rangle$	$\|2\rangle$	$\|3\rangle$
$\langle 1\|$	0	0	0
$\langle 2\|$	0	0	0
$\langle 3\|$	0	1	0

$S(\omega_{2,3}) =$

	$\|1\rangle$	$\|2\rangle$	$\|3\rangle$
$\langle 1\|$	0	0	0
$\langle 2\|$	0	0	1
$\langle 3\|$	0	0	0

$S(\omega = 0) =$

	$\|1\rangle$	$\|2\rangle$	$\|3\rangle$
$\langle 1\|$	1	0	0
$\langle 2\|$	0	1	0
$\langle 3\|$	0	0	1

$S(\bar{\omega} = 0) =$

	$\|1\rangle$	$\|2\rangle$	$\|3\rangle$
$\langle 1\|$	1	0	0
$\langle 2\|$	0	1	1
$\langle 3\|$	0	1	1

Figure 2.2: An illustration of the operators in the partial and fully secular master equations along with a cartoon of the eigenstate energies of the toy system whose dynamics they describe. All operators dealing with an ω are fully secular operators and those dealing with an $\bar{\omega}$ are partial secular operators.

not be accurate despite remaining physical. The partial secular equations also rely on the piecewise flat spectral density approximation, which demands that $\gamma_{\alpha,\beta}(\bar{\omega}, \bar{\omega}) = \gamma_{\alpha,\beta}(\omega, \omega)$ for all ω which have been replaced by $\bar{\omega}$. In other words, it is justifiable to replace the individual jump rates for all frequencies associated with a given nonsecular block by an average jump rate because those rates are identical or very similar. This eventually comes down to an assumption about the structure of the bath which is virtually never precisely satisfied.[125, 272] In many cases this approximation is justified, but care must be taken to assure oneself of this.

There are other, very different master equations applicable to quantum systems under

special circumstances. In cases where the bath correlation times are long in comparison to the system timescales or when the system bath coupling is strong, neither the Redfield equation nor any of its relatives will suffice. An alternative approach is a quantum equivalent to classical Brownian motion.[41] It is, however, beyond the scope of this work as it applies to very different systems and conditions than any that will be addressed here.

Quantum Correlation Functions

Before moving on, a discussion of how bath correlation functions are calculated is warranted, as so far they have been treated as a black box.

The Redfield equations, as well as other methods in quantum dynamics, depend on integrals of correlation functions of the bath in which the bath is an infinite set of harmonic oscillators, usually treated by normal mode representation, and the frequencies of those oscillators are described by a spectral density function, $J(\omega)$. The system bath interaction, H_I, usually couples the system to the position coordinates of the oscillators in the bath. In the correlation function $\langle B(t)B(0)\rangle$ the B bath operators will be a sum over the mass weighted normal modes of the bath, q_j,[187]

$$B = \sum_j c_j q_j = \sum_j c_j \sqrt{\hbar/(2\omega_j)}(a_j^+ + a_j) \tag{2.53}$$

where a_j^+ and a_j are the raising and lowering operators for harmonic oscillator normal mode j and ω_j is its frequency. The raising and lowering operators have time-dependence, $a_j(t) = a_j e^{-i\omega_j t}$ and $a_j^+(t) = a_j e^{i\omega_j t}$. If we use this to expand out $\langle B(t)B(0)\rangle$, we find

$$\langle B(t)B(0)\rangle = \sum_j \frac{c_j^2\hbar}{2\omega_j}\langle a_j^+ a_j^+ + a_j a_j + a_j^+ a_j + a_j a_j^+\rangle \tag{2.54}$$

and eliminate the terms $a_j^+ a_j^+$ and $a_j a_j$ as their averages are zero. The raising operator applied to a ket, $a^+|i\rangle$ produces $\sqrt{i+1}|i\rangle$ and the action of the lowering operator on the same ket produces $\sqrt{n}|n-1\rangle$. The zero averages of the eliminated operators can be seen by considering that $a^+|i\rangle$ is proportional to $|i+1\rangle$ for any harmonic oscillator eigenstate $|i\rangle$, thus $\langle i|a^+a^+|i\rangle$ is proportional to $\langle i|i+2\rangle = 0$ due to the orthogonality of the basis, meaning that the thermal average $Tr[e^{-\beta H}a^+a^+] = 0$. The same is true for the square of the lowering operator. Taking these into account produces,[187]

$$\langle B(t)B(0)\rangle = \sum_j \frac{c_j^2\hbar}{2\omega_j}((n_j+1)e^{-i\omega_j t} + n_j e^{i\omega_j t}) \tag{2.55}$$

where n_j is the average excitation of mode j. This is determined from the Boltzmann distribution to be $n_j = 1/(e^{\beta\hbar\omega_j} - 1)$.

Spectral densities, $J(\omega)$, which describe the oscillator distribution give relations between an analytical function and infinite sums over c_j^2, allowing us to replace the infinite sum

with an integral. Depending on the form of $J(\omega)$, the Fourier transforms of the correlation functions might be exactly solvable, as in the case of an Ohmic spectral density bath at zero temperature,[82] but most will require numerical integration in order to find the solution, often in combination with Kramers-Kronig relations for relating real and imaginary parts of an integral to deal with singularities.[83, 151]

Chapter 3

The Classical Committor

> It is always useful for a university to have a Very Big Thing. It occupies the younger members, to the relief of their elders (especially if the VBT is based at some distance from the seat of learning itself) and it uses up a lot of money, which would otherwise only lie around causing trouble or be spent by the sociology department or, probably, both. It also helps if it pushes back boundaries, and it doesn't much matter what boundaries these are, since as any researcher will tell you that it's the pushing that matters, not the boundary.
>
> Terry Pratchett, *The Science of Discworld: Darwin's Watch*

The committor function is endemic to classical molecular simulation, and we will first seek it out in its natural habitat before concerning ourselves with how the committor adapts in quantum mechanical systems. This will require a brief discussion of classical molecular dynamics and Brownian motion, the equations of motion that are most likely to be employed when determining and using classical committor functions. Classical equations of motion are not our principal interest, merely a means to an end, and will not be discussed in any great depth.

3.1 Closed System Deterministic Dynamics

Classical dynamics for any closed system, meaning that neither energy nor particles are exchanged with the environment and the force is conservative, is fully described by Newton's equations of motion.[187, 100] The positions of the classical particles evolve as

$$\frac{d\boldsymbol{x}_i}{dt} = \frac{\boldsymbol{p}_i}{m_i} \tag{3.1}$$

where $\boldsymbol{x}_i$ is the vector of coordinates for particle i, $\boldsymbol{p}_i$ is the vector of momenta for particle i and m_i is the particle's mass. The momentum of each particle changes as

$$\frac{d\boldsymbol{p}_i}{dt} = -\boldsymbol{F}_i = -\nabla_i U(\boldsymbol{x}) \tag{3.2}$$

where $\boldsymbol{F}_i$ is the force vector on particle i and $U(\boldsymbol{x})$ is the potential energy function, which may depend on all of the particle positions in the system through electrostatic terms, and ∇_i is the gradient operator for particle i.

With these equations in hand, it is possible to describe the evolution of any closed classical system. In practice, solving these equations of motion for more than a few degrees of freedom requires approximations to be made on many fronts. Moreover, a closed classical system which conserves energy, volume, and particle number, known as an NVE ensemble or a microcanonical ensemble,[100] is less commonly of interest than the canonical or NVT ensemble, which models an open system in a constant temperature heat bath with volume and particle number conserved.

3.2 Stochastic Methods

We will purely interest ourselves in the NVT ensemble. Modelling the influence of a constant temperature heat bath is challenging, with numerous different approaches, the most straight forward of which such as velocity rescaling do not sample the proper, equilibrium NVT distribution.[279]

The Langevin Equation

If we concern ourselves only with the whereabouts of a single particle in a classical NVT ensemble, considering all degrees of freedom save for this particle to be a thermal bath whose precise condition is uninteresting to us, we can use the generalized Langevin equation[138] to describe the evolution of the particle of interest.[187, 279] The Langevin equation describes Brownian motion, the way in which a particle moves when subjected to random interactions with a thermal bath surrounding it.[55] The Langevin equation and its relatives have been known for more than a century and continue to provide new insights today.[117] The generalized Langevin equation in one dimension is

$$\frac{d^2x(t)}{dx^2} = -\frac{1}{m}\frac{\partial U(x(t))}{\partial x} - \int_0^t Z(t-\tau)\frac{dx(\tau)}{d\tau}\,d\tau + \frac{1}{m}R(t). \tag{3.3}$$

Here, U is the potential energy operator for the particle, m is the mass of the particle, $R(t)$ is a Gaussian distributed random force representing interaction of the bath degrees of freedom which are not modelled explicitly, and $Z(t-\tau)$ is a memory term. The integral over the memory term reflects the influence of past states of the system on its future evolution, mediated through the bath.[187]

If the relaxation dynamics in the non-explicitly modeled bath are very fast in comparison to the timescales over which the particle of interest moves, the system can be assumed to be Markovian, without any memory, and $Z(t-\tau)$ becomes $\gamma\delta(t-\tau)$, where δ is the Dirac delta function. This results in the non-generalized Langevin equation,

$$\frac{d^2x(t)}{dx^2} = -\frac{1}{m}\frac{\partial U(x(t))}{\partial x} - \gamma\frac{dx(t)}{dt} + \frac{1}{m}R(t), \tag{3.4}$$

where γ is called the friction coefficient.[187]

The mean value of the random force is zero to represent that the bath has no net impact on the system. In order to thermalize to the proper temperature, the fluctuation-dissipation relationship must be maintained, requiring that

$$\langle R(t)R(t')\rangle = 2m\gamma k_B T\delta(t-t'), \tag{3.5}$$

which states that there is no correlation between the random force at two different times, and relates the square of the force at time t to the temperature and friction.[187] This can be understood intuitively to state that the energy added by the random force $R(t)$ must be counteracted by the friction in order to avoid increasing the average velocity of particles of the system and thus changing its temperature.

Numerous variations on the classical Langevin equation exist, describing specialized situations such as high friction, but all are simulated in the same way on a computer. An initial system state is defined and then the Langevin equation is integrated numerically for all desired time steps.[81] At each time step random numbers are selected to determine the stochastic force.

Despite its many variations and its attractive, low cost of simulation,[81] the Langevin equation approach is often inappropriate for modeling complicated molecular systems. Chemical detail is often more easily encoded in and extracted from the simulation results of molecular mechanics calculations.

3.3 Molecular Mechanics

Molecular mechanics is the general approach of building a model of a molecular system, designed to imitate within a computer the results of an experiment on an equivalent, real system. A model of a molecular system must include the energy of bonds stretching and bending as well as electrostatic interactions between molecules.[107, 229] The entire description of how the potential energy of the system is calculated, from bonds and electrostatic terms, is known as the force field.[107, 237, 100] There are numerous force fields with countless means of addressing bonds and electrostatics. Different force fields are appropriate for different systems and different problems, and trade offs between computational time and accuracy must be considered, with choice of the proper potential energy functions being critical for successful modelling.[203] For example, despite their importance in some cases, many-body interaction terms are not usually included in molecular mechanics calculations due to the extremely high cost of computation, with only two body terms typically being used.[160, 290]

A major distinction is made between all atom force fields, which represent every single atom in all molecules in the system explicitly, and coarse grained or united atom force fields, which group several atoms together into working units and do not model every atom explicitly.[129] A united atom force field might represent a methyl group as a single type of

particle. United atom force fields typically sacrifice some accuracy in return for computational efficiency.

After applying a force field and determining an initial condition for the system, numerical integration routines designed to approximate the solutions to Newton's equations propagate the system forwards in time, taking a step of size Δt forward until, eventually, the final desired time is reached.[100, 107] There are numerous approaches to this approximate integration. One of the most popular means to integrate a molecular mechanics simulation is the Velocity Verlet method. This integration method does not strictly conserve energy in a closed system. However, it does conserve a property closely related to the total energy, sometimes called the shadow energy and, as such, performs well over long periods of time resulting in little energy drift and easily computable bounds on the accuracy.[286, 114]

Molecular mechanics in closed systems is reasonably straightforward to integrate and is deterministic given a specific initial condition. Introducing thermostats to impose a constant temperature on the system and produce an NVT ensemble requires careful consideration. Solutions, such as the Nosé-Hoover thermostat, exist which guarantee that a molecular mechanics simulation appropriately reproduces dynamics from the specified conditions without bias introduced by brute force velocity rescaling algorithms.[189, 121, 100, 279] Nosé-Hoover is a deterministic method to model the dynamics in an NVT ensemble. Barostats, of several different kinds and with several different limitations, can be used to control pressure in a simulation to sample an NPT ensemble, with special care needed in the choice if one would like to run the dynamics backwards for any reason.[226]

Simulations made with molecular mechanics, or the Langevin equation, can produce information that is extremely difficult or impossible to obtain by any physical experiment carried out on the system modelled including our principal interest, dynamical information about how a reaction occurs.

3.4 Reaction Coordinates and the Transition State

Having given an overview of how a classical molecular system is treated on a computer, we can now discuss reactive events with the assurance that there is, in fact, a way to compute dynamics for model molecular systems undergoing these processes.

Consider the simplest abstract classical reaction, moving a ball originally from a valley on the left over the top of a mountain pass separating it from a valley on the right. The mountain pass is the highest energy state that the ball will pass through on its journey. The potential energy surface associated with this situation is illustrated in Figure 3.1. Provided that there is no prevailing wind, if the ball is placed at rest at $R = 0$ it has equal probability to roll to the left into the first valley from whence it came or to the right into the second valley which it has not yet visited. In this situation, the mountain pass defines a transition state, a point at which the reaction is as likely to complete as not. The transition state is located at a particular value of the particle's horizontal position, the coordinate R. Specifically, the transition state is at $R = 0$ and R itself is known as the reaction coordinate. A perfect

reaction coordinate, such as R in our simple case, completely characterizes the progress of the reaction so that no additional information is necessary to know how likely the reaction is to proceed.[210, 23] The reaction coordinate and the transition state give us critical information

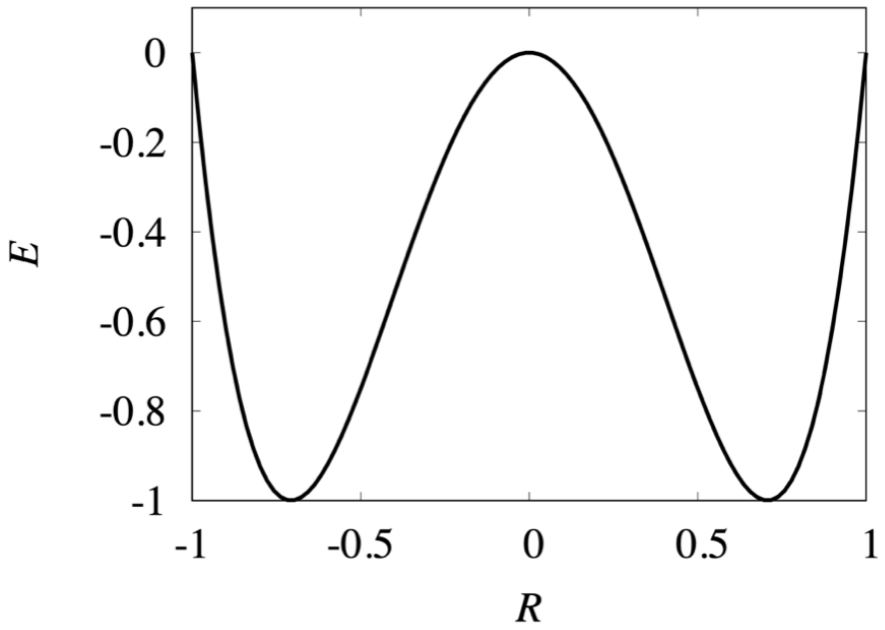

Figure 3.1: A potential energy surface with two stable wells and a transition state between them located at $R = 0$.

about how a reaction occurs. If we inspect a transition state in a chemical system undergoing a reaction, the positions of the atoms may tell us which bonds break and how.

Transition State Theory

Knowing the energy of the transition state allows applications of theories such as transition state theory or Grote-Hynes theory to determine the rate of a reaction. Transition state theory is one of the simplest theories for calculating a reaction rate. Transition state theory assumes that equilibration to a Boltzmann distribution within the reactant and product wells is very fast in comparison to the timescales over which the reaction occurs. This is justified if the barrier is large in comparison to $k_B T$. Transition state theory also assumes that recrossing events, where a trajectory crosses the barrier from reactants to products but then crosses back to reactants without reaching the products, never happen.[187, 288, 206] This is not usually a well justified approximation and corrections are often applied to transition state theory to adjust for recrossing.[246, 281]

The transition state theory rate is found from the forward flux at the transition state, meaning the net flux at the transition state moving from products to reactants. Generically, the transition state theory rate in one dimension can be written as

$$k_{TST} = P(x^*)\langle v_R \rangle \tag{3.6}$$

where $P(x^*)$ is the probability to reach the transition state located at x^* and $\langle v_R \rangle$ is the average velocity in the direction of the reaction at x^*.[187] The fast equilibration assumption allows calculation of the probability to be in the transition state using the Boltzmann distribution as

$$P(x^*) = \frac{e^{-\beta U(x^*)}}{\int_{RW} e^{-\beta U(x)} dx} \tag{3.7}$$

where $U(x)$ is the potential energy of x and RW indicates that the integral is carried out over the reactant well only, not the entire system. Knowing the transition state and its energy is a necessity for this calculation. The average velocity may be calculated from the Boltzmann distribution as,

$$\langle v_R \rangle = \frac{\int_0^\infty v e^{-\beta m v^2/2}}{\int_{-\infty}^\infty v e^{-\beta m v^2/2}} = \frac{1}{\sqrt{2\pi\beta m}}, \tag{3.8}$$

where m is the particle mass. This equation may be simplified by a harmonic approximation when the potential energy surface is nearly parabolic.[187]

Transition state theory has its shortcomings, but it has been proven very useful in determining ballpark estimates for transition rates. Many more powerful reaction rate theories, including Kramers theory[134], Grote-Hynes theory,[112] and Marcus electron transfer theory[161] are all built on the foundation laid by transition state theory and all depend on knowing the transition state.

From the transition state we may acquire useful rate information, but the transition state may not provide us enough information to understand the mechanism of the reaction, such as the order of bonds breaking or atoms rearranging. Determining a good reaction coordinate to describe the progress of the reaction will prove more helpful. However, even finding the transition state, let alone a reaction coordinate to provide physical insight, is more easily said than done.

Reaction Coordinates in Multidimensional Systems

It may be obvious in a very simple system what the reaction coordinate should be. For example, consider a gas phase molecule consisting of any two atoms, X_2, undergoing dissociation. The only relevant coordinate is the $X - X$ bond distance, R. The bond distance serves as the reaction coordinate and gives us all of the information we need about the current progression of the reaction. At a certain special R we will find the transition state. However, in a system with even two relevant degrees of freedom, a good reaction

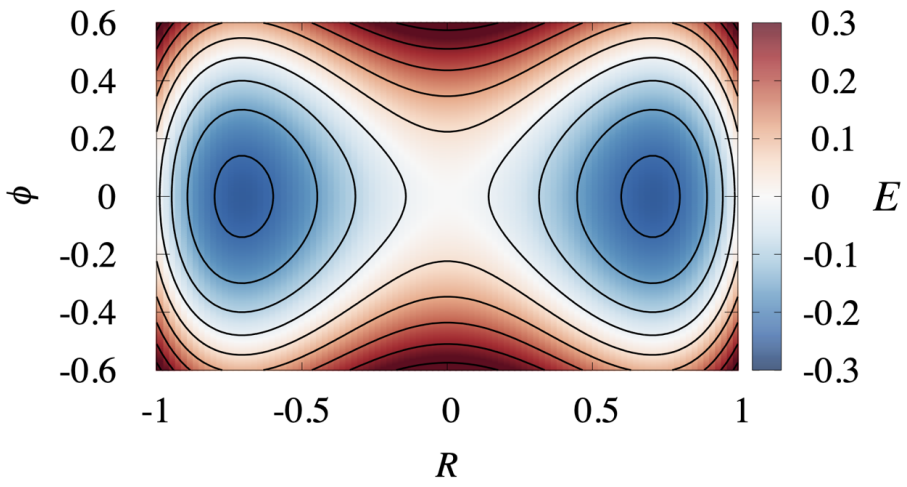

Figure 3.2: A heat map of a symmetric potential energy surface with two metastable wells and a transition state located at $R = 0$. Energy is given in arbitrary units designated by the contours and color.

coordinate may not be so easy to find. We could be lucky. Perhaps, when we plot our two dimensional potential energy surface we find a neat, symmetric system as in Figure 3.2 where it is apparent that R is still a good reaction coordinate and $R = 0$, regardless of the value of the perpendicular coordinate ϕ, is a transition state. To see this, consider the one dimensional potential energy surfaces obtained by cutting through the two dimensional surface of Fig. 3.2 at fixed values of ϕ. These are shown in Figure 3.3. Regardless of where the cut is made, the highest energy location on the one dimensional potential energy surface is at $R = 0$, and it is apparent that a ball set at $R = 0$ is equally likely to fall to the right or to the left, regardless of the value of ϕ.

However, our potential energy surface is unlikely to be so neat. To return to our mountain metaphor, perhaps the mountain has an unusual shape like the energy surface in Figure 3.4. The coordinate R is no longer a good reaction coordinate as it is not sufficient to designate the transition state in this system. This is evident when we take cuts through the potential energy surface at $R = 0$. When we inspect cuts made at different constant values of ϕ for the potential energy surface in Figure 3.4, we see that $R = 0$ is only a transition state when $\phi = 0$. At $\phi = R = 0$, the ball would stand at the apex between the valleys with equal probability to roll in either direction, but when $\phi = 1.7$ the ball will likely roll down hill into the valley on the left, whereas at $\phi = -1.7$ the ball will likely roll down hill into the valley on the right. This is recrossing, and the recrossing probability is very high for many states where $R = 0$, so $R = 0$ does not adequately describe the transition state and R itself is not a good reaction coordinate. We need information about both R and ϕ in order to determine the progress of the reaction or define a transition state. What would be the reaction coordinate

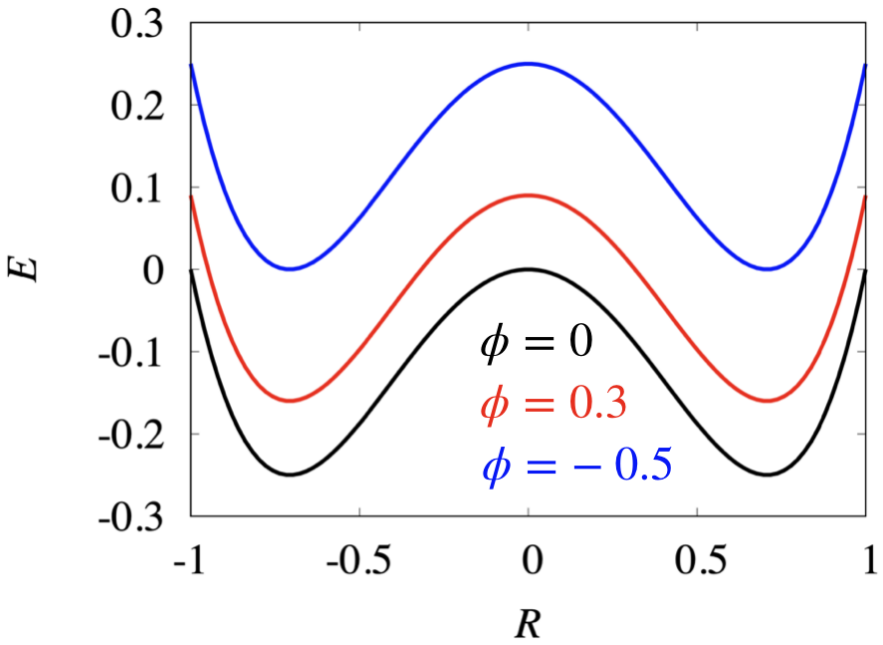

Figure 3.3: Cuts through the heat map of a symmetric potential energy surface shown in Figure 3.2 at varied values of ϕ illustrating that $R = 0$ defines the transition state.

in this system, then? Some $\zeta(R, \phi)$ coordinate should exist such that $\zeta(R, \phi) = 0$ defines the transition state, but its nature is hardly obvious inspecting the potential energy surface. This is only a two dimensional surface. Chemical systems of interest may have dozens or even hundreds of degrees of freedom which are relevant to the reaction. Finding the reaction coordinate and the transition state is extremely difficult in high dimensions where searching for relevant saddle points and paths between them is very expensive and difficult.[235, 5, 178]

The Committor

Our perfect reaction coordinate ζ is, by definition, the committor. The committor is the function that, given the coordinates of all particles in the classical system $\{\boldsymbol{x}\}$, returns the probability for the system to complete the reaction. Less technically, the committor tells us the probability that the system will visit a product state before it visits a reactant state.[210, 132] More technically, the isocommittor surfaces, meaning hyper surfaces in phase space where the committor values are equal, define the perfect reaction coordinate.[287]

The existence of a committor function that we do not know does not help us to characterize reaction mechanisms in complicated systems. However, the committor for any particular

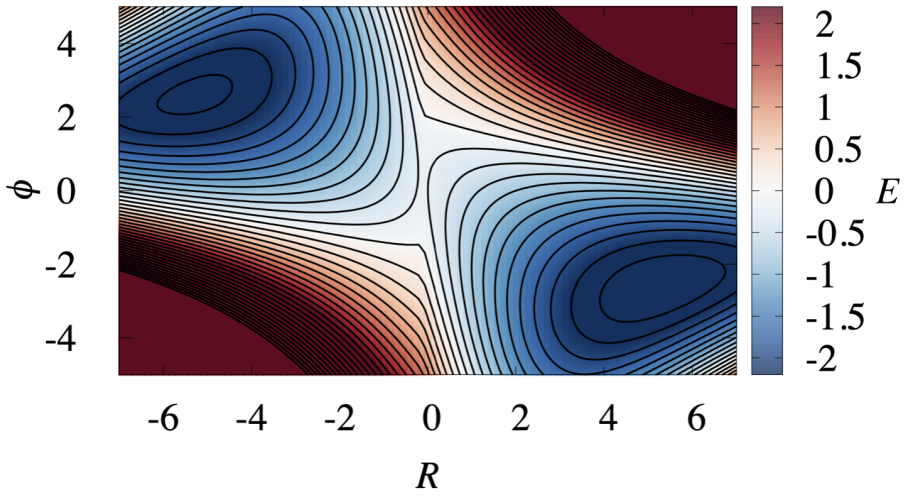

Figure 3.4: A potential energy surface for bond distance R and perpendicular coordinate ϕ. Energy is given in arbitrary units designated by the contours and color.

system state can be calculated by running a series of trajectories from a particular $\{\boldsymbol{x}\}$ and tallying the outcomes,[215] or by more sophisticated approaches.[287] To accomplish this sampling in a deterministic molecular mechanics simulation, numerous trajectories are launched from the given $\{\boldsymbol{x}\}$ with $\{\boldsymbol{p}\}$ randomly sampled from a Boltzmann distribution. For the Langevin equation or another stochastic simulation method, numerous trajectories from the same $\{\boldsymbol{x}\}$ are launched with a different sequence of random noises drawn. Regardless of how they are generated, the number of reactive trajectories is tallied against the number of non-reactive trajectories to determine the committor. Any state where the committor is found to be 0.5 is part of the separatrix, which for our purposes will be referred to as a transition state, although they are not technically synonymous.[210]

This presents an alternate means of dealing with complicated reactions. We can analyze reactive behavior by simulating the system with our chosen equations of motion, be they molecular mechanics or the Langevin equation or an alternate approach, observing reactive events and analyzing the trajectories that resulted in a reaction. By calculating the committor at points along reactive trajectories, we can determine where the transition state is and monitor the reaction's progress.

However, this approach is often not feasible because reactive events in equilibrium systems are usually rare.[277] The energy barrier between states is often very high with respect to the size of energy fluctuations in the system and the probability of crossing the barrier is very low, resulting in long periods of waiting on one side of the barrier followed by a very fast reactive event and then another long period of waiting. This situation is illustrated in the cartoon in Fig. 3.6 where in b) a trajectory in red dallies in the leftmost well, oscillating

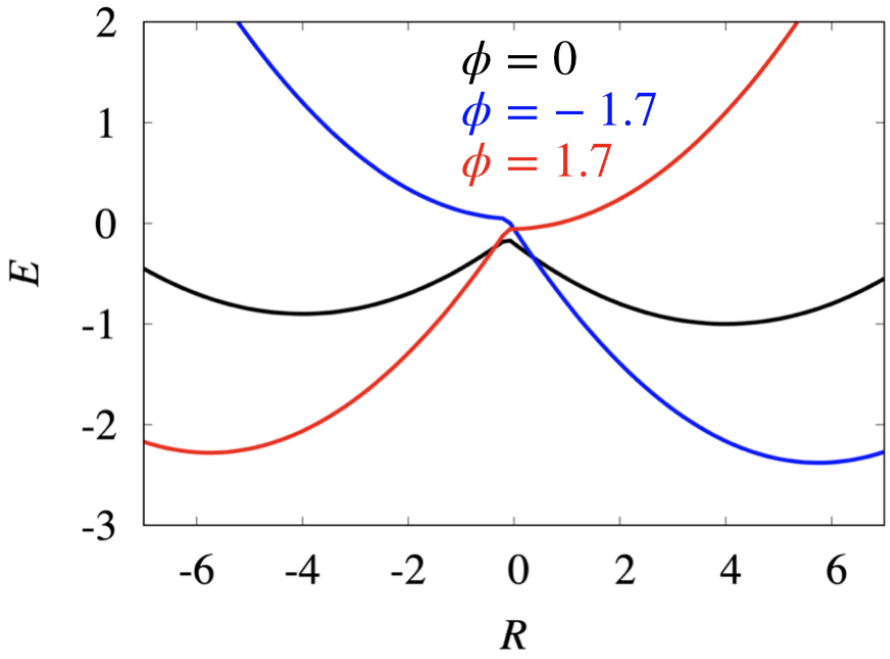

Figure 3.5: Cuts through the heat map of the potential energy surface shown in Figure 3.4 at varied values of ϕ illustrating that $R = 0$ does not define the transition state.

back and forth many times, before quickly crossing the barrier and completing the reaction, after which it dallies in the rightmost well. In Fig. 3.6 a) this behavior is illustrated on an aligned plot showing R and time, t, along with several reactive trajectories. Their R values stay mostly constant for long periods before abruptly transitioning from one extreme to the other. Because of this separation of timescales, it is usually infeasible to generate a significant number of reactive trajectories by brute force simulations. We would spend all of our lives waiting for the trajectories to cross the barrier.

3.5 Transition Path Sampling

Transition path sampling (TPS) is an attractive alternative to brute force sampling of reactive trajectories. The overarching goal of transition path sampling is to quickly obtain an unbiased sample of pathways from the reactive path ensemble.[69, 68] In other words, a set of reactive pathways obtained from transition path sampling should be statistically indistinguishable from a set of pathways obtained by brute force calculations, long observations of the system's undisturbed evolution. These reactive pathways can be easily analyzed

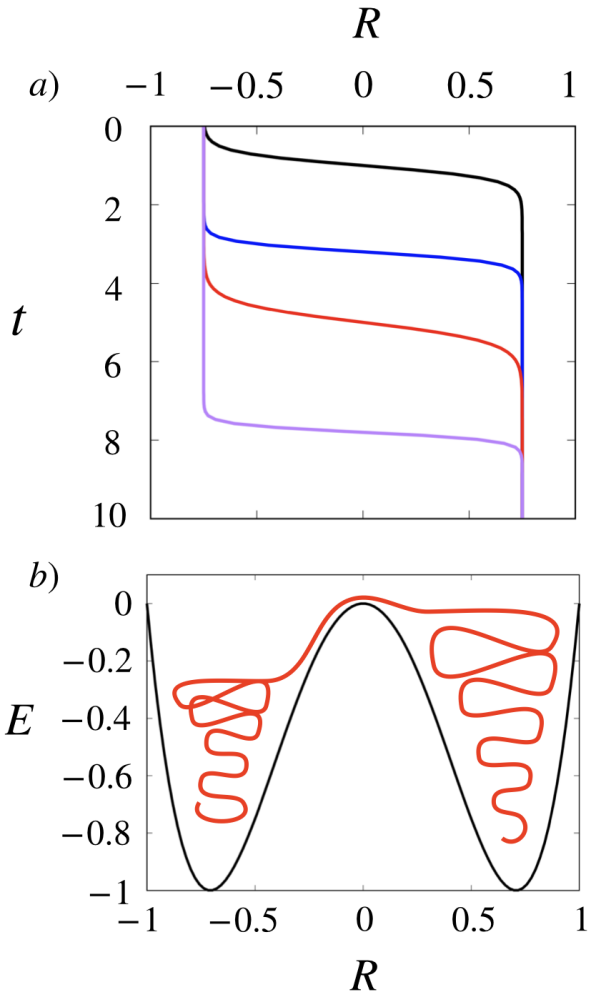

Figure 3.6: A cartoon illustration of the challenge of modelling reactive trajectories due to the timescales. Each colored line in a) represents the position as a function of time of a different trajectory equivalent in behavior to the single trajectory whose position and energy oscillations are shown in b).

for mechanistic information and used in thermodynamic integration to calculate reaction rates.[69, 66] Although we may want to calculate the committor along reactive pathways to identify the transition state, we do not need to know the committor, or any good reaction coordinate, in order to perform transition path sampling. This is a powerful advantage of the method.[69]

Transition path sampling is a Monte Carlo method which randomly perturbs reactive trajectories in order to generate new reactive trajectories. A valid transition path for ini-

tialization must be provided. This initial guess can be obtained in any way. It does not necessarily have to be a reasonable path. It could be a transition observed from brute force calculations or it could be completely artificial. The quality of the guess will affect the efficiency of the sampling procedure, however, with a sufficiently bad guess being unusable.

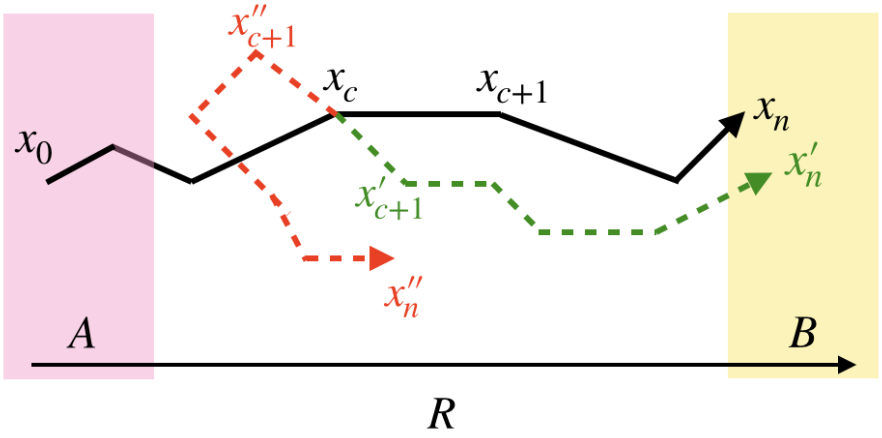

Figure 3.7: An illustration of transition path sampling. The parent path is in black and two child paths are in green and red. The reactant region is shaded pink and the product region shaded yellow. The parent begins in the reactants and ends in the products. The red child path ends outside of the product region and is rejected whereas the green child path ends in the product region and is accepted.

At each iteration of the algorithm, transition path sampling selects a Monte Carlo move, a kind of perturbation, to perform on the trajectory. A common kind of move is a shooting move. In the simplest case, a forward shooting move, a time step of the trajectory is randomly selected and all time steps after that are erased then regenerated to form a new trajectory.[68, 66] If the dynamics are stochastic, the child trajectory will be different from the parent which generated it if a new set of random noises are chosen. If the dynamics are not stochastic, the system state at the selected location will be perturbed by modifying the momentum while preserving the total energy.[36] The resulting child trajectory is tested to determine whether it is reactive and whether it meets additional acceptance criteria imposed by the Monte Carlo sampling procedure to guarantee that an unbiased reactive path ensemble is sampled. If the child trajectory is accepted, it then becomes the parent and is added to the reactive path ensemble. If the child is rejected the parent remains unchanged. This process is depicted in Fig. 3.7 with one parent trajectory in black, one rejected child in red and one accepted child in green. Monte Carlo moves are repeated, harvesting the resulting reactive trajectories until a sufficient number have been acquired.[36, 68, 66]

In order to sample reactive trajectories from the correct ensemble, transition path sampling must satisfy detailed balance conditions. This implies that[68]

$$P[X]\Gamma[X \to X'] = P[X']\Gamma[X' \to X] \tag{3.9}$$

where $P[X]$ is the probability to observe pathway X, and $\Gamma[X \to X']$ is the probability to obtain child pathway X generated from parent pathway X', including the probability to accept the proposed child pathway. As long as the detailed balance requirement is met, the proper distribution will be sampled eventually. Like all Monte Carlo methods, sampling problems can occur if the initial guess is sufficiently bad or it is otherwise very difficult to generate child pathways that are significantly different from the parent pathway. It is important to keep track of the number of rejected pathways and modulate the kinds of Monte Carlo moves between options such as shifting, shooting, forward shooting, backward shooting or more sophisticated shooting from the top approaches in order to achieve successful, unbiased sampling.[37]

As an example of how to solve for acceptance probabilities for a transition path sampling Monte Carlo move, consider the case of a forward shooting move in a stochastic system where trajectories are of fixed length, meaning they consist of the same number of discrete time steps.[68] Note that backwards shooting moves are often not available in stochastically evolving systems as it may not be possible to run the dynamics backwards in time. A fixed-length trajectory X can be described as a discrete number of system states, $\{x_0, x_1, x_2...x_n\}$. A reactive trajectory begins in the reactant states A and ends in the product states B. Indicator functions, $h_A(x_i)$ and $h_B(x_i)$ will return the probability that x_i is a reactant state A or product state B respectively. In a classical system, these indicator functions will return 1 or 0 only.

With our trajectory and the product and reactant states defined, a forward shooting move selects c, a time step along path X, then regenerates all time steps after c to obtain a path X'. Up until time step c, X and X' are identical. The probability to observe reactive pathway X is given by

$$P[X] = \frac{h_A(x_0)\rho(x_0)\Pi_{i=0}^{n} p(x_i \to x_{i+1})h_B(x_n)}{C}, \tag{3.10}$$

where C is a normalization constant, $\rho(x_0)$ is the equilibrium probability to start in x_0, and $p(x_i \to x_{i+1})$ is the probability that state x_i transitions to state x_{i+1} in one time step. The two indicator functions impose starting and ending conditions on the trajectory, forcing it to be a part of the reactive ensemble.

The probability $\Gamma[X \to X']$ has two components, the probability to generate pathway X' from pathway X and the probability to accept the Monte Carlo move from X to X', $P(\text{accept } [X \to X'])$. Solving the detailed balance equation Eq. 3.9 to find the ratio of

acceptance probabilities yields,

$$\frac{P(\text{accept } [X \to X'])}{P(\text{accept } [X' \to X])} = \frac{h_B(x'_n)}{h_B(x_n)} \frac{\rho(x'_0)\ \Pi_{i=0}^{n-1} p(x'_i \to x'_{i+1})}{\rho(x_0)\ \Pi_{i=0}^{n-1} p(x_i \to x_{i+1})} \frac{P(\text{select } x_c)\ \Pi_{i=c}^{n} p(x_i \to x_{i+1})}{P(\text{select } x'_c)\ \Pi_{i=c}^{n} p(x'_i \to x'_{i+1})}, \tag{3.11}$$

which can be immediately simplified if the probability to select x_c is equal for all c while taking into account that this is a forward shooting move and $x'_i = x_i$ up until point c, including at the first point, x_0. This results in all terms cancelling except for the product state indicator functions giving

$$\frac{P(\text{accept } [X \to X'])}{P(\text{accept } [X' \to X])} = \frac{h_B(x'_n)}{h_B(x_n)}, \tag{3.12}$$

as the ratio of acceptance probabilities. This shows that the ratio of acceptance probabilities is 0 if $h_B(x'_n)$ is 0 and can be one otherwise given that $h_B(x_n)$ must be 1. Detailed balance is assured by accepting any new trajectory which is, in fact, a reactive trajectory and rejecting all other trajectories. Acceptance criteria for other kinds of Monte Carlo moves are derived equivalently, often with similarly simple results.

Reaction rates can be calculated from transition path sampling by using thermodynamic integration. The rate, $k(t)$, to transition between A and B is given by the rate of change of the time correlation function $C_{AB}(t)$, which merely gives the probability for the system to be in B at t given that the system was in A at time zero,

$$k(t) = \frac{d\, C_{AB}(t)}{dt} = \frac{d}{dt} \frac{\langle h_A(x_0) h_B(x_t) \rangle}{\langle h_A(x_0) \rangle}, \tag{3.13}$$

where brackets indicate averaging over the equilibrium ensemble and the denominator renormalizes to compensate for the fact that not all trajectories start in reactant states, A. Integrating over the path ensembles yields partition functions

$$Z_A = \int P\,[X]\, h_A(x_0)\ D\,[X] = \langle h_A(x_0) \rangle, \tag{3.14}$$

where $P[X]$ is the probability to observe pathway X and $D[X]$ is the differential,

$$Z_{AQ} = \int P\,[X]\, h_A(x_0) h_Q(x_t)\ D\,[X] = \langle h_A(x_0) h_Q(x_t) \rangle, \tag{3.15}$$

where h_Q is an indicator function describing the likelihood to be in a region defined by Q, with Q being any coordinate that can smoothly describe a transition between A and B. It does not need to be a good reaction coordinate. It simply needs to be capable of connecting products and reactants.

We can redefine the correlation function rate equation in terms of these partition function integrals, finding

$$\frac{d\,C_{AB}(t)}{dt} = \frac{d}{dt}\frac{Z_{AB}(t)}{Z_A(t)}. \tag{3.16}$$

The log of the ratio between the partition functions can be calculated from a thermodynamic integral,

$$ln\frac{Z_{AB}}{Z_A} = \int_0^B \left(\frac{\partial\, ln\,(Z_{AQ})}{\partial Q}\right) dQ, \tag{3.17}$$

which gives the reversible work to move the system from reactants to products.[233, 174] An approximation for the rate without performing a derivative of this term might be obtained by calculating the ratio,

$$k = \frac{1}{t_m}\frac{Z_{AB}(t_m)}{Z_A(t_m)}, \tag{3.18}$$

at an intermediate time, t_m, for which the slope appears to be steady. If the time is too small, k will reflect dynamics only applicable to the start of the reaction, before arriving at a steady state. The rate will also be incorrect if t_m is too large and the system has started to equilibrate.

Transition path sampling is much more efficient than brute force sampling of trajectories, but there are alternative methods that may be easier to use, easier to interpret, easier to parallelize, or more applicable to extremely large systems. One close cousin of transition path sampling is transition path theory.

3.6 Transition Path Theory

Transition path theory (TPT) is a method for committor calculation initially formulated for applications to protein folding problems in thermal equilibrium.[277] Compared to dynamics that can be modeled in molecular mechanics or related methods, folding of a protein is astronomically slow, making study of this process by brute force essentially impossible and even transition path sampling very difficult due to the sheer length and complexity of folding mechanisms. Transition path theory determines a means to answer questions about long processes by running many short trajectories, all of which can be carried out in parallel, and using them to assemble a Markov state model for the system evolution.[168, 85, 170]

A Markov state model consists of a set of states, i, and a transfer matrix T where entry $T_{i,j}$ gives the probability that the system in state i will transition to state j within a time period τ. The first step in transition path theory is partitioning the configuration space into the states in the Markov state model.[202] This requires a large amount of simulation data. This data must sample all configurations likely to be seen during the reaction. Note that, for this discussion, a configuration will mean a unique $\{\boldsymbol{x}\}$ specifying the location of all particles in the system whereas a state will mean a state in the Markov state model consisting of many $\{\boldsymbol{x}\}$ configurations grouped together.

Inclusion of a configuration in any given state is generally based on the average displacement of the particles in a configuration from those designated to define the state. Sorting of configurations into states by this criteria may be accomplished by a partitioning method such as k-means or k-medoids, which are beyond our scope.[39, 3, 123]

A timescale of simulation must be selected such that the behavior of the system described by the model is, in fact, Markovian. All individual configurations which make up a state in the Markov state model must behave indistinguishably over the chosen timescale in order to guarantee that evolution has no memory, meaning that the timescale must be long enough to allow equilibration among all configurations in a state and average out any individual differences between them. The timescale must not be so long that a significant amount of density transfers between states, however, as in this case the model may lose the ability to distinguish two jump pathways between states, $i \to j \to k$, from direct one jump pathways, $i \to k$. Partitioning a system so that all of these conditions are met is very difficult. Markovianity of the model must be carefully checked by inspection of eigenvectors and eigenvalues of the transfer matrix.[39, 123]

Once the Markov state model (MSM) for the system has been obtained and validated, TPT calculations are straightforward. A system of linear equations defines the committor for the system in state i, $P_{B|A}(i)$, with products B and reactants A.

The system of equations is straightforward to derive. The probability that a state that is neither a product or a reactant, i, reaches product states B before reactants state A is the probability that i immediately transitions to some state in B, $\sum_{k\in B} T_{i,k}$ plus the probability that i transitions to any non-product state j times the probability that the system in state j will reach a product state before a reactant state, $P_{B|A}(j)$. Summing over all j results in the system of equations for the committors,[188]

$$P_{B|A}(i) - \sum_{j\in I} T_{i,j} P_{B|A}(j) = \sum_{k\in B} T_{i,k} \tag{3.19}$$

with set I indicating any state which is not in A or B. This system of linear equations can be immediately solved by any linear algebra library, but numerical stability problems can arise and a close eye must be kept on the solutions.

The next step in TPT is to calculate the reactive flux between all pairs of states. Given the committors and π_i, the equilibrium probability to be in state i as obtained from the Boltzmann distribution, the reactive flux for the reaction from A to B through jump $i \to j$ is

$$f_{i,j}^{A,B} = \pi_i P^*_{A|B}(i) T_{i,j} P_{B|A}(j) \quad i \neq j, \tag{3.20}$$

where $P^*_{A|B}(i)$ is the reverse committor, the probability that, under time reversed dynamics, the system in state i will visit A before B. In other words, the reactive flux is the probability to be in state i times the probability that the system arrived in state i from the reactants not the products, times the probability that state i will next transition to state j, times the probability that the system in state j will visit the products first and not the reactants. In

the case that the dynamics satisfy detailed balance and microscopic reversibility, $P^*_{A|B}(i) = P_{A|B}(i) = 1 - P_{B|A}(i)$.[188]

Using the shortcut to calculate $P_{A|B}(i)$ from $P_{B|A}(i)$ is not advisable due to numerical stability concerns. It is better to solve for $P_{A|B}(i)$ and $P_{B|A}(i)$ independently from two different systems of equations and then use the smaller of the two values to adjust the larger value so that their sum is equal to 1 and detailed balance conditions are enforced. This will help minimize the impact of numerical noise. If the value of the larger committor found via enforcement of detailed balance is very different from that found from solving the independent system of equations, there is reason to question the accuracy of TPT results. Similarly, if the reactive pathways found for the forward and reverse reaction are not identical, unless the MSM was generated by a method by which microscopic reversibility should not hold, this likely indicates serious problems with numerical noise.

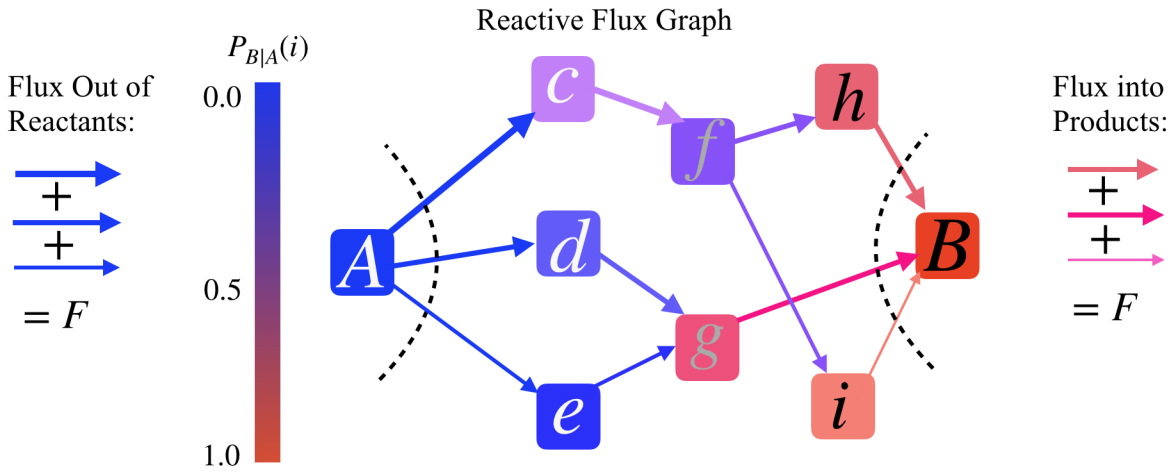

Figure 3.8: An illustration of the net flux graph associated with a transition path theory calculation where A is the reactant state, B is the product state and all others are intermediates. The amount of flux into the product or out of the reactant states gives the total reactive flux. The committor of each state is shown by the color.

The total reactive flux that leaves the reactants or, equivalently, the total reactive flux that arrives in the products is the total reactive flux through the system,[188]

$$F = \sum_{a \in A, j \notin A} f^{A,B}_{a,j} = \sum_{j \notin B, b \in B} f^{A,B}_{j,b}, \tag{3.21}$$

which is related to the total reaction rate, $k_{A|B}$, by dividing by τ, the time over which the

MSM was generated, and also a factor Π_A,

$$k_{A,B} = \frac{F}{\tau \Pi_A}, \tag{3.22}$$

where Π_A is the equilibrium probability that the system is moving forward from A to B, $\Pi_A = \sum_i P_{A|B}(i)^* \pi_i$, or more specifically the total probability that the system is in a state which came from the reactants and can, in fact, complete a reaction by going to the products next.

Transition path theory can provide more detailed mechanistic information than just the committors of every state and the rate. An ensemble of transition pathways can be found by defining the net reactive flux between states i and j as[188]

$$f_{i,j}^{+} = \max[0, f_{i,j}^{A,B} - f_{j,i}^{A,B}], \tag{3.23}$$

and using these as weights of a directed graph. A cartoon example of such a graph, along with the summations leading to the total reactive fluxes, is illustrated in Fig. 3.8, with states color coded by their committor values and the width of arrows between states indicating different $f_{i,j}^{+}$ values. The maximum flux that can pass through a pathway is equal to the minimum flux capacity of any $f_{i,j}^{+}$ it passes through. The pathway through which maximum flux can flow is the pathway along which the bottleneck, the minimum $f_{i,j}^{+}$ encountered, is the largest possible bottleneck for any existing pathway through the system. It is sometimes called the max-min flux pathway as a result. In the graph in Fig. 3.8, the max-min flux pathway is $A \to d \to g \to B$.

To obtain a max-min flux ensemble of reactive pathways through the system, Dijkstra's algorithm is used to find the max-min flux path,[72] and then this pathway is eliminated from the graph. If the bottleneck flux on the path eliminated was f_{min}, then f_{min} is subtracted from every single $f_{i,j}^{+}$ along the pathway, eliminating the bottleneck completely and appropriately reducing the weights of all the other edges along the pathway. Dijkstra's algorithm is then run again on this new graph to find the next max-min flux pathway, repeating the procedure until no pathways remain. Transition states can be assigned to the pathways by identifying states for which the committor value is approximately 0.5.

The max-min flux ensemble is usually the ensemble of greatest interest, but it is not unique.[188] Infinite different pathway ensembles can be traced through the flux graph by employing different algorithms for their extraction. Certain properties of the ensembles are conserved, however, such as the ensemble of transition states identified, meaning they can be used to gain mechanistic insight.

Note that these identified pathways between states reflect the overall movement of probability density through the system but do not reflect the actual dynamical pathways that would be encountered during brute force sampling or transition path sampling as recrossing events and other unproductive dynamics which bring the system no further towards transition are eliminated. This is generally a feature rather than a bug as the complicated, long, raw trajectories obtained from brute force dynamics or TPS simulations are difficult to interpret, often requiring coarse graining of the phase space in order to gain any insight into

dynamics.[123, 39, 188] The TPT reactive path ensemble distills down the important moves along reactive pathways, which are comparatively very simple and easily analyzed.

3.7 A Path Ensemble Point of Note

Analyzing the reactive path ensembles produced by TPT or TPS emphasizes an important, interesting point: just because a system state has a committor value of 0.5, and would be a transition state if a reactive pathway passed through it, does not mean that the system will ever *reach* this state. To return to our mountain metaphor, the peak of a mountain between the two valleys will have a committor value of 0.5, but the mountain pass between the two valleys will also have a committor value of 0.5 and, as the pass is much lower in energy and easier to access than the peak, reactive pathways will travel over the pass, not the peak. The peak is irrelevant to the system's dynamics. A committor value of 0.5 does not imply that a system state is *important*, merely that it would be the transition state along a reactive pathway *if* a reactive pathway were to pass through it. This may virtually never occur.

Chapter 4

The Quantum Committor

> 'Y'know,' he said, 'it's very hard to talk quantum using a language originally designed to tell other monkeys where the ripe fruit is.'
>
> Terry Pratchett, *Night Watch*

Reactions in which quantum effects are important share many of the challenges encountered when addressing classical reactions. Rugged, high dimensional potential energy surfaces complicate the search for transition states and reaction coordinates. New challenges appear as well. Quantum complications such as delocalization and tunneling arise, and make it difficult to apply classical mechanical tricks for analyzing reactive behavior. A different approach is required when treating reactions in quantum systems.

4.1 The Quantum Transition State

What, exactly, is the nature of the transition state in the world of the Heisenberg uncertainty principle[89, 187] where a particle does not have a precise location but is rather characterized by a probability distribution? What is the nature of a transition state when a system may tunnel through energy barriers?

Quantum mechanical extensions to transition state theory[171, 271] usually depended on instantons, or path integral based centroids, to characterize the transition states.[282, 173] An instanton is an orbit in imaginary time. Instanton theories are often effective at accounting for the effects of tunneling on reaction rates in quantum mechanical systems.[225] However, although based in rigorous quantum mechanical principles, instanton theories may be difficult to interpret and they do not provide any close approximation to the transition path ensemble of a classical system.

Quantum Jump Trajectories

A solution to this conundrum can be found by employing a trajectory based method of quantum mechanics, such as the unravelled GKSL master equation, which describes an ensemble of wavefunctions rather than a single density matrix by equating the density matrix to the expectation value, $\mathbb{E}[]$, of the outer product of the ensemble of wavefunctions,

$$\sigma = \mathbb{E}[|\Psi\rangle\langle\Psi|] = \sum_i P(|\Psi_i\rangle)|\Psi_i\rangle\langle\Psi_i| \tag{4.1}$$

where $|\Psi\rangle$ is treated as a stochastic variable which takes values $|\Psi_i\rangle$ with probability $P(|\Psi_i\rangle)$.[41, 65, 25, 63, 79, 45]

There are several possible unravelling of the GKSL equation, each of which can be equated to a different physical process of monitoring the state of a system.[289] The most commonly employed method, known as the Lindblad jump master equation or wavefunction Monte Carlo,[176, 280, 41] corresponds to continuous monitoring of the energy change of the bath interacting with the system. This unravelling is the precise theoretical equivalent of the evolution of a quantum system that would be observed if an experimental apparatus recorded every instance that the system and bath exchanged energy, allowing the observer to determine the precise change in energy experienced by the system. The Lindblad jump equation describes the change in the wavefunction at time t as[41, 280, 125, 233]

$$d|\Psi(t)\rangle = -\frac{i}{\hbar}H_{co}|\Psi(t)\rangle dt + \sum_{k\omega}\left(\frac{\sqrt{\gamma_k(\omega)}S_k(\omega)}{\langle\Psi(t)|\gamma_k(\omega)S_k^*(\omega)S_k(\omega)|\Psi(t)\rangle} - 1\right)|\Psi(t)\rangle dN_{k,\omega}, \tag{4.2}$$

with the coherent, non-Hermitian Hamiltonian,

$$H_{co} = H_S - \frac{i}{2}\sum_{k\omega}\gamma_k(\omega)S_k^*(\omega)S_k(\omega), \tag{4.3}$$

with the random variable $dN_{k,\omega}$ being either 0 or 1 at each time step.

The density matrix, $\sigma(t)$, that would be found from propagation of the corresponding deterministic Lindblad master equation is recovered by averaging over an ensemble of wavefunctions generated from the jump master equation,[280, 41]

$$\sigma(t) = \frac{1}{N}\sum_{i=1}^{N}|\Psi_i(t)\rangle\langle\Psi_i(t)| \tag{4.4}$$

where N is the number of stochastic wavefunctions simulated. Note that multiple different ensembles of wavefunctions will produce the same $\sigma(t)$, which will obviously be a mixed state density matrix. In other words, more information is available from inspecting an ensemble of stochastic trajectories than from inspecting a density matrix.[41]

The Lindblad jump equation describes a stochastic process where, at each time step, the wavefunction either evolves smoothly under the effect of H_{co}, an effective, coherent

Hamiltonian which does *not* preserve energy or norm as it is not Hermitian, or undergoes a quantum jump dictated by the selected operator, $S_k(\omega)$, which transforms the wavefunction into a different state.

A formal definition of a stochastic process over Hilbert space and proofs of properties about the expectation values and behaviors of such processes largely exceed our scope.[41] Intuitive arguments will serve our purposes better. If the expectation value of the norm of the wavefunction is not 1, a physically reasonable density matrix could not be constructed as the expectation value of the outer product of the wavefunctions. The expectation values of the coherently evolving term and the stochastic term must, therefore, sum to 1. Coherent evolution of the wavefunction by H_{co} results in decay of the norm. This loss must be accounted for, so the amount of probability lost by decay in coherent evolution has, necessarily, undergone a quantum jump as described by the stochastic term. The probability that a quantum jump occurs at any given time step is equal to the decay of probability observed from coherent dynamics for that time step. In other words, the probability to make a stochastic jump at time t rather than evolve coherently is

$$P(\text{jump}) = (\langle\Psi(t)|\mathbf{1} - \frac{i}{\hbar}H_{co}\,dt|\Psi(t)\rangle) \tag{4.5}$$

where $\mathbf{1}$ is the identity operator. If a jump has occurred, the probability that a particular jump, $S_k(\omega)$, has occurred is proportional to $\langle\Psi(t)|\gamma_k(\omega)S_k^*(\omega)S_k(\omega)|\Psi(t)\rangle$. These probabilities are normalized by the sum for all possible jumps such that the probability for a particular jump operator to effect a jump and evolve the system to a new, normalized $|\Psi(t+1)\rangle$ is,[41, 280, 233]

$$P\left(|\Psi(t+1)\rangle = \frac{\sqrt{\gamma_k(\omega)}S_k(\omega)|\Psi(t)\rangle}{\langle\Psi(t)|\gamma_k(\omega)S_k^*(\omega)S_k(\omega)|\Psi(t)\rangle}\right) = \frac{\langle\Psi(t)|\gamma_k(\omega)S_k^*(\omega)S_k(\omega)|\Psi(t)\rangle}{\sum_{j\omega'}\langle\Psi(t)|\gamma_j(\omega')S_j^*(\omega')S_j(\omega')|\Psi(t)\rangle}. \tag{4.6}$$

Determining the probability of a jump at each time step is computationally expensive. It is easier to find the waiting time distribution, which gives the probability that a jump will occur between times 0 and t, and sample t from the waiting time distribution directly. The waiting time distribution takes a Poisson form,[41, 280]

$$P(t) = 1 - ||e^{\frac{-i}{\hbar}H_{co}t}|\Psi(0)\rangle||^2 \tag{4.7}$$

where $||$ indicates taking the norm. The probability that a transition has occurred at t depends on the loss of the norm of the coherently evolved wavefunction at time t. In practice, this means that determining when a transition should occur is very easy. A uniform random number is drawn from a distribution between 0 and 1. Starting from a normalized wavefunction, the wavefunction is evolved coherently under H_{co} until the square of its norm decays to the chosen random number, at which point a jump operator is selected as detailed by Eqn. 4.6.[280, 233, 41] The wavefunction is operated on by this jump operator and then

normalized. This is an efficient algorithm and that is fortunate because large ensembles, often consisting of many thousands of wavefunctions, must be simulated in order to converge to the density matrix obtained from the equivalent deterministic calculation.

In the case that the Lindblad jump equation represents a secular Redfield equation, the eigenspectrum contains no degeneracies, and baths are uncorrelated, there are only two kinds of operators in the system.[41, 233, 280] The first is the dephasing operator, which corresponds to $\omega_{i,j} = 0$, and, in the energy eigenstate basis, is nonzero only on the diagonal where $i = j$. The action of the dephasing operator is to destroy coherent oscillations in the system.[187, 280] Any operator where $\omega_{i,j} \neq 0$ will have at most one non-zero entry when represented in the energy eigenstate basis and this will not be on the diagonal. Each jump operator instantaneously moves the system state from one individual energy eigenstate into another individual energy eigenstate. This means that three things can happen at each time step as a wavefunction evolves stochastically. No jump can occur and the system can proceed evolving coherently, the dephasing operator can act to damp coherent oscillations, or one of the other jump operators can act. If the system is in a superposition of multiple energy eigenstates, coherent evolution or the action of the dephasing operator will leave the system in a superposition. Any other operator, however, will collapse the wavefunction and destroy the superposition, leaving the system localized in a single energy eigenstate. This collapse to an eigenstate is not reversible. If the system's initial wavefunction, $|\Psi(0)\rangle$ is an energy eigenstate, the entire trajectory will be described as a series of jumps between energy eigenstates only. If the system begins in a superposition, eventually it will collapse to an energy eigenstate after which it will proceed to jump between energy eigenstates only, never returning to a superposition.

An illustration of this process is shown in Fig. 4.1, which shows the average electronic state character, $\langle e_2 \rangle$, of the coherently evolving density matrix of an arbitrary system in black alongside some of the stochastic trajectories that would be averaged to obtain that density matrix. This system was initialized out of equilibrium and allowed to relax. The resulting stochastic trajectories are complicated. They all collapse from a superposition very quickly, and it is difficult to discern any coherent evolution at all. After collapsing, the trajectories make a large number of jumps and although their averages will, of course, match that of the density matrix it is rare for any trajectory to take a value which matches the density matrix, even at long times when the density matrix seems to have achieved an equilibrium value with very little change occurring. This may be reminiscent of classical "dynamic equilibrium" descriptions of a system, in which apparently stationary macroscopic properties in equilibrium belie constant forward and reverse reactions taking place on microscopic scale.[15, 254]

It is important to keep in mind that while this stochastic treatment of the wavefunctions results in norms decaying away to nothing throughout evolution, a wavefunction must always be normalized in order to meet the basic definition of a wavefunction.[187, 261] Prior to recovering the full density matrix evolution by averaging the ensemble, or obtaining any other kind of property, it is necessary to normalize all $|\Psi(t)\rangle$ in the ensemble at all times t.

The stochastic approach to the GKSL equation may be cheaper to simulate than density matrix approaches. Simulating the full Redfield master equation requires time $O(n^3)$[213] at

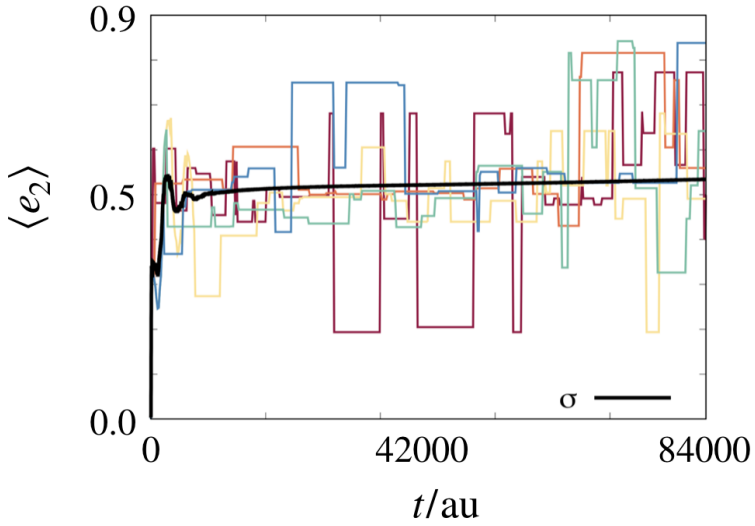

Figure 4.1: The average electronic state character of an evolving density matrix in black along with a subset of the wavefunction jump trajectories, in a variety of colors, which are averaged together to obtain the density matrix evolution. Note how complicated and different the trajectories are and the large number of jumps involved.

each time step, where n is the number of entries in the basis, whereas the stochastic equation requires $O(n^2N)$ time at each time step,[176, 280, 233] where N is the number of trajectories simulated. Depending on the number of trajectories required to converge results this may present significant time savings. Convergence with respect to the number of trajectories may be confirmed by comparing with the deterministic dynamics, running progressively larger trajectory ensembles until $\sigma(t)$ converges, or by averaging together small subensembles of the wavefunction trajectories and confirming that the $\sigma(t)$ for these subensembles matches that for the full ensemble, a procedure called block averaging.

The chief purpose of the unravelling, however, is not time savings. The ensemble of stochastically evolving wavefunction trajectories shares many similarities with the classical trajectory ensembles that TPS and TPT were developed to address. A committor can be defined for a quantum system using this framework and the committor-based methods addressing transition states, reaction coordinates, and transition rates are applicable as well.

4.2 Quantum Transition Path Sampling

Transition path sampling in a quantum system initially seems very appealing now that quantum trajectories have been defined. In one fell swoop, TPS can overcome the problems

of rare event sampling held in common between quantum and classical reactions and define a committor to allow designation of quantum transition states and reaction coordinates.

Quantum stochastic wavefunction trajectories can be sampled in much the same way as classical trajectories can be sampled.[233] In fact, forward shooting Monte Carlo TPS moves can be implemented without any complications at all. The acceptance criteria are identical for wavefunction trajectories as for classical trajectories.[233] If the child trajectory arrives in the product state, meaning it is an actual reactive trajectory, then it is accepted.

Backwards shooting moves may or may not be possible. It is possible to run the Lindblad jump equations backwards in time,[41] but only if the system was never in a superposition of multiple energy eigenstates. There is no jump operator which can recover a superposition from a wavefunction which has collapsed to a single eigenstate, nor is there an anti-dephasing operator that creates the coherent oscillations the dephasing operator destroys. If the reactants and products can be defined in terms of a single eigenstate and no wavefunction superposition is ever involved in the stochastically evolving wavefunctions, backwards shooting moves can be implemented.

By means of forward shooting moves and additional Monte Carlo moves when possible, ensembles of reactive trajectories can be generated for a quantum system as for a classical system and the committor can be calculated for individual states along the trajectory by spawning child trajectories exactly as in the classical stochastic trajectory case, with one caveat. If the trajectory begins in an eigenstate and ends in an eigenstate then we only need to assess the committors for a finite set of states, the energy eigenstates, as the trajectory must always be in one of them. If the trajectory begins in a wavefunction superposition, however, there are potentially an infinite number of different superpositions that the trajectory might visit and are thus potentially an infinite number of states for which the committor must be calculated.

Although reactive trajectory ensembles can be generated, rate calculations involving quantum TPS (QTPS) necessitate defining some kind of coordinate, Q, in order to calculate the thermodynamic integral,

$$ln\frac{Z_{AB}}{Z_A} = \int_0^B \left(\frac{\partial\, ln\,(Z_{AQ})}{\partial Q}\right) dQ, \tag{4.8}$$

which, as reviewed in the previous chapter, is necessary to determine the reaction rate. Although it does not matter whether this coordinate is a good reaction coordinate, it must be possible to strictly define a boundary based on this coordinate such that a trajectory is either between A and Q', where this just designates a particular Q, or is between Q' and B. Otherwise the thermodynamic integral cannot be calculated. This poses a problem. In a general quantum mechanical system, it is unclear how to define a strict boundary based on Q. Energy eigenstate wavefunctions have an exact energy, but the uncertainty principle thwarts any attempt to assign a precise location. Energy eigenstates are delocalized in position space, often very broadly.

There are two possible means of defining a boundary based on the coordinate. We can use the average value of Q for an energy eigenstate as if it were an exact value of Q or we can

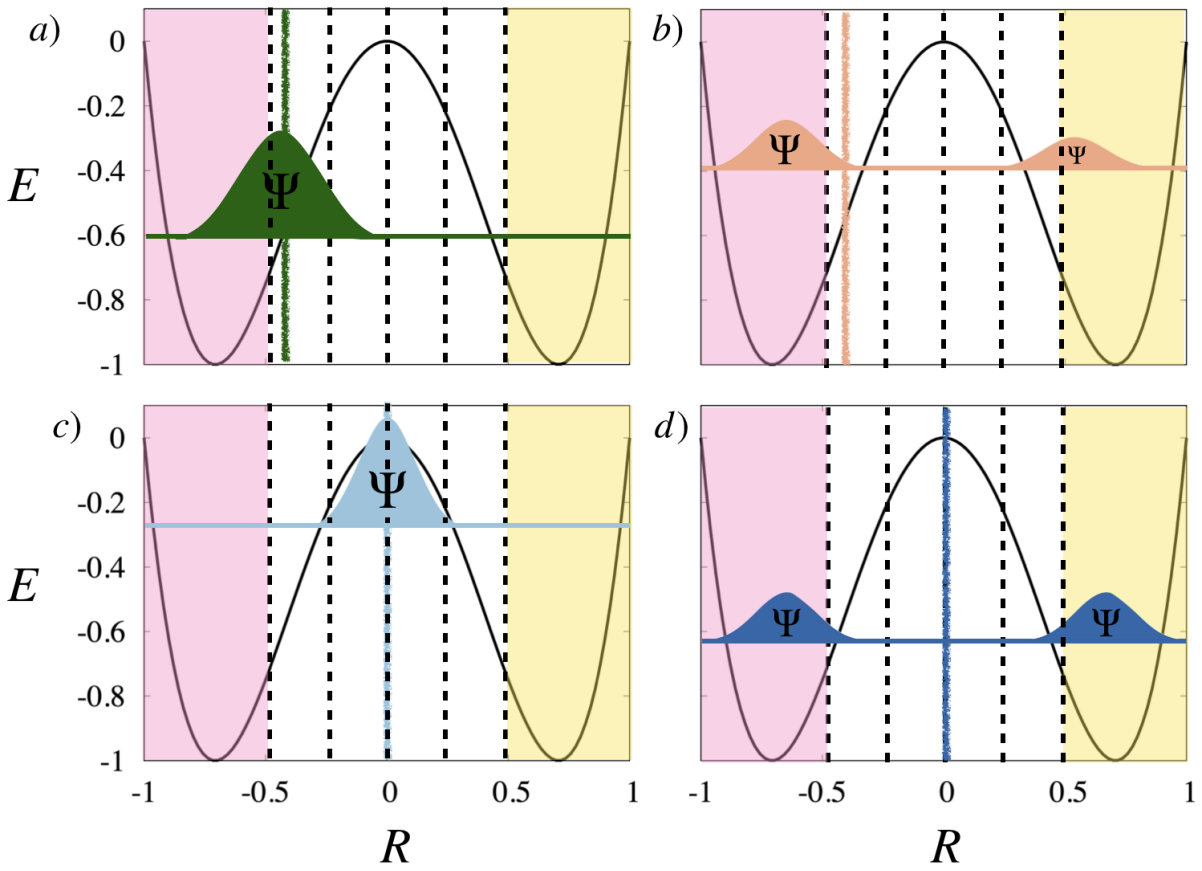

Figure 4.2: An illustration of the challenges in defining a reaction coordinate in a quantum system. The potential energy surface is a black, quartic line. Cartoon wavefunctions are represented in all four panels by one or more Gaussian functions of identical color. The average R for each wavefunction is illustrated by a blurred line of matching color. The reactant region is shaded in pink and the product region is shaded in yellow. Several dotted lines indicate constant values of the reaction coordinate, R. Note that the wavefunctions in c and d and a and b have the same average R but bear no resemblance to each other and represent very different states.

express the state of the system in terms of Q eigenstates and enforce requirements on which Q eigenstates are included in A to Q' versus in Q' to B . However, conceptual problems arise immediately due to delocalization and tunneling.

Pitfalls are illustrated in Fig. 4.2 where our favorite coordinate, R, is taken to be the Q for thermal integration. Panels a) and b) and c) and d) have the same average value of Q. However, these states are very different. There is a significant probability that, should we

measure R for b), we would find it to be in a product state. For the state in a) this probability is negligible. Even more problematic, the state shown in b) has a significant probability to be found in both the product and reactant states. A similar situation is shown in panels c) and d) where two states have the same average, but the state in c) has a significant chance to be measured in neither products nor reactants whereas the state in d) has a significant chance to be found in both products or reactants. In other words, our indicator functions h_A and h_B are no longer necessarily just 1 or 0 and this is resulting in conceptual problems. Using this framework and the average value of Q, there is no way to determine whether a state should be considered to be a reactant state or a product state or neither, let alone whether it should be considered to be between A and Q'.

The second method for defining boundaries based on Q is similarly problematic. The wavefunction, expressed in eigenstates of Q, will usually be a linear combination of many different Q eigenstates with a variety of values, some of which are between A and Q' and some of which are between Q' and B, some of which are in the reactant region and some of which are in the product region. The only way forward is to arbitrarily define some cutoff of probability that must be concentrated between Q' and B in order for the system state to be considered to be between these two values. However, this artificial bound cannot be justified and has the potential to bias the integral and the change of basis obfuscates exactly what influence this may have. There is some reason to suspect that the bound may artificially suppress tunneling contributions to the rate.

Some previous studies of TPS in quantum systems have circumvented this problem by strictly defining a series of energy eigenstates corresponding to an increasing Q.[233] This is only possible, however, in simple systems where we can pick out an approximate reaction coordinate by inspecting the wavefunctions and putting them into a particular order, with this order being the coordinate. It is also possible to use a mixed quantum/classical calculation or surface hopping for TPS rates, using a classical coordinate as the reaction coordinate, but this approach cannot help address fully quantum dynamics described by master equations.[181, 247]

Although it can potentially provide reactive ensembles and committors, QTPS is not as suited to providing rates. The ensembles of trajectories are also often difficult to interpret and complicated, as illustrated by the numerous, often unproductive, jumps seen in trajectories in Fig. 4.1. An alternative approach is quantum transition path theory.

4.3 Quantum Transition Path Theory

Transition path theory is easier to apply to the secular Redfield master equation, which can be written in GKSL master equation form as previously discussed, than to a classical system because the states in the Markov model are already known. This simplicity is easy to see by considering an alternate way to express the secular Redfield master equation,[20]

which states that the populations of the density matrix in the energy eigenbasis evolve as

$$\frac{d\sigma_{ii}}{dt} = D\sigma_{ii} \tag{4.9}$$

where σ_{ii} is a vector containing the populations of the eigenstates. In other words this vector is the diagonal entries of the reduced density matrix in the energy eigenbasis. Assuming for simplicity that $H_I = S \otimes B$, with only a single Hermitian system operator S, the matrix D is given by

$$D_{i,j} = |S_{i,j}|^2 \gamma_k(\omega_{i,j}), \tag{4.10}$$

where i and j are the indices of two eigenstates. In this representation, the coherences of the initial density matrix, provided there are any, undergo exponential decay and will be completely ignored. This is simply the form of a classical master equation describing population transfers between the energy eigenstates.

A classical master equation of this form can be used to generate a Markov state model (MSM).[153, 123, 64, 39] The energy eigenstates are the states of the MSM. The clustering problem necessary to determine the states of the MSM in classical molecular dynamical models are unnecessary. Despite this taking the form of a classical master equation, the rates within are informed by quantum mechanics, so quantum effects such as tunneling are preserved.

Assembling the Markov state model from the master equation is not difficult. The MSM is assembled from propagation of the secular Redfield master equation or equivalent GKSL equation for a short period of time, τ starting from the eigenstate in question then recording the populations observed. In other words, the Markov state model, T, has entries

$$T_{i,j} = \left(e^{D\tau}\sigma_{ii}\right)_{jj} \tag{4.11}$$

where $\sigma_{ii} = |\phi_i\rangle\langle\phi_i|$ and the subscript jj indicates that the jth element of the diagonal of the evolved density matrix has been extracted.

As in the classical case, it is necessary to check that the results obtained from TPT are invariant to the selected τ as, should a large timescale be employed, second order processes may destroy the accuracy of the model. If these "double jumps" are included in a significant fraction, they muddy the interpretation of the results. If the selected time τ is too short, however, the solution may be tainted by numerical problems. Calculations at several values of τ should be completed in order to verify that the results are insensitive to variations around the chosen τ.

Once the Markov state model has been assembled by running a total of n short time density matrix propagation calculations, one for every energy eigenstate in the basis, TPT can be applied to the resulting MSM exactly as in the classical case. An eigenstate (or states) is chosen to represent the reactants, A, and another to represent the products, B. The TPT system of equations can be solved and a committor value assigned to every energy eigenstate in the system. The equilibrium fluxes and net fluxes can also be calculated just as in the classical case, providing a reactive flux graph, along with the thermal reaction rate.

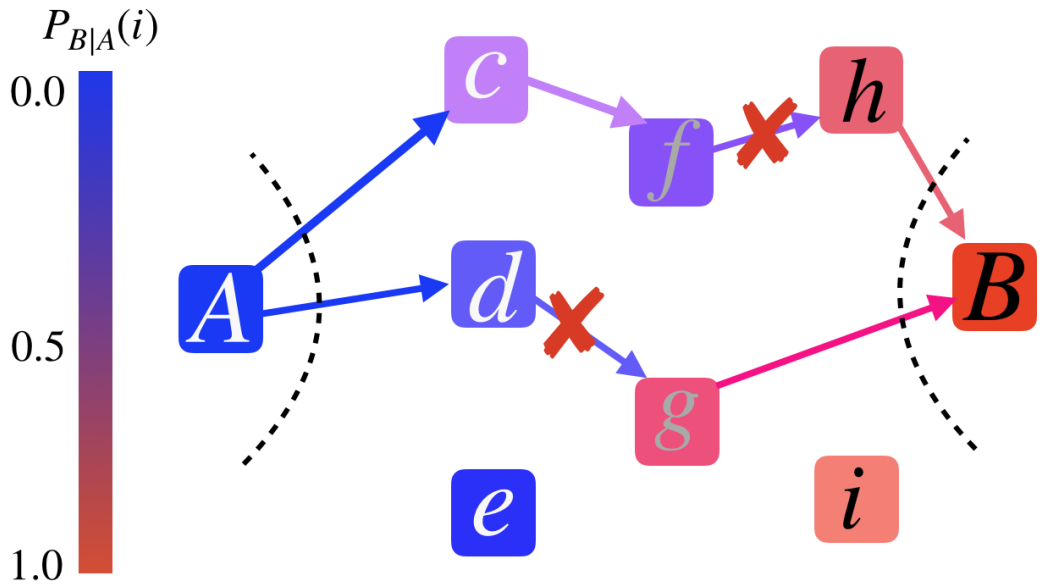

Figure 4.3: An illustration of transition pathways through the net flux graph between eigenstates. Eigenstates are color coded by committor value with transition eigenstates on either side of the red 'x' symbols.

The problem of sampling rare events in a quantum system is addressed in tandem with the problem of defining a committor in a quantum system.

Care must be taken when forming the reactive flux graph. Because the eigenstates are discrete and tunneling processes may occur, there is no guarantee that any eigenstate's committor value will ever be 0.5, or even close to 0.5. However, by definition there must be some point along the reactive pathways through the system at which the committor probability of eigenstate i, $P_{A|B}(i)$ is less than 0.5 followed by a jump to an eigenstate j where $P_{A|B}(j)$ is greater than 0.5. These states i and j are as close as we can come to a committor value of 0.5 and, together, constitute the closest equivalent we can define to a classical transition state. These are called the committor, or transition, eigenstates. An ensemble of reactive pathways can be assembled by Dijkstra's algorithm along with an ensemble of their transition states, the pairs of committor eigenstates. The process of extracting reactive pathways from a graph and assigning committor eigenstates is shown in Fig. 4.3 where two pathways from reactants to products are shown, the eigenstates color coded by their committor values, and a red 'x' marks the critical jump at which the committor changes from below to above 0.5. The committor eigenstate before the jump is called the pre-committor eigenstate and the one after the jump is called the post-committor eigenstate.

Committor eigenstates can provide significant insights into reaction dynamics. For example, comparing the ensemble average energy of the transition eigenstates to the height of the energy barrier between reactants and products will immediately clarify whether tunneling plays a significant role in the mechanism.

Note that the unravelled Lindblad equation is not needed to perform quantum TPT (QTPT). Density matrix propagation is sufficient to determine population dynamics and assemble the MSM, and hence there is no need to consider the ramifications on a physical experiment implied by unravelling a master equation. No particular measurement protocol has been imposed. However, it is often useful conceptually to think about ensembles of jump trajectories when considering what a QTPT result actually means. QTPT describes the average behavior of that ensemble of trajectories jumping between energy eigenstates with all unproductive jumps and the complexity of the raw trajectories in Fig. 4.1 eliminated. In the ensemble of trajectories, at some point, some critically important Lindblad jump operator is responsible for moving a trajectory from a pre-committor eigenstate to a post-committor eigenstate, but another operator might then move it back to the pre-committor eigenstate again. QTPT reactive pathways will never show recrossing events, but remembering the chaotic raw trajectories of Fig. 4.1, we know they likely occur.

Quantum transition path theory does have an unfortunate drawback as formulated. It is designed to address a system which is performing a thermal barrier crossing reaction. If we are interested in addressing a system that has been vertically excited by a photon, TPT is not equipped to provide us information about transition states and reaction pathways. A different approach is necessary to handle photoreactions.

4.4 Quantum Transition Path Theory for Photoreactions

If the system of interest is not in equilibrium, the committor for all eigenstates is still determined as usual by QTPT but there is no longer any means to calculate the reactive flux as the probabilities to be in any given eigenstate are not given by the Boltzmann distribution. This thwarts all immediate attempts to acquire mechanistic or rate information as committor eigenstate identification requires the reactive fluxes.

QTPT can be generalized to address the case of a system relaxing from a nonequilibrium state to equilibrium. The initial, excited system will be a coherent superposition between many system eigenstates. Returning to the stochastic GKSL equation and viewing the evolving system as an ensemble of wavefunction trajectories rather than a single evolving density matrix, a jump operator will eventually result in collapse of the initial, coherent superposition to an eigenstate. It is possible to calculate the probability, $\Pi(C)$, that the eigenstate into which collapse occurs is eigenstate C, given an initial wavefunction $|\Psi(0)\rangle$. This is complicated by actions of the dephasing operator which may occur at any time and change the form of the wavefunction, which prevents us from simply propagating $|\Psi(0)\rangle$

under the action of the coherent H_{co} and cataloguing the departure probability to C at each time step, t,

$$P(|\Psi(t+1)\rangle = |C\rangle) = \sum_{c\omega} \langle \Psi(t)|\gamma_c(\omega) S_c^*(\omega) S_c(\omega)|\Psi(t)\rangle, \tag{4.12}$$

where c and ω index over all Lindblad jump operators which result in collapse of the coherent wavefunction into eigenstate C. Practically, $\Pi(C)$ is obtained by sampling a large number of stochastic trajectories to find their states of initial collapse. After this collapse, Onsager's regression hypothesis[197, 198, 270], and Markovianity, imply that the system is ignorant as to how it arrived in its current state and its relaxation pathways will be identical to those which would be found in a Boltzmann distributed system which had arrived in C due to equilibrium fluctuations. This allows us to make use of the same logic for deriving fluxes as in equilibrium QTPT.

Consider a system which has been excited into a coherent wavefunction superposition of many states and then collapsed into eigenstate C. This excited state will relax and will eventually reach either the reactants, A, or products, B. The reactive flux from C to A along the edge i, j is

$$f_{i,j}^{C,A} = P_{C|AB}^*(i) \pi_i T_{i,j} P_{A|CB}(j), \tag{4.13}$$

where $P_{C|AB}^*(i)$ indicates the probability that the system in state i came from C before A or B and $P_{A|CB}$ indicates the probability that the system will reach A before B or C . This is very similar to the equilibrium QTPT equation for the reactive flux and derived from the same logic. The total flux from C to A is given by the sum $F^{C,A} = \sum_{j \neq C,B} f_{C,j}^{C,A}$. Finding the total flux along i, j into A following vertical excitation requires summing over all possible C states into which the initial superposition could collapse as

$$f_{i,j}^{A} = \sum_{C} f_{i,j}^{C,A} \frac{\Pi(C)}{F^{C,A}}. \tag{4.14}$$

The contributions of reactive flux from different initial C sources must be renormalized by dividing by $F^{C,A}$ so that all initial sources have unit exiting flux before they can be weighted by $\Pi(C)$ and added together to find the total flux. A net flux graph is then trivially assembled, with the weight of the edges given by $f_{i,j}^{A+} = \max\left[0, f_{i,j}^{A} - f_{j,i}^{A}\right]$ for edge i, j. Summing over all edges entering A gives the total flux into A, $\sum_{a \in A\ j \notin A,B} f_{j,a}^{A} = F^{A}$, excluding the usually negligible edge case in which the system collapses directly to A.

This procedure is extremely numerically unstable. The initial eigenstates occupied following collapse usually have very high energies, making their equilibrium probabilities exceedingly small. This leads to tiny total reactive fluxes, resulting in large errors when their weights are renormalized by dividing by $F^{C,A}$ prior to the summation.

The flux graph describing the relaxation to A is equivalently obtained by brute force propagation of wavefunction jump trajectories from the initially excited state, $|\Psi_0\rangle$, continuing propagation only until either A or B is reached. The total number of jumps from eigenstate i to eigenstate j carried out by all trajectories in the ensemble is denoted $J_{i,j}$.

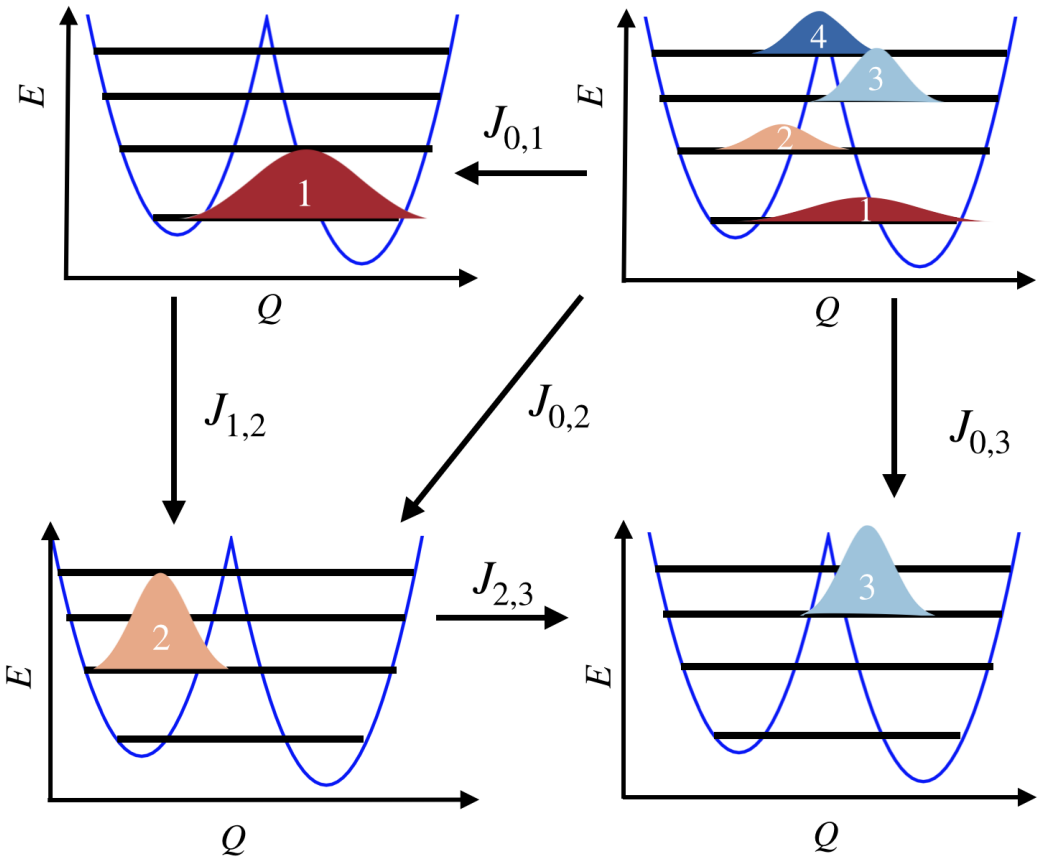

Figure 4.4: A schematic of the procedure for assembling a flux graph from brute force relaxation calculations. Collapse occurs from any superposition that results from coherent evolution and the dephasing operator, with all such states called state 0, to an eigenstate. Every time a jump is observed in a relaxing trajectory, its source and destination state are recorded. The total number of jumps between each source and destination state, $J_{i,j}$, normalized by the full number of jumps throughout propagation, estimates the reactive flux. Note that not all possible $J_{i,j}$ are shown on this cartoon for the sake of cleanliness.

Figure 4.4 is a cartoon showing a superposition of four different eigenstates which then collapses, illustrating the meaning of $J_{i,j}$. Any uncollapsed wavefunction state is referred to as state 0 for convenience, even though it may take one of infinite different forms, and $J_{0,i}$ is the number of observed collapses from any superposition to eigenstate i.

Before calculating J values or performing other post processing, trajectories must be sorted into conditioned ensembles depending on whether they arrive in A before B or B before A. Trajectories are propagated only until they reach either A or B and terminated at that point, so this means that trajectories are sorted based on their ending states. The

number of jumps $i \to j$ in the ensemble conditioned to arrive in A, $J^A_{i,j}$, divided by the total number of trajectories, N,

$$f^A_{i,j} \approx \frac{J^A_{i,j}}{N} \tag{4.15}$$

is an unbiased estimate of $f^A_{i,j}$. Block averaging can be employed to determine whether the trajectory ensembles are of sufficient size.

The $f^A_{i,j}$ fluxes can be used to generate a net flux graph as in equilibrium QTPT, resulting in each edge of the net flux graph having weight $f^{A+}_{i,j} = \min\{f^A_{i,j} - f^A_{j,i}, 0\}$. The special state 0 contains within it an infinite number of different coherent superpositions of the eigenstates; any state which has not yet collapsed to an eigenstate is considered to be in state 0. Examining the hidden degrees of freedom within state 0 for individual trajectories would provide information about what kinds of superpositions are most likely to collapse to which energy eigenstates, but in order to trace relaxation pathways with Dijkstra's algorithm a finite number of states is required and state 0 must encompass all uncollapsed wavefunctions, losing any information about the system prior to collapse. Dijkstra's algorithm produces a reactive path ensemble of pathways from 0 to A from the ensemble conditioned to arrive in A and from 0 to B from the ensemble conditioned to arrive in B.

Once an ensemble of relaxation pathways has been extracted from the graph, there are two kinds of committor behavior that may be observed. Consider the relaxation pathways from 0 to A. The committor of the eigenstate, i, to which the system collapses along a pathway, $P_{A|B}(i)$ may be less than 0.5 or it may be greater than 0.5. In the case that the committor is less than 0.5, a set of committor eigenstates along the relaxation pathway are selected just as in equilibrium QTPT. In the case that $P_{A|B}(i)$ is greater than 0.5, commitment occurred at some point when the system was in the superposition state 0 or as it collapsed into i. In a sense, 0 and i are the committor eigenstates, but as 0 could represent any superposition of system eigenstates and take practically any form, there is no true pre-committor eigenstate, and it is impossible to say whether the system had committed prior to the collapse to the first eigenstate.

Nonequilibrium QTPT can produce committor eigenstates and relaxation mechanisms. It cannot, however, produce any rate information. The trajectories in the relaxing ensembles can be of any length. There is no timescale τ associated with the fluxes. Because it uses a trajectory based approach, its results are associated with a particular measurement protocol, specifically with measuring all exchanges of energy between the system and bath. Despite these drawback it is still a very useful tool for understanding nonequilibrium quantum reactions.

The equilibrium and nonequilibrium incarnations of QTPT are equipped to address many systems. However, they are both built on the secular approximation to the Redfield master equations. Although this approximation is often justified, there are cases where it is not valid, and a different approach is necessary in order to appreciate the full influence of quantum effects on the system.

Chapter 5

The Committor and Quantum Coherent Effects

> If you thought that science was certain–well, that is just an error on your part.
>
> Richard Feynman

5.1 The Generalized Quantum Committor

The methods presented so far can assign committor values to all energy eigenstates within a system only by making the secular approximation, which is a strong assumption which is not valid in some cases. Near degeneracies between energy eigenstates call the secular approximation into question. The size of the energy gap between states at which nonsecular effects, the influence of quantum coherences, become relevant depends strongly on the rates of transfer between eigenstates of the system. In cases where nonsecular effects are important the QTPT methods detailed previously are not usable as they will not be able to accurately describe the coherent effects of the system, losing the impact of important dynamics.

However, an alternative means of defining the committor is available. This more general definition depends on the partial secular approximation and can treat quantum coherent effects. This method allows the committor to be efficiently defined for any quantum state, any density matrix, provided the propagator for the dynamics can be described as a linear, Markovian master equation with the product and reactant states designated as absorbing boundary conditions.

The Time-Independent Committor

The partial secular Redfield master equation described previously was presented in classical master equation form by placing the eigenstate populations into a vector and defining

the propagator, D, for this vector as a matrix such that $\dot{\sigma}(t) = D\sigma(t)$. The coherences were ignored because they were irrelevant. However, it is not necessary to ignore the coherences in order to bring a Redfield master equation into the form in which the system is a vector and a matrix multiplying this vector defines its evolution

To begin, the density matrix is unrolled into a column vector of length n^2, where n is the basis size. This vector includes all populations and coherences in a fixed order. The propagator can then be represented as a matrix of dimension n^2 by n^2. The Redfield and partial secular Redfield master equations define different matrices, but in both cases one can be defined.[47, 90] The process for forming this matrix can be somewhat odious and it may be too cumbersome to deal with in large systems due to its unfavorable scaling with system size, but often it is not necessary to deal with this matrix explicitly. It is merely necessary to recognize that our master equation can be written as,

$$\dot{\sigma}(t) = \mathcal{L}\sigma(t), \tag{5.1}$$

where $\mathcal{L}$ is called the superoperator and this is the superoperator form of the master equation.[201] Many master equations, whether phenomenological or microscopically derived, can be brought into superoperator form.[86]

The superoperator $\mathcal{L}$ can be modified into $\mathcal{L}'$ in which states A and B have been designated as absorbing boundary conditions. This can be done in the superoperator formalism by setting all entries of $\mathcal{L}_{i,A}$ and $\mathcal{L}_{i,B}$ to zero for all i, where A and B are any indexes into the superoperator corresponding to the locations of the populations in the reactants and products, the absorbing boundary states. In the partial secular Redfield master equation, this procedure can be performed by setting jump rates to zero for any operator corresponding to density departing from states in A or B. This can be done without explicitly forming the superoperator. This is only a valid operation to perform if coherent effects between A and B are irrelevant. In other words, there must be no potential for quantum coherent effects between A or B and any states which are not also in A or B respectively. In the partial secular Redfield equation, this means that all states in the reactants, A, must be in a nonsecular block or nonsecular blocks which contain other states in A only. The same must be true of the products, B.

If the system is initialized in $\sigma(0)$ and then propagated to $t = \infty$ under $\mathcal{L}'$,

$$\sigma(t = \infty) = \left(\lim_{t\to\infty} e^{\mathcal{L}'t}\sigma(0)\right), \tag{5.2}$$

all population will be found in A or B, depending on which was reached first. These populations at infinite time, then, are precisely the definition of the quantum mechanical committor for $\sigma(0)$, our initial state.

This provides us with a general means of calculating a committor in a quantum system. However, much greater power is afforded by considering a complete basis for σ. The density matrix can be written as a linear combination of basis states $\sigma_{i,j}$ where $\sigma_{i,j} = |\phi_i\rangle\langle\phi_j|$. Specifically,

$$\sigma = \sum_{c_{i,j}} c_{i,j}|\phi_i\rangle\langle\phi_j|, \tag{5.3}$$

with complex coefficients, $c_{i,j}$, which must satisfy certain relations including $c_{i,j} = c^*_{j,i}$ to guarantee a physical density matrix. We will define the time integrated flux,

$$V_{A|B}(\sigma_{ij}) = \left(\lim_{t\to\infty} e^{\mathcal{L}'t}\sigma_{ij}\right)_A \tag{5.4}$$

where the subscript indicates that we are extracting the population in state A from the resulting density matrix at infinite time. This time integrated flux can be used to calculate the committor for any quantum state as

$$P_{A|B}(\sigma) = \sum_{c_{i,j}} c_{i,j} V_{A|B}(\sigma_{ij}), \tag{5.5}$$

requiring at most n^2 calculations to define the initial basis before the calculation for any σ can be done instantly. The partial secular Redfield equation formalism tells us which coherences will have $V_{A|B}$ of zero; only the coherences contained within nonsecular blocks can have a nonzero contribution to the committor. This dramatically decreases the cost of calculating $V_{A|B}$ for the full basis as the contribution of many coherences is known to be zero.

This provides a very fast and straightforward method for calculating the committor for any quantum state provided that dynamics for the system can be described by a linear master equation to which absorbing boundary conditions can be applied. It also allows precise quantification of the effect that any coherence in the density matrix has on the committor, and hence the outcome of the reaction.

Time-Dependent Committor

The time-dependent committor, $P_{A|B}(t, \sigma)$, rather than giving the probability that the system will visit A before B, asks for the probability that the system will arrive in A by time t. The general definition for the time-dependent committor is very straightforward. The integrated flux is now time-dependent,

$$V_{A|B}(t, \sigma_{ij}) = \left(e^{\mathcal{L}'t}\sigma_{ij}\right)_A \tag{5.6}$$

and the time-dependent committor is the same sum over components as for the time-independent committor.

The time-dependent committor can provide information that the time-independent committor cannot, such as whether any given quantum coherence changed the dynamics of the relaxation at an intermediate point, not just whether it had an impact on the final fate of the system.

The General Committor Derivation

Although the general committor definition presented is very intuitive, a more formal exploration of the general committor is warranted. Recall Eq. 4.2, which showed the unravelling of the secular Redfield master equation allowing the density matrix propagation to

be calculated as an average over an ensemble of stochastically evolving wavefunctions governed by a Poisson jump process. An equivalent wavefunction unravelling may be derived for the partial secular Redfield master equation, with its only differences from Eq. 4.2 being modification of rates and operators as ω is replaced by $\bar{\omega}$. A stochastic equation for the evolution of the density matrix, σ, may also be obtained, related to the stochastic wavefunction evolution by[131]

$$d\sigma(t) = d(|\Psi(t)\rangle\langle\Psi(t)|) = d|\Psi(t)\rangle\langle\Psi(t)| + |\Psi(t)\rangle d\langle\Psi(t)| + d|\Psi(t)\rangle d\langle\Psi(t)|. \tag{5.7}$$

Using the Itô rules which state that $dN_{k,\bar{\omega}}(t)dN_{k',\bar{\omega}'}(t) = \delta(k,k')\delta(\bar{\omega},\bar{\omega}')dN_{k,\bar{\omega}}(t)$, one eventually arrives at,

$$\begin{aligned} d\hat{\sigma}(t) = \hat{\mathcal{L}}\hat{\sigma}(t) = \Bigg(& -i[H_S + H_{LS}, \hat{\sigma}(t)] + \sum_{k,\bar{\omega}} \gamma_k(\bar{\omega}) \\ & \left(\frac{-1}{2}\{S_k^*(\bar{\omega})S_k(\bar{\omega}), \hat{\sigma}(t)\} + Tr[S_k^*(\bar{\omega})\hat{\sigma}(t)S_k(\bar{\omega})]\ \hat{\sigma}(t) \right) \Bigg)\ dt + \\ & \left(\sum_{k,\bar{\omega}} \frac{S_k^*(\bar{\omega})\hat{\sigma}(t)S_k(\bar{\omega})}{Tr[S_k^*(\bar{\omega})\hat{\sigma}(t)S_k(\bar{\omega})]} - \hat{\sigma}(t) \right)\ dN_{k,\bar{\omega}}(\hat{\sigma}(t)) \end{aligned} \tag{5.8}$$

where the expectation value of performing a particular jump defined by the operator $S_k(\bar{\omega})$,

$$\mathbb{E}[dN_{k,\bar{\omega}}(\hat{\sigma}(t))] = \gamma_k(\bar{\omega})Tr[S_k^*(\bar{\omega})\hat{\sigma}(t)S_k(\bar{\omega})]dt, \tag{5.9}$$

is the expectation value needed to calculate the average behavior of this system and the decorated density matrix, $\hat{\sigma}$, and superoperator, $\hat{\mathcal{L}}$, indicate that the equation refers to a single stochastically evolving density matrix rather than to a deterministic evolution.[41, 131, 289, 8] By taking the expectation value of $d\hat{\sigma}(t)$, $\mathbb{E}[d\hat{\sigma}(t)]$, and cancelling terms, it is easy to see that the expectation value of this unravelling is the partial secular master equation. As in the case of wavefunction unravellings, this stochastic process is not unique. The averages of several different stochastic processes would all yield the same expectation value. This one, however, will be very conceptually useful.

As in the case of the stochastic wavefunction trajectories, there are two processes that may occur at any time step as $\hat{\sigma}$ evolves. The system may undergo a jump which may move it between nonsecular blocks or it may evolve coherently and deterministically within nonsecular blocks. The final two terms in Eq. 5.8 represent a jump process in which operators $S_k(\bar{\omega})$ may move the stochastically evolving density matrix from one nonsecular block into another nonsecular block. Not all operators will result in a jump between blocks. The dephasing operator, for example, will not change the nonsecular block which the density matrix inhabits. If the system does not undergo a jump it will evolve deterministically according to the first three terms in Eq. 5.8. This will result in the density matrix evolving throughout the nonsecular block. Note that the system may be in a mixed state within this block. In this sense, the stochastic density matrix equation differs sharply from the

stochastic wavefunction equation as the latter describes the evolution of an ensemble of pure states. If the nonsecular block is of size one, then there is no nontrivial coherent evolution as the system remains in that single eigenstate until a jump operator moves it to a new nonsecular block.

Although it covers an unusual state space, Eq. 5.8 is merely a Poisson jump process over nonsecular blocks and the committor for this Poisson jump process is easily defined. By definition, the committor is the probability that product states B will be visited before reactant states A. In the simplest and most convenient treatment, we demand that A and B are defined by two nonsecular blocks. Given an initial density matrix state, $\sigma(0)$, the committor probability to B, $P_{B|A}(\sigma(0))$, is the probability that a stochastic trajectory initialized at $\sigma(0)$ will visit B before A. To determine the committor given a current state of $\sigma(0)$ we must average the probability of arriving in B before A over all realizations of a stochastic process beginning from this initial condition.

This expectation value could be obtained by simulating an infinite number of independent stochastic density matrix trajectories initialized in $\sigma(0)$, observing their evolution and recording whether A or B was visited first. This approach is valid only because A and B are defined by different nonsecular blocks, thus the system may not be in a superposition involving a state in A or B and any state not in either A or B respectively, and because the probability of the system performing two jumps simultaneously vanishes under the Redfield weak system-bath coupling approximation, thus the system arrives in either A or B first, not both at once.

Because dynamics after reaching A or B are irrelevant to the question of whether reactants or products are reached first, we are free to alter the equation of motion such that no jump process exists which moves a trajectory out of A or B. These jump processes represent dynamics which occur exclusively after the point at which a stochastic trajectory's evolution would be terminated. The propagator, $\hat{\mathcal{L}}$, becomes $\hat{\mathcal{L}}'$, with all jump rates associated with leaving A or B set to zero. This merely guarantees that any stochastic trajectory arriving in A or B will remain there for all time. Under these modified dynamics, the committor $P_{B|A}(\sigma(0))$ is the expectation value of a trajectory being in B after infinite time,

$$P_{B|A}(\sigma(0)) = \mathbb{E}[(\lim_{t\to\infty} e^{\hat{\mathcal{L}}'t}\hat{\sigma}(0))_B] \tag{5.10}$$

where the subscript B indicates, as usual, that we are extracting the population in B following evolution. Note that, under the conditions imposed, each individual realization of the stochastic evolution will result in a population in B of either 1 or 0 after infinite time.

The expectation value in Eq. 5.10 is precisely equal to Eq. 5.2. Note that although a particular unravelling and jump definition, hence a particular measurement protocol imposed on the quantum system,[289, 41] was used to derive the general quantum committor, the density matrix propagation which defines the general committor does not involve any particular unravelling and is independent of measurement protocol.

The basis decomposition for calculating the committor is a purely mathematical consequence which does not have physical meaning, as it is physically impossible for a system's

density matrix to have coherence but no population. The Markovianity and linearity of the propagator $\mathcal{L}'$ guarantees the validity of Eq. 5.5 without taking into account any underlying stochastic process.

The derivation of the time-dependent general quantum committor is equivalent to the time independent case. The limit taking t to infinity is replaced by a finite time throughout the derivation.

5.2 The Generalized Transition State

Given a generalized definition for the time-independent quantum committor which can be applied to any quantum state, it is possible to define the transition state in any quantum system. It is given by the usual criteria, $P_{A|B}(\sigma) = 0.5$. Unlike the case of quantum transition path theory, the committor has been defined as a continuous function of σ's elements and a transition state with a committor of precisely 0.5 will exist. However, there is no guarantee that, throughout the course of a calculation, a σ for which $P_{A|B}(\sigma) = 0.5$ will ever be encountered. If the system is initialized in a state, $\sigma(0)$, which has a committor of $P_{A|B} > 0.5$, the density matrix may relax to equilibrium without passing through any transition state.

In the partial secular Redfield master equation, each individual nonsecular block may or may not contain any states with a committor value of 0.5. If a nonsecular block does contain one such point, it will likely contain infinitely many points, although an edge case in which there is only one is conceivable. Because the master equation is linear, the transition state will constitute a hyperplane in the multidimensional space defined by the nonsecular block. In the limit that the nonsecular block contains only two states, the eigenstates in the nonsecular block define a Bloch sphere and the plane constituting the transition state can be visualized on this Bloch sphere. In any dimensions higher than two it will not be possible to visualize the transition state.

5.3 The Generalized Committor and Quantum Control

The generalized quantum committor can identify transition states, where the committor is 0.5, but it can also identify states where the committor approaches 1.0. In other words, it can determine which states are most likely to complete a reaction. QTPT can also do this in cases where it is applicable. This is very useful.

Consider the situation in Fig. 5.1. A ground state wavefunction, $|\Psi_0\rangle$ which is localized at 0 of the coordinate Q_t, may be excited by two different laser pulses to either a left wavefunction, $|\Psi_L\rangle$ or a right wavefunction, $|\Psi_R\rangle$. These two wavefunctions then relax into one of the wells of the blue potential energy surface. A common control problem is to determine the product of a photoreaction in such a system by forcing the system to relax

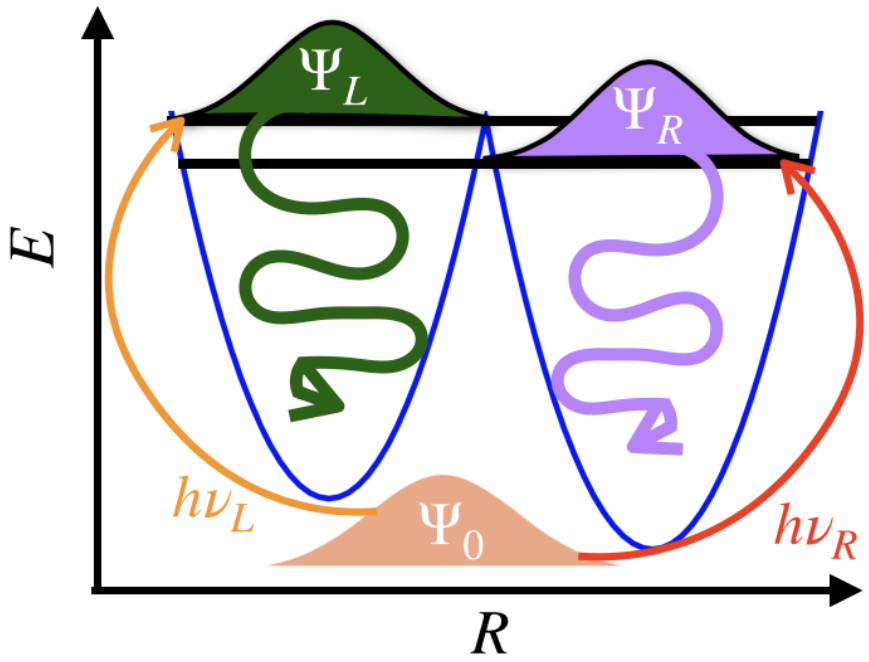

Figure 5.1: A cartoon of a photoexcitation from ground wavefunction Ψ_0 to preferentially selected wavefunctions, Ψ_L and Ψ_R, which relax to either side of a barrier on the blue potential energy surface.

only into the left well or only into the right well. Coherent quantum control protocols employ carefully crafted laser pulses to form the initial wavefunction in order to determine the dynamics of the system.[26, 13] Determining what initial state the laser should target, however, is a difficult problem to solve.

We now have an easy way to select optimal $|\Psi_L\rangle$ and $|\Psi_R\rangle$ states. Presuming that it is possible to designate A and B as states localized at the bottom of the two wells of interest, the generalized quantum committor provides a formula for acquiring the optimal initial wavefunctions. After solving for $V_{A|B}(\sigma_{ij})$ for the system, we can optimize $P_{A|B}(\sigma)$ over the coefficients $c_{i,j}$ to obtain the optimal desired wavefunctions. Similarly, QTPT can provide the values of maximum committor eigenstates in cases where it is certain that coherences will not impact relaxation. If only a subset of the general committor σ basis is available due to physical constraints, the optimization can be carried out in precisely the same way, simply cutting out those elements of the matrix which are unavailable. A constrained optimization will always be required to ensure that the initial wavefunction is physical. Optimizing over a mixed state density matrix to determine an initial state requires greater care than dealing with a pure state as there are a larger number of independent variables and an optimized

pure state is likely preferred.

Relaxation Pathways and the Transition State

As detailed in the general committor derivation section, it is possible to formulate the density matrix relaxation of the partial secular Redfield equations as a sum over an ensemble of stochastically evolving wavefunctions as in the secular unravelling case. Calculating the committor along these trajectories would allow generation of an ensemble of transition states for the relaxation which would provide more information than could be obtained from the relaxation of a single density matrix, as one density matrix can correspond to a multitude of different stochastic trajectory ensembles. This avenue has not been sufficiently explored thus strong claims of its efficacy cannot be made.

Chapter 6

Quantum Committor Theories for Conical Intersections

> Physicists like to think that all you have to do is say, these are the conditions, now what happens next?
>
> Richard Feynman

Conical intersections, once thought to be a mathematical curiosity and little more, are actually extremely common phenomena present in nearly all large molecules and serving very important roles.[293] At a conical intersection, two or more potential energy surfaces are degenerate. This means that, following photoexcitation to an electronically excited state, a molecule may thermally relax, passing through a conical intersection to return to its ground electronic state quickly and without emitting a photon.[184, 164, 60] This serves an important role in photoprotection, including in DNA.[24] Conical intersections play a part in energy capture by photosynthetic light harvesting complexes.[274, 194] They also serve key roles in reaction mechanisms in molecular photoswitches, systems that change their geometry following excitement by absorbing a photon. Photoswitches have numerous existing and potential engineering applications.[242, 21] Molecular photoswitches have appeared in holographic materials, information storage materials, communication devices, and methods for controlling the firing of individual neuron ion channels.[252, 186, 11, 255, 102]

Due to their important roles, conical intersection dynamics are a busy field of study, with many theorists attempting to better understand their mechanistic behavior or control the outcomes of relaxation through them.[1, 146, 243, 143] Experimentalists are similarly interested and groups using lasers tuned with coherent control protocols have successfully manipulated wavepackets passing through conical intersections,[13, 150] although determining these protocols can be challenging, commonly leading to feedback based control wherein a machine learning algorithm tunes the laser.[26]

Theoretical treatment of dynamics around conical intersections to understand mechanisms or propose means for controlling reaction outcomes poses several challenges. The

solvent environment, especially polarity and viscosity, is known to have a large impact on dynamics in nonadiabatic systems, so gas phase calculations are generally insufficient for learning substantial information about a system's behavior.[244, 58, 120, 21] Conical intersections also include nonadiabatic dynamics, in which the vibrational motion of the nuclei and the electronic dynamics occur on similar timescales, requiring that both be treated explicitly by quantum dynamical methods.[291, 142] In many other systems we can employ the Born-Oppenheimer approximation and adiabtic dynamics in order to simplify our treatment, but near a conical intersection this option is unavailable.[1]

6.1 Adiabatic and Nonadiabatic Dynamics

The potential energy surfaces of a chemical system can be expressed in different ways. Electronic structure calculations return one set of surfaces, but infinite different change of basis operations may be performed to mix these surfaces together to produce new ones. Two kinds are commonly used: adiabatic and diabatic potential energy surfaces.[17, 302] In the same way that all toads are frogs but not all frogs are toads, any surface which is not adiabatic may be called nonadiabatic. A diabatic surface is nonadiabatic, but a nonadiabatic surface is not necessarily diabatic, as this has a very specific meaning. The adiabatic potential energy surfaces, generally obtained from electronic structure theory programs, arise from the Born-Oppenheimer approximation.

Adiabatic Dynamics: The Born-Oppenheimer Approximation

Most of this section follows the discussion in *Chemical Dynamics in Condensed Phases* by Abraham Nitzan.[187] Discussions can be found in many papers and textbooks.[261, 89]

In the most general case, the Hamiltonian of a closed molecular system can be stated as[187]

$$H(\boldsymbol{r}, \boldsymbol{R}) = H_N(\boldsymbol{R}) + H_{N-e}(\boldsymbol{R}, \boldsymbol{r}) + H_e(\boldsymbol{r}) \tag{6.1}$$

Where $\boldsymbol{r}$ refers to the position coordinates of the electrons, $\boldsymbol{R}$ refers to the position coordinates of the nuclei, and the Hamiltonians giving the energy for the nuclear degrees of freedom, nuclear-electron interaction, and electron degrees of freedom are given by $H_N(\boldsymbol{R})$, $H_{N-e}(\boldsymbol{R}, \boldsymbol{r})$ and $H_e(\boldsymbol{r})$ respectively. Because, in most cases, the timescales of motion for the light electrons and massive nuclei, which are about one thousand times heavier than the electrons, are so disparate, we can view the nuclei as being stationary in comparison to the electrons. This simplification is known as the Born-Oppenheimer approximation.[38]

Under this simplification, the Born-Oppenheimer (BO) wavefunction, $|\Psi(\boldsymbol{r}, \boldsymbol{R})\rangle$ is split into two components, the nuclear wavefunction, $|\chi_{i,j}(\boldsymbol{R})\rangle$, and the electronic wavefunction $|\phi_i(\boldsymbol{r}, R)\rangle$ in which the positions of the nuclei are treated as a parameter, not a variable, and

[1] This chapter is based on work submitted to *The Journal of Chemical Physics*[10] and submitted to arXiv.[8]

hence are not in bold. An eigenstate wavefunction under the Born-Oppenheimer approximation has form

$$|\Psi_{i,j}(\boldsymbol{r},\boldsymbol{R})\rangle = |\chi_{i,j}(\boldsymbol{R})\rangle|\phi_i(\boldsymbol{r},R)\rangle, \tag{6.2}$$

a product of a nuclear and electronic wavefunction. The full wavefunction of the system is a sum over many Born-Oppenheimer eigenfunctions. The electronic BO wavefunction is found from

$$H_{BO}(\boldsymbol{r},R) = \left(H_e(\boldsymbol{r}) + H_{N-e}(\boldsymbol{r},R)\right)|\phi_i(\boldsymbol{r},R)\rangle = E_e^i(R)|\phi_n(\boldsymbol{r},R)\rangle, \tag{6.3}$$

where H_{BO} is the Born-Oppenheimer Hamiltonian. The electronic energy eigenstate i for nuclear positions R is $E_e^i(R)$. The BO potential energy surface, known as the adiabatic potential energy surface, for electronic state i is given by $E^i(R) = E_e^i(R) + V_N(R)$ where the potential component of $H_N(\boldsymbol{R})$, which consists of nuclear-nuclear repulsion terms, has been extracted to give $V_N(R)$. The nuclear wavefunction can then be determined as

$$\begin{aligned}&(H_{BO}(\boldsymbol{r},R) + H_N(\boldsymbol{R}))|\phi_i(\boldsymbol{r},R)\rangle|\chi_{i,j}(\boldsymbol{R})\rangle = \\ &(T_N(\boldsymbol{R}) + E^i(R))|\phi_i(\boldsymbol{r},R)\rangle|\chi_{i,j}(\boldsymbol{R})\rangle = E^{i,j}(\boldsymbol{R})|\phi_i(\boldsymbol{r},R)\rangle|\chi_{i,j}(\boldsymbol{R})\rangle,\end{aligned} \tag{6.4}$$

where $T_N(\boldsymbol{R})$ is the nuclear kinetic energy operator. The nuclear (vibrational) BO energy eigenstates are given by $E^{i,j}(\boldsymbol{R})$ with i specifying the electronic state and j specifying the vibrational state.

The Born-Oppenheimer approximation assumes complete independence of system evolution on separate adiabatic states, greatly reducing many challenges associated with solving the full Schrödinger equation. The evolution of the electronic BO wavefunction is given by the usual time-dependent Schrödinger equation,

$$|\phi(\boldsymbol{r},R,t)\rangle = e^{-iH_{BO}t/\hbar}|\phi(\boldsymbol{r},R,0)\rangle, \tag{6.5}$$

which shows that if the system begins in an electronic eigenstate, it will remain there for all future times. The system can be pictured as a sum of wavefunctions evolving along adiabatic potential energy surfaces, with no interaction between those surfaces. A greater simplification that is sometimes made presumes that only a single electronic state is relevant, in which case the system can be viewed as evolving along a single adiabatic potential energy surface.[187, 17, 291]

The BO approximation neglects the coupling between electronic states through the nuclear kinetic energy operator. The full Hamiltonian acting on a BO eigenstate in which the nuclear degrees of freedom for the electronic states are not frozen gives

$$\begin{aligned}&(T_N(\boldsymbol{R}) + V_N(\boldsymbol{R}) + H_{BO}(\boldsymbol{r},R))|\phi_i(\boldsymbol{r},\boldsymbol{R})\rangle|\chi_{i,j}(\boldsymbol{R})\rangle = \\ &\left(-\sum_K \frac{\hbar^2\partial^2}{2M_K\partial R_K^2} + E^i(\boldsymbol{R})\right)|\phi_i(\boldsymbol{r},\boldsymbol{R})\rangle|\chi_{i,j}(\boldsymbol{R})\rangle,\end{aligned} \tag{6.6}$$

and we focus in on the term providing the momentum for each of the K nuclei in the system, each of which has mass M_K. Applying the partial derivative operators with the product rule

yields,

$$\begin{aligned}
&-\sum_K \frac{\hbar^2\partial^2}{2M_K\partial R_K^2}|\phi_i(\boldsymbol{r},\boldsymbol{R})\rangle|\chi_{i,j}(\boldsymbol{R})\rangle = \\
&-\sum_K \frac{\hbar^2}{2M_K}\left(\frac{\partial^2}{\partial R_K^2}|\phi_i(\boldsymbol{r},\boldsymbol{R})\rangle\right)|\chi_{i,j}(\boldsymbol{R})\rangle \\
&-\sum_K \frac{\hbar^2}{M_K}\left(\frac{\partial}{\partial R_K}|\phi_i(\boldsymbol{r},\boldsymbol{R})\rangle\right)\left(\frac{\partial}{\partial R_k}|\chi_{i,j}(\boldsymbol{R})\rangle\right) \\
&-\sum_K \frac{\hbar^2}{2M_K}|\phi_i(\boldsymbol{r},\boldsymbol{R})\rangle\left(\frac{\partial^2}{\partial R_K^2}|\chi_{i,j}(\boldsymbol{R})\rangle\right)
\end{aligned} \tag{6.7}$$

Taking the inner product with a BO wavefunction in a different adiabatic electronic state yields three terms,

$$\begin{aligned}
&-\langle\phi_l(\boldsymbol{r},\boldsymbol{R})|\langle\chi_{l,m}(\boldsymbol{R})|\sum_K \frac{\hbar^2}{2M_K}\left(\frac{\partial^2}{\partial R_K^2}|\phi_i(\boldsymbol{r},\boldsymbol{R})\rangle\right)|\chi_{i,j}(\boldsymbol{R})\rangle \\
&-\langle\phi_l(\boldsymbol{r},\boldsymbol{R})|\langle\chi_{l,m}(\boldsymbol{R})|\sum_K \frac{\hbar^2}{M_K}\left(\frac{\partial}{\partial R_K}|\phi_i(\boldsymbol{r},\boldsymbol{R})\rangle\right)\left(\frac{\partial}{\partial R_k}|\chi_{i,j}(\boldsymbol{R})\rangle\right) \\
&-\langle\phi_l(\boldsymbol{r},\boldsymbol{R})|\langle\chi_{l,m}(\boldsymbol{R})|\sum_K \frac{\hbar^2}{2M_K}|\phi_i(\boldsymbol{r},\boldsymbol{R})\rangle\left(\frac{\partial^2}{\partial R_K^2}|\chi_{i,j}(\boldsymbol{R})\rangle\right),
\end{aligned} \tag{6.8}$$

the first of which is the nuclear kinetic energy. The second term, which can be rewritten as,

$$-\sum_K f_{l,i}^K\langle\chi_{l,m}(\boldsymbol{R})|\frac{\hbar^2}{M_K}\frac{\partial}{\partial R_K}|\chi_{i,j}(\boldsymbol{R})\rangle, \tag{6.9}$$

contains the derivative coupling,

$$f_{l,i}^K = \langle\phi_l(\boldsymbol{r},\boldsymbol{R})|\frac{\partial}{\partial R_K}|\phi_i(\boldsymbol{r},\boldsymbol{R})\rangle, \tag{6.10}$$

which links BO adiabatic energy surfaces to each other. The final term, the diagonal or BO correction, modifies the energies of the adiabtic states to compensate for nonadiabatic effects. It is generally small and often neglected, despite the fact that it can become large and influence dynamics in some cases.[106, 275, 116] In many cases, the derivative coupling term can be neglected as well, but when two adiabatic potential energy surfaces draw near to each other, this term will become large and it cannot be ignored. In this case, nuclear degrees of freedom and electronic degrees of freedom must all be explicitly modeled without any BO simplifications. In fact, the magnitude of the derivative coupling is proportional to $1/(E^{i,j}(R) - E^{l,j}(R))$, so at locations where two adiabatic surfaces touch, this term becomes infinite.[293, 291, 187]

Diabatic Potential Energy Surfaces

Modeling chemical dynamics using adiabatic, BO, potential energy surfaces is problematic at conical intersections or avoided crossings. The latter are locations at which adiabatic surfaces narrowly avoid touching, the former cases where they actually do. It is more convenient to change the basis of representation to avoid the problem of the diverging derivative coupling term. One may perform a basis rotation and work in a nonadiabatic basis.

Anything that is not an adiabatic basis is a nonadiabatic basis. The diabatic representation is a very specific nonadiabatic representation in which the nonadiabatic coupling operator is eliminated by applying a rotation resulting in a representation in which the nuclear kinetic energy operator is diagonal. The derivative coupling in Eq. 6.10 vanishes for a true diabatic state.[293] The transformation is accomplished by applying a unitary operation, $U_{i,j}(R)$, to all adiabatic wavefunctions, $|\phi_j^{db}(\boldsymbol{R},\boldsymbol{r})\rangle = \sum_i U_{i,j}(R)|\phi_i(\boldsymbol{r},R)\rangle$, where $|\phi_j^{db}\rangle$ is the new, diabatic basis such that

$$f_{j,i}^K = \langle\phi_j^{db}(\boldsymbol{r},\boldsymbol{R})|\frac{\partial}{\partial R_K}|\phi_i^{db}(\boldsymbol{r},\boldsymbol{R})\rangle = 0 \;\forall\; i,j,K \tag{6.11}$$

which presents a problem which can be solved easily in diatomic molecules where there is only one K coordinate, the interatomic distance. When there are additional coordinates, the partial differential equations which result can only be solved if certain conditions hold to allow for path integration, and generally they do not. A true diabatic basis, thus, does not exist for molecules of nontrivial size.[293, 256, 115, 16, 167] Whenever the diabatic basis is discussed, an approximately diabatic basis is implied. Many different method exist for attempting to determine approximate diabatic states with the field constantly improving.[113, 209, 260] For the rest of this discussion, we will assume that a suitably accurate approximately diabatic basis is available for use during our simulations.

Landau-Zener Theory

Landau-Zener theory is a means of determining how a system will behave at an avoided crossing.[137, 294, 259] The Landau-Zener problem is sometimes framed as the problem of what happens when two molecules collide with one another so that the distance between them, R, is time dependent.[187] The Hamiltonian for this system in the diabatic basis with diabatic electronic states $|\phi_1\rangle$ and $|\phi_2\rangle$, is

$$H = E_1(R)|\phi_1\rangle\langle\phi_1| + E_2(R)|\phi_2\rangle\langle\phi_2| + V_{1,2}\left(|\phi_1\rangle\langle\phi_2| + |\phi_2\rangle\langle\phi_1|\right), \tag{6.12}$$

where the coupling between diabatic potential energy states, $V_{1,2}$, is presumed to be time independent, and E_i refers to the energy of diabatic state i. At time $t = 0$, $E_1(R)$ and $E_2(R)$ are presumed to be very disparate but at a special time t^* and a certain R, R^*, the diabatic surfaces cross, leading to an avoided crossing. At infinite time, the energies of the diabatic surfaces will be very disparate again. The question posed in the Landau-Zener problem is whether the system passing through the avoided crossing will change its diabatic character

and maintain its adiabatic character or whether it will change its adiabatic character and maintain its diabatic character. In other words, will the system passing through the intersection in Fig. 6.1 maintain its color or its dash type as it passes the vicinity of the avoided crossing? Population transfer between two states in a quantum system will not occur when

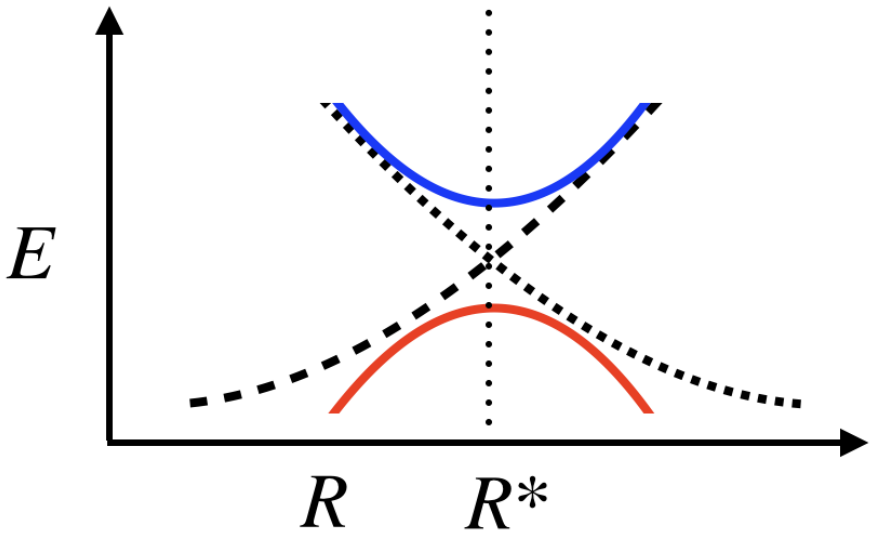

Figure 6.1: Two adiabatic potential energy surfaces in blue and red at an avoided crossing with a single degree of freedom involved, R. The diabatic potential energy surfaces are dashed. The vertical dotted line marks the avoided crossing at R^*. The adiabatic surfaces are obtained by diagonalizing the diabatic Hamiltonian of $|\phi_1\rangle$ and $|\phi_2\rangle$ at each point.

the coupling between them is too small in comparison to the energy difference,[187] so the Landau-Zener solution approximates that all appreciable population transfer occurs near enough to R^* that all necessary information to calculate the probability of the transfer can be calculated from values at R^* only.

Evaluating the evolution of the two level system, the probability to transition between diabatic states is[187, 265, 70]

$$P(|\phi_1\rangle \rightarrow |\phi_2\rangle) = 1 - \exp\left[-\frac{2\pi|V_{1,2}|^2}{\hbar\,\dot{R}|F_2(R^*) - F_1(R^*)|}\right] \tag{6.13}$$

where $F_i = -\partial E_i/\partial R$, the forces on the system on each diabatic surface, are evaluated at R^*, as is the derivative $\dot{R} = \partial R/\partial t$.

Two limits of behavior exist in the Landau-Zener problem. The first is the limit in which the coupling is small in comparison to $\dot{R}$, in other words the system moves very

quickly through the avoided crossing region with comparatively small coupling. From Taylor expanding the exponential of e^{-x} when x is small to find $e^{-x} \approx 1 - x$, this gives us a limiting case of[187, 265, 70]

$$P(|\phi_1\rangle \to |\phi_2\rangle) = \frac{2\pi |V_{1,2}|^2}{\hbar \, \dot{R} |F_2(R^*) - F_1(R^*)|} \tag{6.14}$$

which, given our initial assumptions, indicates that there is a very low probability of transfer between the two diabatic surfaces. This is called the nonadiabatic limit as, by remaining on its diabatic surface, the system changes adiabatic state.

The opposite limit, in which the coupling is large in comparison to $\dot{R}$, is called the adiabatic limit. In this case, the large negative value in the exponential results in $P(|\phi_1\rangle \to |\phi_2\rangle) \approx 1$. The system is nearly assured to maintain its adiabatic state and change diabatic states as a result of strong coupling and slow R velocity.[187]

Although formulated for avoided crossing models, these ideas of adiabatic and nonadiabatic limiting behaviors have been applied to conical intersections in several forms and will prove useful for our discussions.[155, 92]

6.2 Conical Intersection Barrier Crossing Reactions

In order to properly engineer a photoswitch for any given application, the thermal isomerization rate needs to be controlled. If one desires a memory device, a slow speed of isomerization will be necessary,[11, 255] but for any kind of information transfer device, a faster rate will be needed.[102, 255] Numerous studies on tuning the behavior of photoswitches have been carried out.[42, 71] Simeth and coworkers had demonstrated that it is possible to radically modify the rate of isomerization by modifying the potential energy surfaces of the conical intersection with the addition of methyl groups.[255] Solvent effects can significantly influence isomerization rates, too, as well as dynamics including the isomerization pathways.[19, 21] Open questions remain, however, and a systematic understanding is far off.[244] As conical intersections are a key component of photoswitches, we focus in on thermal barrier crossing dynamics in their vicinity.

To investigate the impact of the conical intersection's geometry on isomerization rate, we applied QTPT to a simple model of a conical intersection undergoing a thermal barrier crossing, adjusting a key parameter of the potential energy surfaces and observing the impact on the barrier crossing rate. The conical intersection was described by a simple model, a set of two two dimensional harmonic oscillators constituting the diabatic electronic states. The vibrational coordinates in these states are the tuning coordinate, Q_t, and the coupling coordinate, Q_c, so called because the two diabatic states are linked through Q_c. The full Hamiltonian of the system is[133, 52, 232, 233]

$$H_S = \sum_{k=1,2} |e_k\rangle h_k \langle e_k| + \left(|e_1\rangle\langle e_2| + |e_2\rangle\langle e_1|\right) \lambda Q_c, \tag{6.15}$$

where the Hamiltonians of the diabatic states are,

$$h_k = \frac{1}{2}\sum_{j=c,t} \hbar\omega_j \left\{P_j^2 + Q_j^2\right\} + E_k + \kappa_k Q_t \tag{6.16}$$

where $|e_i\rangle$ are the diabatic electronic states, λ constitutes the diabatic coupling parameter, E_k are energy adjustments added to each diabatic state, κ_k are tuning coordinate shifts for each diabatic state, and ω_j are the oscillator frequencies for the coupling and tuning modes. The oscillators are in dimensionless coordinates, where $Q_i = \sqrt{1/2}(a^+ + a)$ $i = c, t$, given that a^+ and a are the raising and lowering operators, and momentum is similarly dimensionless, $P_i = -i/\sqrt{2}(a^+ - a)$. See Table 6.1 for parameters used in this model. When plotting figures in dimensionless coordinates for this system, Q_0, a reference value, will be the average of the Q_t values at the minima of the two potential energy wells. The coupling between the system and the bath is described by

$$V = (|e_1\rangle\langle e_1| + |e_2\rangle\langle e_2|)\sum_{\alpha}\sum_{j=c,t} c_{\alpha,j} q_{\alpha,j} Q_j, \tag{6.17}$$

where q_α are the coordinates of individual oscillators in the bath and $c_{\alpha,j}$ is a coupling strength parameter related to the bath spectral density. This coupling describes two statistically independent oscillator baths interacting bilinearly with both the coupling and the tuning modes. To use a classical metaphor, the noise causing decay of vibrations in the Q_c direction is independent from the noise causing decay of oscillations in the Q_t direction. In some other cases, a single bath may be coupled to both coordinates. This represents physics in which noise on both coordinates is perfectly correlated, which is not the circumstances we expect for this system in a disordered solvent. The spectral density of the independent baths, which describes their distributions of harmonic oscillator frequencies, takes a Debye form,

$$\begin{aligned} J_j(\omega) &= \sum_{\alpha} c_{\alpha,j}^2 \delta(\omega - \omega_{\alpha,j}) \\ &= \eta \frac{\omega}{\omega^2 + \omega_b^2}, \end{aligned} \tag{6.18}$$

where η is the coupling strength parameter and ω_b, called the cutoff frequency of the bath, describes the frequency at which the largest proportion of oscillators is located.

Solving for the adiabatic energy surfaces from the diabatic potential energy surfaces constitutes finding the solution to the eigenvalue problem,

$$\begin{bmatrix} h_1 & \lambda Q_c \\ \lambda Q_c & h_2 \end{bmatrix}, \tag{6.19}$$

in order to produce potential energy functions without explicit off-diagonal coupling to each other in the Hamiltonian. This produces an upper potential energy surface which resembles

a cone, hence the conical intersection name, and a lower potential energy surface with a double well structure. The resulting potential energy surfaces are

$$g(Q_t, Q_c) = 0.5 * \Big(E_1 + E_2 + \kappa_1 Q_t + \kappa_2 Q_t + \omega_t Q_t^2 + \omega_c Q_c^2 \pm \sqrt{(E_1 - E_2)^2 + 2E_1 Q_t(\kappa_1 - \kappa_2) + E_2 Q_t(\kappa_1 - \kappa_2) + (\kappa_1 Q_t - \kappa_2 Q_t)^2 + 4\lambda^2 Q_c^2}\Big), \tag{6.20}$$

the upper and lower potential energy surfaces respectively.

The vibrational degrees of freedom for the diabatic states, as they are shifted harmonic oscillators, were modeled with a basis of unshifted harmonic oscillator functions, 40 for Q_c and 110 for Q_t. After Hamiltonian diagonalization, the lowest 240 energy eigenstates were kept for the model. Basis convergence was confirmed by increasing the number of basis functions in both the Q_c and Q_t direction as well as the total number of eigenstates kept in the model until no change in results was observed with an increase.

In our study of geometry's influence on barrier crossing dynamics, we focused in on a single parameter in the above Hamiltonian, λ. The diabatic coupling parameter, λ, drastically influences the shape of the conical intersection, although its precise influence is not easily inferred from the adiabatic energy surface equations. As can be seen in Fig. 6.2, a small value of λ results in a high barrier in the lower potential energy surface whereas a high λ results in a low, broad potential energy barrier.

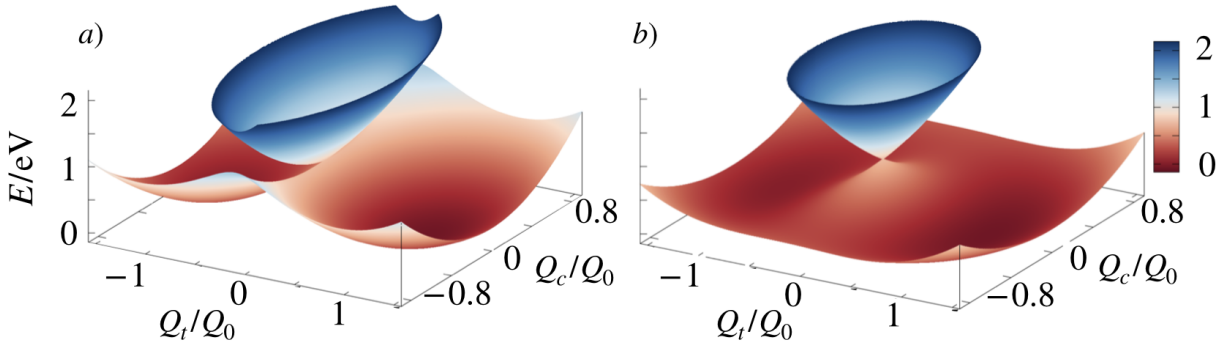

Figure 6.2: Two conical intersection potential energy surfaces, with the blue cone being the upper adiabatic potential energy surface and the red double well structure being the lower adiabatic potential energy surface, for a) a weak coupling $\lambda/\lambda_0 = 0.3$ case, and b) a strong coupling $\lambda/\lambda_0 = 1.3$ case, where λ_0 is a reference value given in Tab. 6.1.

To apply QTPT, we designated the reactants, state A, to be the lowest energy eigenstate in the rightmost, stable well whose minima is approximately $Q_t/Q_0 = 1$ and B to be the lowest energy eigenstate in the leftmost, metastable well whose minima is approximately $Q_t/Q_0 = -1$. Transition path theory analysis produced barrier crossing rates as a function

of increasing λ relative to a reference value, λ_0. The most obvious feature is that the barrier crossing reaction rate depicted in Fig. 6.3 a) increases drastically with increasing λ. This is not at all surprising given that the magnitude of the barrier in the potential energy surface decreases with λ. The Arrhenius classical rate equation implies that barrier crossing rates should be proportional to $e^{-\beta\Delta E}$[169, 166] where ΔE is the activation energy, the difference between the ground state and the transition state energy, classically assumed to be the height of the barrier.

However, in a quantum system there is no reason to assume that the barrier height in the potential energy surface will be equal to the transition state energy due to quantum tunneling effects (or that the Arrhenius equation should apply at all depending on what sort of quantum effects are afoot) and, in fact, transition path theory can easily determine that the transition state is not always at the barrier energy.

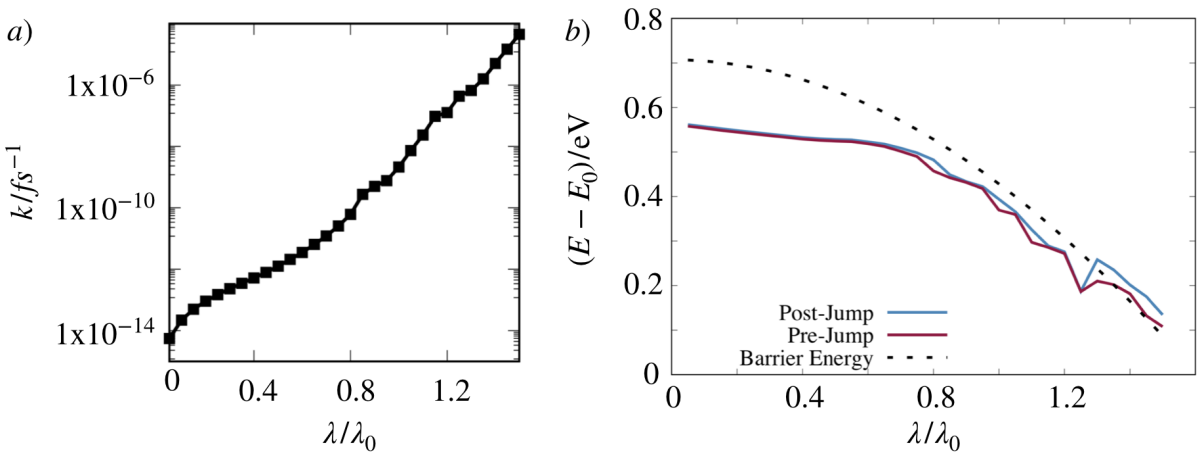

Figure 6.3: a) Barrier crossing rate in the conical intersection as a function of λ/λ_0 showing marked increase of rate with diabatic coupling strength. b) Energies of the committor eigenstates in blue and red compared with the energy of the barrier in dashed black, all relative to the energy of the lowest eigenstate in the system, E_0.

Consider Fig. 6.3 b), which shows the average energy of all the committor eigenstates in the system. To obtain this information, a reactive path ensemble was determined for each value of λ and for each pathway the committor eigenstates were determined. The energies of these committor eigenstates were then averaged, weighted by the amount of reactive flux which passes through the given committor eigenstate pair along the pathway from which they were obtained. At low λ, the energies of the transition eigenstates are well below the dotted black line which indicates the height of the barrier in the system, meaning that most or all of the reactive pathways in this system are tunneling pathways. At higher λ, however, the committor eigenstate energies are approximately at the height of the barrier, meaning

that these systems include many, or all, more classically inclined barrier crossing pathways and dynamics in the system are not dominated by tunneling.

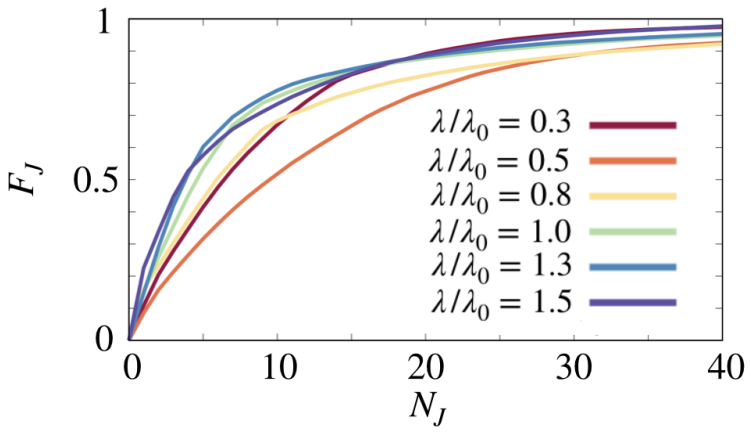

Figure 6.4: Fraction of total reactive flux, F_J, accounted for by the first N_J pathways in the reactive path ensemble, with the pathways in the ensemble ordered by decreasing reactive flux, at several different λ values. Note that only on the order of 10 pathways are required to account for the majority of reactive flux in all cases.

Averages of energies can sometimes be deceiving as outliers could influence the results. The conclusions determined from the averaging can, however, be confirmed easily by inspecting individual reactive pathways and individual committor eigenstate pairs. In determining whether we can inspect a small number of pathways for representative information, the number of pathways in the transition path ensemble and the distribution of flux between them must be scrutinized. Inspecting the dominant pathway for mechanistic information is ineffective if a very large number of pathways, all accounting for similar amounts of reactive flux, exist in the system, potentially representing a multitude of different reaction mechanisms and transition states. We can visualize the distribution by defining the proportion of reactive flux accounted for by each pathway as f_i and the cumulative reactive flux accounted for by the first N_J pathways as $F_J = \sum_{i=1,N_J} f_i/F$ where F is the total reactive flux. In this system, for all λ values, approximately 50% of the total reactive flux is accounted for by the first ten pathways, as is evident in Fig. 6.4, with the dominant pathway accounting for as much as 10% of the total reactive flux and the distributions at different values of λ being largely similar. This degree of dominance by a small number of pathways allows us to analyze the committor eigenstates of the highest flux pathways with confidence that they hold significant meaning.

We first examine the dominant relaxation pathway's progress for several λ. The dominant pathway means the first pathway extracted by Dijkstra's algorithm, the pathway with the maximum reactive flux capacity of any pathway that can be extracted. Inspecting the

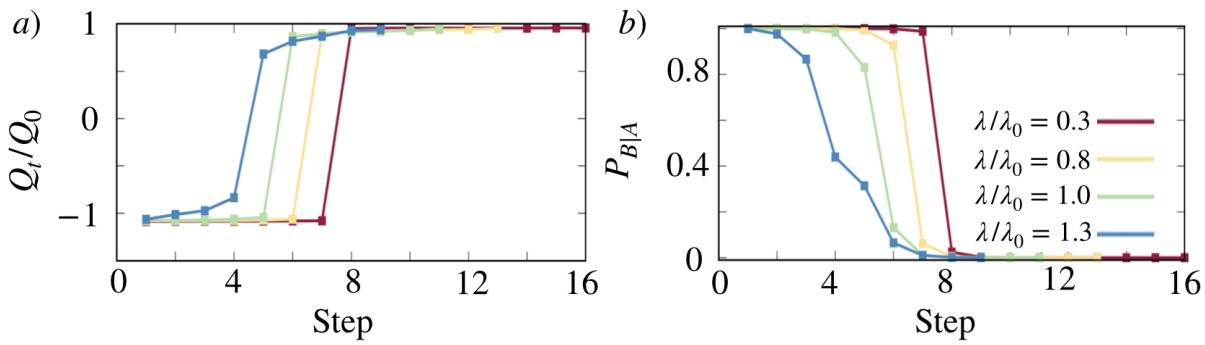

Figure 6.5: a) Eigenstate's average Q_t/Q_0 as a function of steps taken along the dominant reaction pathway identified by QTPT. b) Committor probability to the higher energy well as a function of steps taken along the dominant pathway identified by QTPT. Note the close inverse relationship between the two which identifies Q_t as an acceptable reaction coordinate in this case.

properties of the energy eigenstates along the reactive pathways at different values of λ can impart significant information about the reaction mechanisms and about reaction coordinates. In Fig. 6.5, the average Q_t/Q_0 tuning position and $P_{B|A}$ committor value of the eigenstate are displayed as a function of the number of steps taken along the pathway, with each step constituting a single eigenstate along the pathway. Note that different λ values have dominant pathways with different numbers of steps, ranging from 9 at the highest λ to 16 at the lowest λ. The greater number of steps for lower λ is attributed to the higher barrier in lower diabatic coupling cases, which, intuitively, should require a longer series of jumps to overcome.

The pathways are superficially similar to instanton pathways,[219, 225] which are another means of analyzing quantum transition pathways and rates. The properties remain largely static for long periods, remaining centered in either well, before changing suddenly. Inspecting the committment probability of the eigenstate as a function of step and comparing it to the Q_t/Q_0 as a function of step, it can be seen that tuning position is a good indicator of committment probability in these systems, with the two being strongly correlated for pathways travelling from B to A. It is not a perfect coordinate, however, as exact values of relative position never precisely correspond with the committor value. None the less, for thermal barrier crossing reactions average Q_t appears to be a good reaction coordinate for this system. The behavior of diabatic electronic character with step along the path is not displayed as it provides redundant information; it correlates very well with Q_t and $P_{B|A}$, indicating that diabatic character, too, is a good reaction coordinate for this system.

Some differences in behavior of pathways at different λ are evident from average $P_{B|A}$ in Fig. 6.5, where pathways at large λ change committor values gradually in comparison to the

sudden, sharp changes for low λ cases. This is suggestive of a tunneling mechanism in the low diabatic coupling case, something we expected given the average energies in Fig. 6.3. The high diabatic coupling case, also as expected, appears to describe a classical barrier crossing in which the energy barrier is overcome. Inspection of the wavefunction densities for the

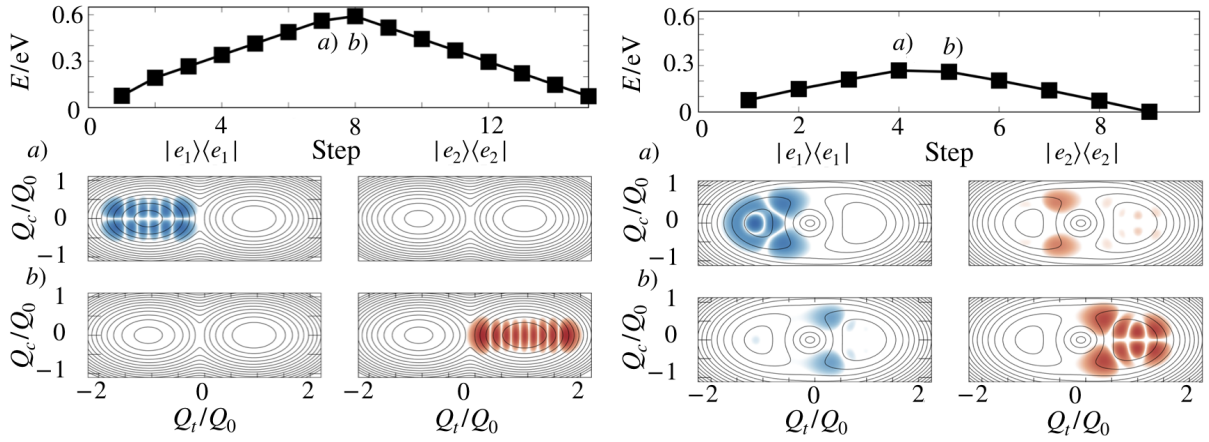

Figure 6.6: The energies of the eigenstates along the dominant reactive pathways at $\lambda/\lambda_0 = 0.3$ (left) and $\lambda/\lambda_0 = 1.3$ (right). In each case, the probability density, $\langle\Psi|\Psi\rangle$, for both committor eigenstates is displayed overlaid on an energy contour plot of the lower adiabatic surface, with the density in the two electronic states displayed separately.

committor eigenstates allows us to confirm our supposition. In Fig. 6.6, the energies at each step along the dominant pathway for a low and high diabatic coupling case are displayed along with the wavefunction densities of their committor eigenstates, both of which are, as expected given their set role as the equivalent of transition states, the highest energy states along the pathway. At low λ, the energies passed through along the dominant pathway remain well below the barrier height of approximately 0.7 eV and the committor eigenstates are nearly completely localized in their respective diabatic electronic state wells showing no significant overlap. Visually, these states resemble highly excited harmonic oscillator wavefunctions. Taken together, this is clearly the deep tunneling pathway other evidence suggested. This is in stark contrast to the representative pathway and eigenstates at large λ, where the energies of the committor eigenstates reach the barrier height of approximately 0.3 eV and are neither localized in a single well nor a single diabatic electronic state. They overlap with each other significantly and concentrate density in the vicinity of the conical intersection's sides, indicating that this pathway traverses around the conical intersection in a manner similar to a classical barrier crossing mechanism, as expected from our other evidence.

A change of regime from transitions occurring by tunneling to transitions occurring by

traversing around the conical intersection appears to take place in Fig. 6.3 at approximately $\lambda/\lambda_0 = 0.8$, where the energies of the committor eigenstates begin to approach the barrier height. We could argue that this change in mechanism is accompanied by a change in the scaling of rate with λ/λ_0, but the trend is too subtle to be considered more than suggestive. Even mild skeptics would not accept our assertion.

Our results align well with the simplified picture proposed by Ferretti and coworkers for extending Landau-Zener type models and the idea of nonadiabatic and adiabatic limits to conical intersections.[92] In the low diabatic coupling limit, nonadiabatic behavior is closely equivalent to that in the Landau-Zener avoided crossing model in which the system evolves along diabatic surfaces and the chance to transition between the two diabatic surfaces is small. In this regime we observe tunneling dominated dynamics. At larger λ, Ferretti and coworkers argue that excitations in the coupling coordinate become important to the process of population transfer, which then becomes much more efficient.[92] Our observation of high λ systems in an apparent adiabatic regime traversing around the conical intersection, with density found at large Q_c values, is largely in accord with Ferretti and coworkers' arguments.

6.3 Nonequilibrium Conical Intersections

At least as important as the thermal behavior of a conical intersection is the relaxation behavior following photoexcitation. There are several criteria required for a photoswitch[71, 42] but the most obvious is that a photoswitch is not a good photoswitch, or perhaps not a photoswitch at all, if it does not efficiently isomerize following irradiation with a laser.[21] As relaxation following vertical photoexcitation is not an equilibrium reaction, it must be addressed with the modified QTPT adapted for this purpose. The definitions of A and B are unchanged, but rather than modelling a thermal reaction between A and B, we vertically excite the system from a harmonic oscillator ground state in some hypothetical electronic state whose minima is at $Q_t = Q_c = 0$ into electronic state 1. In this vertical excitation the initial wavefunction is assumed to be promoted to a higher energy electronic state so quickly that it has no time to change shape and is still the ground state harmonic oscillator wavefunction for the electronic state from which it was excited. This state is easily prepared in a computer because the original basis used to construct the Hamiltonian is the unshifted harmonic oscillator basis; all initial density is placed in the lowest energy vibrational state of electronic state 1 and then the Hamiltonian is diagonalized and the initial state transformed into the basis of the Hamiltonian to carry out simulations.[52]

Addressing an identical conical intersection model to the thermal barrier crossing case, the effect of λ on behavior was again investigated, except the single number of primary importance is now not rate but photoyield, meaning the probability to change diabatic electronic state from diabatic state 1, the higher energy, metastable well, to state 2, the lower energy, stable well, during relaxation. A relaxing trajectory arriving in B indicates no change in diabatic state whereas arriving in A indicates a change in state.

Ensembles consisting of 10000 raw wavefunctions undergoing stochastic dynamics until

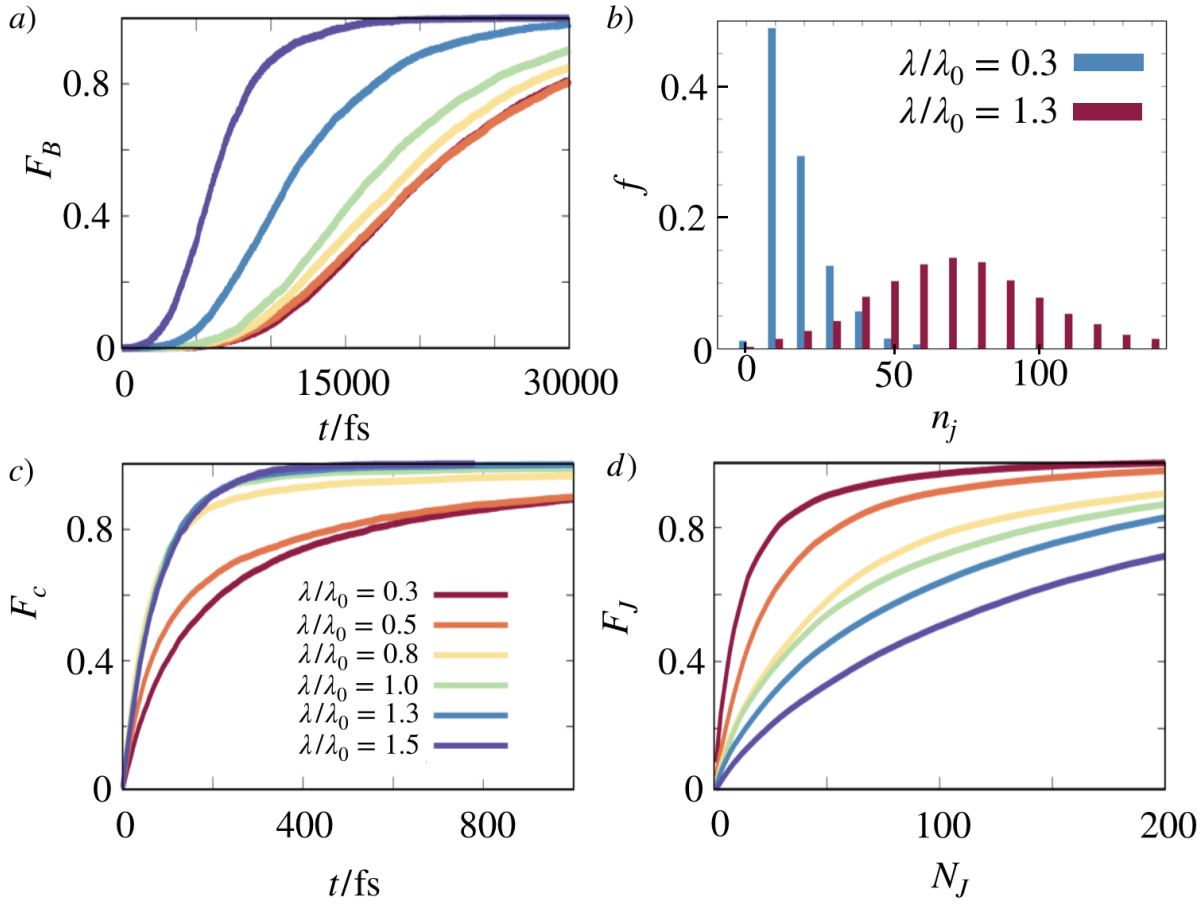

Figure 6.7: a) The fraction of raw trajectories bound for state B in electronic state 1 which have arrived in B, F_B. b) The fraction of raw trajectories, f, at low and high coupling strengths with a number of distinct eigenstate to eigenstate jumps, n_j, in the indicated range, with the location of the scale indicating the low bound of each 10 wide bin. c) The fraction, F_c of raw trajectories which have collapsed to an eigenstate as a function of time for several different diabatic coupling strengths. d) The fraction of cumulative flux, F_J, accounted for by the first N_J processed QTPT trajectories with trajectories ordered by decreasing flux.

they reached either A or B were simulated. All the jumps were catalogued to determine the fluxes. Other statistics about the ensembles were also of interest. Information from the raw jump trajectories themselves can be nearly as illuminating as that obtained from QTPT processing. In Fig. 6.7 a), the fraction of trajectories bound for B which have arrived in B as a function of time, F_B, shows that for the high diabatic coupling cases the full

relaxation process is much faster than for the low cases. The fraction of trajectories that have collapsed from a superposition to a single eigenstate, F_c, in Fig. 6.7 c) shows a similar trend. Somewhat paradoxically, the distribution of the number of distinct intereigenstate jumps in the trajectories, shown for a weak and strong diabatic coupling case in the histogram in Fig. 6.7 b), shows a much broader distribution over number of jumps and a much higher average number of jumps for the strong diabatic coupling cases, indicating that at high λ the system makes many jumps quickly, most of which are not very useful for the relaxation process. In contrast, the low λ system makes many fewer jumps with long waiting times between them but these jumps must be very effective at moving the system towards its inevitable destination.

The larger variety of trajectories at larger λ that Fig. 6.7 b) suggests is borne out in the number of processed relaxation pathways from QTPT which are required to account for a given proportion of reactive flux. In Fig. 6.7 d), the weakest diabatic coupling case only requires a handful of trajectories to account for 50% of the reactive flux, but the strongest diabatic coupling case requires almost 100. There are still dominant relaxation pathways, but the dominant pathways are far more dominant at low λ than at high λ. Taken together, this information from raw trajectories and QTPT processing suggests that higher diabatic coupling relaxation results in more exploration of state space with many ineffective jumps before the system finally arrives at its final destination. Effectively, the relaxing system wanders more when coupling is stronger, already an interesting result.

Photoyields observed in 6.10 a) range from approximately 20% to nearly 65%, with the lowest yields being associated with the lowest λ and the highest yields being associated with the highest λ. The initial plateau of yield reached at approximately $\lambda/\lambda_0 = 0.5$, followed by increasing yield once more, suggests a change in mechanistic regime. We can inspect

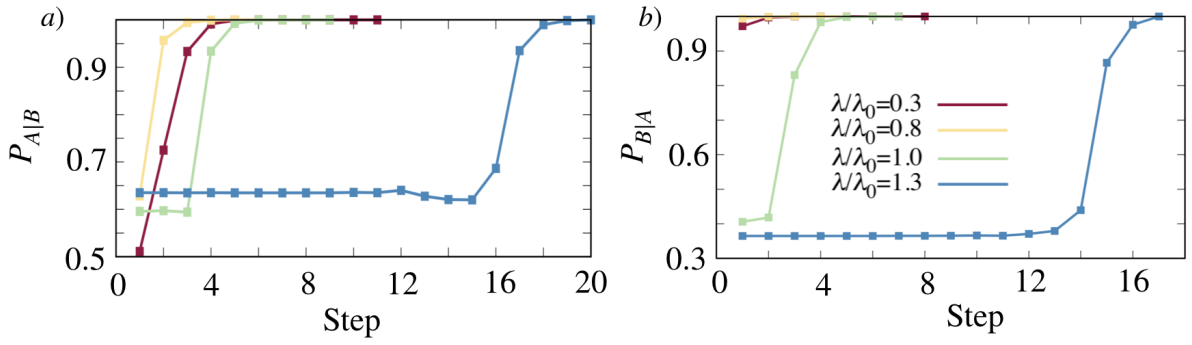

Figure 6.8: The committor value as a function of step along the dominant relaxation pathway following vertical excitation at several different coupling strengths for relaxation pathways bound for A (left) and for B (right).

dominant relaxation pathways for mechanistic behavior as in the equilibrium case, keeping

in mind that there are a greater number of relaxation pathways available at higher λ, meaning we must carefully cross check information obtained from inspecting the dominant relaxation pathway in the larger coupling case to make sure that it is representative of the relaxation behavior as many other pathways of similarly high reactive flux exist. In this case, the dominant relaxation pathway is quite similar to other pathways of high flux in the system in the sense that they are of similar lengths and the last few eigenstates visited in the relaxation are generally similar. In the case of high λ relaxation to B, most large flux pathways share the same post-committor eigenstate and sometimes the same pre-committor eigenstate as well.

Inspection of the committor along dominant relaxation pathways in Fig. 6.8 reveals very different behavior depending on λ for pathways bound for both A and B. At high λ the pathways maintain the nearly instantonic appearance of the equilibrium relaxation pathways, maintaining an approximately constant, moderate $P_{A|B}$ for several steps before transitioning rapidly to a fully committed state with $P_{A|B}$ approaching 1. In contrast, low λ pathways either collapse directly into states which are fully committed if they are destined for B in Fig. 6.8 b) or collapse into states with moderate committor values and proceed quickly to fully committed states without tarrying in any moderately committed states if destined for A in Fig. 6.8 a). This is further evidence that a very different mechanism dominates relaxation at low and high diabatic couplings.

Inspecting relaxation pathway committor eigenstates for mechanistic information is complicated in this case by the lack of true committor eigenstates in most relaxation pathways. Because diabatic state 2 has a significantly lower energy than diabatic state 1, high energy, delocalized eigenstates usually have $P_{A|B} > 0.5$, thus relaxation pathways bound for diabatic state 2 usually undergo collapse from the initial wavefunction superposition into an eigenstate which is already committed to its final destination, but this committment probability is simply the average committment of the system states and is not necessarily meaningful in the same way as a definitive switch between a committor value below and above 0.5. Low λ pathways bound for diabatic state 1 also usually collapse into an eigenstate which is already committed, not because this is the average committment of the system's high energy eigenstates, however. This is a different kind of behavior.

Of four example relaxation pathways displayed in Fig. 6.9, one each to diabatic state 1 and 2 for one low and one high coupling strength, only the high λ relaxation pathway to diabatic state 1 has true committor eigenstates, both of which are displayed. The other pathways display the first eigenstate on the pathway, the state of initial collapse, which can be considered the post-committor eigenstate, along with another interesting eigenstate from further along the relaxation pathway.

Both of the low λ relaxation pathways in the top row of Fig. 6.9 are similarly short and the post-committor eigenstates are largely localized in one well, although the first eigenstate along the pathway bound for diabatic state 1 is more localized, as is to be expected given that this is the higher energy, metastable well, more easily escaped. A state fully committed to this well must necessarily be more localized and likely lower energy than a state fully committed to its rival. Wavefunctions of interest further along the relaxation pathways for low λ are

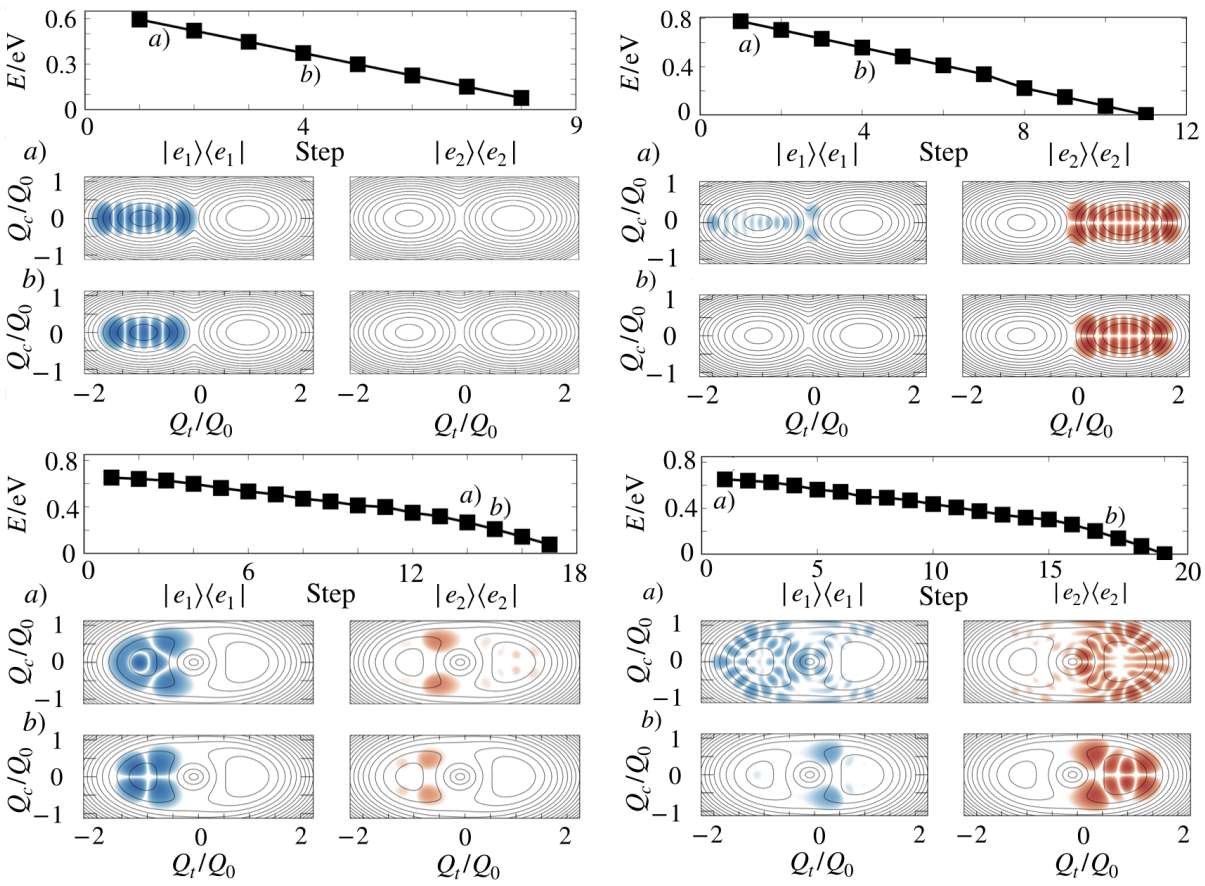

Figure 6.9: Dominant relaxation pathways following vertical excitation into electronic state 1 at $\lambda/\lambda_0 = 0.3$ (top) and $\lambda/\lambda_0 = 1.3$ (bottom) with a destination of electronic state 1 (left) and 2 (right) showing the probability density of the committor eigenstates in the sole case where they exist (bottom left) and the state into which the system collapses as well as another state of interest in all other cases. The densities in the two electronic states are displayed separately, overlaid on energy contours of the lower adiabatic surface.

even more localized. The states of initial collapse can be considered true post-committor eigenstates, with a caveat. The state of the system prior to collapse is unknown as it could be one of an infinite number of different wavefunction superpositions and it is not possible to say whether that superposition was committed prior to collapse or not. Nevertheless, the first eigenstate along the pathways at low λ indicates by its localization that the committor is not high simply because the average committor of the system for high energy eigenstates is high. These states are truly committed. Treating these as post-committor eigenstates is acceptable but when using the energies of the initial state of collapse to determine the average

energy of the post-committor eigenstate, our inability to keep track of the wavefunction and committor prior to collapse could make the post-committor eigenstates appear artificially low in energy and we must keep this in mind. Prior to its collapse into the post-committor eigenstates, dephasing processes and the coherent Hamiltonian are the only influences on the wavefunction. The trajectory's fate is determined by dephasing effects and the collapse itself, which have localized the wavefunction and determined its fate in this low coupling, diabatic limit where crossing between diabatic states is very rare.

For the high λ pathway bound for A, the state of initial collapse is technically the post-committor eigenstate for the relaxation pathway, as displayed in the lower right quadrant of Fig. 6.9 but this state is highly delocalized, appearing like an octopus spread across both electronic states, and although it is technically committed to its final destination, that is merely a result of the lower energy of the stable well biasing the committor of all highly excited states in this system, as previously described. The initial states into which all high λ trajectories collapse, regardless of their final destinations, are generally delocalized like this. Following collapse, it takes on the order of ten or more jumps for the system to become localized in one diabatic well. The designation of the state of initial collapse in the high λ relaxation pathway to diabatic state 2 in the bottom right of Fig. 6.9 is misleading. This can be seen from inspecting the high λ relaxation pathway to diabatic state 1 in the lower left quadrant of Fig. 6.9, the path with proper committor eigenstates. Commitment occurs along this pathway after more than ten jumps, when the system is largely localized into one well. This means that the vast majority of relaxation pathways leading to diabatic state 1 decide their destiny long after initial collapse to an eigenstate, and by necessity pathways bound for diabatic state 2 make their decision here as well by deciding *not* to commit to diabatic state 1. The initial relaxation pathways at large λ are not generally distinguishable by destination until the eigenstate energy is approximately equal to the height of the barrier. The trajectory's fate is determined by dissipation effects and relaxation at the barrier height, not by the dephasing operator or nature of the initial collapse.

Examining the average post-committor eigenstate energies for pathways relaxing into diabatic state 1 is a legitimate exercise because the large λ relaxations have true pairs of pre and post-committor eigenstates for this destination and the post-committor eigenstates for low λ may, at worst, be underestimates of the energy at which committment occurs. The difference in mechanism at different λ is evident in Fig. 6.10 b) where we compare energy of the post committor eigenstates for relaxation to electronic state 1 to the barrier height. At low λ, committment occurs at a very high energy, much higher than the barrier height. At higher λ, there is a proper pre and post-committor eigenstate pair found at approximately the height of the barrier. The change in regime between low λ dephasing mediated committment and high λ dissipation mediated committment occurs at approximately $\lambda = 0.6$, corresponding with the point at which photoyield in Fig. 6.10 a), which had plateaued, begins to increase quickly again, indicating that there is an apparent limit to the efficiency of dephasing mediated commitment where photoyield is concerned.

The observed dependence of mechanism on λ is consistent with previous works exploring the behavior of conical intersections following vertical excitation. A multi-level Redfield in-

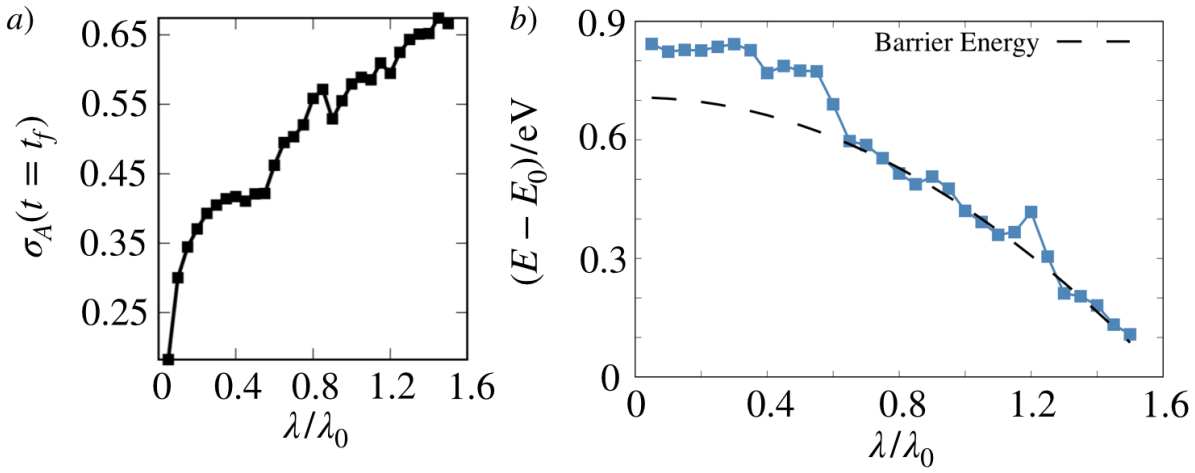

Figure 6.10: a) Photoyield, meaning percentage of trajectories which changed their electronic state from 1 to 2, following vertical excitation as a function of λ/λ_0. The time at which the trajectory concludes is t_f. b) The energy of the post-committor eigenstates, which may be part of a committor eigenstate pair or may be the first state into which the system collapses, as a function of λ/λ_0, compared to the barrier height in dashed black. All energies are relative to the lowest energy eigenstate in the system, E_0.

vestigation by Lan and coworkers found that λ was a limiting factor on the rate of internal conversion, a radiationless electronic state change, of the pyrole-pyridine complex.[136] Doubling λ doubled the rate of internal conversion. This is similar to the trend seen here where λ limits photoyield. Manthe and Köppel studied dynamics in several different conical intersection models, all under closed quantum dynamics conditions following vertical excitation, finding three separate regimes dependent on λ. [158] At low λ they observed a nonadiabatic regime, equivalent to nonadiabatic behavior in the Landau-Zener problem previously discussed,[137, 294, 187] in which wavepackets moved on the diabatic potential energy surfaces. At high λ they observed the adiabatic limit, wavepackets moving on the adiabatic potential energy surfaces. At intermediate regimes, interplays between the two effects arose. Despite studying open systems, we have likewise observed a regime change between nonadiabatic behavior for small λ, dephasing dominated relaxation in which the diabatic state at collapse seals a trajectory's fate, and adiabatic behavior at large λ, dissipation controlled relaxation where the system chooses its fate at the energy barrier and moves between diabatic states easily prior to this point.

6.4 Nonsecular, Nonequilibrium Conical Intersections

The previous inquiries assumed that the secular Redfield master equation is applicable to the conical intersections in question. Given our understanding of the system and the analysis methods, applying the general quantum committor should not change results in the systems previously discussed as they have few near eigenstate degeneracies. However, near energy eigenvalue degeneracies and their resulting quantum coherent effects can be relevant in conical intersections and populations during relaxation calculated using the secular Redfield equations in this system do not correspond perfectly with the nonsecular Redfield dynamics. Secular dynamics usually appear to be smoothed in comparison to nonsecular dynamics, missing little details related to quantum coherences. Previous works have studied dynamics in conical intersections, both experimentally and theoretically, in attempts to understand the role that quantum coherent effects play in their relaxation.[217, 77] To study quantum

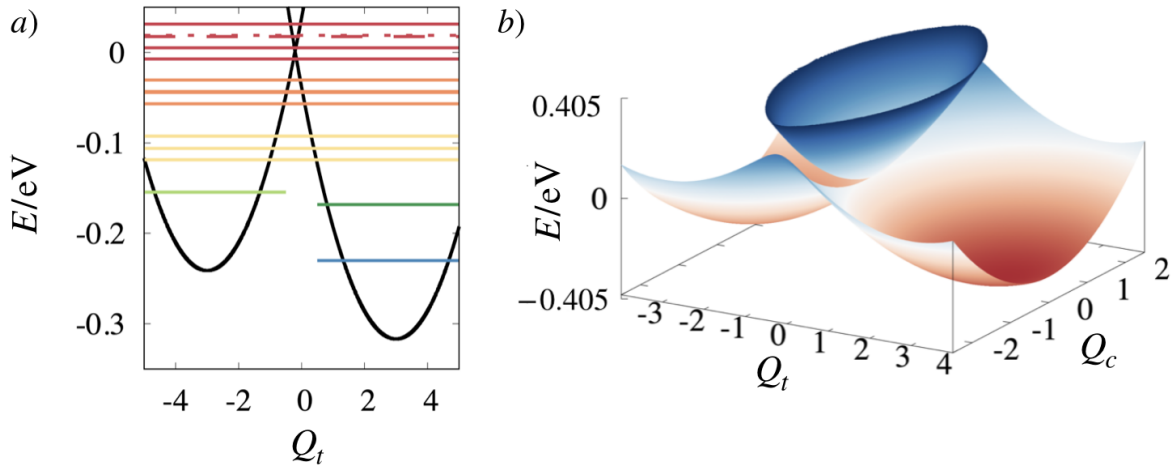

Figure 6.11: a) Energies of the lowest fifteen energy eigenstates in the system, color coded by nonsecular block, with the bottom three eigenstates each constituting a single block, the next block containing three eigenstates, the next four, and the final block five. The black parabolas are the diabatic potential energy curves at $Q_c = 0$. b) The two adiabatic potential energy surfaces of the system, which appears to be a low dibatic coupling limit system. Both Q_t and Q_c are in dimensionless coordinates.

coherent effects, we inspected a conical intersection with the same Hamiltonian structure but different parameters, given in Table 6.1, imitating a system studied previously. [232, 52, 77, 78, 217] The basis for Q_c was given dimension 40 and that for Q_t was given dimension 90. After diagonalization of the Hamiltonian the basis was trimmed down to include only the lowest fifteen energy eigenstates. We then applied the generalized quantum committor

to systematically characterize the roles of quantum coherences on the system's relaxation behavior. The system was organized into a total of six nonsecular blocks. These blocks and their individual eigenstate members are depicted by color coding in Fig. 6.11 a), with Fig. 6.11 b) showing the entire potential energy surface. The lowest three eigenstates are each the sole inhabitants of their respective nonsecular blocks. Eigenstate 3 is the lowest energy eigenstate in the metastable well and constituted the product state B whereas eigenstate 1, the lowest eigenstate in the stable well, constituted the reactants, A. The second lowest eigenstate in the stable well, eigenstate 2, can be included in A without affecting the results in this case. These are equivalent to our previous definitions.

The eigenspectrum for this system reveals a near degeneracy between eigenstates 13 and 14, suggesting that quantum coherences between these two eigenstates may have significant impacts on dynamics. Calculating $V_{B|A}$ for the basis for the density matrix including the lowest fifteen energy eigenstates in this system and focusing in on eigenstates 13 and 14 revealed that $P_{A|B}(|\phi_{13}\rangle\langle\phi_{13}|) \approx 0.85$ and $P_{B|A}(|\phi_{14}\rangle\langle\phi_{14}|) \approx 0.85$. These eigenstates are somewhat delocalized, as seen in Fig. 6.12, with approximately 85% of density in one electronic state and 15% in the other for both eigenstates 13 and 14, meaning the diabatic state character matches nearly exactly with the committor values, a phenomenon seen in the previous conical intersection model in the low coupling, nonadiabatic limit. Meanwhile, $V_{B|A}(|\phi_{13}\rangle\langle\phi_{14}|)$ was very large, indicating significant coherent effects between these two eigenstates which influence the relaxation outcomes in this system. Any superposition of $|\phi_{13}\rangle$ and $|\phi_{14}\rangle$ can be written as $|\Psi_S\rangle = a|\phi_{13}\rangle + b|\phi_{14}\rangle$ and, employing the basis representation of the density matrix, the committor of this superposition can be written as

$$\begin{aligned} P_{A|B}(|\Psi_S\rangle\langle\Psi_S|) =& a^2 V_{A|B}(|\phi_{13}\rangle\langle\phi_{13}|) + b^2 V_{A|B}(|\phi_{14}\rangle\langle\phi_{14}|) + \\ & a^* b V_{A|B}(|\phi_{13}\rangle\langle\phi_{14}|) + a b^* P_{A|B}(|\phi_{14}\rangle\langle\phi_{13}|), \end{aligned} \tag{6.21}$$

and we can optimize over a and b, given the restriction that $a^2 + b^2 = 1$, in order to find the maximum and minimum values of $P_{A|B}$ for any superposition of these two eigenstates. The resulting optimized initial wavefunctions, $|\Psi_A\rangle = -0.36|13\rangle + 0.93|14\rangle$ and $|\Psi_B\rangle = 0.93|13\rangle + 0.37|14\rangle$, achieve nearly 100% committment to states A and B respectively. The symmetry in the wavefunction parameters, accompanied by a change of sign, is expected. A value of 0.93 and 0.36 for a and b maximizes the influence of the coherent effect on the committor. Negating one value and swapping their locations will invert the influence of the coherent effect, minimizing the committor which was previously maximized. The results of the optimization are impressive. Starting from $\sigma(0) = |\Psi_A\rangle\langle\Psi_A|$ in Fig. 6.13 a) relaxation occurs without any density at all arriving into state B. However, over a period of 50000 au, not all density reaches either states A or states B. This phenomenon can be understood by inspecting a graph of the net movement of population over the simulated period. Every time a jump operator moves population from one nonsecular block to another during propagation, this movement is recorded, resulting in a tally of the population flux between all nonsecular blocks which can be transformed to a net flux graph similar to that obtained from an equilibrium QTPT calculation, with one important difference. These

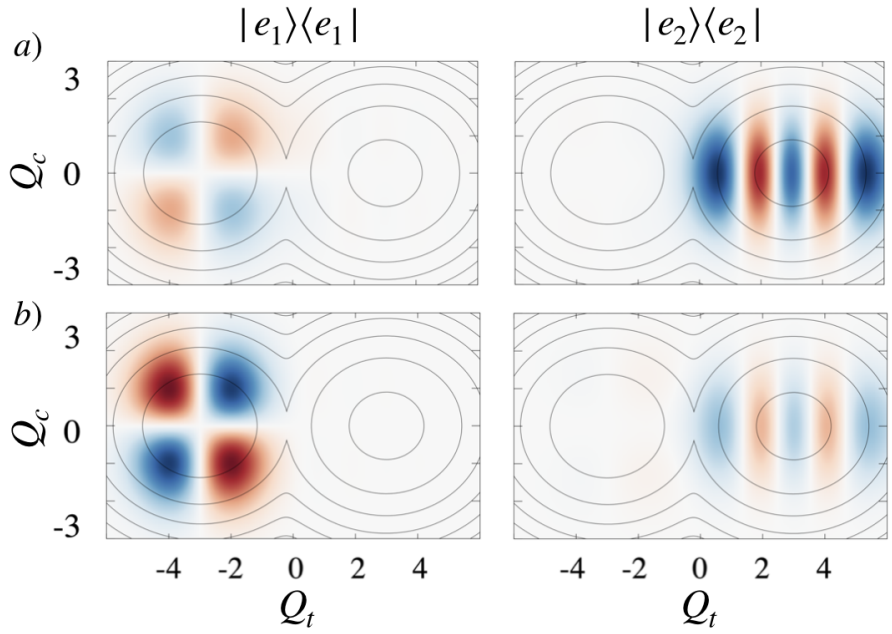

Figure 6.12: The phase of the real part of the wavefunction in both diabatic electronic states, $|e_1\rangle$ and $|e_2\rangle$ for eigenstate 13, a), and 14, b) plotted on the contours of the lower energy adiabatic potential surface. Both states are significantly delocalized.

general committor net flux graphs do not track movement of population between eigenstates but rather between nonsecular blocks which have a hidden internal state. Density arriving in block 5 may arrive in one of an infinite number of different internal states of block 5, with this hidden state determining the population dynamics moving forward. From the flux graph in Fig. 6.13 c) we see that density moves from block 6 to 5 to 4 to 2 to 1, with a significant amount still stuck in 2, but on its way to 1 at the calculation's conclusion. Inspecting the relaxation from $\sigma(0) = |\Psi_B\rangle\langle\Psi_B|$ in Fig. 6.13 b) some similarities and some differences are found. There are two distinct relaxation pathways, one passing through nonsecular block five and one passing through nonsecular block four. The pathway passing through nonsecular block 5 moves through quickly, with virtually no density remaining in this nonsecular block after 50000 au. A significant amount of density passing through block 4, however, does not leave this nonsecular block during the simulation duration. This was initially believed to be the result of a dark state trap from a coherent superposition into which the system had evolved as it does pass through some coherent superpositions which may influence jump rates, but after closer inspection, a population of approximately 0.1 in eigenstate 6, which is the chiefly occupied entry of nonsecular block 4, is close to the equilibrium distribution expected. This does not affect the overall success of the optimization procedure, which has

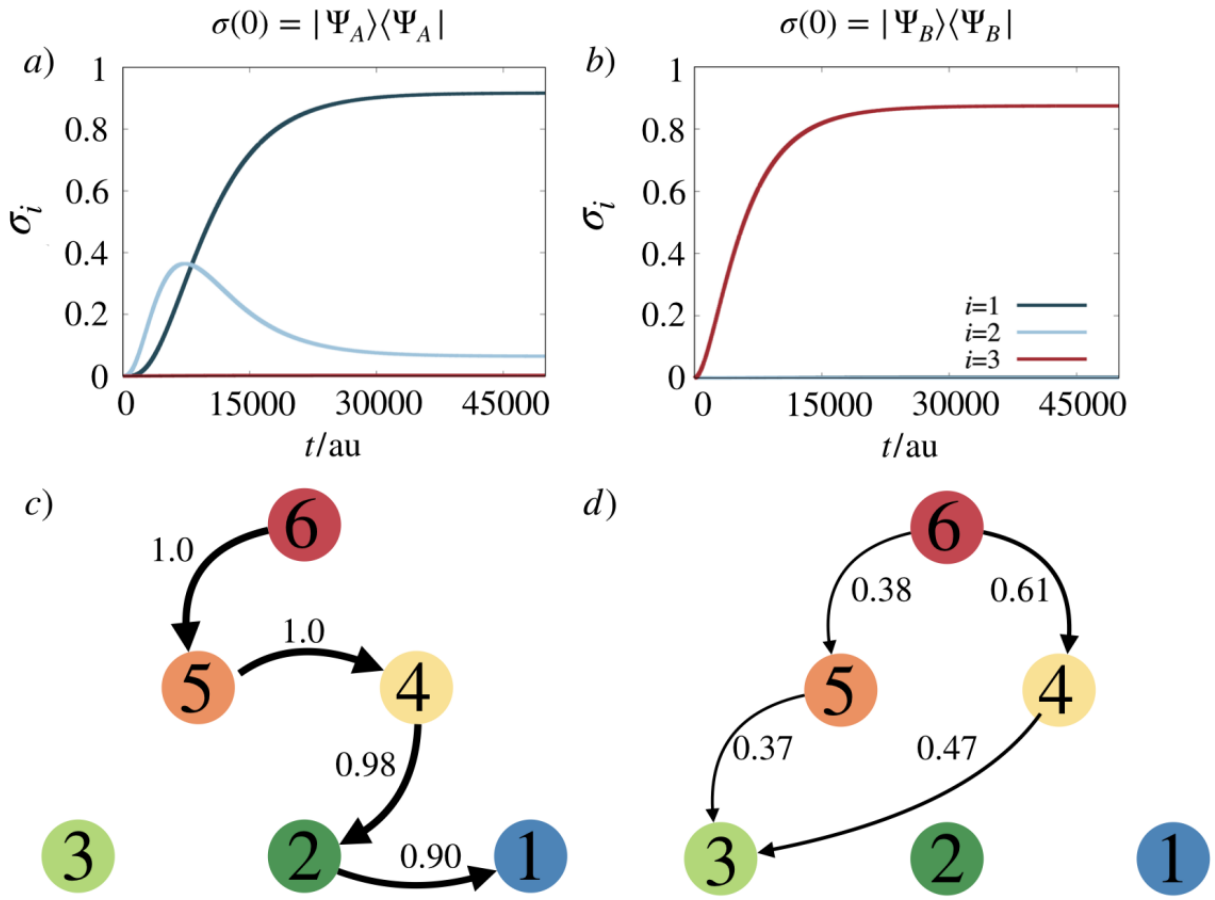

Figure 6.13: a) Populations in the lowest three eigenstates as relaxation occurs from initialization in state $\sigma(0) = |\Psi_A\rangle\langle\Psi_A|$, with σ_i indicating the population in eigenstate i. b) Populations in the lowest three eigenstates as relaxation occurs from initialization in state $\sigma(0) = |\Psi_B\rangle\langle\Psi_B|$, with σ_i indicating the population in eigenstate i. c) A graph showing the transfer of flux through the system for the relaxation process depicted in a). d) A graph showing the transfer of flux through the system for the relaxation process depicted in b).

directed all density into one equilibrium well or the other.

To understand what the optimization procedure has actually achieved, we turn to the initial wavefunctions themselves. It is evident that the optimization procedure has effectively localized the initial excitation into one diabatic state or the other. The wavefunction $|\Psi_A\rangle$ in Fig. 6.14 a) is completely localized in the lower energy well, electronic state $|e_2\rangle$, whereas $|\Psi_B\rangle$ in Fig. 6.14 b) is completely localized in the higher energy, metastable well, electronic state $|e_1\rangle$.

For both optimized initializations, the localization persists throughout the relaxation

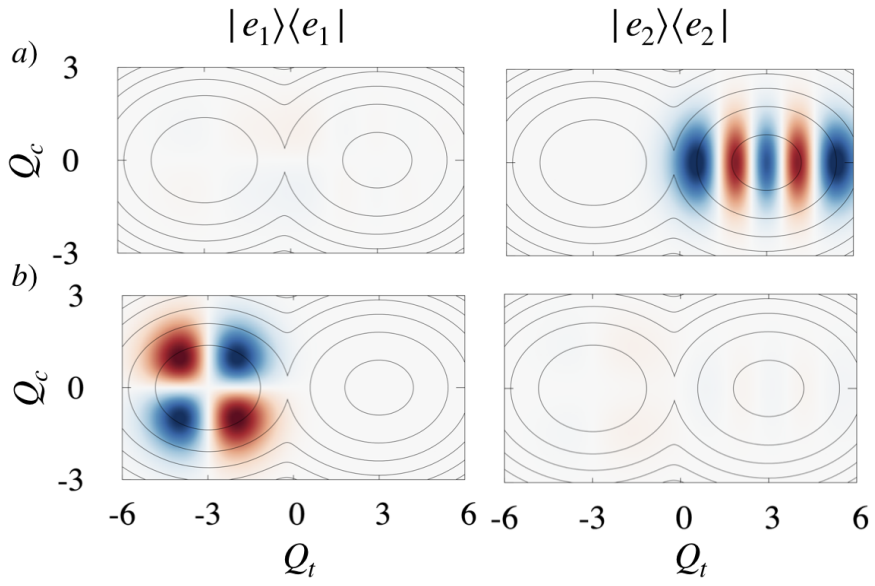

Figure 6.14: The phase of the real part of the wavefunctions for two superpositions formed from eigenstates 13 and 14, both of which are localized in opposite electronic states, plotted on top of the energy contours of the lower adiabatic potential energy surface. a) The wavefunction is $|\Psi_A\rangle$. b) The wavefunction is $|\Psi_B\rangle$.

process. The most dramatic part of the relaxation happens very quickly, in the sense that by 15000 au the vast majority of the density has arrived in states A or B respectively. Inspecting the wavefunction density for both pathways over the first 50000 au in Fig. 6.15, the fast relaxation is evident in changes taking place over the short time period, all of which serve to localize the density further in its well. In both cases, the relaxation dynamics further confirm that the purpose of our initial optimization was only to localize the wavefunction in the desired state, where it will remain, relaxing quickly towards the bottom of the selected well. Our initial wavefunction choice does not appear to influence dynamics in any other way.

In this apparent low coupling, nonadiabatic limit conical intersection where changing diabatic state is rare, it is unsurprising that localization of the initial states is necessary to optimize the committor. Moreover, even in a system behaving adiabatically, optimization is expected to achieve the same result, electronic state localization, if the eigenstates we are targeting are approximately at the height of the barrier. The barrier is where dissipation decides the trajectory's destination. We learned this from our previous exploration of relaxation following vertical excitation in high diabatic coupling cases, so localization, regardless of whether the system is behaving adiabatically or nonadiabatically, would likely be the

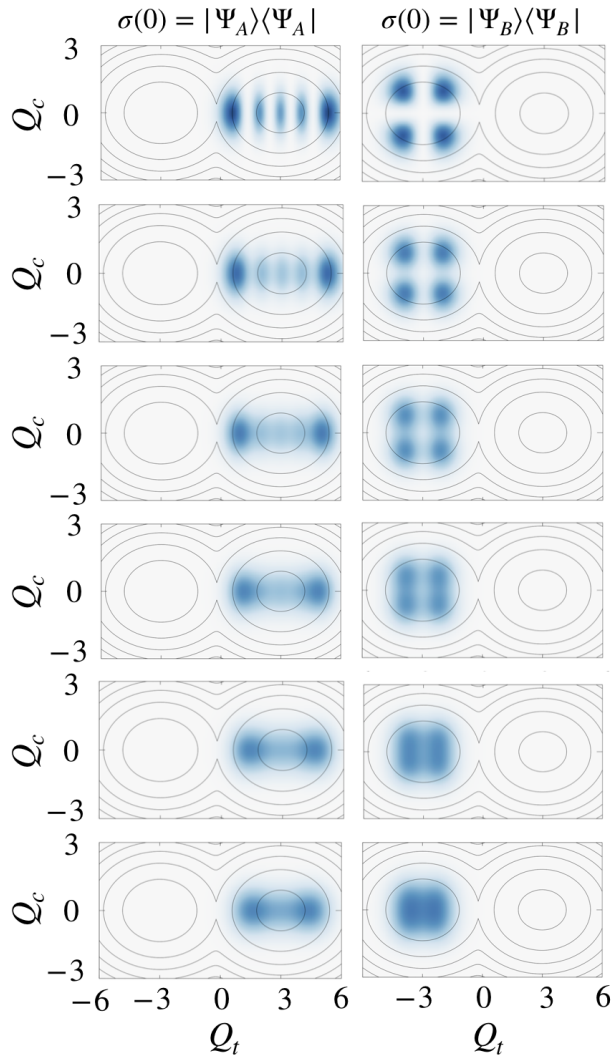

Figure 6.15: Probability densities as relaxation takes place following excitation into $\sigma(0) = |\Psi_A\rangle\langle\Psi_A|$ (left) and $\sigma(0) = |\Psi_B\rangle\langle\Psi_B|$ (right) at times, from top to bottom, of 0, 10000, 20000, 30000, 40000, and 50000 au superimposed on an energy contour of the lower adiabatic potential energy surface.

outcome of committor optimization for coherent eigenstate superpositions near the barrier height.

This might not be the case when treating eigenstates well above the energy of the barrier and eigenstates 13 and 14 are certainly not the only pair of nearly degenerate states where quantum coherent effects lend themselves to committor optimization. In this system eigenstates 19 and 20 are also nearly degenerate, delocalized states, both spatially and elec-

tronically. This delocalization is likely a necessity for nearly degenerate states at or above barrier height in conical intersections. Although optimization of this higher energy pair for this weak diabatic coupling case would also likely arrive at a solution in which the initial states were localized into diabatic wells, it is unclear what the result of optimizing the committor for a superposition of eigenstates like 19 and 20 would achieve for a high diabatic coupling case. It is not even clear whether it would be possible to optimize the committor at all using a superposition of a pair of high energy, nearly degenerate states in a system behaving adiabatically. This is a topic for future inquiry.

6.5 Implications for Photoswitches

Low photoyields are associated with nonadiabatic behavior and deep tunneling barrier crossing reactions. Higher photoyields are associated with adiabatic behavior, dissipation mediated committment and thermal isomerization by traversing around the conical intersection. This is a much faster process than the deep tunneling behavior observed in the nonadiabatic regime. This means that it is difficult to achieve a high photoyield and a long lived metastable state, at least for the subset of systems investigated here. This holds some parallels with challenges observed in experimental works. Researchers attempting to optimize the behavior of photoswitches for engineering applications have noted that it is difficult to assure addressability of the photoswitch, meaning the ability to excite only one isomer of the molecule, while also guaranteeing a long lifetime of the metastable state.[42] Addressability is a complex function of the molecule[71] influenced by many factors not captured by our model so it is difficult to say whether our observed conundrum, in which high photoyield results in short metastable state lifetimes, demonstrates the same phenomenon. Recent inquiries have had some success in engineering photoswitches with high addressability and very long metastable state lifetimes, however, indicating that this trade off is not inescapable,[42] so perhaps we might escape the confines of ours as well. Our investigation modified only a single parameter of the conical intersection potential energy surface and others influence the behavior at the conical intersection. It is possible that a high λ in conjunction with larger values of κ, shifting the wells further from $Q_t = 0$, might result in longer lived metastable states achieved alongside high photoyield, although this is not certain. If the mechanisms of reaction do not change with a modified κ which increases the width of the barrier, nonadiabatic limit tunneling mechanisms would certainly slow down, but adiabatic traversal mechanisms at high λ might not be slowed significantly, which would not help us to escape from our trade. It is also possible that increasing κ would result in mechanistic changes decreasing the photoyield at high λ, again thwarting our attempt to escape our trade off. This warrants further investigation.

Our final inquiries into controlling relaxation outcomes suggest an alternate means by which to overcome this problem: tailor an initialization state using quantum interference effects in order to optimize relaxation destination, and hence photoyield, while maintaining a low λ, high barrier, nonadiabatic limit system with a long lived metastable state. Ex-

perimentalists have studied quantum control in conical intersection traversal[13] though this often involved complicated feedback control mechanisms using machine learning.[26] Many theorists have worked on means of determining ideal laser control pulses to guide systems through conical intersections to desired states[1, 146]. Our work provides a new, powerful means for planning quantum control protocols, in conical intersections and elsewhere. It must be noted that individual eigenstates in the system where we demonstrated coherent control are already completely committed to one diabatic state well or the other. Whether reaching a coherent superposition initialization or a single eigenstate initialization would be a more convenient means for exciting any given system experimentally is unknown, so it is unclear how useful this optimization approach could be in practice in real systems. None the less, the information about the system provided by the general quantum committor is extremely useful for mechanistic studies and the method for obtaining it is generally applicable to any quantum system, provided that a suitably descriptive model of the system can be obtained in the partial secular Redfield theory formalism. Moving forward, there is a great deal more information that these methods can offer for systematic studies of mechanisms around conical intersections.

Parameter	Nonsecular System (atomic units unless specified)	Secular System (atomic units unless specified)
β	1052.584413	1052.584413
ω_b	0.01	0.004836
η	0.1 (unitless)	$9.345 * 10^{-9}$
E_1	-0.00139	0.1547
E_2	0.00139	0.1448
ω_c	0.004116	0.0004336
ω_t	0.002279	0.0002720
κ_1	-0.006836	0.01316
κ_2	0.006836	-0.01158
λ or λ_0	0.00091153	0.009628

Table 6.1: Parameters employed during simulation of the conical intersection models. The secular system is the first system, modeled via QTPT. The nonsecular system is the second system, addressed with the general committor definition. Note that these simulations are carried out with $Q_{c,t}$ and $P_{c,t}$ in dimensionless units.

Chapter 7

Quantum Committor Theories for Polaritons

> 'Madam, I quite understand your feelings myself–it takes ages to get any real coherence out of them. Alas, that is the curse of academia...'
>
> Terry Pratchett, *Judgment Day: Science of Discworld IV*

Throughout the 1970s into the early 1980s, advances in laser technology triggered a flurry of novel research and the rise of a new field that hoped to spawn a revolution in chemistry with laser-catalyzed reactions.[295, 141] Several different forms of laser catalysis arose in small molecules, yielding mixed success.[34, 98, 99] The white whale, however, was selective bond breaking in large molecules. Researchers proposed that by tuning a laser to excite an individual bond in a large molecule, this bond could be severed. It was referred to as a "chemists dream" by Nobel Prize winner Ahmed Zewail, writing for *Physics Today* in 1980.[295] However, in order for this method to prove successful, it was not just the power of the laser that was important, but the behavior of the target molecule as well. Energy placed in a target bond must stay there for a significant period of time as photons are absorbed. If energy placed in one bond of the molecule redistributes quickly throughout the other modes, no selectivity can be achieved.[266] Theoreticians and occasionally experimentalists argued back and forth about whether laser selective chemistry in large molecules was possible, eventually reaching the disappointing conclusion that no, in the general case it is not possible. Energy redistributes throughout the molecule's degrees of vibrational freedom exceedingly quickly and no selectivity is achieved by focusing a laser on one bond's frequency in particular.[35, 40, 199] Recent advances, however, have suggested an alternative means by which chemists might achieve the dream of selectively breaking bonds in large molecules.[1]

[1]This chapter is based on work submitted to *The Journal of Physical Chemistry Letters*[9] and arXiv.[8]

7.1 Polaritons

Polaritons are light-matter hybrid states, quasiparticles displaying characteristics of both their components. A polariton contains one photon degree of freedom as well as a matter degree of freedom. This matter degree of freedom may be an exciton, meaning an electron-hole pair in a solid material, a phonon, meaning a vibrational mode in a solid, a vibrational mode in a molecule, or a plasmon, meaning a collective mode of charge density oscillation.[239] A cartoon showing the formation of a polariton is depicted in Figure 7.1. In this case, hybridization takes place between a proton vibrational mode where the gaps between energy eigenstates are equal to the gaps between energy eigenstates for a photon. The proton, which has an associated electron which is not pictured for simplicity, is conceptualized to be moving freely between two negatively charged ions which are fixed at their respective locations.[251] This results in an approximately quartic potential energy surface with frequency ω_s obtained by making a harmonic approximation to each of the wells. When ω_s and the natural frequency of a microcavity, ω_c, meaning the frequency of the photon which would be present in the cavity were there a photon in the cavity, are approximately equal, hybridization of the light and matter state occurs. This produces two states of mixed light-matter character. The energy difference between the two formed polariton states, the upper and lower polariton states in purple in Fig. 7.1, is called the Rabi splitting, $\hbar\Omega_R$, where Ω_R is the Rabi frequency.[224] Larger Rabi splittings are associated with stronger light-matter coupling and a greater degree of mixing of photon and proton character. Numerous ap-

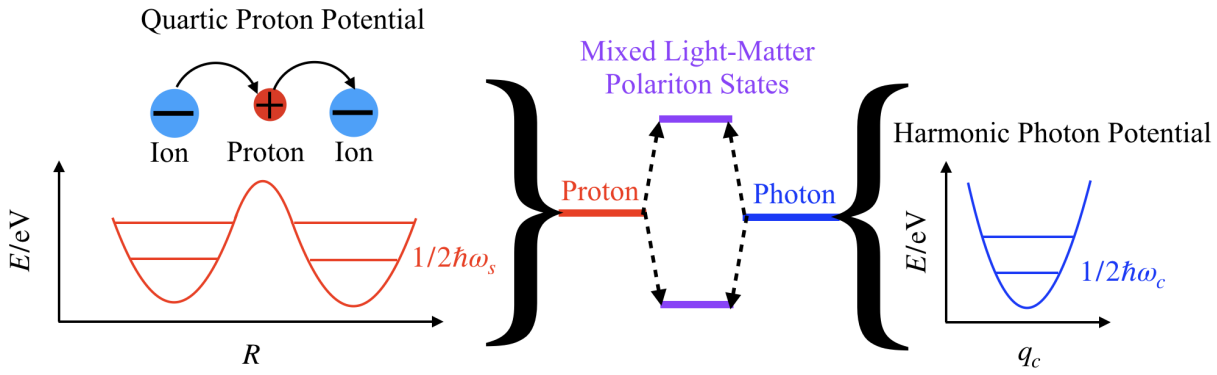

Figure 7.1: A cartoon of the formation of polariton light-matter hybrid states from resonance conditions between a proton vibrational mode and a photon vibrational mode whose frequencies, ω_c for the photon and approximately ω_s for the proton, are nearly identical.

plications for polaritons have been suggested in nanotechnologies, where exciton polaritons may be applicable for high temperature Bose-Einstein condensate engineering and efficient lasing.[147, 80, 296, 212] Polaritons have been demonstrated to enhance photochemical reactions,[185] non-radiative transfer between molecules at significant distances,[300] and charge

conductivity.[200, 224] Polariton effects are regarded as promising frontiers of research in many chemical fields.

Polariton Rate Modification

The effect of interest to us is polaritonic resonance rate modification. Several papers have reported that confinement of a molecule to a microcavity in which the vacuum photon mode is in resonance with a vibrational mode of the molecule, meaning the bond frequency matched the cavity frequency, resulted in modulation of the rate of bond breaking reactions in that system. This sometimes resulted in an increased rate, sometimes resulted in a decreased rate, and allowed inversion of the ratio of molecules produced in a case in which there were two competing products for the reaction.[267, 268, 140] These reactions occur in dark microcavities, so the problems encountered with laser catalyzed reactions half a century ago are not relevant. However, the physics underlying this rate modulation is not well understood.

The suppression or enhancement of rates observed on resonance conditions in polaritonic systems has been a subject of a great deal of debate. Many studies have attempted to apply classical transition state theory[43, 299, 144, 101] to understand the change in rates. Others have applied Grote-Hynes theory or quantum transition state theory. Grote-Hynes theory[112] is a classical theory able to capture certain kinds of dynamical recrossing effects, with some researchers proposing that dynamical caging, an effect of the potential energy surface geometry in conjunction with thermal bath effects,[145] is a potential source of polariton resonance suppression. Others employed quantum transition state theories which address tunneling effects using instanton path integral approaches.[283, 44] However, none of these approaches have recovered the proper sharp resonance behavior, whether addressing a single molecule or attempting to study an ensemble in a microcavity and considering the collective effects for the billions of molecules present.[157, 144, 43, 101, 149, 145, 75]

The failure of the classical studies indicates that quantum mechanics of some flavor is likely afoot in these systems. Fully quantum investigations have indicated that the rate suppression is probably a quantum dynamical effect.[149] Even quantum statistical effects, implemented by ring polymer molecular dynamics, do not appear to be sufficient to explain the observed resonance rate modulation effects.[94] The potential for using polaritonic rate suppression or enhancement to selectively break bonds in large molecules is intriguing. An understanding of the mechanism behind the suppression could be extremely helpful for designing reactions to selectively break bonds, and as this appears to be a fully quantum dynamical effect it is a good proving ground for QTPT.

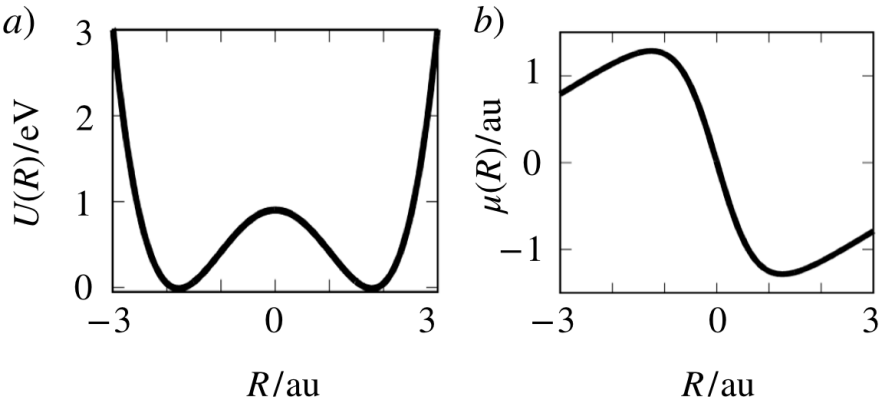

Figure 7.2: a) The quartic potential energy surface of the polaritonic system. b) The matter dipole function of the polaritonic system.

7.2 Secular Polariton Systems

A simple polariton model was selected to apply QTPT. The model in question is similar to the Shin-Metiu model pictured in Fig. 7.1.[251] The Hamiltonian is given by[145]

$$H_S = P^2/(2M) + U(R) + p_c^2/2 + \frac{\omega_c^2}{2}\left(q_c + \sqrt{2/(\hbar\omega_c^3)}\chi\mu(R)\right)^2, \tag{7.1}$$

in atomic unites where P and R are the momentum and position of the proton, $U(R)$ is the quartic potential energy surface of the proton, $\mu(R)$ is the dipole moment of the proton, p_c and q_c are the momentum and position of the photon, ω_c is the frequency of the photon, and χ is a parameter influencing the coupling strength. The matter dipole and potential are displayed in Fig. 7.2 b) and a) respectively, showing the quartic well which represents $U(R)$ along with its corresponding dipole operator. In our simulations $\hbar = 1$ but in this particular case it is included explicitly in the Hamiltonian for clarity. This kind of Hamiltonian is called the Pauli-Fierz Hamiltonian, a formulation in which light and matter coordinates are treated identically.[205, 76] This approach includes several approximations including the long wavelength approximation and the dipole approximation for addressing the electromagnetic, photon, field in the cavity, but maintains the dipole self-interaction term, the term in which $\mu(R)^2$ appears.[214, 56] The dipole self-interaction term is sometimes eschewed despite being important to modeling many kinds of physics. Neglecting it in this case would artificially modify the potential energy barrier height leading to incorrect results.[145]

The light-matter coupling strength for this Hamiltonian, η_c, is proportional to χ/ω_c,[145]

$$\eta_c = \frac{\partial\mu(R)}{\partial R}\Big|_{R_0}\sqrt{\frac{\hbar}{2\omega_s M}}\frac{\chi}{\hbar\omega_c}, \tag{7.2}$$

where M is the proton mass and ω_s is the approximate harmonic frequency at the bottom of the quartic wells defined by $U(R)$. The minimum of the quartic well is given by R_0. The derivative term involving the dipole of the proton is evaluated at the minimum of the quartic well. In our formulation of this problem, a very small linear bias is added to the potential energy surface in order to break the degeneracy in the system which would result in wavefunctions being delocalized across both wells. Breaking the degeneracy results in two R_0 values but the difference between them is too small to be of note. Precise definitions for $U(R)$ and $\mu(R)$ are found at the end of this chapter.

The system is coupled to the bath linearly through the proton coordinate R,

$$H_I = \sum_k c_k R_k q_k \tag{7.3}$$

where q_k are the positions of the bath oscillators described and c_k are coupling constants, all specified by Ohmic spectral density,

$$J(\omega) = \sum_k c_k^2 \delta(\omega - \omega_k) = \eta \omega e^{-|\omega|/\omega_b}, \tag{7.4}$$

where η is the system-bath coupling strength and ω_b is the bath cutoff frequency. Because there is no bath coupling to the photon coordinate, q_c, there is no cavity loss in this system, which would physically imply that the mirrors on the cavity are perfect, reflecting 100% of incident light. This is never the case, but this model should be appropriate for the low cavity loss limit. Complete parameter information for this model is found in Table 7.1.

With this minimal polariton model we use QTPT to search for resonance rate suppression effects by holding η_c constant while adjusting ω_c and calculating the rate of barrier crossing for each adjustment. Changing the photon frequency has a dramatic effect on the shape of the potential energy surface as demonstrated in Fig. 7.3, where increasing ω_c results in a steadily narrower, compressed potential surface. However, this gradual change gives no indication as to why any kind of resonance effect would arise in this system, save potentially Grote-Hynes dynamical caging arguments which have not, previously, been found to support the sharp resonance behavior observed by experiment[268] but rather broad rate suppression.[145] Designating the lowest energy eigenstates in each well, eigenstates 1 and 2, as our reactants A and products B respectively, we can apply equilibrium QTPT straightforwardly. The Markov state model used $\tau = 2500$ au, with calculations carried out with τ at half and twice this size producing indistinguishable results and hence indicating that this was an acceptable delay time which was neither capturing double jumps nor suffering from numerical problems. The final basis contained 200 eigenstates, but the initial Hamiltonian was constructed with a harmonic oscillator basis of dimension 70 for the photon. The proton was described with a Colbert-Miller Discrete Variable Representation (DVR) basis[57], in which basis functions are proportional to $sinc(x) = sin(x)/x$ centered along the R coordinate at intervals of δ. The DVR basis had dimension of 101 and $\delta = 0.1$ au. This means that a *sinc* function was centered at $R = -5.0$ au, -4.9 au, -4.8 au, ... 4.9 au, 5.0 au. The

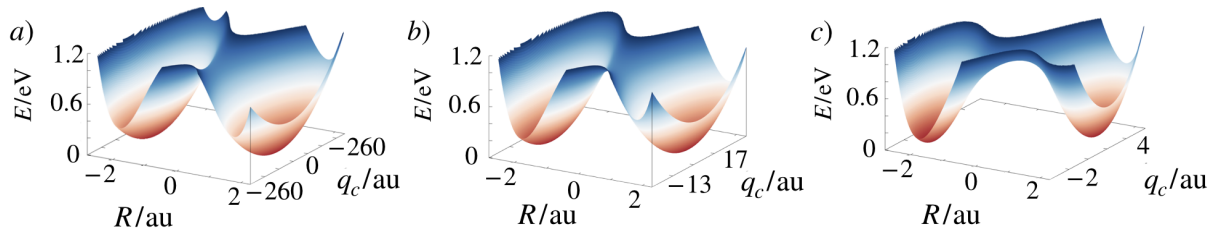

Figure 7.3: Potential energy surfaces, $H_S - p_c^2/2 - P^2/2M$ showing the polaritonic system as ω_c/ω_s changes with a) $\omega_c/\omega_s = 0.1$, b) $\omega_c = \omega_s$ and c) $\omega_c/\omega_s = 10$.

Colbert-Miller DVR basis is popular because there is an analytical form for the approximate kinetic energy operator and the potential operator is diagonal with the value for each basis function being simply the potential energy evaluated at the R at which the *sinc* basis function is centered. This makes it very easy to calculate the Hamiltonian in this basis. Basis set convergence was tested to make sure there was sufficient resolution, that δ was sufficiently small, and that enough functions were used to cover all relevant regions of R.

In Fig. 7.4 a) QTPT identified resonant rate suppression at approximately $\omega_c/\omega_s = 0.9$, which is not precisely the $\omega_c/\omega_s = 1$[268] observed in experiment. However, the quartic potential modeled here only has an approximate harmonic frequency, and it was possible to identify energy gaps in the eigenspectrum of the proton model completely decoupled from the photon,

$$H_S = P^2/(2M) + U(R), \tag{7.5}$$

which match exactly with the photon frequency at $\omega_c/\omega_s \approx 0.9$, the precise resonance condition under which polaritons are expected to form. It should be noted that these resonance gaps occur between excited energy eigenstates, not the ground state and first excited state, which is why the approximate harmonic frequency differs to such a large degree from the resonance frequency. This system has a very high barrier in comparison to k_BT and thus it is not at all surprising that resonances involving higher energy eigenstates might be involved in the reaction, although this occurrence alone does not provide us sufficient information to understand what, exactly, causes the resonance rate suppression observed.

The rate suppression in Fig. 7.4 a) is most noticeable for the highest light-matter coupling strength in black, which shows multiple peaks, meaning that several different eigenstate pairs are likely involved, each forming a resonance with ω_c in turn as ω_c/ω_s is adjusted. It is not surprising that the lower coupling cases show fewer resonances. The larger the light-matter coupling strength, the more disparate the gap in the uncoupled proton eigenspectrum can be from perfect resonance with ω_c while still allowing for light-matter hybridization. At the smallest coupling strength in red, only one extremely sharp resonance rate suppression condition is observed, the nearly perfect match between ω_c and an eigenstate gap found at $\omega_c/\omega_s \approx 0.9$.

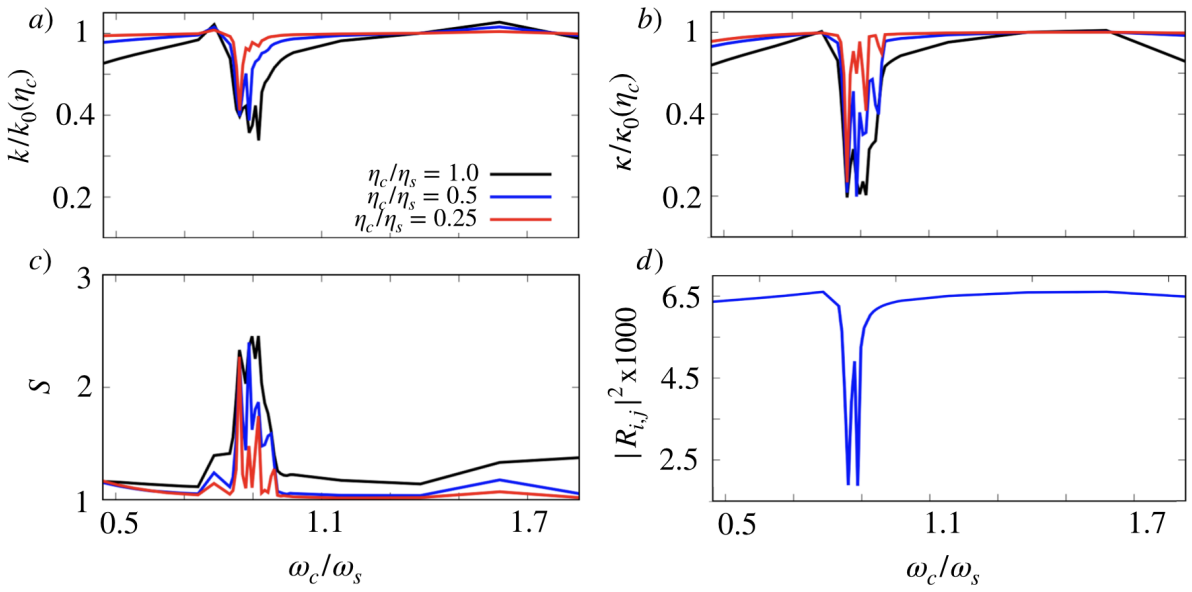

Figure 7.4: a) The barrier crossing rate in the polaritonic system as a function of ω_c/ω_s at three different light-matter coupling strengths, with the default $\eta_s = 0.02$. Note that this system is in the low friction, energy-dissipation bounded, limit if we consider the photon as a form of friction interacting with the proton. Increasing the value of η_c, the friction, results in an increase in barrier crossing rate. This necessitates normalization by a light-matter coupling dependent factor, $k_0(\eta_c)$, in order to compare rates for different light-matter coupling strengths on the same set of axes. b) The transmission coefficient, κ, normalized by $\kappa_0(\eta_c)$, for the dominant reactive pathway of the barrier crossing reaction as a function of ω_c/ω_s at three different light-matter coupling strengths. c) The path entropy describing the variety of different reaction pathways in the system for three different light-matter coupling strengths. d) The element of the system portion of the system-bath coupling operator, $|R|^2$, which links the committor eigenstates for the dominant transition pathway as a function of ω_c/ω_s. The reference values of $k_0(\eta_c)$ and $\kappa_0(\eta_c)$ are displayed in Table 7.3.

In order to understand the source of resonance rate suppression, we inspect the dominant transition pathways on and off resonance. In this system, the dominant barrier crossing pathways identified by QTPT carry upwards of 30% of the total reactive flux, sometimes even as much as 70% of the total reactive flux, so the dominant reaction pathways' committor eigenstates provide a representative account of the reaction mechanisms in these systems. In Fig. 7.5, three pairs of committor eigenstates are shown together on contour plots of the potential energy surfaces at three difference ω_c/ω_s. These are clearly the committor eigenstates of deep tunneling pathways, evident because they are localized in opposite wells

and show no overlap with each other, allowing pairs to be conveniently plotted together on a single energy contour map. The off resonance cases in a) and c) look quite similar. Both show wavefunction nodes which are close to vertical. They resemble harmonic oscillator eigenstates for R, excitations purely in the proton coordinate. The on resonance case in b), however, is very different. The angle of the wavefunction node is close to 45°, or not even a proper angle at all, with the wavefunctions appearing more like Yin-Yang symbols than harmonic oscillator wave functions. This is an actual polariton wavefunction, excitations shared between photon and proton coordinates, meaning that QTPT has identified that formation of a polariton wavefunction is associated with suppression of the thermal barrier crossing rate. This is already a success, proof that quantum mechanical methods, or rather

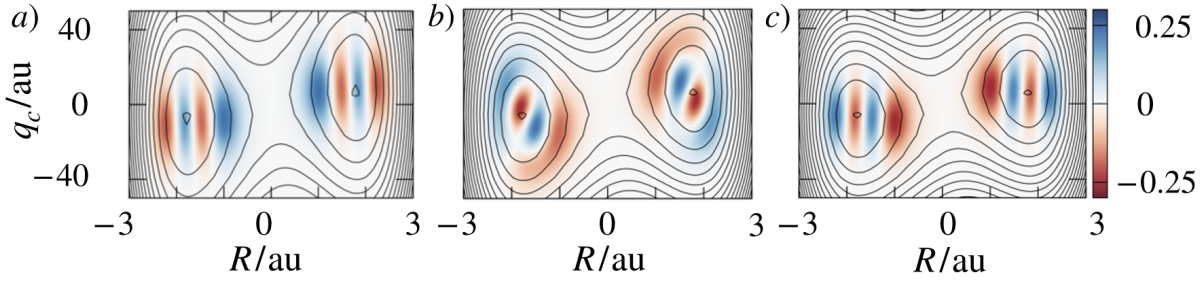

Figure 7.5: The phase of the real part of the wavefunction for the committor eigenstates, pre and post-committor plotted together on the same energy contour map, for the polaritonic system when a) ω_c/ω_s is below resonance, b) ω_c/ω_s is on resonance and c) ω_c/ω_s is above resonance. Energy contours are 0.01 au apart.

QTPT in particular, are able to model polaritonic rate suppression phenomena which match qualitatively with experimental observations. However, QTPT is able to provide much more, enough information for us to precisely explain the cause of the rate suppression.

The first clue is provided by κ for the dominant reaction pathway in Fig. 7.4 b) where $\kappa = k/\exp[-\beta\Delta E^\dagger]$ is a transmission coefficient calculated from k, the barrier crossing rate, and $\Delta E^\dagger$, the activation energy. The activation energy is the difference in energy between the lowest energy eigenstate and the higher energy of the committor eigenstates, be that the pre or the post-committor eigenstate, on the reactive pathway. The transmission coefficient quantifies how relatively likely a reaction is to occur once the activation energy has been reached. If κ were to remain approximately constant throughout the resonant suppression regime, this would indicate that the change in rate is caused by a change in $\Delta E^\dagger$ of the reaction, but κ does not stay constant. Rather, the transmission coefficient shows resonant rate suppression as well, indicating that it is not a change in activation energy that results in resonance rate suppression. Another factor is at work.

The second clue is provided by path entropy, defined as $S = -\sum_{i=1}^{N} f_i \ln(f_i)$ where f_i is the fraction of reactive flux carried by pathway i of the max-min flux ensemble which includes

N total reactive pathways. The path entropy measures the variety of different pathways represented in the ensemble. In the limit that all flux passes through a single pathway, $S = 0$. A wider variety of pathways will result in an increasingly larger S. Observing S as a function of ω_c/ω_s in Fig. 7.4 c), we find a spike in entropy at the location of resonant suppression, indicating that there is a greater variety of pathways in the reactive path ensemble on resonance. This tells us that the dominant pathway, which carries a large proportion of the reactive flux in this system, has become less dominant. This can be confirmed by inspecting the reactive path ensembles and observing that a lower proportion of reactive flux travels along the dominant reactive pathway during resonance conditions, leading, necessarily, to a larger fraction of the flux travelling along smaller, alternative pathways which in turn leads to a larger S.

Taken together, this indicates that the formation of the polariton wavefunctions in the committor eigenstates has resulted in a decrease in efficiency for this critical jump on the transition pathway resulting in smaller contribution of the dominant pathway to the overall rate and a decrease in the overall rate. There are two possible causes for this inefficiency. Under secular Redfield theory, the rate, $r_{i\to j}$ to jump between two eigenstates, i, and j, in the system can be written as,[20]

$$r_{i\to j} = |R_{i,j}|^2 \int_0^\infty dt\, e^{-i\omega_{i,j}t}\langle B(0)B(t)\rangle_B + |R_{i,j}|^2 \int_0^\infty dt\, e^{-i\omega_{j,i}t}\langle B(t)B(0)\rangle_B, \tag{7.6}$$

which consists of the Fourier transforms of the bath correlation functions, B being the bath portion of the system bath coupling operator, times a coupling element $|R_{i,j}|^2$, due to the use of R as the system component of the system-bath coupling operator.[41, 187] Thus, the only two options for the cause of the rate suppression are the Fourier transforms of the bath correlation functions and the coupling operator element, $R_{i,j}$. There is no reason to think that the Fourier transform of the bath correlation functions should change as a result of system behavior. However, $R_{i,j}$ might well change.

Inspecting the value of $|R_{i,j}|^2$ where i and j are the pre and post-committor eigenstates along the dominant reaction pathway as a function of ω_c/ω_s, we find resonance suppression that corresponds very well with the suppression observed in rates. In Fig. 7.4 d) the twin suppression spikes in $|R_{i,j}|^2$ for the the moderate light-matter coupling case correspond precisely with the suppression spikes observed in the rate in Fig. 7.4 a). The magnitude of the suppression in $|R_{i,j}|^2$ is more dramatic than the actual rate suppression observed because the dominant pathway does not constitute the only reaction pathway in the system and the other pathways are not necessarily suppressed by the formation of polaritons.

This presents a complete view of one potential mechanism of rate suppression in polaritonic systems. Under high barrier, weak cavity loss, weak system-bath coupling conditions which lead to deep tunneling reaction mechanisms, resonance between energy levels of the matter coordinate and the vacuum photon mode results in the formation of polaritons in the committor eigenstates. The bath interactions which facilitate the tunneling transitions between the committor eigenstates are more efficient for wavefunctions with solely matter

character than for mixed light-matter character polariton wavefunctions. This is a fundamentally quantum dynamical phenomenon which is detected only because QTPT is able to explicitly model the formation of a polariton wavefunction and the interaction of that wavefunction with the bath. Any method which cannot do both of these things will not detect this phenomenon, which explains why classical endeavours[145] and quantum statistical investigations[94] with path integrals have failed to detect this kind of rate suppression but a recent HEOM study has found polaritonic resonance phenomena.[149]

There are a few caveats in these results and opportunities for further investigation. First, this system has no cavity loss, and the low cavity loss limit is not realistic for most real systems. Because the nature of the system-bath coupling is critical to the rate suppression phenomenon observed, different dynamics are likely to be observed if cavity loss is significant, meaning its interaction with the system is comparable in strength to the interaction of the solvent modes coupled to R. It seems likely that if cavity loss were the dominant bath interaction, meaning that the system portion of the coupling operator only included q_c, the trend observed here might be reversed with the bath only effectively facilitating transitions between polaritonic eigenstates rather than matter excitations leading to resonance rate enhancement, a phenomenon that has also been seen in experiment.[267, 268, 140] Further investigation on this front is warranted.

The second caveat regards the barrier height and mechanism. This system involves a barrier so large that virtually all reaction mechanisms proceed by deep tunneling and the mechanism of suppression is specific to tunneling mechanisms. It is unclear whether similar suppression would occur if the energy barrier were lower and tunneling did not play a major role in the reaction. Further investigation is certainly warranted on this point as well. It is unlikely that all observed reactions demonstrating polariton rate suppression proceed by tunneling.

The third caveat is that polaritonic effects are generally observed experimentally in ensembles where billions of molecules are concentrated in a microcavity together. Many have argued that polaritonic rate suppression must involve collective effects,[208, 264, 253] and it is not clear whether the phenomenon observed here for a single molecule, with all other molecules treated as merely another aspect of the harmonic bath, would extend to describe rate suppression in a large ensemble. This simple model could be extended to include several proton degrees of freedom and observe trends in rate suppression. Further investigation in this direction is warranted.

7.3 Nonsecular Polariton Systems

When investigating polariton rate suppression effects, comparisons were made between secular Redfield, nonsecular Redfield and numerically exact hierarchical equation of motion[88, 87, 263] calculation in order to confirm that the critically important rates in the system, the jump rates between the committor eigenstates upon which all of the mechanistic analysis rests, were calculated correctly by secular Redfield despite the fact that some near

degeneracies did exist in the eigenspectrum. Agreement was very good. The good performance of secular Redfield is likely attributed to the large energy barrier resulting in small intereigenstate transfer rates despite the near degeneracies. As long as the departure rates from an eigenstate to its neighbors are small in comparison to the energy gap between the states, the secular approximation is likely to hold.

Nonsecular effects could certainly arise in other polaritonic systems. A recent study suggested that narrow band laser excitation in a cavity can influence the outcome of the reaction but that this is merely a result of the initial state targeted by the laser.[207] It is unclear whether quantum coherences might be involved in this behavior. Given the prevalence of near eigenstate degeneracies, an investigation of quantum coherent effects in polaritonic systems is warranted. Employing a very different potential energy surface, we explored the impact of nonsecular quantum coherent effects in a polaritonic system which could, potentially, result in a dramatic change in reaction outcome if the system were excited by different coherent laser pulses.

The system Hamiltonian has a similar structure to that addressed previously and describes the same kind of Shin-Metiu[251] model and Pauli-Fierz[205] approach but follows a simpler method for defining the light matter coupling strength, η_c.[149] Otherwise, all of the variables maintain their previous definitions leading to,[149]

$$H_S = \frac{P^2}{2M} + U(R) + \frac{p_c^2}{2} + \frac{\omega_c^2}{2}\left(q_c + \sqrt{\frac{2}{\omega_c}}\eta_c\mu(R)\right)^2, \tag{7.7}$$

where the system-bath coupling is bilinear and independent for both the proton and cavity

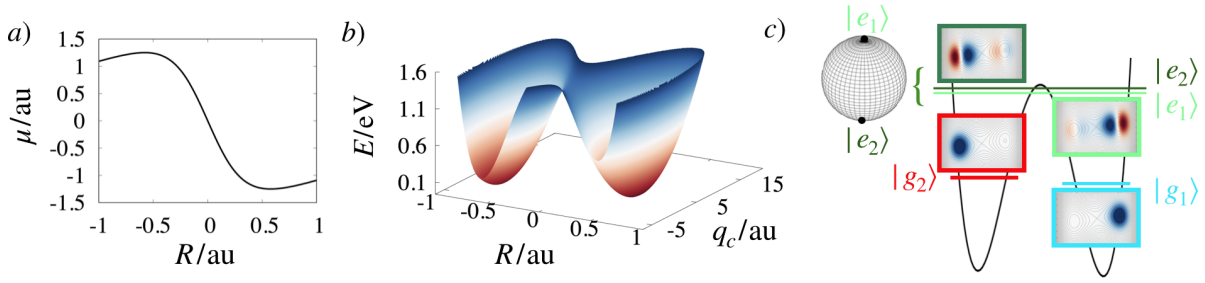

Figure 7.6: a) The matter dipole operator for the polariton system. b) The potential energy surface $H_S - P^2/2M - p_c^2/2$ for the polariton system. c) A cartoon illustrating the placement of the four eigenstates modeled for the system. The phase of the real part of the eigenstate wavefunctions superimposed on an energy contour plot are shown along with the Bloch sphere defined for the nonsecular block consisting of $|e_1\rangle$ and $|e_2\rangle$.

modes,

$$H_I = R \otimes \sum_k c_{k,1} r_{k,1} + q_c \otimes \sum_k c_{k,2} r_{k,2}, \tag{7.8}$$

with $r_{k,i}$ being the positions of the harmonic oscillators in the baths, meaning that this model does include cavity loss. The system again employed a Colbert-Miller DVR basis for R[57] and a harmonic oscillator basis for q_c with dimensions of 81 and 60 respectively and a δR for the DVR basis of 0.03 au. Convergence tests were performed as usual. Parameters for the Hamiltonian are found in Table 7.2.

In order to examine quantum coherent effects closely in a context where they are easily visualized, the system was trimmed down to only four eigenstates after diagonalizing the Hamiltonian. The spectral density describing the coupling strengths, $c_{k,\alpha}$, for each bath $\alpha = \{1, 2\}$ is,

$$J_\alpha(\omega) = \sum_k c_{k,\alpha}^2 \delta(\omega - \omega_{k,\alpha}) = \eta\omega e^{-|\omega|/\omega_b}, \tag{7.9}$$

which is, again, an Ohmic exponential form.

The dipole operator for this system is shown in Fig. 7.6 a) and the full potential energy surface is shown in Fig. 7.6 b). Fig. 7.6 c) shows a cartoon of the system potential energy surface showing the locations of the four eigenstates modeled, with the phases of the real parts of the eigenstates displayed, overlaid on an energy contour plot. Note that in this polaritonic system there are only four eigenstates at or below barrier height, the four which we model, in contrast to our previous system of study with QTPT which had dozens of eigenstates at or below barrier height. We now concern ourselves not with the rate of thermal barrier crossing reactions, which would certainly be very different for this system, but with the definition of the transition state and how it can be influenced by quantum coherent effects.

Because we have chosen to model a minimal system with only four states, there are only a total of three nonsecular blocks in the system. The localized ground states in either well, called $|g_1\rangle$ and $|g_2\rangle$ in Fig. 7.6 c) each comprise their own nonsecular blocks and are designated A and B respectively. The two states at the barrier height, $|e_1\rangle$ and $e_2\rangle$, are in a nonsecular block together. This nonsecular block of dimension two can be visualized as a Bloch sphere with $|e_1\rangle$ and $|e_2\rangle$ at the poles with coordinates $(x, y, z) = (0, 0, 1)$ and $(x, y, z) = (0, 0, -1)$ respectively. The general quantum committor allows us to define a committor probability for any location on the Bloch sphere, with locations where the committor is equal to 0.5 constituting a transition state. We can gain a much deeper understanding of the quantum coherent effects described by the partial secular Redfield equation by visualizing them on this Bloch sphere.

There are two distinct kinds of dynamics described by the partial secular Redfield master equation: jump processes which result in density moving between different nonsecular blocks and coherent processes that change the quantum state within a nonsecular block without moving density out of the nonsecular block, including actions of the dephasing operator and H_{LS}. The latter dynamics evolves the system to a new (x, y, z) location on the block sphere. The interplay of coherent evolution within and departure from the nonsecular block determines the behavior of the system. There are two possible extreme limits, the case in which the rate of departure from the nonsecular block is fast in comparison to coherent dynamics within the nonsecular block and the case in which the coherent dynamics within

the nonsecular block are fast in comparison to the rate of departure from the block.[2]

These two cases are illustrated in Fig. 7.7. The left column, a) and c), shows heat maps of the committor as a function of x and y for a slice through the Bloch sphere describing the nonsecular block of $|e_1\rangle$ and $|e_2\rangle$ at $z = 0.111$. The right column, b) and d), show heat maps of the same slice depicting the proportion of the probability that departs from the block to $|g_1\rangle$ rather than to $|g_2\rangle$. This is called the instantaneous departure probability as it refers to a ratio of jump rates obtained over a single time step for a specific location on the Bloch sphere. The upper row, a) and b), shows the limit of fast departure rates and slow coherent evolution. In this case, the committor probability is almost indistinguishable from the instantaneous departure rates because the density departs quickly from the nonsecular block without having a chance to move significantly to new locations which have different instantaneous departure probabilities, thus whether density arrives in A or B is decided by the instantaneous departure rates in a very small proportion of the Bloch sphere. The opposite limit is depicted in c) and d). The instantaneous departure rate heat map is effectively unchanged from b), meaning the ratio of instantaneous departure rates is unchanged. However, the committor heat map in c) is completely different from that in a). It is effectively a single color. This is due to the fast coherent dynamics which result in the system evolving through the density matrix quickly with small amounts of density departing for $|g_1\rangle$ and $|g_2\rangle$ from many different (x, y, z) locations with vastly different instantaneous departure rates. Averaging over many locations, hence departure rates, removes all dependence of the committor on x and y coordinates of the Bloch sphere, eliminating essentially all influences of quantum coherence, although for this system the z coordinate, meaning the relative population of $|e_1\rangle$ versus $|e_2\rangle$, does influence the committor, indicating that coherent evolution averages over more x and y coordinates than z coordinates. Whether the system matches the fast departure limit in a) and b) or the slow departure limit in c) and d), was determined by the light-matter coupling strength, η_c, which was set to two very extreme values, 0.5 (unitless) and 0.05 (unitless) respectively to achieve the fast and slow departure limits. The bath facilitates transitions out of the nonsecular block much more quickly for higher light-matter coupling strength, possibly because the eigenstates for larger η_c have more photon character allowing them to interact more strongly with the bath coupled to q_c which, given that the average q_c value in this system is larger than the average R significantly, is likely an effectively stronger bath. Regardless of the precise explanation, it is clear that an increase in η_c increases certain departure rates from the nonsecular block relative to the rate of coherent evolution within the block.

Using our basis definition of the committor, we can calculate the committor contributions of the basis states described by locations on the Bloch sphere, which are the Pauli matrices σ_x, σ_y, σ_z, and the identity, 1. It is then trivial to solve for $0.5 = xV_{A|B}(\sigma_x) + yV_{A|B}(\sigma_y) +$

[2]A word of warning is appropriate here: numerical linear algebra libraries may abruptly change the signs of eigenvectors for these systems as η_c or any other system parameter is adjusted. This can result in apparently abrupt inversion of the x and y axis of the Bloch sphere. This is physically meaningless, merely an inevitable side effect of numerical simulation. Checking and standardizing the signs of eigenvectors is advisable.

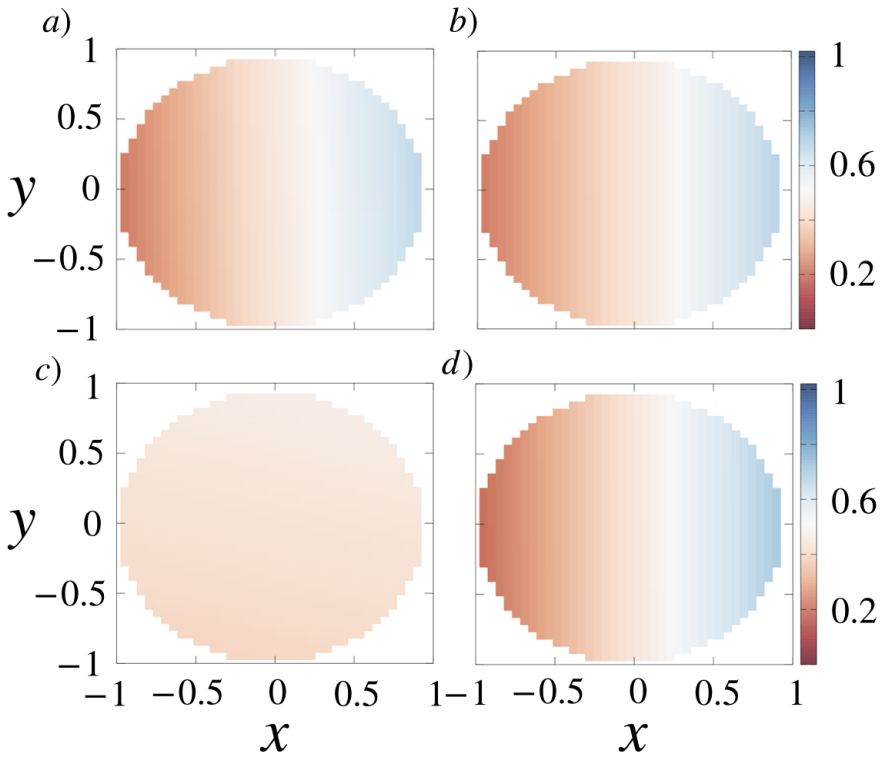

Figure 7.7: Heat maps of the the Bloch sphere defined by $|e_1\rangle$ and $|e_2\rangle$ at a fixed value of $z = 0.111$. a) The committor in the fast departure rate limit. b) The proportion of instantaneous departures to A versus B in the fast departure rate limit. c) The committor in the slow departure rate limit. d) The proportion of instantaneous departure to A versus B in the slow departure rate limit.

$zV_{A|B}(\sigma_z)+dV_{A|B}(1)$ to determine the equation for the plane through the Bloch sphere which defines the transition state in this system (although one must be wary of the placement of factors of 1/2 when employing this method). In the extreme case in Fig. 7.7 a) the location at which the committor is equal to 0.5 constitutes a nearly vertical plane through the Bloch sphere, whereas in the alternate extreme in Fig. 7.7 c) a nearly flat plane will define the transition state. More interesting effects can develop in intermediate regimes where the departure rates and coherent evolution are on comparable timescales, resulting in a plane that is neither flat, constant z, nor vertical, constant x.

In Fig. 7.8, three polaritonic systems with increasing light-matter coupling strengths have been selected and in each case the committor plane as calculated from the partial secular Redfield equation has been plotted alongside the plane obtained from the fully secular quantum master equation, which has no coherent effects by definition and must define a single

value of z as the committor plane. For all three couplings this value is $z \approx -0.3$, the secular plane changing very little with η_c. The committor plane designated by the partial secular quantum master equation, in contrast, changes drastically as η_c increases. At the lowest value of light-matter coupling in Fig. 7.8 a) the partial secular committor plane is nearly flat. It does not exactly match the committor plane designated by the secular approximation, however, and this is due to the piecewise flat spectral density approximation. This leads to a discrepancy between the partial secular and fully secular committor plane even in the limit that there are no significant coherent effects.

As η_c increases to 0.1 in Fig. 7.8 b), quantum coherent effects start to become important. The tilt of the plane in the x and y directions shows the increasing influence on the committor by the coherences in the density matrix. The slope in the x direction is significantly larger than the slope in the y direction indicating that it is largely the real part of the coherences, σ_x, that affects the committor in this system rather than the imaginary part, σ_y. A further increase in light-matter coupling strength in Fig. 7.8 c) results in an even more extreme tilt of the committor plane, still mostly in the x direction, so it is again the real parts of the coherences which are largely responsible. An increase in light-matter coupling strength radically increases the influence of quantum coherent effects in the system, moving through a range of intermediate values between the extremes depicted in Fig. 7.7.

It is interesting to examine relaxation dynamics starting from three different density matrices marked on the surface of the Bloch sphere for Fig. 7.8 c), $\sigma_1 = (x, y, z) = (-0.87, -0.17, -0.31)$, $\sigma_2 = (0.87, 0.383, -0.31)$ and $\sigma_3 = (0.87, 0.17, 0.46)$. Both σ_1 and σ_2 are on the secular committor plane whereas σ_3 is on the nonsecular committor plane. Although they are both on the secular committor plane, σ_1 and σ_2 show radically different relaxation behavior under partial secular evolution in Fig. 7.9 a), where less than 20% of density reaches $|g_1\rangle$ for initialization in σ_1 and more than 50% reaches it for σ_2. Meanwhile, σ_3 which has similar x and y values to σ_2 but a radically different z value, ends with a population of 50% in $|g_1\rangle$, as it must given its location on the nonsecular committor plane.

Given the discrepancy observed between the partial secular committor plane and the fully secular committor plane in Fig. 7.8 a), it is important to assess the relative magnitude of quantum coherent effects and the impact of the piecewise flat spectral density approximation. In Fig. 7.9 b) dynamics starting from σ_2 in Fig. 7.8 c) for three different methods of propagation are compared. One, in red, is the fully secular Redfield equation. One, in dark blue, is the partial secular Redfield equation and the last, in light blue, is a special modification of the partial secular Redfield equation in which, at every single time step, all off diagonal elements, meaning all coherences, in the density matrix are set to zero. This effectively eliminates all quantum coherent effects from the propagation. The only effect left which can cause a discrepancy between this zeroed coherence evolution and the fully secular evolution is the piecewise flat spectral density approximation. Indeed, the zeroed coherence partial secular propagation does not precisely match the secular propagation, however, it is vastly closer to the fully secular dynamics and very far removed from the partial secular dynamics. This indicates that, in this system, the effect of the piecewise flat spectral density approximation is small in comparison to the effect of quantum coherences and employing

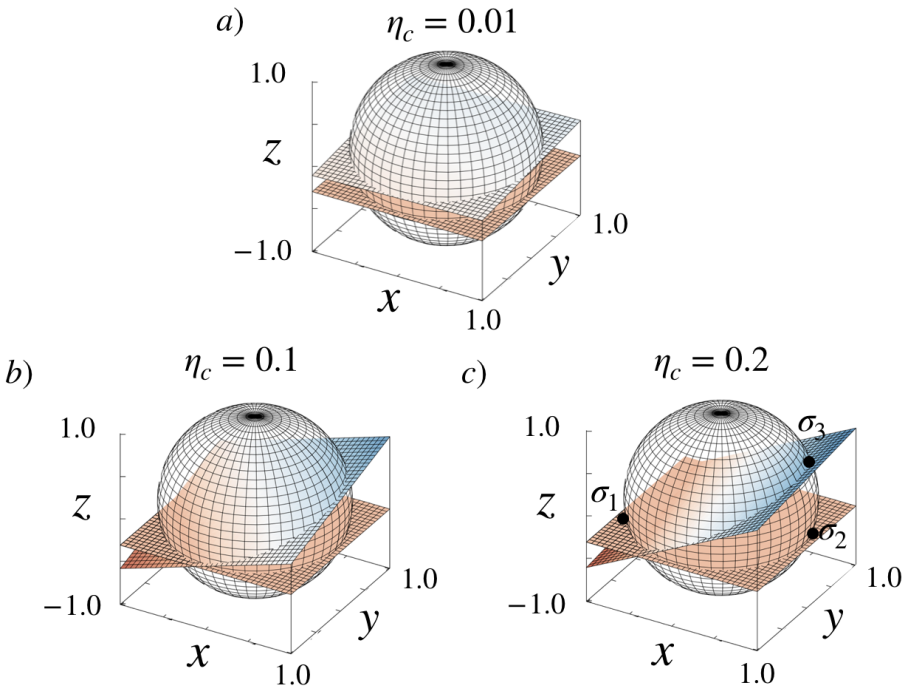

Figure 7.8: The fully secular (always completely flat) and partial secular (tilted) committor planes in the a) low light-matter coupling $\eta_c = 0.01$ case, b) moderate light-matter coupling $\eta_c = 0.1$ case, and c) strong light-matter coupling $\eta_c = 0.2$ case.

the secular Redfield equations will lead one far astray from the correct dynamics.

Quantum coherent effects are very important in this polariton model at higher light-matter coupling strengths and it is certainly possible that quantum coherent effects could have a significant influence on dynamics of polaritonic systems in practice. As in the polariton analyzed with QTPT, these striking effects on the transition states themselves are a fully quantum dynamical phenomenon which cannot be modelled without a means of describing a fully quantum mechanical system in which light-matter hybrid states can form and interact explicitly with the bath.

It should be noted that this system has been intentionally simplified to the greatest possible degree in order to allow us to clearly visualize the effects of quantum coherences on the transition state. In reality, the nonsecular block for which we modeled the Bloch sphere would likely contain four or more energy eigenstates. Coherent effects would certainly still be important in this more complicated system, though it is difficult to say precisely what the effect of adding in more degrees of freedom would be. This model also studies only one ω_c value which is not precisely on resonance for the relevant eigenstates in this system, as is evident from the lack of obvious polaritonic character in the eigenstates. Large polaritonic

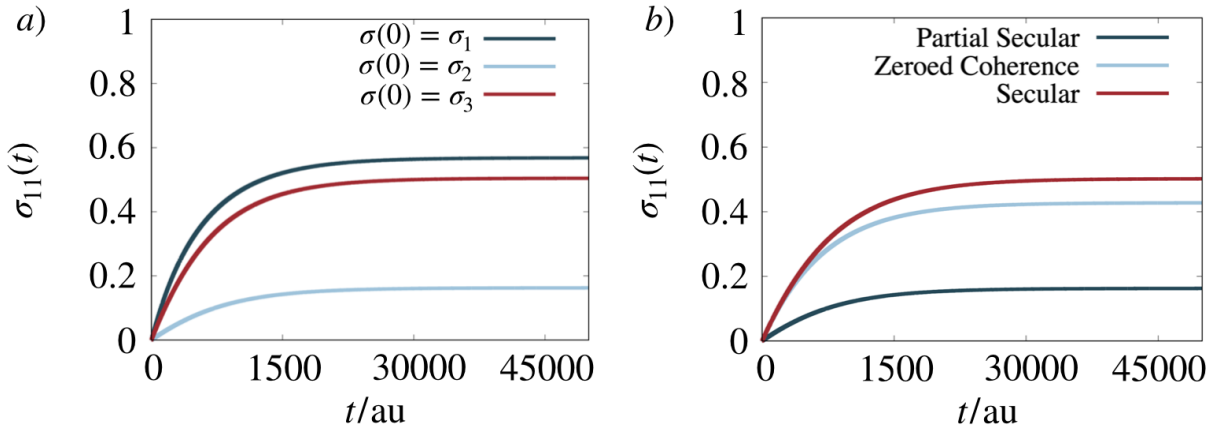

Figure 7.9: a) Population in $|g_1\rangle$ during propagation with the partial secular Redfield master equations following initialization into the three different density matrices marked in Fig. 7.8 c). Population in $|g_1\rangle$ during propagation starting from σ_2 in Fig. 7.8 with the Redfield equation which is fully secular, partial secular, and partial secular with coherences manually set to zero.

character would manifest as a significant deviation from a 90° angle in the wavefunction nodes in Fig. 7.6 c. Future work might explore the interplay of resonance and quantum coherent effects by scanning over ω_c. It is also worth considering the implications for quantum control problems in this system. Depending on what location of the Bloch sphere is targeted by a laser, the outcome of the system's relaxation could be very different. Quantum coherences may influence the optimal state into which a system should be excited by a laser in order to determine its final destination state.

7.4 Implications for Polaritonic Systems

Our initial QTPT exploration in a secular polaritonic system revealed, in great detail, a mechanism for resonance rate suppression in equilibrium barrier crossing reactions which matches with experimental observations. This is only one particular mechanism for one very specific set of circumstances: no cavity loss and a high barrier without explicit modelling of collective effects, but is still intriguing as it explains in such detail exactly how and why resonance rate suppression occurs. Our investigation of potential nonsecular effects in a smaller polaritonic system has indicated that, at high light-matter coupling strengths, nonsecular effects may significantly alter the transition state of a polaritonic system. Not only is this an extremely interesting and novel demonstration of quantum coherences changing the transition state of the system, but also a discovery with potentially serious implications for attempts to manipulate this system with lasers in coherent quantum control. Any study

Parameter	value (atomic units unless specified)
β	1052.584413
ω_s	0.00677687
ω_b	0.006269431
M	1836
χ_0 *	0.002535471
η	0.0018228 (unitless)
η_s	0.02

Table 7.1: Parameters employed during simulation of the many level polariton model addressed with QTPT.*Note that χ_0 is the value of χ when $\omega_c/\omega_s = 1$ and $\eta_c/\eta_s = 1$

of quantum control in polaritons must take the potential for these kinds of coherent effects into account.

The polaritonic systems explored here are systems heavily influenced by quantum dynamical effects, and any attempts going forward to understand dynamics in polariton systems, whether in or out of equilibrium, must acknowledge this. The modelling method employed needs to be able to, at the very least, explicitly model the formation of polariton states and the interaction of those polariton states with the bath in order to recover correct dynamics. In some cases, the method must be able to treat quantum coherent effects as well; the secular approximation to Redfield theory or similar approximations may not be sufficient.

7.5 Simulation Parameters

In the system treated with QTPT, the dipole operator is given by,

$$\mu(R) = -1.90249 \tanh(1.26426\ R) + 0.37044\ R, \tag{7.10}$$

and the proton potential is,

$$U(R) = -0.021088\ R^2 + 0.0033108\ R^4 + 0.033161 + 3.6749 \times 10^{-6}\ R + H_{ls} \tag{7.11}$$

with the correction

$$H_{ls} = \omega_b \eta R^2/(M\pi), \tag{7.12}$$

which is so small that it is negligible under most circumstances.

Parameter	atomic units unless specified
β	1052.584413
ω_b	0.05
ω_c	0.025344
η	0.2
c_{ob}	0.8
c_{eb}	0.05
M	1836
c_{cu}	0.004
v	-1.7
y	3.0 (unitless)
z	0.6

Table 7.2: Parameters employed during simulation of the four level polariton model.

η_c	$k_0(\eta_c)$/au $^{-1}$	$\kappa_0(\eta_c)$/ au^{-1}
η_s	7.643×10^{-17}	1.667×10^{-8}
$\eta_s/2$	9.782×10^{-17}	2.180×10^{-8}
$\eta_s/4$	1.042×10^{-16}	2.331×10^{-8}

Table 7.3: Parameters employed in rate and transmission constant specifications for the many level polariton model addressed with QTPT.

In the system treated with the general quantum committor, the dipole operator is given by,

$$\mu(R) = v\tanh(y\ R) + z\ R, \tag{7.13}$$

and the proton potential is,

$$U(R) = \frac{c_{ob}^4}{16c_{eb}}\ R^4 - \frac{c_{ob}^2}{2} - c_{cu}\ R^3, \tag{7.14}$$

with parameters in Table 7.2.

Chapter 8

A Time-Dependent Committor Analysis of the Fenna-Matthews-Olson Complex

> Nobody ever figures out what life is all about, and it doesn't matter. Explore the world. Nearly everything is really interesting if you go into it deeply enough.
>
> Richard Feynman

8.1 The Fenna-Matthews-Olson Complex

The Fenna-Matthews-Olson (FMO) complex is a small light-harvesting complex found in photosynthetic bacteria. It consists of either seven or eight chromophores, depending on the model, each of which is a Bacteriochlorophyll A molecule.[130, 54] FMO, the first chlorophyll complex whose structure was solved for from X-ray spectroscopy,[54, 91] plays a key role in the process of photosynthesis for some bacteria where it serves to capture energy in the form of an exciton and facilitate transfer of that excitonic energy to a reaction center where it is harnessed for the electron transport chain to oxidize water.[108, 183] The FMO complex's long history and small size make it a convenient and popular model system for researchers attempting to understand energy transport in photosynthesis. Under the right conditions, the FMO complex may transfer energy to the reaction center with 98% efficiency,[108, 54, 18] an impressive feat which is critical for the success of photosynthetic organisms. Numerous researchers have attempted to understand the efficient energy transfer within the FMO complex through experimental studies with 2D spectroscopy[152, 269] and theoretical methods.[54, 240] Observation of apparent long-lived quantum beating in relaxation dynamics in the FMO complex has led to many other experimental and theoretical investigations attempting to explain the origin of these phenomena and their potential impact on the FMO complex's efficiency[183, 130, 18, 183, 250, 130] with several experimental

papers arguing that these long-lived beats are not indicative of electronic coherences and rather attributable to vibrational coherences from vibronic coupling between excited states and the ground state.[269, 152] Several theoretical groups have measured large quantum entanglement or otherwise argued that quantum effects are important for the energy transfer process in FMO.[108, 183] Whether quantum effects are important in the FMO complex or related, larger photosynthetic systems remains a topic of debate.

It is known that the secular Redfield equation is insufficient to model some photosynthetic systems[54] including the FMO complex.[190] The full, nonsecular Redfield equations have frequently been used to model FMO and other photosynthetic light harvesting complexes with reasonable accuracy when the low system-bath coupling limit is in effect, with arguments against the Redfield equation modelling, according to Jeske and coworkers, often conflating weaknesses of the secular approximation with inherent weaknesses in Redfield theory.[54, 108, 126]

Given the ongoing debate about quantum effects in this system and the apparent importance of nonsecular Redfield terms, this is an interesting case in which to apply the partial secular Redfield equation and carry out committor calculations seeking to quantify the influence of quantum coherent effects on the system behavior.

8.2 Model System

When a photon of sufficient energy is absorbed by a system, an electron is excited from the highest occupied molecular orbital to the lowest unoccupied molecular orbital of the system, forming a quasiparticle known as an exciton. Excitons can move throughout a system, residing on different sites capable of hosting an electron-hole pair, due to electrostatic interactions which couple these different sites.[159] The FMO complex model we will investigate consists of several chromophores, each treated as an exciton site, and is small, leading to large couplings between chromophores and delocalization of excitons. The system state is a superposition of excitations on different chromophore sites. This can be modelled using a Frenkel exciton Hamiltonian where the state of the system will consist of a linear combination of excitations of the chromophores whose basis states are the site basis denoted $|i\rangle$,[223, 54]

$$H_S = \sum_{i=1}^{N} \epsilon_i |i\rangle\langle i| + \sum_{i<j} J_{i,j}(|i\rangle\langle j| + |j\rangle\langle i|) \tag{8.1}$$

where N is the number of chromophore sites which can host an excitation, ϵ_i is the energy of each site, and $J_{i,j}$ are the exciton couplings between chromophores i and j which are often determined by calculating the interaction of the chromophore dipoles, although there is evidence that a more powerful method may be necessary in some cases to handle this coupling.[97, 54] The energies of the chromophores themselves are determined by a combination of calculations and fitting to experimental spectroscopic data.[6, 2] Each chromophore site is presumed to interact with a solvent environment independently of the other chromophores,

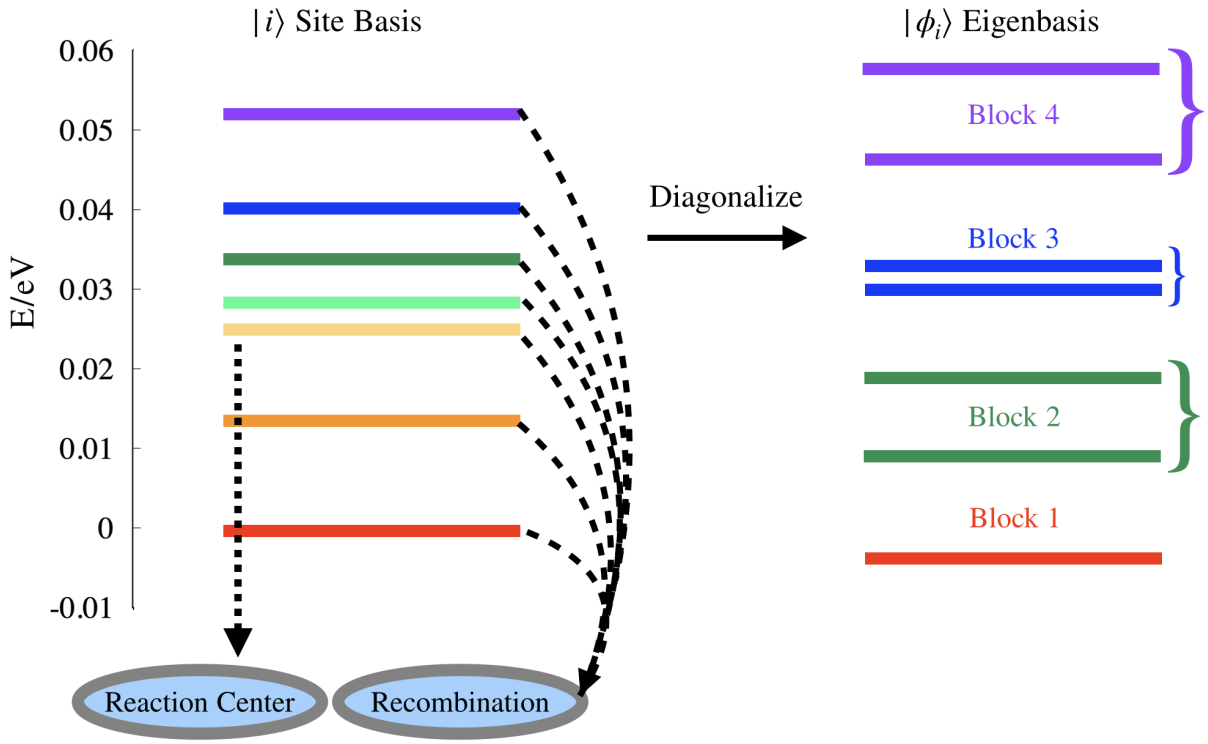

Figure 8.1: The energies of the seven sites in the model, $|i\rangle$, with cartoons illustrating the processes of recombination and transfer to the reaction center, alongside the energy eigenbasis, $|\phi_i\rangle$ that results from diagonalizing the Hamiltonian and consists of four nonsecular blocks.

so each is coupled to an independent bosonic bath,

$$H_I = \sum_{i=1}^{N} \sum_{j} |i\rangle\langle i| c_{i,j} q_{i,j} \tag{8.2}$$

where i sums over the N chromophores and j sums over an infinite oscillator bath as usual with $c_{i,j}$ being a coupling strength parameter and $q_{i,j}$ being the position of an oscillator in the bath.[6, 175, 130]

More recent experiments have indicated that an eighth chromophore is involved in the system, which can result in different energy transfer pathways through the system but does not appear to significantly influence the efficiency.[175, 6] The efficiency of energy transfer in the system is maintained even with significant disruptions to the chromophores, including completely removing a subset of them and drastically changing environmental interactions,[18] and for this reason the choice of an eight state or seven state model is likely not of critical

importance when assessing the potential impact of quantum coherences on dynamics in the FMO complex. We will use the older, more commonly studied seven chromophore model originally fit to experimental spectroscopy data by Adolphs and coworkers.[2, 126] Our brief exploratory calculations with an eight site model did not suggest that the additional site would lead to significant changes.

We employ the Debye spectral density model of Moix and coworkers[175],

$$J_i(\omega) = \eta \frac{\omega}{\omega^2 + \omega_b^2} = \sum_j c_{i,j}^2 (\delta\omega - \omega_{i,j}) \tag{8.3}$$

with $\eta = 7.612 * 10^{-8}$ au and $\omega_b = 4.7733 * 10^{-4}$ au at a temperature of 77 K for our initial calculations. This is the temperature at which most spectroscopic measurement is carried out, although obviously not the temperature relevant to biological processes.

The Fate of an Excitation

There are two potential fates for the excitation: it can migrate to chromophore 3 in the system which is strongly coupled to the reaction center and then pass energy along the transport chain to the next steps of photosynthesis, or it can undergo recombination at any site, with the excitation energy dissipating or being emitted as a photon and the electron returning to its natural place to fill the hole.[125, 54, 175] These two potential processes are illustrated in the cartoon in Fig. 8.1. Efficiency of light harvesting depends on the recombination occurring much more slowly than the transfer to the reaction center.

Models fitted to experiment set the recombination as a process with a constant rate of 1 ns^{-1} occurring at all chromophores in the system whereas the transfer to the reaction center occurs only from chromophore 3 but happens 1000 times more quickly.[125, 175, 221] The initial excitation, which will eventually make its way either to the reaction center or recombine, is sometimes thermally distributed throughout the system, but more frequently placed on chromophore site $|1\rangle$ or $|6\rangle$.[175, 125] We will place it on chromophore site $|1\rangle$.

To handle this model within the partial secular Redfield formalism, two dummy states are added to the density matrix. The energy of these states is irrelevant as they will be treated as the sinks and their entrance and exit rates will be set without regard to the spectral density. They are not coupled to any states by the Hamiltonian, rather, to model the jump to the reaction center the following Lindblad jump operator is artificially introduced to the system,

$$L_r = \gamma_r |r\rangle\langle 3|, \tag{8.4}$$

which moves density from chromophore $|3\rangle$ to the dummy reaction center state, $|r\rangle$, with rate $\gamma_r = 1$ ps^{-1}. A total of seven Lindblad jump operators must be introduced to handle the recombination loss occurring at all sites, presuming that recombination at different sites is uncorrelated.[175] Each of the seven operators has the structure,

$$L_c = \gamma_c |c\rangle\langle i| \tag{8.5}$$

where i ranges from 1 to 7, $\gamma_c = 1$ ns^{-1} is the recombination rate and $|c\rangle$ is the dummy state representing recombination.

Diagonalizing the system Hamiltonian to arrive at the energy eigenbasis, where states of the energy eigenbasis will be denoted as $|\phi_i\rangle$ in contrast to the simple $|i\rangle$ denotation of the site basis, and inspecting the energies and intereigenstate transfer rates indicates that there are a total of four nonsecular blocks in this system, as illustrated in Fig. 8.1. State $|\phi_1\rangle$ is alone in a single block and the other eigenstates are paired with their nearest neighbors in blocks of two. Due to the mixing of sites by diagonalization, recombination and transfer to the reaction center may occur from any eigenstate. Note that, because they have no coupling, the dummy reaction transfer and recombination states, $|r\rangle$ and $|c\rangle$, are unchanged by diagonalization and identical to the states $|\phi_r\rangle$ and $|\phi_c\rangle$ representing transfer to the reaction center and recombination in the energy eigenbasis. In preforming committor calculations, we will designate $A = |\phi_r\rangle$ and $B = |\phi_c\rangle$.

8.3 Time-Dependent Committor Calculations

Applying the partial secular approximation with an excitation placed on chromophore $|1\rangle$ results in long-lived oscillations in the site basis in Fig. 8.2 a). These are consistent with those observed in previous studies.[175, 126, 183, 130] Over the period modelled these oscillations decay to nothing and the majority of population is transferred to the reaction center with only a tiny fraction of density undergoing recombination. The time-independent committor calculation reveals that $V_{A|B}(\sigma)$ is on the order of 0.01 or less for all $\sigma = |i\rangle\langle j|$ where $i \neq j$, meaning that quantum coherent effects do not appear to have any significant influence on the overall outcome of energy transfer, hence the efficiency, of the FMO complex.

This does not rule out the potential importance of quantum coherent effects on dynamics at intermediate times, however. Quantum coherences might still have an impact on how quickly energy is transferred or what pathway it takes through the system. The time-dependent quantum committor can elucidate one aspect of this, revealing whether there is any time during the propagation at which the amount of recombination loss is significantly impacted by the value of any coherence in the initial density matrix.

Certain $V_{A|B}(t, \sigma)$ were calculated for the FMO complex, displayed in Fig. 8.2 b), with the coherent contribution, $V_{A|B}(t, |\phi_2\rangle\langle\phi_3| + |\phi_3\rangle\langle\phi_2|)$, compared to $V_{A|B}(t, |\phi_2\rangle\langle\phi_2|)$ and $V_{A|B}(t, |\phi_3\rangle\langle\phi_3|)$. This pair of states have the largest $V_{A|B}$ for the coherence between them of any eigenstate pair. At very early times, long before the oscillation of population between sites $|1\rangle$ and $|2\rangle$ have decayed, $V_{A|B}(t, |\phi_2\rangle\langle\phi_3| + |\phi_3\rangle\langle\phi_2|)$ is larger than $V_{A|B}(t, |\phi_3\rangle\langle\phi_3|)$, but the latter value quickly begins to grow and $V_{A|B}(t, |\phi_2\rangle\langle\phi_2|)$ is always large in comparison. Only at trivially small times is there any impact from quantum coherences on energy transfer in this system. Long lived, apparently coherent oscillations in the site basis do not necessarily imply that quantum coherent effects are important for the overall outcome of the reaction.

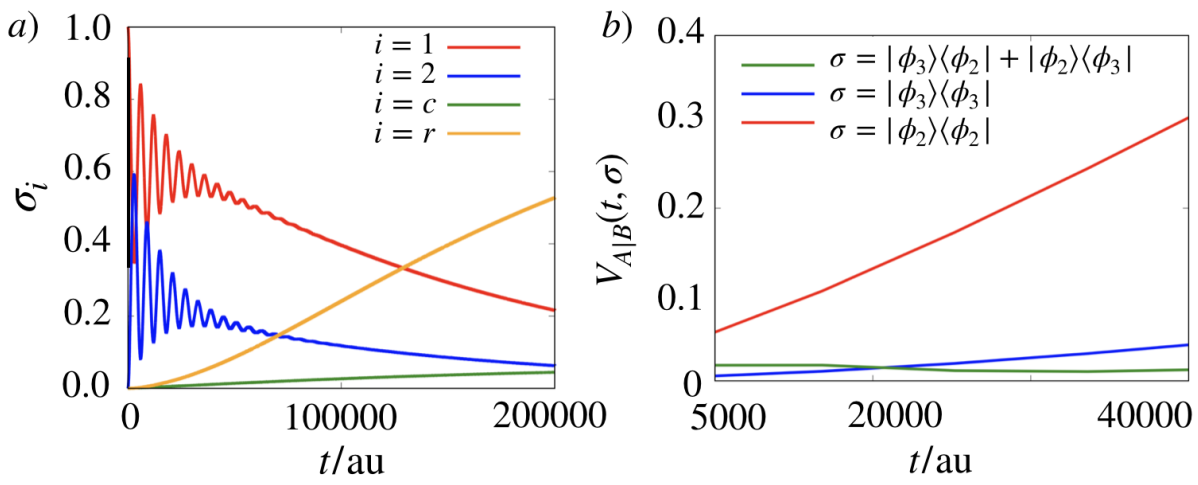

Figure 8.2: a) The populations in the chromophore site basis states $|1\rangle$ and $|2\rangle$ and the reaction center, $|r\rangle$ and recombination $|c\rangle$ as a function of time. b) The integrated flux, $V_{A|B}(t, \sigma)$ as a function of time for three different energy eigenbasis state contributions to the time-dependent committor, two populations and the real part of the coherence between them.

This is a somewhat uninspiring determination; perhaps coherent effects can be found with slight model adjustments. The parameters for recombination rates and bath interactions are all fitted to experimental determinations, but given that the bacteria in which FMO is found may live in hot springs with temperatures above 50° C,[18, 284] there is potentially leeway in modifying bath parameters, temperature and otherwise, in an attempt to find cases in which quantum coherent effects would be of importance in this system.

In the interest of seeking out regimes in which quantum coherent effects might be important, several calculations were run with a variety of bath cutoff frequencies, ω_b, system-bath coupling strengths, η, and temperatures. Without physical justification, purely for the purpose of satisfying curiosity as to whether quantum coherent effects would emerge if the rate of recombination rivaled that of transfer to the reaction center, some calculations had recombination rates at all sites increased by a factor of 10. Population dynamics for six calculations carried out with a variety of parameters are displayed in Fig. 8.3. A case of high bath cutoff frequency in Fig. 8.3 b) resulted in longer lived oscillations. Increasing the temperature in Fig. 8.3 a) and e) resulted in more quickly damped oscillation, as did decreasing ω_b in f), d), and c), regardless of how η had been modified. A wide variety of dynamics are displayed among these six trials, however, no modification made to the bath parameters had any significant impact on the efficiency of the process, with variations in efficiency only on the order of a few percent. These modifications may impact the timescale over which transfer occurs, as in Fig. 8.3 c) but the only means of influencing the efficiency

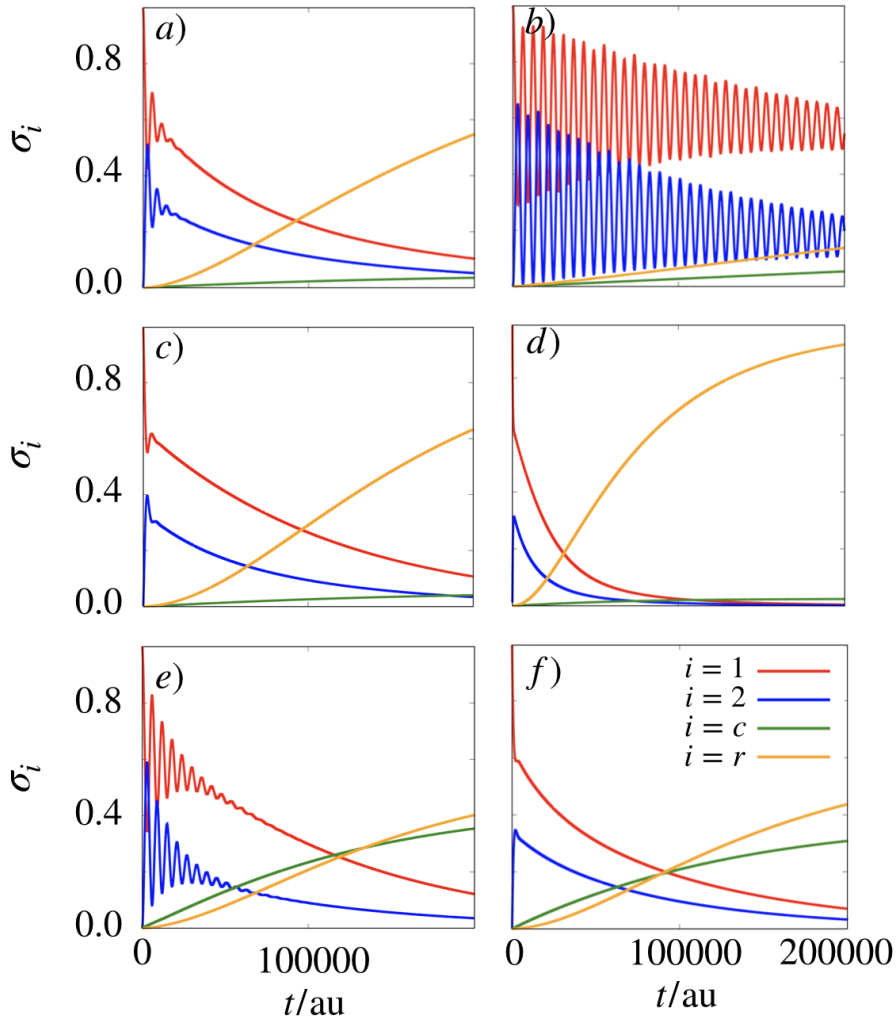

Figure 8.3: The populations in the chromophore site basis states $|1\rangle$ and $|2\rangle$ and the reaction center, $i = r$ and recombination $i = c$ as a function of time for six different modifications of the bath and system parameters. a) The bath temperature has been modified from 77 K to 300 K. b) The bath frequency ω_b has been multiplied by 5. c) The bath frequency ω_b has been multiplied by 1/5 and the system-bath coupling η has been multiplied by 1/2. d) The bath frequency ω_b has been multiplied by 1/5 and the system-bath coupling η has been multiplied by 3.0. e) The recombination rate has been multiplied by 10 at all sites. f) The bath frequency ω_b has been multiplied by 1/10, the system-bath coupling η has been multiplied by 1/4 and the recombination rate has been multiplied by 10 at all sites.

of the system significantly was increasing the recombination rate, which was carried out in the cases of Fig. 8.3 e) and f) resulting in a large decrease in efficiency.

Investigating $V_{A|B}(t, \sigma)$ between eigenstates in the same six modified systems studied in Fig. 8.2, we find in Fig. 8.3 that the influence of the initial coherence in the eigenbasis on the reactive outcome is, in all cases, minimal. The contributions to the committor from populations in energy eigenstates $|\phi_2\rangle$ and $|\phi_3\rangle$ grow quickly with t whereas contribution from the real part of their coherence attains at most a minuscule value of approximately 0.03, leveling off at a plateau value in all cases except for Fig. 8.3 b) which shows oscillatory behavior of $V_{A|B}(t, (|\phi_2\rangle\langle\phi_3| + |\phi_3\rangle\langle\phi_2|))$, an interesting occurrence and perhaps not surprising given the large, long-lived oscillations in site basis population observed in Fig. 8.2 b). Although the influence of the coherence is minimal, for certain systems it can have a small positive influence on the amount of density reaching the reaction center from the FMO complex at certain times and a small negative influence at others, which is quite interesting.

8.4 Analysis of the Initial Coherence in the Site Basis

As the long lived oscillations observed in the population graphs are between states $|1\rangle$ and $|2\rangle$ in the site basis, not the energy eigenbasis, examining the impact of initial coherences in the site basis also seems merited. It is possible to calculate the generalized quantum committor for any density matrix that strikes our fancy, including the populations and coherences in the site basis. However, the interpretation is not straightforward when a basis other than the energy eigenbasis is employed. The partial secular approximation preserves quantum coherent effects between energy eigenstates. When calculating $V_{A|B}(t, \sigma)$ for a basis other than the energy eigenbasis, it is not possible to attribute the contribution of a coherence to nonsecular effects in the Hamiltonian. Terms which were coherences in the site basis may become populations in the eigenbasis and vice versa. Nonsecular quantum effects and basis transformation effects are convoluted and nothing can be said about whether quantum coherent effects, as we defined them in previous chapters, are changing the outcome. However, calculating the time-dependent committor in the site basis allows us to determine whether initial coherences between chromophore sites might influence the outcome of the reaction. We focus in on the coherence between $|1\rangle$ and $|2\rangle$.

In Fig. 8.5 b) the $V_{A|B}(t, \sigma)$ values for the population in the first site basis state, $\sigma = |1\rangle\langle 1|$, as well as that in the second site basis state, $|2\rangle\langle 2|$, and the real part of the coherence between them, $|1\rangle\langle 2| + |2\rangle\langle 1|$, are shown for a modified system with a recombination rate enhanced by a factor of 10 in an attempt to give the coherence every chance to prove its relevance. At short times, 25000 au and less, the coherence's contribution to the committor rivals that of the populations, indicating that the nature of the initial superposition between the two chromophores can influence how much recombination occurs over this period. However, $V_{A|B}(t, \sigma)$ for the committor quickly levels off, having reached a maximum value of 0.1, and eventually begins to decrease. Meanwhile, $V_{A|B}(t, \sigma)$ for the populations increases steadily, and the relevance of the initial coherence fades. Optimizing over a and b in

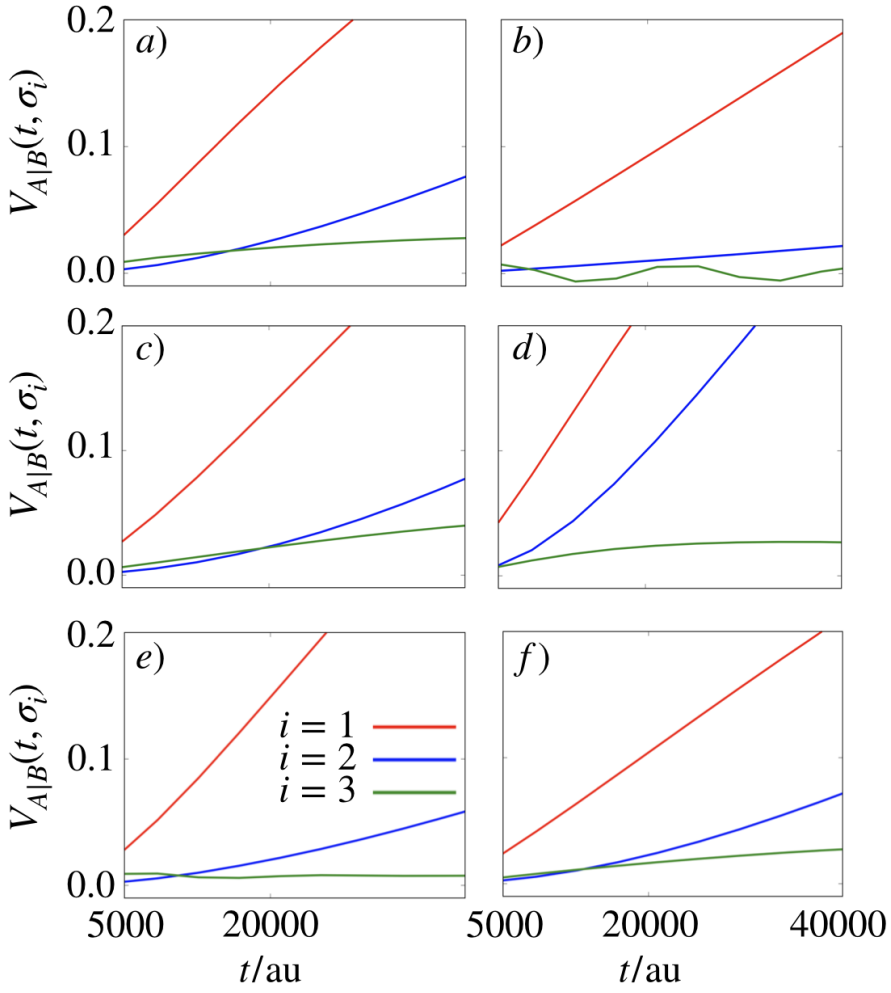

Figure 8.4: The time integrated flux, $V_{A|B}(t,\sigma)$ into $|r\rangle$, the reaction center, over finite time t for three different density matrices, $\sigma_1 = |\phi_2\rangle\langle\phi_2|$, $\sigma_2 = |\phi_3\rangle\langle\phi_3|$ and $\sigma_3 = |\phi_2\rangle\langle\phi_3| + |\phi_3\rangle\langle\phi_2|$, under six modifications of the initial system conditions. a) The bath temperature has been modified from 77 K to 300 K. b) The bath frequency ω_b has been multiplied by 5. c) The bath frequency ω_b has been multiplied by 1/5 and the system-bath coupling η has been multiplied by 1/2. d) The bath frequency ω_b has been multiplied by 1/5 and the system-bath coupling η has been multiplied by 3.0. e) The recombination rate has been multiplied by 10 at all sites. f) The bath frequency ω_b has been multiplied by 1/10, the system-bath coupling η has been multiplied by 1/4 and the recombination rate has been multiplied by 10 at all sites.

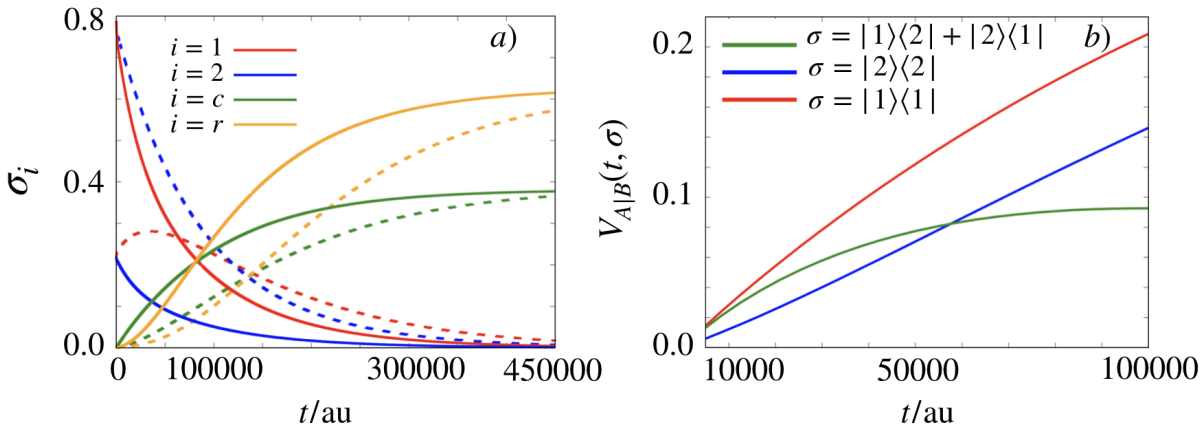

Figure 8.5: The system has been modified by increasing the recombination rate at all sites by a factor of 10, multiplying the bath frequency ω_b by 1/10 and the system-bath coupling by 1/4. a) The populations, σ_i, in the site basis states $|1\rangle$ and $|2\rangle$ and the reaction center, $|r\rangle$, $i = r$, and recombination $|c\rangle$, $i = c$, for two different initial coherent conditions, dashed lines indicating the coherent initialization chosen to minimize arrival in the reaction center at 100000 au and the solid lines chosen to maximize arrival in the reaction center at 100000 au. b) The time-dependent flux into the reaction center, $V_{A|B}(t, \sigma)$, for $\sigma_a = |1\rangle\langle 1|$, $\sigma_b = |2\rangle\langle 2|$, and $\sigma_c = |1\rangle\langle 2| + |2\rangle\langle 1|$.

$\sigma(0) = a^2|\phi_1\rangle\langle\phi_1| + b^2|\phi_2\rangle\langle\phi_2| + a^*b|\phi_1\rangle\langle\phi_2| + b^*a|\phi_2\rangle\langle\phi_1|$ to find the minimum and maximum value of $P_{A|B}(100000 \text{ au}, \sigma) = a^2 V_{A|B}(100000 \text{ au}, |\phi_1\rangle\langle\phi_1|) + b^2 V_{A|B}(100000 \text{ au}, |\phi_2\rangle\langle\phi_2|) + a^*b V_{A|B}(100000 \text{ au}, |\phi_1\rangle\langle\phi_2|) + ab^* V_{A|B}(100000 \text{ au}, |\phi_2\rangle\langle\phi_1|)$ and propagating from the resulting initial $\sigma(0)$ values results in the dynamics in Fig. 8.5 a) where significant differences in the population of the reaction center and the recombination state are evident at early times, with both transfer to the reaction center and recombination happening vastly more quickly in the case that $P_{A|B}(100000 \text{ au}, \sigma)$ was maximized. However, by 450000 au, the point at which nearly all the density has either reached the reaction center or undergone recombination, the gap has closed. No significant bias towards or away from the reaction center has been achieved. Performing this procedure with other variations on the bath parameters achieved similar results.

We were not able to use the generalized quantum committor applied to the site basis to optimize the overall efficiency of recombination or reaction center trapping to any significant degree. However, the optimization did modify the rate of trapping. By the time 200000 au have passed, the maximized calculation, solid lines in Fig. 8.5 a), has nearly completed whereas the minimized reaction will require another 100000 au to reach equivalent completion. Rate of energy transfer through photosynthetic complexes is important for the system to function effectively, thus the initial coherent superposition is not irrelevant to the

performance of the complex.

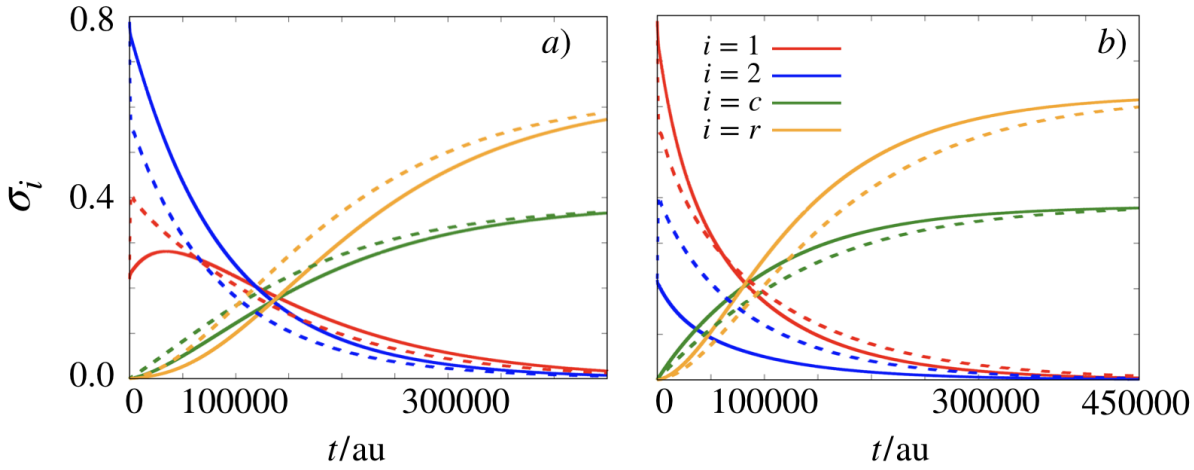

Figure 8.6: The system has been modified by increasing the recombination at all sites by a factor of 10, multiplying the bath frequency ω_b by 1/10 and the system-bath coupling by 1/4. a) The populations in the chromophore site basis states $|1\rangle$ and $|2\rangle$ and the reaction center, $i = r$ and recombination $i = c$ for two different initial coherent conditions, dashed lines indicating the coherent initialization chosen to minimize arrival in the reaction center at 100000 au and the solid lines being the equivalent incoherent initialization, meaning density matrix populations were maintained but coherences set to zero. b) The populations in the chromophore site basis states $|1\rangle$ and $|2\rangle$ and the reaction center, $i = r$ and recombination $i = c$ for two different initial conditions, dashed lines indicating the coherent initialization chosen to maximize arrival in the reaction center at 100000 au and the solid lines being the equivalent incoherent initialization, meaning density matrix populations were maintained but coherences set to zero.

The magnitude of this effect is put in perspective, however, by considering the equivalent incoherent initializations. If the a and b values used to maximize and minimize the committor are employed to determine the initial populations but the coherences are set to zero, an equivalent incoherent initial state has been chosen. In Fig. 8.6, the two coherent initializations are shown beside their incoherent counterparts. The incoherent initializations are dashed lines in Fig. 8.6 a) and b). Direct comparison shows that the change in dynamics induced by the coherent initializations is minimal. There is some small enhancement or suppression of the rate of transfer to the reaction center and rate of recombination, the same phenomenon observed in Fig. 8.5 a) but the advantage is very small and, as previously seen, no significant bias in the overall efficiency of the system is observed with the final population transfer to the reaction center and to recombination being virtually identical regardless of coherent or incoherent initialization.

8.5 Implications for Quantum Effects in the FMO Complex

This work can only answer questions within the purview of the model assumptions and cannot address questions about the potential impact of an eighth chromophore on dynamics[175], address the potential impact of vibrational coherences which are not being modeled explicitly,[152] or address potential non-Markovian bath effects that some have argued are at work in the complex.[183] However, there are several strong statements that can be made within the confines of our model and method.

Nonsecular quantum coherent effects in the FMO complex model can slightly influence the population dynamics at short times but quickly become negligible and provide a tiny bias, if any, to the ratio of recombination to reaction center transfer which occurs. A wide variety of bath parameters were sampled and never did we observe a significant influence on the committor from any coherence between energy eigenstates in the density matrix. The initial coherence between site $|1\rangle$ and $|2\rangle$, when studied in a modified system tailored to help it prove its relevance in any way possible, can have a moderate impact on dynamics at short times, potentially modifying the rate of energy transfer through the system, but it does not change the final outcome, the efficiency, of energy transfer. Comparing these optimized, coherent initializations with their incoherent counterparts shows a minimal modification of the dynamics providing little, if any, advantage in rate of energy transfer and no change in overall efficiency.

It seems that quantum coherences are of little importance to dynamics in the FMO complex. The influence of nonsecular effects in the energy eigenbasis is minimal. Coherent versus incoherent initialization of the system in site basis states $|1\rangle$ and $|2\rangle$ has, potentially, a small impact on rate but no influence on efficiency. This result is in accord with previous work by Cui and Oh who studied the impact of coherent initializations on the efficiency of the FMO complex.[59] They used a similar model and master equation approach, also seeking out optimal initial coherent superpositions, and observed similarly small changes in efficiency.

We have found the FMO complex to be very robust to manipulation, with no choice from a wide variety of bath parameters significantly changing the amount of recombination compared to energy transfer which occurred. Different parameters did change the rate at which that transfer occurred, but the only way to significantly impact the efficiency of the system was to radically adjust the rate of recombination to an unphysical value. This result is in accord with previous studies noting the robust efficiency of the FMO complex,[152, 18] and an important note to takeaway. The most important lesson to learn, however, is that presence of long-lived oscillations of population between two states, or long lived quantum coherences in a given basis, does not necessarily imply that those coherences are important to the outcome of a reaction or that nonsecular effects have significant impact on the system.

Chapter 9

Conclusion

> What is a university for if it isn't to tell you that everything you think you know is wrong
>
> Terry Pratchett, *A Collegiate Casting-Out of Devilish Devices*

Quantum transition path theory in its original form has identified changes of regime in thermal barrier crossing around conical intersections and found a potential mechanism for rate suppression resonance effects in polariton systems. Quantum transition path theory adapted to address photoreactions has identified a change in mechanistic regime around conical intersections undergoing relaxation following photoexcitation which, taken together with knowledge from the thermal barrier crossing case, shows a trade off of photoyield and thermal isomerization rate reminiscent of trade offs encountered in experimental works.

The more advanced, general committor definition has identified cases where quantum coherent effects significantly alter the committor in conical intersections and polaritonic systems, suggesting future avenues by which these systems might be manipulated with coherent quantum control approaches in order to guarantee the desired reactive outcomes. The time dependent general committor definition applied to the Fenna-Matthews-Olson complex has clearly indicated that coherent oscillation in a quantum system does not necessarily indicate that quantum coherent effects have significant impacts on the outcome or rate of the reaction. The lack of influence of coherences is in accord with previous studies of the FMO complex which have emphasized the remarkable versatility of its efficiency with respect to modification of the system itself, not just the parameters governing its interaction with the bath.

The quantum committor methods explored in this work are all based on a few basic assumptions: the quantum system's important degrees of freedom can be identified and fit to a potential energy surface without becoming computationally intractable, the system can be modelled as having a weak interaction with a bath, and the bath is Markovian. To apply quantum transition path theory, the secular approximation implying no coherent effects between energy eigenstates must also apply.

There are numerous quantum systems where these assumptions will hold, including realistic models of molecules like pyrazine or rhodopsin as well as small models of polaritonic systems. In these cases a set of tools has been provided which can produce a breadth of information about reaction mechanisms, providing a new means to analyze quantum reactions. Quantum transition path theory in its simplest form is easy to perform provided that a model of the desired system exists. Secular Redfield theory is a comparatively very simple quantum dynamics method and the transition path theory that must be implemented on top of the results is also fairly simple, with the same post-processing procedures capable of being applied to any Markov state model regardless of its origin. The coherence analysis methods are somewhat more involved to implement but not drastically so. Taken together, the ease of implementation and fairly wide applicability make for a set of mechanistic analysis tools with significant potential.

Numerous avenues exist for improving the general committor method. As any linear propagator can be employed to generate a general quantum committor, other quantum dynamics methods could be employed in place of partial secular Redfield theory. Trajectory based approaches to the general quantum committor formulation are possible and can potentially provide more detailed mechanistic information than obtained from the aggregated flux graphs.

With numerous engineering challenges looming alongside energy and food security challenges at the dawn of the second century of quantum chemical computation, better means of studying and controlling quantum reactions are highly desirable. Our inquiries into the nature and applications of the quantum committor represent a significant step forward in the study of mechanisms in quantum reactions, both towards greater understanding of reactions and greater ability to manipulate reactions.

Bibliography

[1] Mayumi Abe et al. "Optimal control of ultrafast cis-trans photoisomerization of retinal in rhodopsin via a conical intersection". In: *The Journal of Chemical Physics* 123.14 (2005).

[2] Julia Adolphs and Thomas Renger. "How proteins trigger excitation energy transfer in the FMO complex of green sulfur bacteria". In: *Biophysical Journal* 91.8 (2006), pp. 2778–2797.

[3] Mohiuddin Ahmed, Raihan Seraj, and Syed Mohammed Shamsul Islam. "The k-means algorithm: A comprehensive survey and performance evaluation". In: *Electronics* 9.8 (2020), p. 1295.

[4] Seihwan Ahn et al. "Design and optimization of catalysts based on mechanistic insights derived from quantum chemical reaction modeling". In: *Chemical Reviews* 119.11 (2019), pp. 6509–6560.

[5] Devendra Alhat, Vernet Lasrado, and Yan Wang. "A review of recent phase transition simulation methods: Saddle point search". In: *International design engineering technical conferences and computers and information in engineering conference*. Vol. 43253. 2008, pp. 103–111.

[6] Marcel Schmidt Am Busch et al. "The eighth bacteriochlorophyll completes the excitation energy funnel in the FMO protein". In: *The Journal of Physical Chemistry Letters* 2.2 (2011), pp. 93–98.

[7] Graziano Amati et al. "Quasiclassical approaches to the generalized quantum master equation". In: *The Journal of Chemical Physics* 157.23 (2022).

[8] Michelle C Anderson et al. "Coherent control from quantum committment probabilities". In: *arXiv:2403.19533* (2024).

[9] Michelle C Anderson et al. "On the mechanism of polaritonic rate suppression from quantum transition paths". In: *Journal of Physical Chemistry Letters* 14.30 (2023), pp. 6888–6894.

[10] Michelle C. Anderson, Addison J. Schile, and David T. Limmer. "Nonadiabatic transition paths from quantum jump trajectories". In: *The Journal of Chemical Physics* 157.16 (2022), p. 164105.

[11] Joakim Andréasson et al. "All-photonic multifunctional molecular logic device". In: *Journal of the American Chemical Society* 133.30 (2011), pp. 11641–11648.

[12] Tetsuya Aoki. "Application of Magnetism to Automobiles". In: *Magnetic Material for Motor Drive Systems: Fusion Technology of Electromagnetic Fields* (2019), pp. 407–421.

[13] Yasuki Arasaki et al. "Monitoring the effect of a control pulse on a conical intersection by time-resolved photoelectron spectroscopy". In: *Physical Chemistry Chemical Physics* 13.19 (2011), pp. 8681–8689.

[14] Judith P Araújo and Maikel Y Ballester. "A comparative review of 50 analytical representation of potential energy interaction for diatomic systems: 100 years of history". In: *International Journal of Quantum Chemistry* 121.24 (2021), e26808.

[15] Peter Atkins and Julio De Paula. *Physical Chemistry*. Vol. 1. Macmillan, 2006.

[16] Michael Baer. "Adiabatic and diabatic representations for atom-molecule collisions: Treatment of the collinear arrangement". In: *Chemical Physics Letters* 35.1 (1975), pp. 112–118.

[17] Michael Baer. "Introduction to the theory of electronic non-adiabatic coupling terms in molecular systems". In: *Physics Reports* 358.2 (2002), pp. 75–142.

[18] Lewis A Baker and Scott Habershon. "Robustness, efficiency, and optimality in the Fenna-Matthews-Olson photosynthetic pigment-protein complex". In: *The Journal of Chemical Physics* 143.10 (2015).

[19] Amirhossein Bakhtiiari, Gustavo J Costa, and Ruibin Liang. "On the Simulation of Thermal Isomerization of Molecular Photoswitches in Biological Systems". In: *Journal of Chemical Theory and Computation* 19.18 (2023), pp. 6484–6499.

[20] Birgit Balzer and Gerhard Stock. "Modeling of decoherence and dissipation in nonadiabatic photoreactions by an effective-scaling nonsecular Redfield algorithm". In: *Chemical Physics* 310.1 (2005), pp. 33–41. ISSN: 0301-0104.

[21] HM Dhammika Bandara and Shawn C Burdette. "Photoisomerization in different classes of azobenzene". In: *Chemical Society Reviews* 41.5 (2012), pp. 1809–1825.

[22] Sudhish Chandra Banerjee. *Spontaneous Combustion of Coal and Mine Fires*. Netherlands, 1985.

[23] Polina V Banushkina and Sergei V Krivov. "Optimal reaction coordinates". In: *Wiley Interdisciplinary Reviews: Computational Molecular Science* 6.6 (2016), pp. 748–763.

[24] Mario Barbatti et al. "Relaxation mechanisms of UV-photoexcited DNA and RNA nucleobases". In: *Proceedings of the National Academy of Sciences* 107.50 (2010), pp. 21453–21458.

[25] Alberto Barchielli and Viacheslav P Belavkin. "Measurements continuous in time and a posteriori states in quantum mechanics". In: *Journal of Physics A: Mathematical and General* 24.7 (1991), p. 1495.

[26] Christopher J Bardeen et al. "Feedback quantum control of molecular electronic population transfer". In: *Chemical Physics Letters* 280.1 (1997), pp. 151–158. ISSN: 0009-2614.

[27] PS Bardell. "The Origins of Alloy Steels". In: *History of Technology Volume 9* (2016), p. 1.

[28] Yasemin Basdogan, Alex M Maldonado, and John A Keith. "Advances and challenges in modeling solvated reaction mechanisms for renewable fuels and chemicals". In: *Wiley Interdisciplinary Reviews: Computational Molecular Science* 10.2 (2020), e1446.

[29] Michael H Beck et al. "The multiconfiguration time-dependent Hartree (MCTDH) method: A highly efficient algorithm for propagating wavepackets". In: *Physics Reports* 324.1 (2000), pp. 1–105.

[30] Lloyd V Berkner and LC Marshall. "On the origin and rise of oxygen concentration in the Earth's atmosphere". In: *Journal of Atmospheric Sciences* 22.3 (1965), pp. 225–261.

[31] Ralf Betzholz, Bruno G Taketani, and Juan Mauricio Torres. "Breakdown signatures of the phenomenological Lindblad master equation in the strong optomechanical coupling regime". In: *Quantum Science and Technology* 6.1 (2020), p. 015005.

[32] Saurabh Bhandari, Srinivas Rangarajan, and Manos Mavrikakis. "Combining computational modeling with reaction kinetics experiments for elucidating the in situ nature of the active site in catalysis". In: *Accounts of Chemical Research* 53.9 (2020), pp. 1893–1904.

[33] Martin P Bircher et al. "Nonadiabatic effects in electronic and nuclear dynamics". In: *Structural Dynamics* 4.6 (2017).

[34] Nicolaas Bloembergen and Eli Yablonovitch. "Infrared-laser-induced unimolecular reactions". In: *Physics Today* 31.5 (1978), pp. 23–30.

[35] Nicolaas Bloembergen and Ahmed H Zewail. "Energy redistribution in isolated molecules and the question of mode-selective laser chemistry revisited". In: *The Journal of Physical Chemistry* 88.23 (1984), pp. 5459–5465.

[36] Peter Bolhuis. "Sampling ensembles of deterministic transition pathways". In: *Faraday Discussions* 110 (1998), pp. 421–436.

[37] PG Bolhuis and C Dellago. "Practical and conceptual path sampling issues". In: *The European Physical Journal Special Topics* 224.12 (2015), pp. 2409–2427.

[38] Max Born and Werner Heisenberg. "Zur quantentheorie der molekeln". In: *Annalen der Physik* 379.9 (1924), pp. 1–31.

[39] Gregory R Bowman. "An overview and practical guide to building Markov state models". In: *An Introduction to Markov State Models and Their Application to Long Timescale Molecular Simulation* (2014), pp. 7–22.

[40] DM Brenner. "Is bond selective chemistry possible?" In: *Conference on Lasers and Electro-Optics*. Optica Publishing Group. 1982, THJ1.

[41] H P Breuer and Francesco Petruccione. *The Theory of Open Quantum Systems*. Oxford: Oxford University Press on Demand, 2002.

[42] Joaquín Calbo et al. "Tuning azoheteroarene photoswitch performance through heteroaryl design". In: *Journal of the American Chemical Society* 139.3 (2017), pp. 1261–1274.

[43] Jorge A. Campos-Gonzalez-Angulo and Joel Yuen-Zhou. "Polaritonic normal modes in transition state theory". In: *The Journal of Chemical Physics* 152.16 (2020), p. 161101.

[44] Jianshu Cao and Gregory A. Voth. "A unified framework for quantum activated rate processes. I. General theory". In: *The Journal of Chemical Physics* 105.16 (1996), pp. 6856–6870.

[45] Howard Carmichael. *An open systems approach to quantum optics: Lectures presented at the Université Libre de Bruxelles, October 28 to November 4, 1991*. Vol. 18. Springer Science & Business Media, 2009.

[46] Marco Cattaneo et al. "Local versus global master equation with common and separate baths: Superiority of the global approach in partial secular approximation". In: *New Journal of Physics* 21.11 (2019), p. 113045.

[47] Marco Cattaneo et al. "Symmetry and block structure of the Liouvillian superoperator in partial secular approximation". In: *Physical Review A* 101.4 (2020), p. 042108.

[48] Chun-Ran Chang, Zheng-Qing Huang, and Jun Li. "The promotional role of water in heterogeneous catalysis: Mechanism insights from computational modeling". In: *Wiley Interdisciplinary Reviews: Computational Molecular Science* 6.6 (2016), pp. 679–693.

[49] Sambarta Chatterjee and Nancy Makri. "Real-time path integral methods, quantum master equations, and classical vs quantum memory". In: *The Journal of Physical Chemistry B* 123.49 (2019), pp. 10470–10482.

[50] S Chaturvedi and F Shibata. "Time-convolutionless projection operator formalism for elimination of fast variables. Applications to Brownian motion". In: *Zeitschrift für Physik B Condensed Matter* 35.3 (1979), pp. 297–308.

[51] Liangzhou Chen et al. "Reaction pathways and cyclic chain model of free radicals during coal spontaneous combustion". In: *Fuel* 293 (2021), p. 120436.

[52] Lipeng Chen et al. "Dissipative dynamics at conical intersections: Simulations with the hierarchy equations of motion method". In: *Faraday Discussions* 194 (2016), pp. 61–80.

[53] Gui-Juan Cheng et al. "Computational organic chemistry: Bridging theory and experiment in establishing the mechanisms of chemical reactions". In: *Journal of the American Chemical Society* 137.5 (2015), pp. 1706–1725.

[54] Yuan-Chung Cheng and Graham R Fleming. "Dynamics of light harvesting in photosynthesis". In: *Annual Review of Physical Chemistry* 60 (2009), pp. 241–262.

[55] L Cohen. "A review of Brownian motion based solely on the Langevin equation with white noise". In: *Mathematical Analysis, Probability and Applications–Plenary Lectures: ISAAC 2015, Macau, China 10* (2016), pp. 1–35.

[56] Claude Cohen-Tannoudji, Jacques Dupont-Roc, and Gilbert Grynberg. "Quantum Electrodynamics in the Coulomb Gauge". In: *Photons and Atoms*. Hoboken: John Wiley & Sons, Ltd, 1997, pp. 169–252. ISBN: 9783527618422.

[57] Daniel T. Colbert and William H. Miller. "A novel discrete variable representation for quantum mechanical reactive scattering via the S-matrix Kohn method". In: *The Journal of Chemical Physics* 96.3 (1992), pp. 1982–1991.

[58] SH Courtney and GR Fleming. "Photoisomerization of stilbene in low viscosity solvents: Comparison of isolated and solvated molecules". In: *The Journal of Chemical Physics* 83.1 (1985), pp. 215–222.

[59] B Cui, XX Yi, and CH Oh. "Excitation energy transfer in light-harvesting systems: Effect of the initial state". In: *Journal of Physics B: Atomic, Molecular and Optical Physics* 45.8 (2012), p. 085501.

[60] Basile FE Curchod and Todd J Martínez. "Ab initio nonadiabatic quantum molecular dynamics". In: *Chemical Reviews* 118.7 (2018), pp. 3305–3336.

[61] Artur Czerwinski. "Dynamics of open quantum systems—Markovian semigroups and beyond". In: *Symmetry* 14.8 (2022), p. 1752.

[62] Artur Czerwinski. "Entanglement dynamics governed by time-dependent quantum generators". In: *Axioms* 11.11 (2022), p. 589.

[63] Jean Dalibard, Yvan Castin, and Klaus Mølmer. "Wave-function approach to dissipative processes in quantum optics". In: *Physical Review Letters* 68.5 (1992), p. 580.

[64] E Brian Davies. "Markovian master equations". In: *Communications in Mathematical Physics* 39 (1974), pp. 91–110.

[65] Edward B Davies. "Quantum stochastic processes". In: *Communications in Mathematical Physics* 15.4 (1969), pp. 277–304.

[66] Christoph Dellago and Peter G Bolhuis. "Transition path sampling and other advanced simulation techniques for rare events". In: *Advanced Computer Simulation Approaches for Soft Matter Sciences III* (2009), pp. 167–233.

[67] Christoph Dellago, Peter G Bolhuis, and David Chandler. "Efficient transition path sampling: Application to Lennard-Jones cluster rearrangements". In: *The Journal of Chemical Physics* 108.22 (1998), pp. 9236–9245.

[68] Christoph Dellago, Peter G Bolhuis, and Phillip L Geissler. "Transition path sampling". In: *Advances in Chemical Physics* 123 (2002), pp. 1–78.

[69] Christoph Dellago et al. "Transition path sampling and the calculation of rate constants". In: *The Journal of Chemical Physics* 108.5 (1998), pp. 1964–1977.

[70] Francesco Di Giacomo and Evgenii E Nikitin. "The Majorana formula and the Landau–Zener–Stückelberg treatment of the avoided crossing problem". In: *Physics-Uspekhi* 48.5 (2005), p. 515.

[71] Derk Jan van Dijken et al. "Acylhydrazones as widely tunable photoswitches". In: *Journal of the American Chemical Society* 137.47 (2015), pp. 14982–14991.

[72] E. W. Dijkstra. "A note on two problems in connection with graphs". In: *Journal of Numerical Mathematics* 1 (1 1959), pp. 269–271.

[73] Richard J Dimelow et al. "Exploring reaction pathways with transition path and umbrella sampling: Application to methyl maltoside". In: *The Journal of Chemical Physics* 124.11 (2006).

[74] GC Dismukes et al. "The origin of atmospheric oxygen on Earth: The innovation of oxygenic photosynthesis". In: *Proceedings of the National Academy of Sciences* 98.5 (2001), pp. 2170–2175.

[75] Matthew Du, Jorge A Campos-Gonzalez-Angulo, and Joel Yuen-Zhou. "Nonequilibrium effects of cavity leakage and vibrational dissipation in thermally activated polariton chemistry". In: *The Journal of Chemical Physics* 154.8 (2021).

[76] Matthew Du, Yong Rui Poh, and Joel Yuen-Zhou. "Vibropolaritonic reaction rates in the collective strong coupling regime: Pollak–Grabert–Hänggi theory". In: *The Journal of Physical Chemistry C* 127.11 (2023), pp. 5230–5237.

[77] Hong-Guang Duan, R. J. Dwayne Miller, and Michael Thorwart. "Impact of Vibrational Coherence on the Quantum Yield at a Conical Intersection". In: *The Journal of Physical Chemistry Letters* 7.17 (2016), pp. 3491–3496.

[78] Hong-Guang Duan et al. "Signature of the geometric phase in the wave packet dynamics on hypersurfaces". In: *Chemical Physics* 515 (2018), pp. 21–27.

[79] R Dum, P Zoller, and H Ritsch. "Monte Carlo simulation of the atomic master equation for spontaneous emission". In: *Physical Review A* 45.7 (1992), p. 4879.

[80] Adam D Dunkelberger et al. "Vibration-cavity polariton chemistry and dynamics". In: *Annual Review of Physical Chemistry* 73 (2022), pp. 429–451.

[81] Burkhard Dünweg. "Langevin methods". In: *Computer Simulations of Surfaces and Interfaces*. Springer, 2003, pp. 77–92.

[82] Dassia Egorova, Axel Kühl, and Wolfgang Domcke. "Modeling of ultrafast electron-transfer dynamics: Multi-level Redfield theory and validity of approximations". In: *Chemical Physics* 268.1-3 (2001), pp. 105–120.

[83] Dassia Egorova et al. "Modeling of ultrafast electron-transfer processes: Validity of multilevel Redfield theory". In: *The Journal of Chemical Physics* 119.5 (2003), pp. 2761–2773.

[84] Jan Willem Erisman et al. "How a century of ammonia synthesis changed the world". In: *Nature Geoscience* 1.10 (2008), pp. 636–639.

[85] Fernando A Escobedo, Ernesto E Borrero, and Juan C Araque. "Transition path sampling and forward flux sampling. Applications to biological systems". In: *Journal of Physics: Condensed Matter* 21.33 (2009), p. 333101.

[86] Thomas P Fay, Lachlan P Lindoy, and David E Manolopoulos. "Electron spin relaxation in radical pairs: Beyond the Redfield approximation". In: *The Journal of Chemical Physics* 151.15 (2019).

[87] Thomas P. Fay. "A simple improved low temperature correction for the hierarchical equations of motion". In: *The Journal of Chemical Physics* 157.5 (2022), p. 054108.

[88] Thomas Patrick Fay. *`heom-lab`: A Matlab code for performing HEOM calculations*. `https://github.com/tomfay/heom-lab`. 2022.

[89] Michael D Fayer. *Elements of quantum mechanics*. eng. Oxford: Oxford University Press, 2001. ISBN: 9780195141955.

[90] Anthony K Felts, W Thomas Pollard, and Richard A Friesner. "Multilevel Redfield treatment of bridge-mediated long-range electron transfer: A mechanism for anomalous distance dependence". In: *The Journal of Physical Chemistry* 99.9 (1995), pp. 2929–2940.

[91] RE Fenna and BW Matthews. "Chlorophyll arrangement in a bacteriochlorophyll protein from Chlorobium limicola". In: *Nature* 258.5536 (1975), pp. 573–577.

[92] Alessandro Ferretti, Alessandro Lami, and Giovanni Villani. "Quantum dynamics of a model system with a conical intersection". In: *The Journal of Chemical Physics* 106.3 (1997), pp. 934–941.

[93] Jonathan H Fetherolf and Timothy C Berkelbach. "Linear and nonlinear spectroscopy from quantum master equations". In: *The Journal of Chemical Physics* 147.24 (2017).

[94] Marit R Fiechter et al. "How quantum is the resonance behavior in vibrational polariton chemistry?" In: *The Journal of Physical Chemistry Letters* 14.36 (2023), pp. 8261–8267.

[95] Chris Fleming et al. "The rotating-wave approximation: Consistency and applicability from an open quantum system analysis". In: *Journal of Physics A: Mathematical and Theoretical* 43.40 (2010), p. 405304.

[96] GW Ford and RF O'Connell. "The rotating wave approximation (RWA) of quantum optics: Serious defect". In: *Physica A: Statistical Mechanics and its Applications* 243.3-4 (1997), pp. 377–381.

[97] Th Förster. "Zwischenmolekulare energiewanderung und fluoreszenz". In: *Annalen der Physik* 437.1-2 (1948), pp. 55–75.

[98] Heinz Frei, Leif Fredin, and George C Pimentel. "Vibrational excitation of ozone and molecular fluorine reactions in cryogenic matrices". In: *The Journal of Chemical Physics* 74.1 (1981), pp. 397–411.

[99] Heinz Frei and George C Pimentel. "Selective vibrational excitation of the ethylene–fluorine reaction in a nitrogen matrix. I". In: *The Journal of Chemical Physics* 78.6 (1983), pp. 3698–3712.

[100] Daan Frenkel and Berend Smit. *Understanding Molecular Simulation: From Algorithms to Applications*. Academic Press San Diego, 2002.

[101] Javier Galego et al. "Cavity Casimir-Polder forces and their effects in ground-state chemical reactivity". In: *Physical Review X* 9 (2 2019), p. 021057.

[102] Jaume García-Amorós and Dolores Velasco. "Recent advances towards azobenzene-based light-driven real-time information-transmitting materials". In: *Beilstein Journal of Organic Chemistry* 8.1 (2012), pp. 1003–1017.

[103] Phillip L Geissler, Christoph Dellago, and David Chandler. "Kinetic pathways of ion pair dissociation in water". In: *The Journal of Physical Chemistry B* 103.18 (1999), pp. 3706–3710.

[104] Michael Genkin and Eva Lindroth. "Description of resonance decay by Lindblad operators". In: *Journal of Physics A: Mathematical and Theoretical* 41.42 (2008), p. 425303.

[105] Ahmet Ozan Gezerman. "A critical assessment of green ammonia production and ammonia production technologies". In: *Kemija u industriji: Časopis kemičara i kemijskih inženjera Hrvatske* 71.1-2 (2022), pp. 57–66.

[106] Rami Gherib et al. "On the inclusion of the diagonal Born-Oppenheimer correction in surface hopping methods". In: *The Journal of Chemical Physics* 144.15 (2016).

[107] Miguel A González. "Force fields and molecular dynamics simulations". In: *École thématique de la Société Française de la Neutronique* 12 (2011), pp. 169–200.

[108] B González-Soria and F Delgado. "Quantum Entanglement in Fenna—Matthews—Olson Photosynthetic Light—Harvesting complexes: A Short Review of Analysis Methods". In: *Journal of Physics: Conference Series*. Vol. 1540. 1. IOP Publishing. 2020, p. 012026.

[109] Vittorio Gorini, Andrzej Kossakowski, and Ennackal Chandy George Sudarshan. "Completely positive dynamical semigroups of N-level systems". In: *Journal of Mathematical Physics* 17.5 (1976), pp. 821–825.

[110] Beverley Green and William W Parson. *Light-harvesting antennas in photosynthesis*. Vol. 13. Springer Science & Business Media, 2003.

[111] Harald Gröger et al. "Industrial landmarks in the development of sustainable production processes for the β-lactam antibiotic key intermediate 7-aminocephalosporanic acid (7-ACA)". In: *Sustainable Chemistry and Pharmacy* 5 (2017), pp. 72–79.

[112] Richard F. Grote and James T. Hynes. "The stable states picture of chemical reactions. II Rate constants for condensed and gas phase reaction models". In: *The Journal of Chemical Physics* 73.6 (1980), pp. 2715–2732.

[113] Yafu Guan et al. "High-fidelity first principles nonadiabaticity: Diabatization, analytic representation of global diabatic potential energy matrices, and quantum dynamics". In: *Physical Chemistry Chemical Physics* 23.44 (2021), pp. 24962–24983.

[114] KD Hammonds and DM Heyes. "Shadow Hamiltonian in classical NVE molecular dynamics simulations: A path to long time stability". In: *The Journal of Chemical Physics* 152.2 (2020).

[115] Seungsuk Han, Hinne Hettema, and David R Yarkony. "Radiationless decay of the 1, 2, 3 3Πg states of Al2: A fully first principles treatment using adiabatic and rigorous diabatic states". In: *The Journal of Chemical Physics* 102.5 (1995), pp. 1955–1964.

[116] Nicholas C Handy, Yukio Yamaguchi, and Henry F Schaefer III. "The diagonal correction to the Born–Oppenheimer approximation: Its effect on the singlet–triplet splitting of CH2 and other molecular effects". In: *The Journal of Chemical Physics* 84.8 (1986), pp. 4481–4484.

[117] Peter Hänggi and Fabio Marchesoni. "Introduction: 100 years of Brownian motion". In: *Chaos: An Interdisciplinary Journal of Nonlinear Science* 15.2 (2005), p. 026101.

[118] Gabriel Hanna and Raymond Kapral. "Nonadiabatic dynamics of condensed phase rate processes". In: *Accounts of Chemical Research* 39.1 (2006), pp. 21–27.

[119] Werner Heisenberg. "Über den anschaulichen Inhalt der quantentheoretischen Kinematik und Mechanik". In: *Zeitschrift für Physik* 43.3 (1927), pp. 172–198.

[120] JM Hicks et al. "Polarity-dependent barriers and the photoisomerization dynamics of molecules in solution". In: *Chemical Physics Letters* 135.4-5 (1987), pp. 413–420.

[121] William G Hoover. "Canonical dynamics: Equilibrium phase-space distributions". In: *Physical Review A* 31.3 (1985), p. 1695.

[122] Hrant P Hratchian and H Bernhard Schlegel. "Finding minima, transition states, and following reaction pathways on ab initio potential energy surfaces". In: *Theory and Applications of Computational Chemistry*. Elsevier, 2005, pp. 195–249.

[123] Brooke E Husic and Vijay S Pande. "Markov state models: From an art to a science". In: *Journal of the American Chemical Society* 140.7 (2018), pp. 2386–2396.

[124] Sajad Hussain et al. "Photosynthesis research under climate change". In: *Photosynthesis Research* 150 (2021), pp. 5–19.

[125] Jan Jeske and Jared H Cole. "Derivation of Markovian master equations for spatially correlated decoherence". In: *Physical Review A* 87.5 (2013), p. 052138.

[126] Jan Jeske et al. "Bloch-Redfield equations for modeling light-harvesting complexes". In: *The Journal of Chemical Physics* 142.6 (2015).

[127] Bogumil Jeziorski, Robert Moszynski, and Krzysztof Szalewicz. "Perturbation theory approach to intermolecular potential energy surfaces of van der Waals complexes". In: *Chemical Reviews* 94.7 (1994), pp. 1887–1930.

[128] Concepción Jiménez-González et al. "Key green engineering research areas for sustainable manufacturing: A perspective from pharmaceutical and fine chemicals manufacturers". In: *Organic Process Research & Development* 15.4 (2011), pp. 900–911.

[129] Soumil Y Joshi and Sanket A Deshmukh. "A review of advancements in coarse-grained molecular dynamics simulations". In: *Molecular Simulation* 47.10-11 (2021), pp. 786–803.

[130] Adam Kell et al. "On uncorrelated inter-monomer Förster energy transfer in Fenna–Matthews–Olson complexes". In: *Journal of the Royal Society Interface* 16.151 (2019), p. 20180882.

[131] Dustin Keys and Jan Wehr. "Poisson stochastic master equation unravelings and the measurement problem: A quantum stochastic calculus perspective". In: *Journal of Mathematical Physics* 61.3 (2020).

[132] Andrei Kolmogoroff. "Über die analytischen Methoden in der Wahrscheinlichkeitsrechnung". In: *Mathematische Annalen* 104 (1931), pp. 415–458.

[133] H Köuppel, Wolfgang Domcke, and Lorenz S Cederbaum. "Multimode molecular dynamics beyond the Born-Oppenheimer approximation". In: *Advances in Chemical Physics* (1984), pp. 59–246.

[134] Hendrik Anthony Kramers. "Brownian motion in a field of force and the diffusion model of chemical reactions". In: *Physica* 7.4 (1940), pp. 284–304.

[135] Vasileios Kyriakou et al. "An electrochemical Haber-Bosch process". In: *Joule* 4.1 (2020), pp. 142–158.

[136] Zhenggang Lan et al. "Photochemistry of hydrogen-bonded aromatic pairs: Quantum dynamical calculations for the pyrrole–pyridine complex". In: *Proceedings of the National Academy of Sciences* 105.35 (2008), pp. 12707–12712.

[137] LD Landau. "On the theory of transfer of energy at collisions II". In: *Phys. Z. Sowjetunion* 2.46 (1932), p. 118.

[138] Paul Langevin. "On the theory of Brownian motion." In: *Comptes rendus de l'Académie des Sciences (Paris)* 146 (1908), p. 530.

[139] DG Joakim Larsson. "Pollution from drug manufacturing: Review and perspectives". In: *Philosophical Transactions of the Royal Society B: Biological Sciences* 369.1656 (2014), p. 20130571.

[140] Jyoti Lather et al. "Cavity catalysis by cooperative vibrational strong coupling of reactant and solvent molecules". In: *Angewandte Chemie International Edition* 58.31 (2019), pp. 10635–10638.

[141] VS Letokhov. "Use of lasers to control selective chemical reactions". In: *Science* 180.4085 (1973), pp. 451–458.

[142] Benjamin G Levine and Todd J Martínez. "Isomerization through conical intersections". In: *Annual Review of Physical Chemistry* 58 (2007), pp. 613–634.

[143] Hui Li et al. "Quantum Control of Atom-Ion Charge Exchange via Light-Induced Conical Intersections". In: *The Journal of Physical Chemistry A* 127.29 (2023), pp. 5979–5985.

[144] Tao E. Li, Abraham Nitzan, and Joseph E. Subotnik. "On the origin of ground-state vacuum-field catalysis: Equilibrium consideration". In: *The Journal of Chemical Physics* 152.23 (2020), p. 234107.

[145] Xinyang Li, Arkajit Mandal, and Pengfei Huo. "Theory of mode-selective chemistry through polaritonic vibrational strong coupling". In: *The Journal of Physical Chemistry Letters* 12.29 (2021), pp. 6974–6982.

[146] Chelsea Liekhus-Schmaltz et al. "Coherent control using kinetic energy and the geometric phase of a conical intersection". In: *The Journal of Chemical Physics* 145.14 (2016).

[147] TCH Liew, IA Shelykh, and G Malpuech. "Polaritonic devices". In: *Physica E: Low-dimensional Systems and Nanostructures* 43.9 (2011), pp. 1543–1568.

[148] Goran Lindblad. "On the generators of quantum dynamical semigroups". In: *Communications in Mathematical Physics* 48 (1976), pp. 119–130.

[149] Lachlan P. Lindoy, Arkajit Mandal, and David R. Reichman. "Resonant cavity modification of ground-state chemical kinetics". In: *The Journal of Physical Chemistry Letters* 13.28 (2022), pp. 6580–6586.

[150] Na Liu et al. "Optical Control of Crossing the Conical Intersection in β-Carotene". In: *The Journal of Physical Chemistry Letters* 14.41 (2023), pp. 9215–9221.

[151] Valerio Lucarini et al. *Kramers-Kronig Relations in Optical Materials Research*. Vol. 110. Springer Science & Business Media, 2005.

[152] Margherita Maiuri et al. "Coherent wavepackets in the Fenna–Matthews–Olson complex are robust to excitonic-structure perturbations caused by mutagenesis". In: *Nature Chemistry* 10.2 (2018), pp. 177–183.

[153] Dmitrii E Makarov. "The master equation approach to problems in chemical and biological physics". In: *Reviews in Computational Chemistry* 30 (2017), pp. 257–287.

[154] Harri Mäkelä and M Möttönen. "Effects of the rotating-wave and secular approximations on non-Markovianity". In: *Physical Review A* 88.5 (2013), p. 052111.

[155] João Pedro Malhado and James T Hynes. "On the Landau–Zener approach to nonadiabatic transitions for a vertical conical intersection". In: *Chemical Physics* 347.1-3 (2008), pp. 39–45.

[156] Vincenzo Manca, Roberto Pagliarini, and Simone Zorzan. "A photosynthetic process modelled by a metabolic P system". In: *Natural Computing* 8 (2009), pp. 847–864.

[157] Arkajit Mandal, Xinyang Li, and Pengfei Huo. "Theory of vibrational polariton chemistry in the collective coupling regime". In: *The Journal of Chemical Physics* 156.1 (2022).

[158] Uwe Manthe and H Köppel. "Dynamics on potential energy surfaces with a conical intersection: Adiabatic, intermediate, and diabatic behavior". In: *The Journal of Chemical Physics* 93.3 (1990), pp. 1658–1669.

[159] Adriana Marais et al. "Decoherence-assisted transport in quantum networks". In: *New Journal of Physics* 15.1 (2013), p. 013038.

[160] Gianluca Marcelli and Richard J Sadus. "Molecular simulation of the phase behavior of noble gases using accurate two-body and three-body intermolecular potentials". In: *The Journal of Chemical Physics* 111.4 (1999), pp. 1533–1540.

[161] Rudolph A Marcus. "Chemical and electrochemical electron-transfer theory". In: *Annual Review of Physical Chemistry* 15.1 (1964), pp. 155–196.

[162] Jordi Martí, Félix S Csajka, and David Chandler. "Stochastic transition pathways in the aqueous sodium chloride dissociation process". In: *Chemical Physics Letters* 328.1-2 (2000), pp. 169–176.

[163] Vincenzo Mascoli, Luca Bersanini, and Roberta Croce. "Far-red absorption and light-use efficiency trade-offs in chlorophyll f photosynthesis". In: *Nature Plants* 6.8 (2020), pp. 1044–1053.

[164] Spiridoula Matsika. "Three-state conical intersections in nucleic acid bases". In: *The Journal of Physical Chemistry A* 109.33 (2005), pp. 7538–7545.

[165] Spiridoula Matsika and Pascal Krause. "Nonadiabatic events and conical intersections". In: *Annual Review of Physical Chemistry* 62 (2011), pp. 621–643.

[166] Donald Allan McQuarrie and John Douglas Simon. *Physical Chemistry: A Molecular Approach*. Vol. 1. Sausalito, CA: University science books, 1997.

[167] C Alden Mead and Donald G Truhlar. "Conditions for the definition of a strictly diabatic electronic basis for molecular systems". In: *The Journal of Chemical Physics* 77.12 (1982), pp. 6090–6098.

[168] Yilin Meng et al. "Transition path theory analysis of c-Src kinase activation". In: *Proceedings of the National Academy of Sciences* 113.33 (2016), pp. 9193–9198.

[169] M Menzinger and Re Wolfgang. "The meaning and use of the Arrhenius activation energy". In: *Angewandte Chemie International Edition in English* 8.6 (1969), pp. 438–444.

[170] Philipp Metzner, Christof Schütte, and Eric Vanden-Eijnden. "Illustration of transition path theory on a collection of simple examples". In: *The Journal of Chemical Physics* 125.8 (2006), p. 084110.

[171] William H Miller. "Quantum mechanical transition state theory and a new semiclassical model for reaction rate constants". In: *The Journal of Chemical Physics* 61.5 (1974), pp. 1823–1834.

[172] Daniel B Mills et al. "Eukaryogenesis and oxygen in Earth history". In: *Nature Ecology & Evolution* 6.5 (2022), pp. 520–532.

[173] G Mills et al. "Generalized path integral based quantum transition state theory". In: *Chemical Physics Letters* 278.1-3 (1997), pp. 91–96.

[174] Michael J Mitchell and J Andrew McCammon. "Free energy difference calculations by thermodynamic integration: Difficulties in obtaining a precise value". In: *Journal of Computational Chemistry* 12.2 (1991), pp. 271–275.

[175] Jeremy Moix et al. "Efficient energy transfer in light-harvesting systems, III: The influence of the eighth bacteriochlorophyll on the dynamics and efficiency in FMO". In: *The Journal of Physical Chemistry Letters* 2.24 (2011), pp. 3045–3052.

[176] Klaus Mølmer, Yvan Castin, and Jean Dalibard. "Monte Carlo wave-function method in quantum optics". In: *The Journal of the Optical Society of America B* 10.3 (1993), pp. 524–538.

[177] Andrés Montoya-Castillo, Timothy C Berkelbach, and David R Reichman. "Extending the applicability of Redfield theories into highly non-Markovian regimes". In: *The Journal of Chemical Physics* 143.19 (2015).

[178] Klaus Müller. "Reaction paths on multidimensional energy hypersurfaces". In: *Angewandte Chemie International Edition in English* 19.1 (1980), pp. 1–13.

[179] Ellen Mulvihill and Eitan Geva. "A Road Map to Various Pathways for Calculating the Memory Kernel of the Generalized Quantum Master Equation". In: *The Journal of Physical Chemistry B* 125.34 (2021), pp. 9834–9852.

[180] Ellen Mulvihill et al. "A modified approach for simulating electronically nonadiabatic dynamics via the generalized quantum master equation". In: *The Journal of Chemical Physics* 150.3 (2019).

[181] Anja Muzdalo et al. "Cis-to-trans isomerization of azobenzene derivatives studied with transition path sampling and quantum mechanical/molecular mechanical molecular dynamics". In: *Journal of Chemical Theory and Computation* 14.4 (2018), pp. 2042–2051.

[182] Sadao Nakajima. "On quantum theory of transport phenomena: Steady diffusion". In: *Progress of Theoretical Physics* 20.6 (1958), pp. 948–959.

[183] Peter Nalbach, Daniel Braun, and Michael Thorwart. "Exciton transfer dynamics and quantumness of energy transfer in the Fenna-Matthews-Olson complex". In: *Physical Review E* 84.4 (2011), p. 041926.

[184] Simon P Neville et al. "Substituent effects on dynamics at conical intersections: Allene and methyl allenes". In: *The Journal of Chemical Physics* 144.1 (2016).

[185] Charlene Ng et al. "Waveguide-Plasmon Polariton Enhanced Photochemistry". In: *Advanced Optical Materials* 3.11 (2015), pp. 1582–1590.

[186] Maxim Nikolaev and Denis Tikhonov. "Light-Sensitive Open Channel Block of Ionotropic Glutamate Receptors by Quaternary Ammonium Azobenzene Derivatives". In: *International Journal of Molecular Sciences* 24.18 (2023), p. 13773.

[187] Abraham Nitzan. *Chemical Dynamics in Condensed Phases: Relaxation, Transfer and Reactions in Condensed Molecular Systems*. Oxford: Oxford University Press, 2006.

[188] Frank Noé et al. "Constructing the equilibrium ensemble of folding pathways from short off-equilibrium simulations". In: *Proceedings of the National Academy of Sciences* 106.45 (2009), pp. 19011–19016.

[189] Shuichi Nosé. "A unified formulation of the constant temperature molecular dynamics methods". In: *The Journal of Chemical Physics* 81.1 (1984), pp. 511–519.

[190] Vladimir Novoderezhkin, Markus Wendling, and Rienk Van Grondelle. "Intra-and interband transfers in the B800-B850 antenna of Rhodospirillum m olischianum: Redfield theory modeling of polarized pump-probe kinetics". In: *The Journal of Physical Chemistry B* 107.41 (2003), pp. 11534–11548.

[191] Raymond Kwesi Nutor et al. "Accelerated emergence of CoNi-based medium-entropy alloys with emphasis on their mechanical properties". In: *Current Opinion in Solid State and Materials Science* 26.6 (2022), p. 101032.

[192] Kenji Ohmori. "Wave-packet and coherent control dynamics". In: *Annual Review of Physical Chemistry* 60 (2009), pp. 487–511.

[193] MJ Olascoaga and FJ Beron-Vera. "Exploring the use of Transition Path Theory in building an oil spill prediction scheme". In: *Frontiers in Marine Science* 9 (2023), p. 1041005.

[194] Gloria Olaso-González, Manuela Merchán, and Luis Serrano-Andrés. "Ultrafast electron transfer in photosynthesis: Reduced pheophytin and quinone interaction mediated by conical intersections". In: *The Journal of Physical Chemistry B* 110.48 (2006), pp. 24734–24739.

[195] Alexandra Olaya-Castro et al. "Efficiency of energy transfer in a light-harvesting system under quantum coherence". In: *Physical Review B* 78.8 (2008), p. 085115.

[196] Moshood Onifade and Bekir Genc. "A review of research on spontaneous combustion of coal". In: *International Journal of Mining Science and Technology* 30.3 (2020), pp. 303–311.

[197] Lars Onsager. "Reciprocal relations in irreversible processes. I." In: *Physical Review* 37.4 (1931), p. 405.

[198] Lars Onsager. "Reciprocal relations in irreversible processes. II." In: *Physical Review* 38.12 (1931), p. 2265.

[199] Izhack Oref and B Seymour Rabinovitch. "Do highly excited reactive polyatomic molecules behave ergodically?" In: *Accounts of Chemical Research* 12.5 (1979), pp. 166–175.

[200] E Orgiu et al. "Conductivity in organic semiconductors hybridized with the vacuum field". In: *Nature Materials* 14.11 (2015), pp. 1123–1129.

[201] Benoit Palmieri, Darius Abramavicius, and Shaul Mukamel. "Lindblad equations for strongly coupled populations and coherences in photosynthetic complexes". In: *The Journal of Chemical Physics* 130.20 (2009).

[202] Vijay S Pande, Kyle Beauchamp, and Gregory R Bowman. "Everything you wanted to know about Markov State Models but were afraid to ask". In: *Methods* 52.1 (2010), pp. 99–105.

[203] Eric Paquet, Herna L Viktor, et al. "Molecular dynamics, Monte Carlo simulations, and Langevin dynamics: A computational review". In: *BioMed Research International* 2015 (2015).

[204] Jinhyung Park et al. "Ab initio potential energy surfaces calculation via restricted Hartree–Fock for molecular dynamics simulation: A comprehensive review". In: *Journal of the Korean Physical Society* (2024), pp. 1–16.

[205] W. Pauli and M. Fierz. "Zur Theorie der Emission langwelliger Lichtquanten". In: *Il Nuovo Cimento (1924-1942)* 15 (3 1938), pp. 167–188.

[206] Philip Pechukas. "Transition state theory". In: *Annual Review of Physical Chemistry* 32.1 (1981), pp. 159–177.

[207] Juan B Pérez-Sánchez et al. "Collective polaritonic effects on chemical dynamics suppressed by disorder". In: *Physical Review Research* 6.1 (2024), p. 013222.

[208] Juan B Pérez-Sánchez et al. "Simulating molecular polaritons in the collective regime using few-molecule models". In: *Proceedings of the National Academy of Sciences* 120.15 (2023), e2219223120.

[209] Maurizio Persico and Giovanni Granucci. "An overview of nonadiabatic dynamics simulations methods, with focus on the direct approach versus the fitting of potential energy surfaces". In: *Theoretical Chemistry Accounts* 133 (2014), pp. 1–28.

[210] Baron Peters. "Reaction coordinates and mechanistic hypothesis tests". In: *Annual Review of Physical Chemistry* 67 (2016), pp. 669–690.

[211] Baron Peters. *Reaction Rate Theory and Rare Events*. Elsevier, 2017.

[212] Johannes D Plumhof et al. "Room-temperature Bose–Einstein condensation of cavity exciton–polaritons in a polymer". In: *Nature Materials* 13.3 (2014), pp. 247–252.

[213] W Thomas Pollard and Richard A Friesner. "Solution of the Redfield equation for the dissipative quantum dynamics of multilevel systems". In: *The Journal of Chemical Physics* 100.7 (1994), pp. 5054–5065.

[214] Edwin Albert Power and S. Zienau. "Coulomb gauge in non-relativistic quantum electro-dynamics and the shape of spectral lines". In: *Philosophical Transactions of the Royal Society A* 251.999 (1959), pp. 427–454.

[215] Lawrence R Pratt. "A statistical method for identifying transition states in high dimensional problems". In: *The Journal of Chemical Physics* 85.9 (1986), pp. 5045–5048.

[216] Jingzhi Pu, Jiali Gao, and Donald G Truhlar. "Multidimensional tunneling, recrossing, and the transmission coefficient for enzymatic reactions". In: *Chemical Reviews* 106.8 (2006), pp. 3140–3169.

[217] Da-Long Qi et al. "Tracking an electronic wave packet in the vicinity of a conical intersection". In: *The Journal of Chemical Physics* 147.7 (2017).

[218] Sara L Quaytman and Steven D Schwartz. "Reaction coordinate of an enzymatic reaction revealed by transition path sampling". In: *Proceedings of the National Academy of Sciences* 104.30 (2007), pp. 12253–12258.

[219] Srinath Ranya and Nandini Ananth. "Multistate ring polymer instantons and nonadiabatic reaction rates". In: *The Journal of Chemical Physics* 152.11 (2020).

[220] Anthony K Rappe and Carla J Casewit. *Molecular Mechanics Across Chemistry*. University Science Books, 1997.

[221] Patrick Rebentrost et al. "Environment-assisted quantum transport". In: *New Journal of Physics* 11.3 (2009), p. 033003.

[222] Alfred G Redfield. "The theory of relaxation processes". In: *Advances in Magnetic and Optical Resonance*. Vol. 1. Elsevier, 1965, pp. 1–32.

[223] Thomas Renger, Volkhard May, and Oliver Kühn. "Ultrafast excitation energy transfer dynamics in photosynthetic pigment–protein complexes". In: *Physics Reports* 343.3 (2001), pp. 137–254.

[224] Raphael F Ribeiro et al. "Polariton chemistry: Controlling molecular dynamics with optical cavities". In: *Chemical Science* 9.30 (2018), pp. 6325–6339.

[225] Jeremy O Richardson. "Ring-polymer instanton theory". In: *International Reviews in Physical Chemistry* 37.2 (2018), pp. 171–216.

[226] SMJ Rogge et al. "A comparison of barostats for the mechanical characterization of metal–organic frameworks". In: *Journal of Chemical Theory and Computation* 11.12 (2015), pp. 5583–5597.

[227] Frank Roschangar et al. "A deeper shade of green: Inspiring sustainable drug manufacturing". In: *Green Chemistry* 19.1 (2017), pp. 281–285.

[228] Ho Ryu et al. "Pitfalls in computational modeling of chemical reactions and how to avoid them". In: *Organometallics* 37.19 (2018), pp. 3228–3239.

[229] Celeste Sagui and Thomas A. Darden. "Molecular dynamics simulations of bio: Long-range electrostatic effects". In: *Annual Review of Biophysics and Biomolecular Structure* 28.1 (1999), pp. 155–179.

[230] George C Schatz. "Fitting potential energy surfaces". In: *Reaction and Molecular Dynamics: Proceedings of the European School on Computational Chemistry, Perugia, Italy, July (1999)*. Springer. 2000, pp. 15–32.

[231] George C Schatz. "The analytical representation of electronic potential-energy surfaces". In: *Reviews of Modern Physics* 61.3 (1989), p. 669.

[232] Addison J Schile and David T Limmer. "Simulating conical intersection dynamics in the condensed phase with hybrid quantum master equations". In: *The Journal of Chemical Physics* 151.1 (2019).

[233] Addison J Schile and David T Limmer. "Studying rare nonadiabatic dynamics with transition path sampling quantum jump trajectories". In: *The Journal of Chemical Physics* 149.21 (2018).

[234] Addison Jon Schile. *Journey Before Destination: Understanding Quantum Dynamical Phenomena in Condensed Phases*. University of California, Berkeley, 2021.

[235] H Bernhard Schlegel. "Exploring potential energy surfaces for chemical reactions: An overview of some practical methods". In: *Journal of Computational Chemistry* 24.12 (2003), pp. 1514–1527.

[236] Tim Schleif et al. "Solvation effects on quantum tunneling reactions". In: *Accounts of Chemical Research* 55.16 (2022), pp. 2180–2190.

[237] Tamar Schlick. *Molecular Modeling and Aimulation: An Interdisciplinary Guide*. Vol. 2. Springer, 2010.

[238] Sidsel Birkelund Schmidt, Marion Eisenhut, and Anja Schneider. "Chloroplast transition metal regulation for efficient photosynthesis". In: *Trends in Plant Science* 25.8 (2020), pp. 817–828.

[239] C Schneider et al. "Exciton-polariton trapping and potential landscape engineering". In: *Reports on Progress in Physics* 80.1 (2016), p. 016503.

[240] Gregory D Scholes. "Long-range resonance energy transfer in molecular systems". In: *Annual Review of Physical Chemistry* 54.1 (2003), pp. 57–87.

[241] Wolfgang J Schreier, Peter Gilch, and Wolfgang Zinth. "Early events of DNA photodamage". In: *Annual Review of Physical Chemistry* 66 (2015), pp. 497–519.

[242] Thomas Schultz et al. "Mechanism and dynamics of azobenzene photoisomerization". In: *Journal of the American Chemical Society* 125.27 (2003), pp. 8098–8099.

[243] Franziska Schüppel; et al. "Waveform control of molecular dynamics close to a conical intersection". In: *The Journal of Chemical Physics* 153.22 (2020).

[244] Michael S Schuurman and Albert Stolow. "Dynamics at conical intersections". In: *Annual Review of Physical Chemistry* 69 (2018), pp. 427–450.

[245] Thomas P Senftle et al. "The ReaxFF reactive force-field: Development, applications and future directions". In: *npj Computational Materials* 2.1 (2016), pp. 1–14.

[246] Onise Sharia and Graeme Henkelman. "Analytic dynamical corrections to transition state theory". In: *New Journal of Physics* 18.1 (2016), p. 013023.

[247] MC Sherman and SA Corcelli. "Nonadiabatic transition path sampling". In: *The Journal of Chemical Physics* 145.3 (2016).

[248] Qiang Shi and Eitan Geva. "A new approach to calculating the memory kernel of the generalized quantum master equation for an arbitrary system–bath coupling". In: *The Journal of Chemical Physics* 119.23 (2003), pp. 12063–12076.

[249] Fumiaki Shibata, Yoshinori Takahashi, and Natsuki Hashitsume. "A generalized stochastic Liouville equation. Non-Markovian versus memoryless master equations". In: *Journal of Statistical Physics* 17 (1977), pp. 171–187.

[250] Sangwoo Shim et al. "Atomistic study of the long-lived quantum coherences in the Fenna-Matthews-Olson complex". In: *Biophysical Journal* 102.3 (2012), pp. 649–660.

[251] Seokmin Shin and Horia Metiu. "Nonadiabatic effects on the charge transfer rate constant: A numerical study of a simple model system". In: *The Journal of Chemical Physics* 102.23 (1995), pp. 9285–9295.

[252] Atsushi Shishido. "Rewritable holograms based on azobenzene-containing liquid-crystalline polymers". In: *Polymer Journal* 42.7 (2010), pp. 525–533.

[253] Dominik Sidler et al. "A perspective on ab initio modeling of polaritonic chemistry: The role of non-equilibrium effects and quantum collectivity". In: *The Journal of Chemical Physics* 156.23 (2022).

[254] Lee J Silverberg and Lionel M Raff. "Are the Concepts of Dynamic Equilibrium and the Thermodynamic Criteria for Spontaneity, Nonspontaneity, and Equilibrium Compatible?" In: *Journal of Chemical Education* 92.4 (2015), pp. 655–659.

[255] Nadja A Simeth et al. "Tuning the thermal isomerization of phenylazoindole photoswitches from days to nanoseconds". In: *Journal of the American Chemical Society* 140.8 (2018), pp. 2940–2946.

[256] Felix T Smith. "Diabatic and adiabatic representations for atomic collision problems". In: *Physical Review* 179.1 (1969), p. 111.

[257] Theresa Sperger, Italo A Sanhueza, and Franziska Schoenebeck. "Computation and experiment: A powerful combination to understand and predict reactivities". In: *Accounts of Chemical Research* 49.6 (2016), pp. 1311–1319.

[258] Alexandrina Stirbet et al. "Photosynthesis: Basics, history and modelling". In: *Annals of Botany* 126.4 (2020), pp. 511–537.

[259] ECG Stückelberg. "Theorie der unelastischen Stösse zwischen Atomen". In: *Helvetica Physica Acta* 5 (1932), p. 369.

[260] Joseph E Subotnik et al. "The requisite electronic structure theory to describe photoexcited nonadiabatic dynamics: Nonadiabatic derivative couplings and diabatic electronic couplings". In: *Accounts of Chemical Research* 48.5 (2015), pp. 1340–1350.

[261] Attila Szabo and Neil S. Ostlund. *Modern quantum chemistry : Introduction to advanced electronic structure theory*. eng. Mineola, N.Y: Dover Publications, 1996. ISBN: 0486691861.

[262] Kenzi Tamaru. "The history of the development of ammonia synthesis". In: *Catalytic Ammonia Synthesis: Fundamentals and Practice*. Springer, 1991, pp. 1–18.

[263] Yoshitaka Tanimura and Ryogo Kubo. "Time evolution of a quantum system in contact with a nearly Gaussian-Markoffian noise bath". In: *Journal of the Physical Society of Japan* 58.1 (1989), pp. 101–114.

[264] Nguyen Thanh Phuc. "Super-reaction: The collective enhancement of a reaction rate by molecular polaritons in the presence of energy fluctuations". In: *The Journal of Chemical Physics* 155.1 (2021).

[265] A Thiel. "The Landau-Zener effect in nuclear molecules". In: *Journal of Physics G: Nuclear and Particle Physics* 16.7 (1990), p. 867.

[266] Everett Thiele, Myron F Goodman, and James Stone. "Can lasers be used to break chemical bonds selectively?" In: *Optical Engineering* 19.1 (1980), pp. 10–20.

[267] A. Thomas et al. "Tilting a ground-state reactivity landscape by vibrational strong coupling". In: *Science* 363.6427 (2019), pp. 615–619.

[268] Anoop Thomas et al. "Ground-state chemical reactivity under vibrational coupling to the vacuum electromagnetic field". In: *Angewandte Chemie* 128.38 (2016), pp. 11634–11638.

[269] Erling Thyrhaug et al. "Identification and characterization of diverse coherences in the Fenna–Matthews–Olson complex". In: *Nature Chemistry* 10.7 (2018), pp. 780–786.

[270] Benjamin Trendelkamp-Schroer et al. "Estimation and uncertainty of reversible Markov models". In: *The Journal of Chemical Physics* 143.17 (2015).

[271] Donald G Truhlar, Bruce C Garrett, and Stephen J Klippenstein. "Current status of transition-state theory". In: *The Journal of Physical Chemistry* 100.31 (1996), pp. 12771–12800.

[272] Anton Trushechkin. "Unified Gorini-Kossakowski-Lindblad-Sudarshan quantum master equation beyond the secular approximation". In: *Physical Review A* 103 (6 2021), p. 062226.

[273] John C Tully. "Perspective: Nonadiabatic dynamics theory". In: *The Journal of Chemical Physics* 137.22 (2012).

[274] Christophe H Valahu et al. "Direct observation of geometric-phase interference in dynamics around a conical intersection". In: *Nature Chemistry* 15.11 (2023), pp. 1503–1508.

[275] Edward F Valeev and C David Sherrill. "The diagonal Born–Oppenheimer correction beyond the Hartree–Fock approximation". In: *The Journal of Chemical Physics* 118.9 (2003), pp. 3921–3927.

[276] Adri CT Van Duin et al. "ReaxFF: A reactive force field for hydrocarbons". In: *The Journal of Physical Chemistry A* 105.41 (2001), pp. 9396–9409.

[277] Eric Vanden-Eijnden. "Transition path theory". In: *Computer Simulations in Condensed Matter Systems: From Materials to Chemical Biology Volume 1*. Springer, 2006, pp. 453–493.

[278] Patrick Varilly and David Chandler. "Water evaporation: A transition path sampling study". In: *The Journal of Physical Chemistry B* 117.5 (2013), pp. 1419–1428.

[279] Franz J Vesely et al. *Computational Physics*. Springer, 1994.

[280] Nicolas Vogt, Jan Jeske, and Jared H. Cole. "Stochastic Bloch-Redfield theory: Quantum jumps in a solid-state environment". In: *Physical Review B* 88 (17 2013), p. 174514.

[281] Arthur F Voter and Jimmie D Doll. "Dynamical corrections to transition state theory for multistate systems: Surface self-diffusion in the rare-event regime". In: *The Journal of Chemical Physics* 82.1 (1985), pp. 80–92.

[282] Gregory A Voth, David Chandler, and William H Miller. "Rigorous formulation of quantum transition state theory and its dynamical corrections". In: *The Journal of Chemical Physics* 91.12 (1989), pp. 7749–7760.

[283] Gregory A. Voth, David Chandler, and William H. Miller. "Rigorous formulation of quantum transition state theory and its dynamical corrections". In: *The Journal of Chemical Physics* 91.12 (1989), pp. 7749–7760.

[284] Thomas M Wahlund et al. "A thermophilic green sulfur bacterium from New Zealand hot springs, Chlorobium tepidum sp. nov." In: *Archives of Microbiology* 156 (1991), pp. 81–90.

[285] Warren S Warren, Herschel Rabitz, and Mohammed Dahleh. "Coherent control of quantum dynamics: The dream is alive". In: *Science* 259.5101 (1993), pp. 1581–1589.

[286] Hiroshi Watanabe. "Stability of velocity-Verlet-and Liouville-operator-derived algorithms to integrate non-Hamiltonian systems". In: *The Journal of Chemical Physics* 149.15 (2018).

[287] E Weinan, Weiqing Ren, and Eric Vanden-Eijnden. "Transition pathways in complex systems: Reaction coordinates, isocommittor surfaces, and transition tubes". In: *Chemical Physics Letters* 413.1-3 (2005), pp. 242–247.

[288] Eugene Wigner. "The transition state method". In: *Transactions of the Faraday Society* 34 (1938), pp. 29–41.

[289] HM Wiseman and GJ Milburn. "Interpretation of quantum jump and diffusion processes illustrated on the Bloch sphere". In: *Physical Review A* 47.3 (1993), p. 1652.

[290] M Wojcik and E Clementi. "Molecular dynamics simulation of liquid water with three-body forces included". In: *The Journal of Chemical Physics* 84.10 (1986), pp. 5970–5971.

[291] Graham A Worth and Lorenz S Cederbaum. "Beyond Born-Oppenheimer: Molecular dynamics through a conical intersection". In: *Annual Review of Physical Chemistry* 55 (2004), pp. 127–158.

[292] Daiqian Xie, Rongqing Chen, and Hua Guo. "Comparison of Chebyshev, Faber, and Lanczos propagation-based methods for calculating resonances". In: *The Journal of Chemical Physics* 112.12 (2000), pp. 5263–5269.

[293] David R Yarkony. "Nonadiabatic Quantum Chemistry: Past, Present, and Future". In: *Chemical Reviews* 112.1 (2012), pp. 481–498.

[294] Clarence Zener. "Dissociation of excited diatomic molecules by external perturbations". In: *Proceedings of the Royal Society of London. Series A, Containing Papers of a Mathematical and Physical Character* 140.842 (1933), pp. 660–668.

[295] Ahmed H Zewail. "Laser selective chemistry—is it possible?" In: *Physics Today* 33.11 (1980), pp. 27–33.

[296] Long Zhang et al. "Recent developments on polariton lasers". In: *Progress in Quantum Electronics* 83 (2022), p. 100399.

[297] Xiao-Jie Zhang, Cheng Shang, and Zhi-Pan Liu. "Double-ended surface walking method for pathway building and transition state location of complex reactions". In: *Journal of Chemical Theory and Computation* 9.12 (2013), pp. 5745–5753.

[298] Xinhao Zhang, Lung Wa Chung, and Yun-Dong Wu. "New mechanistic insights on the selectivity of transition-metal-catalyzed organic reactions: The role of computational chemistry". In: *Accounts of Chemical Research* 49.6 (2016), pp. 1302–1310.

[299] Vladimir P. Zhdanov. "Vacuum field in a cavity, light-mediated vibrational coupling, and chemical reactivity". In: *Chemical Physics* 535 (2020), p. 110767. ISSN: 0301-0104.

[300] Xiaolan Zhong et al. "Energy transfer between spatially separated entangled molecules". In: *Angewandte Chemie* 129.31 (2017), pp. 9162–9166.

[301] Xin Zhou et al. "Organic semiconductor–organism interfaces for augmenting natural and artificial photosynthesis". In: *Accounts of Chemical Research* 55.2 (2021), pp. 156–170.

[302] Xiaolei Zhu and David R Yarkony. "Non-adiabaticity: The importance of conical intersections". In: *Molecular Physics* 114.13 (2016), pp. 1983–2013.

[303] Kirill Zinovjev and Iñaki Tuñón. "Reaction coordinates and transition states in enzymatic catalysis". In: *Wiley Interdisciplinary Reviews: Computational Molecular Science* 8.1 (2018), e1329.

[304] Robert Zwanzig. "Ensemble method in the theory of irreversibility". In: *The Journal of Chemical Physics* 33.5 (1960), pp. 1338–1341.